Waipapa Taumata Rau
The University of Auckland

Frequency-Filtered Photon Correlations

by
Jacob Peter Kia Ngaha

A thesis submitted in fulfilment of the requirements for the degree of Doctor of Philosophy (PhD) in Physics, the University of Auckland, 2023.

Abstract

In quantum optics, the standard approach for measuring and calculating frequency-filtered photon correlations is to filter the source field of interest with a Lorentzian-type filter, e.g., a tunable single-mode cavity or detector atom. However, given the inverse relation between a filter's bandwidth and temporal response, there is trade-off between the frequency isolation and temporal response of the filter. A broad bandwidth results in a faster temporal response with more accurately measured photon correlations, yet the slow decaying tails of a Lorentzian distribution can allow for non-target frequency photons to pass through the filter. Conversely, a narrow filter bandwidth results in more effective frequency isolation, yet a slow temporal response, potentially changing the nature of the emitted photon correlations.

The aim of this work is to develop a theoretical filtering technique that is simple to implement and offers an effective method of calculating frequency-filtered photon correlations. We model our filter as a *multi-mode array filter*, which consists of an array of tunable single-mode cavities that are equally spaced in frequency. By introducing a mode-dependent phase modulation, we produce a near rectangular frequency response, allowing us to increase the filter bandwidth – and thus the temporal response – without sacrificing frequency isolation. To ensure the filter has no effect on the evolution of the source system, we couple the source system using a *cascaded quantum open systems* approach. The complete lack of back-action of the filter onto the source system allows us to derive a closed set of operator moment equations for source and filter system operators. This provides an extremely effective and computationally efficient way to calculate *frequency-filtered first- and second-order correlation functions*. By coupling the target field into *two* multi-mode array filters, we can set the resonance of the two filters to two different transitions, and thus calculate frequency-filtered *cross-correlation* functions.

We demonstrate this novel filtering method by applying it to two different driven quantum systems: a resonantly driven two-level atom and a three-level ladder-type atom driven at two-photon resonance. We present results of frequency-filtered power spectrum to demonstrate the improved frequency isolation of the multi-mode array filter over the single-mode filter. We then present results for the single-mode and multi-mode array filtered second-order auto- and cross-correlation functions. These are compared against expressions derived in the secular approximation. The improved frequency isolation of the multi-mode array filter allows us to investigate new areas of frequency-filtered photon correlations, such as two-photon *leapfrog* processes, and the effect of vanishing bandwidth on filtered auto-correlation functions.

E whakaihia ana tēnei tuhingaroa ki tōku rangatira, Howard Carmichael.
He toka tū moana he ākinga nā ngā tai.

This thesis is dedicated to my supervisor, Howard Carmichael.
Steadfast as the rock that scorns the lashing tides.

Acknowledgements

Ehara taku toa i te toa takitahi, engari he toa takitini.
My success is not mine alone, it is the success of the collective.

Ko te mihi tuatahi, ko te mihi nui ake, ki tōku rangatira, Howard Carmichael. Ngā mihi nui ki a koe ki tōu mahi kaha, tōu awhi, me tōu tohu. First and foremost I would like to thank my supervisor, Howard Carmichael. In 2017 I started an Honours project with you, not knowing a single thing about quantum optics. In these years, however, I have learnt so much from you. Anytime I wondered about a particular problem, it was most likely mentioned in one of your books, which many of us students treat as our unofficial bible. I feel extremely blessed and privileged to have worked with you these past few years, and am extremely thankful for all the time and effort you have spent into helping me grow as a physicist, a scientist, and a person. Thank you so much for all of your hard work, all of your support, all of your guidance, and all of your "yellow boxes".

Ko te mihi tuarua ki tōku rangatira atu, Scott Parkins. Secondly, I would like to thank Scott Parkins. A lot. This last year has been particularly turbulent, and I am extremely thankful for your continued support and help in getting myself and Geraud through the final part of our PhD studies. In the last year, a lot more work has been placed on your shoulders, and I will always be grateful for the time you have made for us. Thank you, Scott.

Ngā mihi ki tōku whānau me ngōku hoa e awhi ana. Thank you to my family and all my friends, both inside and outside of Te Ao Mātai Ahupūngao. I am ever grateful for your love and support as I undertook this wild journey. To my friend, and fellow student of Howard, Geraud, it has been a rough time, but I am glad we have made it through together.

A special acknowledgement must go to my dear friend and office mate of the past three or so years, Steph. We both started on the exact same day, have gone through the same hōha together, and have come out of it as well. I am incredibly grateful for your support and friendship, for all the quiz scores (both good and bad), and for all of the Munchy breaks.

E mihi ana ki ngā tuaira kua mahi tahi au. A special thanks goes to Tim and Miriam for joining in on the project for their Honour's year. It was a pleasure working with you both, and I truly valued the contributions you both made to this work.

I would also like to thank the Department of Physics and Te Whai Ao, The Dodd Walls Centre, for supporting me through the past few years, and for all the opportunities that have arisen.

Nō reira, ko tēnei te mihi whakamutunga. Heoi anō, ehara i te mihi iti. Ngā mihi nui nui **nui** ki a kōrua, e Maisie kōrua ko Attie. The biggest and most greatest thank you to my loving partner, Maisie, and our little naughty dude, Attie. You have been so amazingly supportive throughout this PhD, and I really could not have done it without you. There were times when it was getting far too much for me, and I would be on the cusp of giving up. Yet you were, and are, always there for me. And to Attie, thank you for all the cuddles over the years, and

also for all of the barking while I have been working at home, during Zoom meetings and online teaching, and also during the last few weeks of writing. I love you both with all of my heart.

Also, a big anti-thank you to Covid.

Contents

List of Figures

1 Introduction

Resonance fluorescence – the scattering of light resonant with an atomic system – of a two-level atom is one of the simplest examples of light interacting with matter, yet it is a key concept in quantum optics. It was found, both theoretically and experimentally, that upon strong coherent excitation, the power spectrum of the two-level atom splits into three components to yield the structure known as the "Mollow triplet" [1–3]. It was then discovered that this splitting phenomenon is due to transitions amongst the atom's "dressed states"; a direct result of the atom interacting with a strong quantised electromagnetic field [4, 5]. This work, so early on in the field of quantum optics, led to a renewed interest in the details of interactions between light and atomic systems [6].

Around the same time that Mollow's papers were originally published, there were also investigations into the quantum nature of the emitted light; of particular interest were *photon correlations*. Photon correlations have long been studied in classical optics; the definitions of *coherence* and *bunched* light – where photons are emitted in packets, or "bunches" – originated from a classical description of light. It was in 1963, however, when Glauber first developed a purely quantum mechanical description of these correlation functions [7, 8]. In 1976, Walls and Carmichael showed that the two-level atom exhibited a purely quantum effect, namely *antibunching* [9–11], with the first experimental observation occurring the following year [12].

In 1977, Eberly and Wódkiewicz formulated a new description of spectra, which they define as a "time dependent physical spectrum of light based on the counting rate of a photodetector" [13]. While this work was set out to solve the discrepancies between power spectra and actual physical measurements, it helped lay the foundation of using Fabry-Pérot interferometers as frequency filters [14–20].

The majority of studies on atomic fluorescence around this time were largely focused on the entire fluorescence spectrum of the atom. It was at the end of the 1970s when Apanasevich and Kilin published one of the first investigations into correlating photons from individual components of the total fluorescence field [21–23]. Soon after, in 1980, Aspect, Roger, Dalibard, and Cohen-Tannoudji reported the first experimental investigation into the photon correlations between photons of the sidebands of the Mollow triplet [24]. They achieved the separation of the two frequency components by splitting the fluorescence into two channels, with each passing through an interference filter tuned to the target wavelength. More research soon followed, and it remains a topic of interest to this day [25–38], thanks, in part, to new capabilities offered by the advent of circuit QED technology.

With a surge of interest in measuring photon correlations from components of the fluorescence spectrum came an interest in the *effect* of frequency filtering [39–42], as well as other methods of calculating and measuring frequency-filtered photon correlations. It was in 2012 that del Valle et al. published their paper "Theory of frequency-filtered and time-resolved N-photon correlations" [43, 44]. Their proposed method consisted of weakly coupling the output

field of a system of interest into N detector atoms, where N is the order of the correlation function of interest. This proved to be an astonishingly simple method to implement, and has been used extensively, in both theoretical and experimental works [45–51]. Other methods have also been discussed over the years, with more of a theoretical leaning, such as: frequency resolved Monte-Carlo, or quantum trajectory methods [52–54]; perturbation approaches [55]; and signal processing methods [56]. Kamide et al. also developed a method based on the eigenvalue decomposition of the Liouvillian superoperators [57, 58]. This theoretically intense method allowed them to model not only Lorentzian filters, but also Gaussian and rectangular filters.

While there is no perfect method of frequency filtering to cover all applications, there are issues with the previous methods. The most common type of frequency filter, and perhaps the easiest in both theoretical and experimental applications, is the tunable interferometer; it can be modelled with relative ease as a single-mode cavity. The most prominent downside to this method is that the natural frequency response of a single-mode cavity is Lorentzian shaped. Why is this limiting? The tails of a Lorentzian distribution extend quite far from the centre and, in fact, never decay entirely. For multi-frequency source systems, such as a strongly driven two-level atom exhibiting the Mollow triplet, the tails of the frequency response can intersect with non-target frequencies. The width of the Lorentzian distribution, i.e., the bandwidth of the filter cavity, is inversely proportional to the temporal response of the filter. Therefore, a trade-off is required between the temporal response and the frequency isolation of the filter.

We therefore arrive at the aim of this thesis: to develop an improved method of frequency filtering and calculating frequency-filtered photon correlations. We require this improved method to be cavity based, such that it could be achieved in a laboratory, and for it to have a more effective frequency response for multi-frequency sources. An ideal filter, in this case, would be a rectangular filter, which can be achieved with the eigenvalue decomposition method of Kamide et al. [57]. This method, however, is entirely mathematical, and cannot be achieved physically.

We also require that the filter model has no effect on the evolution of the source system. The method of del Valle et al. [43] achieves this by assuming a vanishingly small coupling of the source system to the detector atoms, such that any back-action can be neglected. Holdaway et al. [55] take this approach a step further with an algebraic expansion of the source-filter coupled system with respect to the coupling parameter. We can, in fact, ensure there is no back-action by *cascading* the output of the source system as the input for the filter system, using open cascaded systems theory [59, 60], which has been employed in just a few recent works [61, 62].

The novel method we will introduce in this thesis is the *multi-mode array filter*. This filter model consists of an array of tunable, single-mode cavities; the output field of a source system is cascaded equally into each mode, where a mode-dependent phase modulation is applied. The output of each individual mode is then combined, creating an interference that results in an approximately rectangular frequency response.

A further, uncommon approach that we will use for determining filtered photon correlations is by calculating the expectation value of the detection operators. Usually, second-order correlation functions can be calculated via the Lindblad master equation, along with the quantum regression equations formulated by Lax [63, 64]. By solving for the operator averages, or *moment equations*, of a filter system's source operators – such as the photon annihilation operator

– these correlation functions can be solved much more efficiently and accurately. By modelling the filtering process as a cascaded quantum system, thus ensuring there is no back-action of the filter on the source system, the evolution of the source system generates all of the dynamics of the source-filter coupled system. As we will see, this provides a simple and effective method for calculating frequency-filtered correlation functions.

Outline of the Thesis

This thesis is split into two parts: Part I Quantum Optics and Filtering, and Part II Resonance Fluorescence.

In Part I, we set out the important background theory for the entire thesis. We begin in Chapter 2 with a general summary of some of the key concepts of quantum mechanics. We introduce the notion of describing quantum states as vectors, using the language of Dirac notation. With our notation set, we then derive one of the key fundamentals of quantum optics and quantise the electromagnetic field as a discrete collection of harmonic oscillators.

This treatment, however, considers only a closed physical system, with no energy loss. We therefore introduce and derive mathematical methods in Chapter 3 that take into consideration loss of energy into the environment. Using the *Born* and *Markov* approximations, we derive the *Lindblad master equation* for a damped electromagnetic field mode. Under the theory of open quantum systems, the *quantum regression formulae* allow us to derive expressions for the two main quantities discussed in this thesis: *first- and second-order correlation functions*. Finally, we derive the *open cascaded systems master equation*, in which the output of one quantum system is cascaded into another. With this method we are able to model a frequency-filtered quantum system by coupling the output of a target system into a frequency filter.

The frequency filter we will introduce in this thesis – and indeed use for the main results – is the *multi-mode array filter*, which we describe in Chapter 4. We start by discussing the basis of our filtering model, the *Fabry-Pérot interferometer* from the perspective of classical optics. Using the transfer matrix method, we derive expressions for the interferometer's *transmission spectrum* and compare them with expressions derived from a purely quantum model. We then extend the filtering model to the *multi-mode array filter*, which consists of an array of single-mode cavities, with a combined output field. We also derive expressions for the multi-mode array filter's temporal and frequency response.

Part II of this thesis concerns the two source systems we consider in this thesis. In Chapter 5 we will introduce the first of these: the *resonantly driven two-level atom*. We will discuss the dynamics and key physical phenomena of the atom by itself, namely the *Mollow triplet* and photon *antibunching*. The two-level atom will therefore act as the "training wheels" of the multi-mode array filter, which will be the focus of Chapter 6. We investigate the frequency-filtered first- and second-order correlation functions – both auto- and cross-correlation functions – and compare the correlation functions from a single-mode and the multi-mode array filters, highlighting the improved frequency isolation of the multi-mode array filter over the standard single-mode. We therefore demonstrate the improvement of reproducing the idealised dressed state correlations functions as derived in the secular approximation.

Finally, in Chapter 7 we introduce the second source system: the *three-level ladder-type*

atom driven at two-photon resonance. The atomic structure of the three-level atom is based on recent work by Gasparinetti et al. [65, 66], and offers more complex and interesting dynamics than the two-level atom. In particular, when strongly driven the three-level ladder-type atom displays seven distinct frequencies in its power spectrum, corresponding to various transitions amongst its three dressed states. The increased complexity of this system offers an abundance of interesting correlations to explore. We therefore present calculations of frequency-filtered first- and second-order correlation functions for the three-level atom to further demonstrate the effectiveness of the multi-mode array filter over the single-mode filter. We will also investigate cross-correlations between the different transition frequencies, further verifying the dressed state picture. The improved frequency isolation of the multi-mode filter allows us to uncover new areas of correlations, as well as interesting new phenomena. In particular, we find extremely asymmetrical cross-correlations between the different fluorescence peaks of the three-level atom.

Part I

Quantum Optics and Filtering

2 Quantum Mechanics and Quantum Optics

At a very basic level quantum mechanics is based on the idea of *quantisation*, where measured values of physical systems are often discrete quantities. Originally formulated by the likes of Heisenberg, Schrödinger, and Dirac [67–70], the subject is now a central part of the physics curriculum.

We begin this thesis by setting out the fundamentals of quantum mechanics upon which the following chapters build. We summarise the basic postulates of quantum mechanics and the mathematical language we plan to use. We then quantise the electromagnetic field, which leads us to introduce a set of basis states associated with the photon number of a single mode, the so-called *photon-number states* or *Fock states*. Finally, we introduce *coherent states*, a useful representation of the quantum state of laser light.

2.1 Formulation of Quantum Mechanics

While not the focus of this thesis, we aim to give a general summary of quantum mechanics as a way of setting out our notation and methods. We follow the approach of Sakurai and others (Refs. [71, 72]), and give an outline of the formulation of quantum mechanics originally devised by Dirac [69].

2.1.1 Kets, bras, and inner products

We begin by considering a complex vector space, $\mathcal{V}$, where the dimension of this space is determined by the physical system under investigation. Each possible state of the physical system, such as the spin of an atom or the number of photons in a cavity, can be represented by a vector in this vector space, which we will write as a *ket-vector*, $|a\rangle \in \mathcal{V}$. Ket-vectors, or kets, follow similar rules to vectors in a general vector space. That is we can add kets together to form a new ket,

$$|a\rangle + |b\rangle = |c\rangle\,, \tag{2.1}$$

and we can multiply a ket by a complex scalar, $c \in \mathbb{C}$, on the left-hand or right-hand side,

$$c\,|a\rangle = |a\rangle\,c. \tag{2.2}$$

Here we note that the kets $c\,|a\rangle$ and $|a\rangle$ actually represent the same physical state; only the *direction* of the ket vector is physically significant.

An arbitrary ket can be written as a combination of basis states (defined below),

$$|\psi\rangle = c_0\,|a_0\rangle + c_1\,|a_1\rangle + c_2\,|a_2\rangle + \cdots\,, \tag{2.3}$$

where $c_0, c_1, c_2, \ldots$ are complex coefficients.

Where ket-vectors live in a vector space $\mathcal{V}$, *bra-vectors* live in the dual-space, $\mathcal{V}^*$. We denote bra-vectors, or *bras*, by $\langle b| \in \mathcal{V}^*$, and note that they map a ket to a complex number through the inner product

$$(b, a) = (\langle b|) \cdot (|a\rangle) = \langle b|a\rangle \in \mathbb{C}. \tag{2.4}$$

We now introduce two fundamental postulates relating to the inner product. Firstly, the inner products $\langle a|b\rangle$ and $\langle b|a\rangle$ are complex conjugates of each-other,

$$\langle a|b\rangle = \langle b|a\rangle^* , \tag{2.5}$$

and secondly,

$$\langle a|a\rangle \geq 0, \tag{2.6}$$

where the inner product is only zero if $|a\rangle$ is a null-vector. Finally, two non-zero kets, $|a\rangle$ and $|b\rangle$, are said to be orthogonal if

$$\langle a|b\rangle = 0. \tag{2.7}$$

For every ket there is a one-to-one correspondence to a corresponding bra, a property also known as *dual correspondence*. From Eq. (2.5), for the general ket, Eq. (2.3), we have the corresponding bra dual:

$$\langle \psi| = c_0^* \langle a_0| + c_1^* \langle a_1| + c_2^* \langle a_2| + \cdots , \tag{2.8}$$

where we have taken the complex conjugate of the coefficients.

2.1.2 Operators, observables, and expectation values

Where bras map a ket to a complex number, *operators* map one ket (or bra) to another ket (or bra). Operators act on the left of kets,

$$A \cdot (|a\rangle) = A\,|a\rangle \tag{2.9}$$

which in general, but not necessarily, returns a different state. There are, however, particularly useful states, known as the *eigenkets*, or *eigenstates*, of an operator, with eigenvalue equations

$$A\,|a_0\rangle = a_0\,|a_0\rangle , \quad A\,|a_1\rangle = a_1\,|a_1\rangle , \quad A\,|a_2\rangle = a_2\,|a_2\rangle , \quad \cdots , \tag{2.10}$$

where $a_0, a_1, a_2, \cdots \in \mathbb{C}$ are the corresponding eigenvalues.

While there are exceptions, all operators considered in this thesis are linear, with

$$A\,(c_0\,|a_0\rangle + c_1\,|a_1\rangle + \cdots) = c_0 A\,|a_0\rangle + c_1 A\,|a_1\rangle + \cdots . \tag{2.11}$$

Operators can be multiplied, however, they do not generally commute. We therefore define the *commutator* of two operators, A and B, as

$$[A, B] = AB - BA, \tag{2.12}$$

and note that if two operators do commute then $[A, B] = 0$.

Operators can also act on a bra, from the right side,

$$(\langle a|) \cdot A = \langle a| A, \tag{2.13}$$

and, similar to kets, this operation results in another bra. In general, the ket $A|a\rangle$ and the bra $\langle a| A$ are not the duals of one another. Instead we introduce the *Hermitian adjoint* of an operator, $A^\dagger$, defined through the dual correspondence,

$$A|a\rangle \xleftrightarrow{\text{Dual Correspondence}} \langle a| A^\dagger. \tag{2.14}$$

Observables, such as the momentum of a particle or the spin of an atom, can be mathematically represented by an *Hermitian* operator, that is an operator X that is self-adjoint, with

$$X = X^\dagger. \tag{2.15}$$

As previously mentioned, the eigenstates of observables are useful, in that they form a set of orthogonal basis kets in the vector space with real eigenvalues, leading to the expansion of Eq. (2.3). For a complete set of orthogonal basis kets, we also note the useful property of *closure*, also known as the *completeness relation*:

$$\sum_i |a_i\rangle \langle a_i| = \mathbb{1}. \tag{2.16}$$

We can expand on the definition of the inner product of two states with the inclusion of an operator. Recalling that $\langle a| A^\dagger$ is the dual of $A|a\rangle$ we obtain

$$\langle a|A|b\rangle = \langle b|A^\dagger|a\rangle^*. \tag{2.17}$$

Assuming the system state is represented by a linear combination of basis vectors, Eq. (2.3), when a measurement of an operator A is made, the result is one of the eigenvalues of A and the system is cast (assuming no degeneracy) into the corresponding eigenstate $|a_k\rangle$. We do not know which of the eigenstates the system will be cast into, however we postulate that the probability for arriving in a particular state, say $|a_k\rangle$, is given by

$$P(a_k) = |\langle a_k|\psi\rangle|^2 = |c_k|^2. \tag{2.18}$$

From here we define the average, or *expectation value*, of an operator A as

$$\langle A\rangle = \langle\psi|A|\psi\rangle = \sum_{i,j} c_j^* c_i \langle a_j|A|a_i\rangle = \sum_i a_i |c_i|^2, \tag{2.19}$$

where the orthonormality of eigenkets with different eigenvalues has been used (see Ref. [71], p. 15).

2.1.3 The density operator

States that can be written as linear combination of basis states are also known as *pure states*. Pure states are difficult to achieve, however, as experimental settings are not perfect. In most cases, we may know that a physical system can be in one state, $|\psi_i\rangle$, with a probability p_i, out of an ensemble of possible states. When more than one possible state occurs with a non-vanishing probability, the state can no longer be described by a single linear combination of kets, and is instead known as a *mixed state*. We therefore introduce the *density operator*:

$$\rho = \sum_i p_i \left|\psi_i\right\rangle \left\langle\psi_i\right|, \quad \text{with} \quad \sum_i p_i = 1, \quad p_i \geq 0. \tag{2.20}$$

Given a basis set of eigenvectors, the density operator can be written as

$$\rho = \sum_{i,j} \rho_{ij} \left|a_j\right\rangle \left\langle a_i\right|, \tag{2.21}$$

where $\rho_{ij} = \langle a_j|\rho|a_i\rangle \in \mathbb{C}$ defines the *density matrix* in the A-representation. The density operator has two important properties: it is Hermitian, $\rho = \rho^\dagger$, and it has unit trace, $\mathrm{tr}\left[\rho\right] = 1$. With this definition of the density operator, we are able to generalise the expression for the expectation of an operator, Eq. (2.19), to

$$\langle A\rangle = \mathrm{tr}\left[\rho A\right]. \tag{2.22}$$

2.1.4 Time evolution

Whenever a system is not being directly measured, it evolves according to the *time dependent Schrödinger equation*,

$$\frac{\mathrm{d}}{\mathrm{d}t}\left|\psi\right\rangle = \frac{1}{i\hbar} H \left|\psi\right\rangle, \tag{2.23}$$

where H is the system Hamiltonian operator, and $\hbar$ is the *reduced Planck constant*. So long as the Hamiltonian is time independent, we can formally integrate Eq. (2.23) to find

$$\left|\psi(t)\right\rangle = \mathcal{U}(t, t_0) \left|\psi(t_0)\right\rangle, \tag{2.24}$$

where we introduce the *unitary time evolution operator*,

$$\mathcal{U}(t, t_0) = e^{\frac{1}{i\hbar} H(t - t_0)}. \tag{2.25}$$

With this definition, we find that the average value of an operator at some time t may be written as

$$\langle A(t)\rangle = \langle\psi(t)|A|\psi(t)\rangle = \langle\psi(0)|\mathcal{U}^\dagger(t, t_0) A\, \mathcal{U}(t, t_0)|\psi(0)\rangle, \tag{2.26}$$

so that as an alternative to the evolution of the ket vector in the Schrödinger picture, the operator A evolves in the Heisenberg picture as

$$A(t) = \mathcal{U}^\dagger(t, t_0) A(t_0)\, \mathcal{U}(t, t_0). \tag{2.27}$$

From Eqs. (2.25) and (2.27) we obtain the *Heisenberg equation of motion* for an operator A:

$$\frac{\mathrm{d}}{\mathrm{d}t}A = \frac{1}{i\hbar}[A, H]. \tag{2.28}$$

2.2 Quantisation of the Electromagnetic Field

In order to represent the electromagnetic field in terms of quantum mechanical operators, we begin by considering the field to be classical. Following the steps of Walls and Milburn (Ref. [73], Chapter 2), we quantise the field in terms of a vector potential, expanding it over a collection of independent harmonic oscillators.

2.2.1 Plane wave expansion of the field

We start with Maxwell's equations in S.I. units for the electric and magnetic fields in free space, $\boldsymbol{E}(\boldsymbol{r}, t)$ and $\boldsymbol{B}(\boldsymbol{r}, t)$ respectively, at position $\boldsymbol{r}$ and time t:

$$\boldsymbol{\nabla} \cdot \boldsymbol{E}(\boldsymbol{r}, t) = 0, \tag{2.29a}$$

$$\boldsymbol{\nabla} \times \boldsymbol{E}(\boldsymbol{r}, t) = -\frac{\partial}{\partial t}\boldsymbol{B}(\boldsymbol{r}, t), \tag{2.29b}$$

$$\boldsymbol{\nabla} \cdot \boldsymbol{B}(\boldsymbol{r}, t) = 0, \tag{2.29c}$$

$$\boldsymbol{\nabla} \times \boldsymbol{B}(\boldsymbol{r}, t) = \frac{1}{c^2}\frac{\partial}{\partial t}\boldsymbol{E}(\boldsymbol{r}, t), \tag{2.29d}$$

where $c = (\epsilon_0 \mu_0)^{-1/2}$ is the speed of light in a vacuum, and ϵ_0 and μ_0 are the free space electric permittivity and magnetic permeability, respectively. A solution to these equations can be found by choosing a vector potential, $\boldsymbol{A}(\boldsymbol{r}, t)$, such that

$$\boldsymbol{E}(\boldsymbol{r}, t) = -\frac{\partial}{\partial t}\boldsymbol{A}(\boldsymbol{r}, t), \tag{2.30a}$$

$$\boldsymbol{B}(\boldsymbol{r}, t) = \boldsymbol{\nabla} \times \boldsymbol{A}(\boldsymbol{r}, t). \tag{2.30b}$$

We choose a vector potential here, as the divergence of both the electric and magnetic fields are zero in a vacuum. We should note, however, that there is no unique potential that satisfies Eqs. (2.30); a property known as *gauge invariance*. For a given time-independent scalar *gauge function*, $\Lambda(\boldsymbol{r})$, if $\boldsymbol{A}$ is a valid potential then so is

$$\boldsymbol{A}'(\boldsymbol{r}, t) = \boldsymbol{A}(\boldsymbol{r}, t) - \boldsymbol{\nabla}\Lambda(\boldsymbol{r}). \tag{2.31}$$

We therefore find it useful to impose the *Coulomb gauge*,

$$\boldsymbol{\nabla} \cdot \boldsymbol{A}(\boldsymbol{r}, t) = 0, \tag{2.32}$$

where we have eliminated the longitudinal component of the vector potential, leaving us with two *transverse* components. Maxwell's equations now simplify to the wave equation,

$$\boldsymbol{\nabla}^2 \boldsymbol{A}(\boldsymbol{r},t) - \frac{1}{c^2}\frac{\partial^2}{\partial t^2}\boldsymbol{A}(\boldsymbol{r},t) = 0. \tag{2.33}$$

We consider the field to be contained inside a cubic volume $V = L^3$, such that we may extend any solution to neighbouring volumes with periodic boundary conditions, and expand the general solution of Eq. (2.33) in terms of a discrete set of orthogonal mode functions,

$$\boldsymbol{A}(\boldsymbol{r},t) = \sum_{\boldsymbol{k}} \boldsymbol{A}_{\boldsymbol{k}}(t)e^{i\boldsymbol{k}\cdot\boldsymbol{r}} + \boldsymbol{A}^*_{\boldsymbol{k}}(t)e^{-i\boldsymbol{k}\cdot\boldsymbol{r}}, \tag{2.34}$$

with the sum ranging over all wave vectors $\boldsymbol{k} = k_x\hat{\boldsymbol{x}} + k_y\hat{\boldsymbol{y}} + k_z\hat{\boldsymbol{z}}$, where

$$k_x = \frac{2\pi n_x}{L}, \quad k_y = \frac{2\pi n_y}{L}, \quad k_z = \frac{2\pi n_z}{L}, \tag{2.35}$$

with $n_x, n_y, n_z \in \mathbb{Z}$. The mode functions satisfy the transversality condition, Eq. (2.32), if

$$\boldsymbol{k}\cdot\boldsymbol{A} = 0. \tag{2.36}$$

Two polarisation vectors orthogonal to $\boldsymbol{k}$, labelled $\hat{\boldsymbol{e}}_{\boldsymbol{k},\lambda=1,2}$ and corresponding to the two transverse directions of the vector potential, are needed in general, such that this condition holds. The vector potential can then be expanded as

$$\boldsymbol{A}(\boldsymbol{r},t) = \sum_{\boldsymbol{k},\lambda} A_{\boldsymbol{k},\lambda}(t)\hat{\boldsymbol{e}}_{\boldsymbol{k},\lambda}e^{i\boldsymbol{k}\cdot\boldsymbol{r}} + A^*_{\boldsymbol{k},\lambda}(t)\hat{\boldsymbol{e}}_{\boldsymbol{k},\lambda}e^{-i\boldsymbol{k}\cdot\boldsymbol{r}}. \tag{2.37}$$

Substituting this vector potential into the wave equation, Eq. (2.33), and using the fact that the mode functions are orthonormal, Eq. (2.36), yields

$$\boldsymbol{k}^2 A_{\boldsymbol{k},\lambda}(t) + \frac{1}{c^2}\frac{\mathrm{d}^2}{\mathrm{d}t^2}A_{\boldsymbol{k},\lambda}(t) = 0, \tag{2.38}$$

which has solution

$$A_{\boldsymbol{k},\lambda}(t) = A_{\boldsymbol{k},\lambda}e^{-i\omega_{\boldsymbol{k}}t}, \tag{2.39}$$

where we have used the *free space dispersion relation*

$$\omega_{\boldsymbol{k}} = kc. \tag{2.40}$$

Using this vector potential, the electric and magnetic fields may be written as

$$\boldsymbol{E}(\boldsymbol{r},t) = \sum_{\boldsymbol{k},\lambda} i\omega_{\boldsymbol{k}}\hat{\boldsymbol{e}}_{\boldsymbol{k},\lambda}A_{\boldsymbol{k},\lambda}e^{i(\boldsymbol{k}\cdot\boldsymbol{r}-\omega_{\boldsymbol{k}}t)} + \text{c.c.}, \tag{2.41a}$$

$$\boldsymbol{B}(\boldsymbol{r},t) = \sum_{\boldsymbol{k},\lambda} i\left(\boldsymbol{k}\times\hat{\boldsymbol{e}}_{\boldsymbol{k},\lambda}\right)A_{\boldsymbol{k},\lambda}e^{i(\boldsymbol{k}\cdot\boldsymbol{r}-\omega_{\boldsymbol{k}}t)} + \text{c.c.}. \tag{2.41b}$$

2.2.2 The field as a collection of harmonic oscillators

The total energy of the classical electromagnetic field in a cubic volume $V = L^3$ is given by the Hamiltonian

$$\mathcal{H} = \int_V \left[\frac{\epsilon_0}{2} |\boldsymbol{E}(\boldsymbol{r}, t)|^2 + \frac{1}{2\mu_0} |\boldsymbol{B}(\boldsymbol{r}, t)|^2 \right] \mathrm{d}^3\boldsymbol{r}. \tag{2.42}$$

The total energy is a conserved quantity, so we set $t = 0$ and consider

$$\begin{aligned} \mathcal{H} = \int_V \Bigg[& \frac{\epsilon_0}{2} \left(\sum_{\boldsymbol{k},\lambda} i\omega_{\boldsymbol{k}} \hat{\boldsymbol{e}}_{\boldsymbol{k},\lambda} A_{\boldsymbol{k},\lambda} e^{i\boldsymbol{k}\cdot\boldsymbol{r}} + \text{c.c.} \right)^2 \\ & + \frac{1}{2\mu_0} \left(\sum_{\boldsymbol{k},\lambda} i \left(\boldsymbol{k} \times \hat{\boldsymbol{e}}_{\boldsymbol{k},\lambda} \right) A_{\boldsymbol{k},\lambda} e^{i\boldsymbol{k}\cdot\boldsymbol{r}} + \text{c.c.} \right)^2 \Bigg] \mathrm{d}^3\boldsymbol{r}. \end{aligned} \tag{2.43}$$

Noting that the wavevectors, $\boldsymbol{k}$, are orthogonal to the polarisation vectors, $\boldsymbol{e}_{\boldsymbol{k},\lambda}$, and the orthonormality of the mode functions, the total energy simplifies to

$$\mathcal{H} = 2\epsilon_0 V \sum_{\boldsymbol{k},\lambda} \omega_{\boldsymbol{k}}^2 |A_{\boldsymbol{k},\lambda}|^2. \tag{2.44}$$

The Fourier coefficients we have introduced, $A_{\boldsymbol{k},\lambda}$, are generally complex values, therefore we introduce two real variables, $X_{\boldsymbol{k},\lambda}$ and $P_{\boldsymbol{k},\lambda}$, corresponding to the generalised coordinate and conjugate momenta, respectively. We therefore rewrite the Fourier coefficients as

$$A_{\boldsymbol{k},\lambda} = \frac{1}{\sqrt{4\epsilon_0 V}} \left(X_{\boldsymbol{k},\lambda} + i\omega_{\boldsymbol{k}}^{-1} P_{\boldsymbol{k},\lambda} \right), \tag{2.45}$$

which simplifies the Hamiltonian for the electromagnetic field to an infinite set of harmonic oscillators:

$$\mathcal{H} = \sum_{\boldsymbol{k},\lambda} \frac{1}{2} \left(\omega_{\boldsymbol{k}} X_{\boldsymbol{k},\lambda}^2 + P_{\boldsymbol{k},\lambda}^2 \right). \tag{2.46}$$

We make the final step of quantisation by converting the generalised coordinates and conjugate momenta into quantum mechanical operators,

$$X_{\boldsymbol{k},\lambda} \longrightarrow x_{\boldsymbol{k},\lambda}, \quad P_{\boldsymbol{k},\lambda} \longrightarrow p_{\boldsymbol{k},\lambda}, \tag{2.47}$$

with the canonical commutation relation

$$[x_{\boldsymbol{k},\lambda}, p_{\boldsymbol{k}',\lambda'}] = i\hbar\delta_{\boldsymbol{k},\boldsymbol{k}'}\delta_{\lambda,\lambda'}. \tag{2.48}$$

We now introduce the mode annihilation and creation operators,

$$r_{\boldsymbol{k},\lambda} = \frac{1}{\sqrt{2\hbar\omega_{\boldsymbol{k}}}} \left(\omega_{\boldsymbol{k}} x_{\boldsymbol{k},\lambda} + i p_{\boldsymbol{k},\lambda} \right), \tag{2.49a}$$

$$r_{\boldsymbol{k},\lambda}^\dagger = \frac{1}{\sqrt{2\hbar\omega_{\boldsymbol{k}}}} \left(\omega_{\boldsymbol{k}} x_{\boldsymbol{k},\lambda} - i p_{\boldsymbol{k},\lambda} \right), \tag{2.49b}$$

which, from Eq. (2.48), obey the *boson commutation relations*:

$$[r_{\boldsymbol{k},\lambda}, r^\dagger_{\boldsymbol{k}',\lambda'}] = \delta_{\boldsymbol{k},\boldsymbol{k}'}\delta_{\lambda,\lambda'}, \tag{2.50a}$$

$$[r_{\boldsymbol{k},\lambda}, r_{\boldsymbol{k}',\lambda'}] = [r^\dagger_{\boldsymbol{k},\lambda}, r^\dagger_{\boldsymbol{k}',\lambda'}] = 0. \tag{2.50b}$$

Thus, the Hamiltonian for the quantised electromagnetic field is finally cast in the form

$$H = \sum_{\boldsymbol{k},\lambda} \hbar\omega_{\boldsymbol{k}} \left(r^\dagger_{\boldsymbol{k},\lambda} r_{\boldsymbol{k},\lambda} + \frac{1}{2} \right). \tag{2.51}$$

We find the time dependent expression of the annihilation operator by solving the Heisenberg equation of motion, Eq. (2.25),

$$\frac{\mathrm{d}}{\mathrm{d}t} r_{\boldsymbol{k},\lambda} = \frac{1}{i\hbar}[r_{\boldsymbol{k},\lambda}, H] = -i\omega_{\boldsymbol{k}} r_{\boldsymbol{k},\lambda}, \tag{2.52}$$

which has solution

$$r_{\boldsymbol{k},\lambda}(t) = e^{-i\omega_{\boldsymbol{k}} t} r_{\boldsymbol{k},\lambda}(0). \tag{2.53}$$

Finally, we substitute this into Eqs. (2.41) to write the electric and magnetic fields as operators:

$$\boldsymbol{E}(\boldsymbol{r},t) = i\sum_{\boldsymbol{k},\lambda} \sqrt{\frac{\hbar\omega_{\boldsymbol{k}}}{2\epsilon_0 V}} \left[\hat{\boldsymbol{e}}_{\boldsymbol{k},\lambda} r_{\boldsymbol{k},\lambda} e^{i(\boldsymbol{k}\cdot\boldsymbol{r} - \omega_{\boldsymbol{k}} t)} - \text{H.c.} \right], \tag{2.54a}$$

$$\boldsymbol{B}(\boldsymbol{r},t) = i\sum_{\boldsymbol{k},\lambda} \sqrt{\frac{\hbar}{2\epsilon_0 \omega_{\boldsymbol{k}} V}} \left[(\boldsymbol{k} \times \hat{\boldsymbol{e}}_{\boldsymbol{k},\lambda})\, r_{\boldsymbol{k},\lambda} e^{i(\boldsymbol{k}\cdot\boldsymbol{r} - \omega_{\boldsymbol{k}} t)} - \text{H.c.} \right]. \tag{2.54b}$$

It is often useful to decompose the electric field operator into positive and negative frequency contributions:

$$\boldsymbol{E}(\boldsymbol{r},t) = \boldsymbol{E}^{(+)}(\boldsymbol{r},t) + \boldsymbol{E}^{(-)}(\boldsymbol{r},t), \tag{2.55}$$

with

$$\boldsymbol{E}^{(+)}(\boldsymbol{r},t) = i\sum_{\boldsymbol{k},\lambda} \sqrt{\frac{\hbar\omega_{\boldsymbol{k}}}{2\epsilon_0 V}} \hat{\boldsymbol{e}}_{\boldsymbol{k},\lambda} r_{\boldsymbol{k},\lambda}(t) e^{i\boldsymbol{k}\cdot\boldsymbol{r}}, \tag{2.56a}$$

$$\boldsymbol{E}^{(-)}(\boldsymbol{r},t) = \left(\boldsymbol{E}^{(+)}(\boldsymbol{r},t) \right)^\dagger. \tag{2.56b}$$

2.2.3 Harmonic oscillator eigenstates

We now consider only a single wave-vector and polarisation of the quantised electromagnetic field. The Hamiltonian,

$$H = \hbar\omega_{\boldsymbol{k}} \left(r^\dagger_{\boldsymbol{k}} r_{\boldsymbol{k}} + \frac{1}{2} \right), \tag{2.57}$$

has discrete eigenvalues:

$$H\,|E_{n_{\boldsymbol{k}}}\rangle = E_{n_{\boldsymbol{k}}}\,|E_{n_{\boldsymbol{k}}}\rangle\,. \tag{2.58}$$

Using the boson commutation relation, Eq. (2.50), we find that the states $r_{\boldsymbol{k}} |n_{\boldsymbol{k}}\rangle$ and $r_{\boldsymbol{k}}^\dagger |n_{\boldsymbol{k}}\rangle$ are also eigenstates of the Hamiltonian, with eigenvalue equations

$$H r_{\boldsymbol{k}} |E_{n_{\boldsymbol{k}}}\rangle = (E_{n_{\boldsymbol{k}}} - \hbar\omega_{\boldsymbol{k}})\, r_{\boldsymbol{k}} |E_{n_{\boldsymbol{k}}}\rangle\,, \tag{2.59a}$$

$$H r_{\boldsymbol{k}}^\dagger |E_{n_{\boldsymbol{k}}}\rangle = (E_{n_{\boldsymbol{k}}} + \hbar\omega_{\boldsymbol{k}})\, r_{\boldsymbol{k}}^\dagger |E_{n_{\boldsymbol{k}}}\rangle\,. \tag{2.59b}$$

From the two eigenvalue equations we see that the annihilation and creation operators act on a ladder of states, with a set ground state $|E_{n_{\boldsymbol{k}}=0}\rangle$. The ground state energy is fixed by noting that $r_{\boldsymbol{k}} |E_{n_{\boldsymbol{k}}=0}\rangle$ cannot be accepted as an energy eigenstate of the Hamiltonian as its energy would be negative. Equation (2.59a) can only be satisfied by

$$r_{\boldsymbol{k}} |E_{n_{\boldsymbol{k}}=0}\rangle = 0. \tag{2.60}$$

The eigenstate energy ladder then moves up in steps of $\hbar\omega_{\boldsymbol{k}}$,

$$H |n_{\boldsymbol{k}}\rangle = \hbar\omega_{\boldsymbol{k}} \left(n_{\boldsymbol{k}} + \frac{1}{2}\right) |n_{\boldsymbol{k}}\rangle\,, \tag{2.61}$$

where $|n_{\boldsymbol{k}}\rangle$, $n_{\boldsymbol{k}} = 0, 1, 2, \ldots$, is a complete,

$$\sum_{n_{\boldsymbol{k}}=0}^{\infty} |n_{\boldsymbol{k}}\rangle \langle n_{\boldsymbol{k}}| = \mathbb{1}_{\boldsymbol{k}}, \tag{2.62}$$

and orthogonal,

$$\langle n_{\boldsymbol{k}} | m_{\boldsymbol{k}}\rangle = \delta_{n_{\boldsymbol{k}}, m_{\boldsymbol{k}}}, \tag{2.63}$$

set of basis states, known as the *photon number* or *Fock* states; they are eigenstates of the photon number operator:

$$r_{\boldsymbol{k}}^\dagger r_{\boldsymbol{k}} |n_{\boldsymbol{k}}\rangle = n_{\boldsymbol{k}} |n_{\boldsymbol{k}}\rangle\,. \tag{2.64}$$

From Eqs. (2.59) we can see that the annihilation and creation operators have the actions

$$r_{\boldsymbol{k}} |n_{\boldsymbol{k}}\rangle = \beta_1 |n_{\boldsymbol{k}} - 1\rangle\,, \tag{2.65a}$$

$$r_{\boldsymbol{k}}^\dagger |n_{\boldsymbol{k}}\rangle = \beta_2 |n_{\boldsymbol{k}} + 1\rangle\,, \tag{2.65b}$$

where β_1 and β_2 are normalisation constants. To find these normalisation constants we use the definition of the number operator, Eq. (2.64):

$$n_{\boldsymbol{k}} = n_{\boldsymbol{k}} \langle n_{\boldsymbol{k}} | n_{\boldsymbol{k}}\rangle = \langle n_{\boldsymbol{k}} | r_{\boldsymbol{k}}^\dagger r_{\boldsymbol{k}} | n_{\boldsymbol{k}}\rangle = \beta_1^* \beta_1 \langle n_{\boldsymbol{k}} - 1 | n_{\boldsymbol{k}} - 1\rangle = |\beta_1|^2, \tag{2.66a}$$

and

$$n_{\boldsymbol{k}} + 1 = (n_{\boldsymbol{k}} + 1) \langle n_{\boldsymbol{k}} | n_{\boldsymbol{k}}\rangle = \langle n_{\boldsymbol{k}} | r_{\boldsymbol{k}} r_{\boldsymbol{k}}^\dagger | n_{\boldsymbol{k}}\rangle = \beta_2^* \beta_2 \langle n_{\boldsymbol{k}} + 1 | n_{\boldsymbol{k}} + 1\rangle = |\beta_2|^2. \tag{2.66b}$$

We see then that $r_{\boldsymbol{k}}$ and $r_{\boldsymbol{k}}^\dagger$ act as raising and lowering operators for the *ladder* of harmonic oscillation eigenstates:

$$r_{\boldsymbol{k}} \left|n_{\boldsymbol{k}}\right\rangle = \sqrt{n_{\boldsymbol{k}}} \left|n_{\boldsymbol{k}} - 1\right\rangle, \tag{2.67a}$$

$$r_{\boldsymbol{k}}^\dagger \left|n_{\boldsymbol{k}}\right\rangle = \sqrt{n_{\boldsymbol{k}} + 1} \left|n_{\boldsymbol{k}} + 1\right\rangle. \tag{2.67b}$$

2.2.4 Coherent states

Fock states and their superpositions are useful states for fields with small photon numbers, but they are not so useful for high photon numbers such as can be found in a laser field. A state that is better suited for high intensity coherent fields is the *coherent state*, as first discussed in this context in 1963 by Roy Glauber [7, 74]. Typically denoted by $|\alpha_{\boldsymbol{k}}\rangle$ with *coherent amplitude* $\alpha_{\boldsymbol{k}} \in \mathbb{C}$, the coherent state is an eigenstate of the annihilation operator,

$$r_{\boldsymbol{k}} \left|\alpha_{\boldsymbol{k}}\right\rangle = \alpha_{\boldsymbol{k}} \left|\alpha_{\boldsymbol{k}}\right\rangle, \tag{2.68}$$

and has the expansion in Fock states

$$\left|\alpha_{\boldsymbol{k}}\right\rangle = e^{-\frac{1}{2}|\alpha_{\boldsymbol{k}}|^2} \sum_{n_{\boldsymbol{k}}=0}^{\infty} \frac{\alpha_{\boldsymbol{k}}^{n_{\boldsymbol{k}}}}{\sqrt{n_{\boldsymbol{k}}!}} \left|n_{\boldsymbol{k}}\right\rangle. \tag{2.69}$$

Coherent states can also be generated from the vacuum state, $|0\rangle$, by the operation of the *displacement operator* (see Ref. [73], Section 2.3):

$$\left|\alpha_{\boldsymbol{k}}\right\rangle = \mathcal{D}(\alpha_{\boldsymbol{k}}) \left|0\right\rangle, \quad \mathcal{D}(\alpha_{\boldsymbol{k}}) = e^{\alpha_{\boldsymbol{k}} r_{\boldsymbol{k}}^\dagger - \alpha_{\boldsymbol{k}}^* r_{\boldsymbol{k}}}. \tag{2.70}$$

Coherent states are not orthogonal, having the overlap

$$\left\langle\beta_{\boldsymbol{k}}|\alpha_{\boldsymbol{k}}\right\rangle = e^{-\frac{1}{2}\left(|\alpha_{\boldsymbol{k}}|^2 + |\beta_{\boldsymbol{k}}|^2 - 2\alpha_{\boldsymbol{k}}\beta_{\boldsymbol{k}}^*\right)}, \tag{2.71}$$

but they do satisfy the closure relation

$$\frac{1}{\pi} \int \left|\alpha_{\boldsymbol{k}}\right\rangle \left\langle\alpha_{\boldsymbol{k}}\right| \mathrm{d}^2\alpha_{\boldsymbol{k}} = \mathbb{1}_{\boldsymbol{k}}, \tag{2.72}$$

and are therefore overcomplete.

3 Quantum Open Systems

In the previous chapter it was mentioned that quantum systems, when not observed, evolve freely under the time-dependent Schrödinger equation, although this is only true for completely isolated physical systems. *Closed* quantum systems – that is, systems that do not experience energy gain or loss – are not physically realisable in a realistic experimental setting as some form of energy loss will be always present, even though the loss rate might be very small. Also, we are typically interested in a *driven* quantum system where energy is being pumped into an open system, which in turn serves as the source of an output field that is ultimately directed into a filter cavity. To this end, in this chapter we introduce the specific techniques we will use to model *open* quantum systems.

We first formulate a general *master equation* for a system coupled to an environment modelled as a reservoir with an infinite number of degrees of freedom. We then consider the explicit example of a cavity, or resonator, that supports a single mode of the electromagnetic field. The single-mode cavity will form the basis of our initial frequency filtering model. We then introduce two different methods of calculating *two-time correlation functions* from the master equation, using the *quantum regression equations*. Finally, using this frequency filtering model as inspiration, we derive a general master equation for an *open quantum cascaded system*, where one quantum system's output field is cascaded into the input of a second quantum system. We illustrate the general master equation with the explicit example of a single cavity mode driven by a cascaded coherent state source.

3.1 Lindblad Master Equation

We start by considering a system S which is coupled to a reservoir (environment) R through an interaction between the two. We aim to derive an equation of motion that gives us complete information about the evolution of the system with minimal dependence on the total system $S \otimes R$. While we begin with a general formulation for any system-reservoir coupling, we will ultimately consider a single mode of the electromagnetic field (harmonic oscillator) coupled to the full electromagnetic field, Eq. (2.51), as the reservoir.

Following the method of Carmichael (Ref. [75], Chapter 1), we give only a general formulation of the derivation.

3.1.1 Coupled system and reservoir

We consider the generic Hamiltonian

$$H = H_S + H_R + H_{SR}, \tag{3.1}$$

where H_S is the Hamiltonian describing the system, H_R is the Hamiltonian describing the reservoir, and H_{SR} is the Hamiltonian describing the interaction between the two. Introducing the density operator for the total system $S \otimes R$, χ, we define the *reduced density operator* for the system, S, by tracing over the reservoir states:

$$\rho \equiv \mathrm{tr}_R[\chi]. \tag{3.2}$$

The time evolution of the density operator in the Schrödinger picture is given by

$$\frac{\mathrm{d}}{\mathrm{d}t}\chi = \frac{1}{i\hbar}[H, \chi], \tag{3.3}$$

where H is the total Hamiltonian, Eq. (3.1). We transform the density operator into an interaction picture by defining

$$\tilde{\chi}(t) = \mathcal{U}^\dagger(t)\chi(t)\,\mathcal{U}(t), \tag{3.4}$$

with unitary transform operator

$$\mathcal{U}(t) = e^{\frac{1}{i\hbar}(H_S+H_R)t}, \tag{3.5}$$

whence, applying the transformation to Eq. (3.3) and differentiating Eq. (3.4), we obtain

$$\frac{\mathrm{d}}{\mathrm{d}t}\tilde{\chi}(t) = \frac{1}{i\hbar}[\tilde{H}_{SR}(t), \tilde{\chi}(t)], \tag{3.6}$$

where

$$\tilde{H}_{SR}(t) = \mathcal{U}^\dagger(t)H_{SR}(0)\,\mathcal{U}(t) \tag{3.7}$$

is the interaction term transformed into the interaction picture. We can now formally integrate Eq. (3.3) to find a solution,

$$\tilde{\chi}(t) = \tilde{\chi}(0) + \frac{1}{i\hbar}\int_0^t [\tilde{H}_{SR}(t'), \tilde{\chi}(t')]\mathrm{d}t', \tag{3.8}$$

which can then be substituted back into Eq. (3.3) to obtain an exact equation expanded up to second order in the interaction:

$$\frac{\mathrm{d}}{\mathrm{d}t}\tilde{\chi}(t) = \frac{1}{i\hbar}[\tilde{H}_{SR}(t), \tilde{\chi}(0)] - \frac{1}{\hbar^2}\int_0^t [\tilde{H}_{SR}(t), [\tilde{H}_{SR}(t'), \tilde{\chi}(t')]]\mathrm{d}t'. \tag{3.9}$$

3.1.2 Born and Markov approximations

Assuming that when the interaction is turned on, at $t = 0$, there are no correlations between the system and reservoir, the initial density operator factorises as

$$\tilde{\chi}(0) = \chi(0) = \rho(0)R_0, \tag{3.10}$$

where R_0 is the initial density operator for the reservoir. We now take the trace of Eq. (3.9) over the reservoir states to obtain the *master equation*

$$\frac{\mathrm{d}}{\mathrm{d}t}\tilde{\rho}(t) = -\frac{1}{\hbar^2}\int_0^t \mathrm{tr}_R\left\{[\tilde{H}_{SR}(t),[\tilde{H}_{SR}(t'),\tilde{\chi}(t')]]\right\}\mathrm{d}t', \tag{3.11}$$

where we have assumed that the coupling between S and R has zero mean in the initial reservoir state R_0; this allows us to neglect the first commutator in Eq. (3.9):

$$\mathrm{tr}_R\left[\tilde{H}_{SR}(t)R_0\right] = 0. \tag{3.12}$$

As the coupling between the system and the reservoir is weak, we also assume that the density operator can be factorised at any time up to corrections of order H_{SR}. We therefore expand the density operator in powers of the coupling,

$$\tilde{\chi}(t) = \tilde{\rho}(t)R_0 + \mathcal{O}\left(H_{SR}\right), \tag{3.13}$$

and make the *Born approximation* by neglecting all but the first term on the right-hand side of Eq. (3.13):

$$\frac{\mathrm{d}}{\mathrm{d}t}\tilde{\rho}(t) = -\frac{1}{\hbar^2}\int_0^t \mathrm{tr}_R\left\{[\tilde{H}_{SR}(t),[\tilde{H}_{SR}(t'),\tilde{\rho}(t')R_0]]\right\}\mathrm{d}t'. \tag{3.14}$$

The resulting equation of motion still depends, however, on the past behaviour of the system through the integration over $\tilde{\rho}(t')$. Assuming that the reservoir is large compared to the system, changes in the reservoir due to its interaction with the system are expected to dissipate quickly at the location of the system-reservoir coupling . There exists, then, two different time scales: a rapid time scale of decaying reservoir correlations, and a slower time scale governing the evolution of the system. Thus, we make the *Markov approximation* and neglect any effect of the system's past behaviour on its future evolution, allowing us to replace $\tilde{\rho}(t')$ with $\tilde{\rho}(t)$; thus we obtain the *master equation in the Born-Markov approximation*:

$$\frac{\mathrm{d}}{\mathrm{d}t}\tilde{\rho}(t) = -\frac{1}{\hbar^2}\int_0^t \mathrm{tr}_R\left\{[\tilde{H}_{SR}(t),[\tilde{H}_{SR}(t'),\tilde{\rho}(t)R_0]]\right\}\mathrm{d}t'. \tag{3.15}$$

3.1.3 Damped electromagnetic field mode

We now move to an explicit model where the system S is a single electromagnetic field mode (harmonic oscillator) modelled as a ring cavity, as depicted in Fig. 3.1, with frequency ω_0 and ground state energy set to zero. The field mode is coupled to a many-mode electromagnetic field (reservoir) expanded in one dimension, with frequencies ω_j and photon annihilation operators r_j. The Hamiltonians for the system, reservoir, and interaction are:

$$H_S = \hbar\omega_0 a^\dagger a, \tag{3.16a}$$

$$H_R = \sum_j \hbar\omega_j r_j^\dagger r_j, \tag{3.16b}$$

$$H_{SR} = \sum_j \hbar\left(g_j^* a r_j^\dagger + g_j a^\dagger r_j\right) = \hbar\left(a\Gamma^\dagger + a^\dagger\Gamma\right), \tag{3.16c}$$

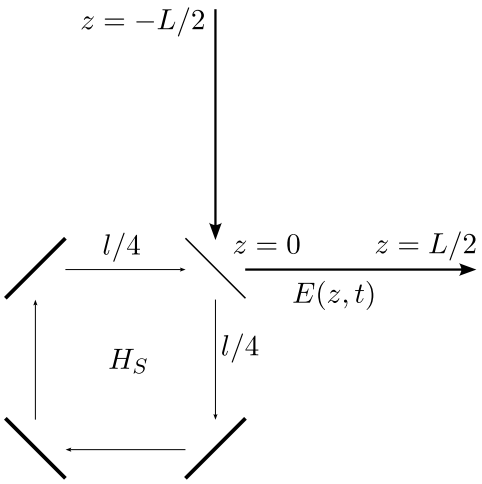

Figure 3.1: Schematic of a ring cavity coupled to a reservoir comprising a free vacuum electromagnetic field expanded in one dimension with quantisation length L. The total cavity round-trip length is l. The cavity has three perfectly reflecting mirrors (bold lines) and one mirror with transmission coefficient $T \ll 1$ (light line).

where g_j is the coupling between the system and the j^{th} reservoir mode.

In one dimension, the ring cavity of round-trip length l has modes separated by the free spectral range $2\pi c/l$. Taking the continuum limit $L \to \infty$, the mode frequencies of the reservoir field are much closer together and described by the one-dimensional mode density

$$\varrho(\omega) = \frac{L}{2\pi c}, \tag{3.17}$$

where $\varrho(\omega)\mathrm{d}\omega$ is the number of modes with frequencies in the interval ω to $\omega + \mathrm{d}\omega$. From Fermi's Golden Rule, we can relate the spectral width of the cavity mode, 2κ, to the mode density and coupling constants according to the standard result for the energy (photon) decay rate [70]:

$$2\kappa = 2\pi\varrho(\omega_0)|g_{\omega_j=\omega_0}|^2. \tag{3.18}$$

From Eq. (3.17) we see that the mode density is independent of frequency, and we therefore approximate the coupling constants to also be frequency independent. Rearranging Eq. (3.18), we then arrive at

$$g_j = \sqrt{2\kappa}\sqrt{\frac{c}{L}}. \tag{3.19}$$

With the coupling constants now established, the explicit form of the master equation in the Born-Markov approximation, from Eq. (3.15), is then

$$\begin{aligned}\frac{\mathrm{d}}{\mathrm{d}t}\tilde{\rho}(t) = \int_0^t \Big\{ &\left[a\tilde{\rho}(t)a - aa\tilde{\rho}(t)\right] e^{-i\omega_0(t+t')}\langle\tilde{\Gamma}^\dagger(t)\tilde{\Gamma}^\dagger(t')\rangle_R + \text{H.c.} \\ &+ \left[a^\dagger\tilde{\rho}(t)a^\dagger - a^\dagger a^\dagger\tilde{\rho}(t)\right] e^{i\omega_0(t+t')}\langle\tilde{\Gamma}(t)\tilde{\Gamma}(t')\rangle_R + \text{H.c.} \\ &+ \left[a\tilde{\rho}(t)a^\dagger - a^\dagger a\tilde{\rho}(t)\right] e^{i\omega_0(t-t')}\langle\tilde{\Gamma}(t)\tilde{\Gamma}^\dagger(t')\rangle_R + \text{H.c.} \\ &+ \left[a^\dagger\tilde{\rho}(t)a - aa^\dagger\tilde{\rho}(t)\right] e^{-i\omega_0(t-t')}\langle\tilde{\Gamma}^\dagger(t)\tilde{\Gamma}(t')\rangle_R + \text{H.c.}\Big\}\,\mathrm{d}t',\end{aligned} \tag{3.20}$$

where, introducing the system and reservoir operators in the interaction picture,

$$\tilde{a}(t) = \mathcal{U}^\dagger(t)a(0)\mathcal{U}(t) = e^{-i\omega_0 t}a, \tag{3.21a}$$

$$\tilde{a}^\dagger(t) = \mathcal{U}^\dagger(t)a^\dagger(0)\mathcal{U}(t) = e^{i\omega_0 t}a, \tag{3.21b}$$

$$\tilde{\Gamma}(t) = \mathcal{U}^\dagger(t)\Gamma(0)\mathcal{U}(t) = \sqrt{2\kappa}\sqrt{\frac{c}{L}}\sum_j e^{-i\omega_j t}r_j, \tag{3.21c}$$

$$\tilde{\Gamma}^\dagger(t) = \mathcal{U}^\dagger(t)\Gamma^\dagger(0)\mathcal{U}(t) = \sqrt{2\kappa}\sqrt{\frac{c}{L}}\sum_j e^{i\omega_j t}r_j^\dagger. \tag{3.21d}$$

The reservoir correlation functions are evaluated with respect to the initial density operator of the reservoir, R_0. For simplicity's sake we assume the reservoir is in the vacuum state and hence the explicit correlation functions are:

$$\begin{aligned}\langle\tilde{\Gamma}(t)\tilde{\Gamma}(t')\rangle_R &= \frac{2\kappa c}{L}\sum_{j,j'} e^{-i\omega_j t}e^{-i\omega_{j'}t'}\mathrm{tr}_R\left[R_0 r_j r_{j'}\right] \\ &= 0,\end{aligned} \tag{3.22a}$$

$$\begin{aligned}\langle\tilde{\Gamma}^\dagger(t)\tilde{\Gamma}^\dagger(t')\rangle_R &= \frac{2\kappa c}{L}\sum_{j,j'} e^{i\omega_j t}e^{i\omega_{j'}t'}\mathrm{tr}_R\left[R_0 r_j^\dagger r_{j'}^\dagger\right] \\ &= 0,\end{aligned} \tag{3.22b}$$

$$\begin{aligned}\langle\tilde{\Gamma}^\dagger(t)\tilde{\Gamma}(t')\rangle_R &= \frac{2\kappa c}{L}\sum_{j,j'} e^{i\omega_j t}e^{-i\omega_{j'}t'}\mathrm{tr}_R\left[R_0 r_j^\dagger r_{j'}\right] \\ &= 0,\end{aligned} \tag{3.22c}$$

and

$$\begin{aligned}\langle\tilde{\Gamma}(t)\tilde{\Gamma}^\dagger(t')\rangle_R &= \frac{2\kappa c}{L}\sum_{j,j'} e^{-i\omega_j t}e^{i\omega_{j'}t'}\mathrm{tr}_R\left[R_0 r_j r_{j'}^\dagger\right] \\ &= \frac{2\kappa c}{L}\sum_j e^{-i\omega_j(t-t')}.\end{aligned} \tag{3.22d}$$

The master equation then reduces to the form

$$\begin{aligned}\frac{\mathrm{d}}{\mathrm{d}t}\tilde{\rho}(t) = \int_0^t \Big\{&\left[a\tilde{\rho}(t)a^\dagger - a^\dagger a\tilde{\rho}(t)\right]e^{i\omega_0(t-t')}\langle\tilde{\Gamma}(t)\tilde{\Gamma}^\dagger(t')\rangle_R \\ &+ \left[a\tilde{\rho}(t)a^\dagger - \tilde{\rho}(t)a^\dagger a\right]e^{-i\omega_0(t-t')}\langle\tilde{\Gamma}(t')\tilde{\Gamma}^\dagger(t)\rangle_R\Big\}\,\mathrm{d}t',\end{aligned} \tag{3.23}$$

where, introducing the density of modes, Eq. (3.17), and noting that the coupling constant is effectively zero as $\omega \to 0$, we extend the integral limits to $-\infty$ and evaluate the correlation function as

$$\begin{aligned}\langle\tilde{\Gamma}(t)\tilde{\Gamma}^\dagger(t')\rangle_R &= \int_{-\infty}^{\infty}\frac{L}{2\pi c}\frac{2\kappa c}{L}e^{-i\omega(t-t')}\mathrm{d}\omega \\ &= 2\kappa\delta\left(t-t'\right).\end{aligned} \tag{3.24}$$

Substituting this into Eq. (3.23) and computing the integral in the time domain we arrive at the master equation in the interaction picture:

$$\frac{\mathrm{d}}{\mathrm{d}t}\tilde{\rho}(t) = \kappa\left(2a\tilde{\rho}(t)a^\dagger - a^\dagger a\tilde{\rho}(t) - \tilde{\rho}(t)a^\dagger a\right) \tag{3.25}$$

Finally, we transform back into the Schrödinger picture to arrive at the *master equation for a damped electromagnetic field mode*:

$$\frac{\mathrm{d}}{\mathrm{d}t}\rho = \frac{1}{i\hbar}[H_S, \rho] + \kappa\left(2a\rho a^\dagger - a^\dagger a\rho - \rho a^\dagger a\right). \tag{3.26}$$

3.1.4 Free and scattered fields

Where the master equation focuses on the dynamics of the system, in this case an electromagnetic field mode, we make direct measurements on the output electromagnetic field. To consider this, we turn to the Heisenberg picture and expand the electric field, Eqs. (2.55) and (2.56), in terms of the reservoir operators. From the Hamiltonians, Eqs. (3.1) and (3.16), we have the coupled equations for the reservoir and cavity mode annihilation operators:

$$\frac{\mathrm{d}}{\mathrm{d}t}a = -i\omega_0 a - i\sum_j g_j r_j, \tag{3.27a}$$

$$\frac{\mathrm{d}}{\mathrm{d}t}r_j = -i\omega_j r_j - ig_j^* a. \tag{3.27b}$$

Then after introducing the slowly varying operators

$$\tilde{a}(t) = ae^{i\omega_0 t}, \quad \tilde{r}_j(t) = r_j e^{i\omega_j t}, \tag{3.28}$$

we formally integrate Eq. (3.27b) to obtain

$$\tilde{r}_j(t) = r_j(0) - ig_j^* e^{i(\omega_j-\omega_0)t}\int_0^t \tilde{a}(t')e^{-i(\omega_j-\omega_0)(t-t')}\mathrm{d}t'. \tag{3.29}$$

We substitute this into the expansion for the electric field operator, Eq. (2.56) in one dimension, which yields

$$\begin{aligned}\hat{\boldsymbol{e}}_0 \cdot \boldsymbol{E}^{(+)}(z,t) = i\sum_j \sqrt{\frac{\hbar\omega_j}{2\epsilon_0 AL}} r_j(0)e^{-i\omega_j(t-z/c)} \\ + e^{-i\omega_0(t-z/c)}\sum_j \sqrt{\frac{\hbar\omega_0}{2\epsilon_0 AL}} g_j^* \int_0^t \tilde{a}(t')e^{-i(\omega_j-\omega_0)(t-t'-z/c)}\mathrm{d}t',\end{aligned} \tag{3.30}$$

where, following Eq. (3.24), we treat the summation over modes as an integral over frequencies, and hence obtain for the second term

$$e^{-i\omega_0(t-z/c)}\int_0^t \tilde{a}(t')\delta\left(t - z/c - t'\right)\mathrm{d}t' = \begin{cases} 0 & \text{if } z < 0 \\ \frac{1}{2}\sqrt{2\kappa}a(t) & \text{if } z = 0 \\ \sqrt{2\kappa}a(t - z/c) & \text{if } 0 < z < ct \end{cases}. \tag{3.31}$$

The electric field, Eq. (3.30), can then be decomposed into two parts,

$$E^{(+)}(z,t) = E^{(+)}_{\text{free}}(z,t) + E^{(+)}_{\text{source}}(z,t), \tag{3.32}$$

where

$$E^{(+)}_{\text{free}}(z,t) = i\sum_j \sqrt{\frac{\hbar\omega_j}{2\epsilon_0 AL}} r_j(0) e^{-i\omega_j(t-z/c)} \tag{3.33}$$

accounts for the freely evolving field, in the absence of the field mode, and

$$E^{(+)}_{\text{source}}(z,t) = \sqrt{\frac{\hbar\omega_0}{2\epsilon Ac}} \times \begin{cases} 0 & \text{if } z < 0 \\ \frac{1}{2}\sqrt{2\kappa}a(t) & \text{if } z = 0 \\ \sqrt{2\kappa}a(t - z/c) & \text{if } 0 < z < ct \end{cases}, \tag{3.34}$$

describes the source field radiated by the cavity mode.

3.2 Two-Time Correlation Functions

The focus of this thesis is frequency-filtered photon correlations from a source system. To this end we must first understand how to calculate unfiltered two-time correlation functions. The two correlation functions discussed in this thesis are the *first- and second-order correlation functions*. The first-order correlation function,

$$G^{(1)}(t,\tau) = \langle E^{(-)}(t) E^{(+)}(t+\tau)\rangle, \tag{3.35}$$

correlates the electric field at two different times, t and $t+\tau$; in the case of a stationary field (correlation function independent of t) its Fourier transform gives the optical spectrum (see, e.g., Ref. [73], Section 3.3). In contrast, the second-order correlation function,

$$G^{(2)}(t,\tau) = \langle E^{(-)}(t) E^{(-)}(t+\tau) E^{(+)}(t+\tau) E^{(+)}(\tau)\rangle, \tag{3.36}$$

quantifies fluctuations in the intensity of the field; it is proportional to the probability of detecting two photons, a first photon at time t and a second at time $t+\tau$ [7, 8].

The master equation we have developed allows us to solve for the density operator of a system interacting with a reservoir as a function of time; thus, it allows us to compute one-time operator averages with Eq. (2.22). What it cannot directly provide, however, are multi-time averages, which our focus on filtered photon correlations relies on. We now discuss how the master equation can be used to compute these averages.

3.2.1 Quantum regression equations

Equations (3.35) and (3.36) yield more complex expressions when the decomposition of the electric field, Eq. (3.32), is considered. Fortunately, however, thermal effects are mostly negligible at optical frequencies. We may therefore take the free field to be in the vacuum state. In this case, the normal and time ordered free field operators drop out, leaving the correlation

functions expressed solely in terms of source operators. In order to calculate these averages, we utilise the *quantum regression equations*. While this work is attributed to Lax (see Refs. [63, 64]), in this section we follow the steps of Carmichael (Ref. [75], Section 1.5).

In view of what follows, it is convenient to recast the master equation Eq. (3.26) in the formal form

$$\frac{\mathrm{d}\rho}{\mathrm{d}t} = \mathcal{L}\rho, \tag{3.37}$$

where $\mathcal{L}$ is the Liouvillian *superoperator*

$$\mathcal{L}\bullet = \frac{1}{i\hbar}[H, \bullet] + \kappa \left(2a \bullet a^\dagger - a^\dagger a \bullet - \bullet a^\dagger a\right). \tag{3.38}$$

Note that a superoperator acts on operators rather than on ket-vectors. Now the average of the product of two general system operators, A and B, evaluated, respectively, at times, t and $t+\tau$ with $\tau \geq 0$, is given by

$$\langle A(t)B(t+\tau)\rangle = \mathrm{tr}_{S\otimes R}\left[\chi(0)A(t)B(t+\tau)\right], \tag{3.39}$$

where the operators satisfy Heisenberg equations of motion, with formal solutions

$$A(t) = e^{-\frac{1}{i\hbar}Ht}A(0)e^{\frac{1}{i\hbar}Ht}, \quad B(t+\tau) = e^{-\frac{1}{i\hbar}H(t+\tau)}B(0)e^{-\frac{1}{i\hbar}H(t+\tau)}. \tag{3.40}$$

Substituting these solutions into Eq. (3.39) and making use of Eq. (3.4) and the cyclic property of the trace, we then obtain

$$\langle A(t)B(t+\tau)\rangle = \mathrm{tr}_S\left\{B(0)\mathrm{tr}_R\left[\mathcal{U}(\tau)\chi(t)A(0)\mathcal{U}^\dagger(\tau)\right]\right\}. \tag{3.41}$$

We now extend the derivation of the master equation to the reduced operator

$$\rho_A(\tau) \equiv \mathrm{tr}_R\left[\mathcal{U}^\dagger(\tau)\chi(t)A(0)\mathcal{U}(\tau)\right], \tag{3.42}$$

assuming that it also satisfies Eq. (3.37), with formal solution

$$\rho_A(\tau) = e^{\mathcal{L}\tau}\left[\rho_A(0)\right] = e^{\mathcal{L}\tau}\left[\rho(t)A(0)\right]. \tag{3.43}$$

Substituting this into Eq. (3.41) we arrive at the two-time correlation function

$$\langle A(t)B(t+\tau)\rangle = \mathrm{tr}_S\left[B(0)e^{\mathcal{L}\tau}\left(\rho(t)A(0)\right)\right]. \tag{3.44}$$

For the second-order correlation function, Eq. (3.36), a similar derivation yields (see Ref. [75], p. 22 for details)

$$\langle A(t)B(\tau)C(t)\rangle = \mathrm{tr}_S\left[B(0)e^{\mathcal{L}\tau}\left(C(0)\rho(t)A(0)\right)\right]. \tag{3.45}$$

3.2.2 Quantum regression equations for a complete set of operators

Rather than working with these formal expressions, we can reduce Eqs. (3.44) and (3.45) to a more familiar and convenient form for making calculations. Specifically, we consider a set of

system operators, $B_1, B_2, \ldots$, whose expectation values obey a set of coupled linear equations with evolution matrix $\boldsymbol{M}$:

$$\frac{\mathrm{d}}{\mathrm{d}t}\langle \boldsymbol{B}\rangle = \boldsymbol{M}\langle \boldsymbol{B}\rangle, \quad \langle \boldsymbol{B}\rangle = \begin{pmatrix} \langle B_1\rangle \\ \langle B_2\rangle \\ \vdots \\ \langle B_n\rangle \end{pmatrix}. \tag{3.46}$$

Following on from Eqs. (3.44) and (3.45) (see Refs. [75], Section 1.5.2 and [63] for details), we find that the two-time correlation functions, $\langle A(t)\boldsymbol{B}(t+\tau)\rangle$ and $\langle A(t)\boldsymbol{B}(t+\tau)C(t)\rangle$, obey the same coupled set of linear equations:

$$\frac{\mathrm{d}}{\mathrm{d}\tau}\langle A(t)\boldsymbol{B}(t+\tau)\rangle = \boldsymbol{M}\langle A(t)\boldsymbol{B}(t+\tau)\rangle, \tag{3.47a}$$

$$\frac{\mathrm{d}}{\mathrm{d}\tau}\langle A(t)\boldsymbol{B}(t+\tau)C(t)\rangle = \boldsymbol{M}\langle A(t)\boldsymbol{B}(t+\tau)C(t)\rangle. \tag{3.47b}$$

3.3 Cascaded Open Quantum Systems

In the previous section we have derived a master equation for a single system S coupled to a reservoir, or environment, R. In this section we aim to take this derivation a step further, by considering a composite model consisting of a source subsystem, whose output is coupled to a target subsystem. While there are many approaches to this problem [60, 76], here we follow the approach of Carmichael (Refs. [59] and [77], Section 19.2).

3.3.1 System-reservoir interaction Hamiltonian

While we can derive this master equation for two general subsystems, we will model the source and target subsystems as two separate ring cavities, as depicted in Fig. (3.2), with Hamiltonians

$$H_{\text{source}} = \hbar\omega_s s^\dagger s, \tag{3.48a}$$

$$H_{\text{target}} = \hbar\omega_a a^\dagger a, \tag{3.48b}$$

where s ($s^\dagger$) and a ($a^\dagger$) are the respective annihilation (creation) operators for the source and target modes. As before, we take the reservoir field to be a collection of harmonic oscillator modes, so the total Hamiltonian, following Eq. (3.1), consists of

$$H_S = H_{\text{source}} + H_{\text{target}}, \tag{3.49a}$$

$$H_R = \sum_j \hbar\omega_j r_j^\dagger r_j, \tag{3.49b}$$

$$H_{SR} = H_{SR}^{\text{source}} + H_{SR}^{\text{target}}, \tag{3.49c}$$

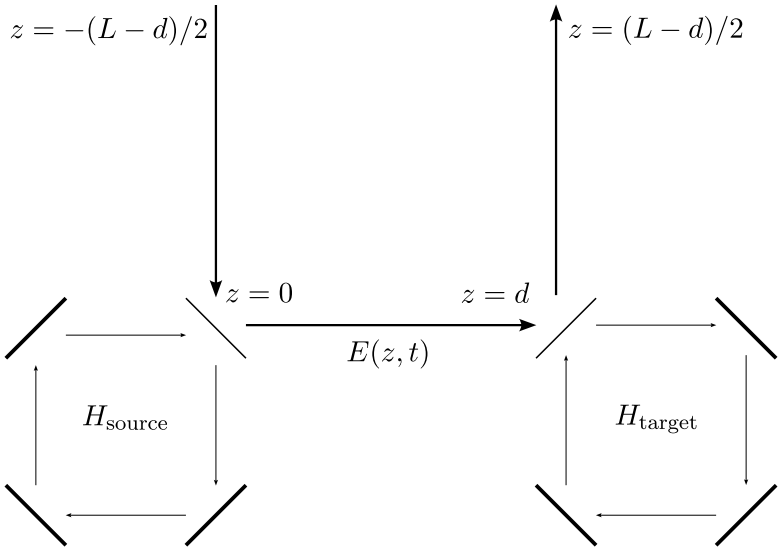

Figure 3.2: Schematic of a cascaded system with the output of a source subsystem, H_{source}, coupled as the input of a target subsystem, H_{target}. The quantisation length of the field is L and the input mirrors of the two subsystems are a distance d apart. As in Fig. 3.1, each cavity has three perfectly reflecting mirrors (bold lines) and one mirror with transmission coefficient $T \ll 1$ (light line).

where

$$H_{SR}^{\text{source}} = \sum_j \hbar \left(g_{s,j}^* s r^\dagger + g_{s,j} s^\dagger r \right), \tag{3.50a}$$

$$H_{SR}^{\text{target}} = \sum_j \hbar \left(g_{a,j}^* a r^\dagger e^{-i\omega_j d/c} + g_{a,j} a^\dagger r e^{i\omega_j d/c} \right). \tag{3.50b}$$

are the interaction terms that account for transmission and reflection of the reservoir field at $z = 0$ and $z = d$. Following from Eq. (3.19), the reservoir coupling coefficients for the two subsystems are:

$$g_{s,j} = \sqrt{2\kappa_s}\sqrt{\frac{c}{L}}, \tag{3.51a}$$

$$g_{a,j} = \sqrt{2\kappa_a}\sqrt{\frac{c}{L}}, \tag{3.51b}$$

where $2\kappa_s$ and $2\kappa_a$ are the spectral widths of the source mode and target mode, respectively. The output field of the source subsystem is carried to the target via the one-dimensional reservoir field where, making the same decomposition as in Eq. (2.55),

$$\hat{\boldsymbol{e}}_0 \cdot \boldsymbol{E}^{(+)}(z,t) = i \sum_j \sqrt{\frac{\hbar\omega_j}{2\epsilon_0 A L}} r_j(t) e^{i(\omega_j z/c + \phi(z))}, \tag{3.52}$$

where

$$\phi(z) \equiv \begin{cases} 0 & \text{if } z \leq 0 \\ \phi_R^{\text{source}} & \text{if } 0 < z \leq d \\ \phi_R^{\text{source}} + \phi_R^{\text{target}} & \text{if } d < z \end{cases}, \tag{3.53}$$

with phase changes upon reflection from the source mirror at $z = 0$, ϕ_R^{source}, and from the target mirror at $z = d$, ϕ_R^{target}. Expressing the reservoir field in units of the photon flux, with

$$\mathcal{E}(z,t) \equiv \sum_j \sqrt{\frac{\omega_j}{\frac{1}{2}(\omega_s + \omega_a)}} \sqrt{\frac{c}{L}} r_j(t) e^{i(\omega_j z/c + \phi(z))}, \tag{3.54}$$

and setting $\omega_j / \frac{1}{2}(\omega_s + \omega_a) \to 1$, the interaction Hamiltonians simplify to

$$H_{SR}^{\text{source}} = \hbar\sqrt{2\kappa_s} \left(s\mathcal{E}^\dagger(0,0) + s^\dagger \mathcal{E}(0,0) \right), \tag{3.55a}$$

$$H_{SR}^{\text{target}} = \hbar\sqrt{2\kappa_a} \left(a\mathcal{E}^\dagger(d,0) + a^\dagger \mathcal{E}(d,0) \right). \tag{3.55b}$$

As previously mentioned, the coupling of the source subsystem to the target is carried by the reservoir field. Following Eq. (3.32), we decompose the reservoir field into three pieces:

$$\mathcal{E}(z,t) = \mathcal{E}_{\text{free}}(z,t) + \mathcal{E}_{\text{source}}(z,t) + \mathcal{E}_{\text{target}}(z,t), \tag{3.56}$$

with free field

$$\mathcal{E}_{\text{free}}(z,t) = \sum_j \sqrt{\frac{c}{L}} r_j(0) e^{-i[\omega_j(t - z/c) - \phi(z)]}, \tag{3.57a}$$

source field

$$\mathcal{E}_{\text{source}}(z,t) = \begin{cases} 0 & z < 0 \\ -i\frac{1}{2}\sqrt{2\kappa_s}\, s(t') & z = 0 \\ -ie^{i\phi(z)}\sqrt{2\kappa_s}\, s(t') & 0 < z < ct \end{cases}, \tag{3.57b}$$

and target field

$$\mathcal{E}_{\text{target}}(z,t) = \begin{cases} 0 & z < d \\ -i\frac{1}{2}\sqrt{2\kappa_a}\, a(t'') & z = d \\ -ie^{i\phi_R^{\text{target}}}\sqrt{2\kappa_a}\, a(t'') & d < z < ct \end{cases}, \tag{3.57c}$$

with $t' = t - z/c$ and $t'' = t - (z-d)/c$.

3.3.2 The cascaded systems master equation

The source and target subsystems are coupled to the reservoir at two different locations, $z = 0$ and $z = d$. At these locations we have two different field operators, $\mathcal{E}(0,0)$ and $\mathcal{E}(d,0)$, which are correlated, so it is not permissible to treat the reservoir interactions as independent. Instead we consider the *time-retarded density operator*

$$\chi_{\text{ret}} \equiv \mathcal{U}_{\text{source}}(-d/c)\, \chi\, \mathcal{U}_{\text{source}}^\dagger(-d/c), \tag{3.58}$$

with

$$\mathcal{U}_{\text{source}}(-d/c) \equiv e^{\frac{1}{i\hbar}(H_{\text{source}}+H_R+H_{SR}^{\text{source}})(-d/c)}. \tag{3.59}$$

The field propagates freely from the source subsystem to the target, i.e., from $z = 0$ to $z = d$, and it carries photons emitted by the source. The time retardation applies only to the source subsystem and its interaction with the reservoir; it is introduced to formally undo the propagation of the source subsystem output field to the target subsystem. The Schrödinger equation now becomes

$$\frac{\mathrm{d}}{\mathrm{d}t}\chi_{\text{ret}} = \frac{1}{i\hbar}[H_{\text{ret}}, \chi_{\text{ret}}], \tag{3.60}$$

where

$$H_{\text{ret}} \equiv H_S + H_R + H_{SR}^{\text{source}} + \left(H_{SR}^{\text{target}}\right)_{\text{ret}}, \tag{3.61}$$

with

$$\left(H_{SR}^{\text{target}}\right)_{\text{ret}} \equiv \hbar\sqrt{2\kappa_a}\left(a\mathcal{E}^\dagger(d_-, d/c) + a^\dagger\mathcal{E}(d_-, d/c)\right), \tag{3.62}$$

and

$$\mathcal{E}(d_-, d/c) \equiv \mathcal{U}_{\text{source}}^\dagger(d/c)\mathcal{E}(d, 0)\mathcal{U}_{\text{source}}(d/c). \tag{3.63}$$

The field operator $\mathcal{E}(d_-, d/c)$ represents the field that arrives at the target subsystem, $z = d$, at the retarded time d/c. Note that this field is the sum of the free field, $\mathcal{E}_{\text{free}}(d, d/c)$, and the output field from the source subsystem, $\mathcal{E}_{\text{source}}(d, d/c)$ – there is no contribution from the target subsystem, i.e., no self-field term. Using the fact that the field propagates freely from the source output, we then obtain

$$\mathcal{E}(d_-, d/c) = e^{i\phi_R^{\text{source}}}\mathcal{E}(0, 0) - i\frac{1}{2}e^{i\phi_R^{\text{source}}}\sqrt{2\kappa_s}s, \tag{3.64}$$

where we have taken the definitions of the fields from Eq. (3.57). After substituting Eq. (3.64) into Eq. (3.62), the total Hamiltonian for the time-retarded system takes the form

$$H_{\text{ret}} = H_S^c + H_R + H_{SR}^c, \tag{3.65}$$

where

$$H_S^c = H_{\text{source}} + H_{\text{target}} + i\hbar\sqrt{\kappa_s\kappa_a}\left(e^{-i\phi_R^{\text{source}}}as^\dagger - e^{i\phi_R^{\text{source}}}a^\dagger s\right), \tag{3.66}$$

and

$$H_{SR}^c = \hbar\left(\sqrt{2\kappa_s}s + e^{-i\phi_R^{\text{source}}}\sqrt{2\kappa_a}a\right)\mathcal{E}^\dagger(0) + \hbar\left(\sqrt{2\kappa_s}s^\dagger + e^{i\phi_R^{\text{source}}}\sqrt{2\kappa_a}a^\dagger\right)\mathcal{E}(0). \tag{3.67}$$

Both the source and target subsystems now couple to the same reservoir operator, $\mathcal{E}(0) \equiv \mathcal{E}(0, 0)$, and we can follow through the method from Section 3.1.3 to arrive at the *master equation for a source subsystem, mode s, cascaded with a target subsystem, mode a, with retardation from the source*:

$$\frac{\mathrm{d}}{\mathrm{d}t}\rho_{\text{ret}} = \frac{1}{i\hbar}[H_S^c, \rho_{\text{ret}}] + \frac{1}{2}\left(2J_c\rho_{\text{ret}}J_c^\dagger - J_c^\dagger J_c\rho_{\text{ret}} - \rho_{\text{ret}}J_c^\dagger J_c\right), \tag{3.68}$$

with cascaded decay operator

$$J_c \equiv \sqrt{2\kappa_s}s + e^{-i\phi_R^{\text{source}}}\sqrt{2\kappa_a}a. \tag{3.69}$$

3.3.3 Coherently driven damped electromagnetic field mode

Where Eqs. (3.66) and (3.68) are for general source and target subsystems, we now move our focus towards a more specific example, namely an idealised laser model coupled into a target cavity mode. As before, we take the source subsystem to be a single cavity mode, however it is now driven by a classical current with amplitude $\mathcal{E}_{\text{current}}$. The cascaded systems master equation then takes the form

$$\begin{aligned}\frac{\mathrm{d}\rho}{\mathrm{d}t} &= -i\omega_s[s^\dagger s,\rho] - i[\mathcal{E}_{\text{current}}e^{-i\omega_s t}s^\dagger + \mathcal{E}^*_{\text{current}}e^{i\omega_s t}s,\rho] + \kappa_s\left(2s\rho s^\dagger - s^\dagger s\rho - \rho s^\dagger s\right)\\ &\quad - i\omega_a[a^\dagger a,\rho] + \kappa_a\left(2a\rho a^\dagger - a^\dagger a\rho - \rho a^\dagger a\right)\\ &\quad + 2\sqrt{\kappa_s\kappa_a}\left(a\rho s^\dagger - \rho s^\dagger a + s\rho a^\dagger - a^\dagger s\rho\right).\end{aligned} \tag{3.70}$$

The density operator for the source subsystem can be obtained by tracing out the target state,

$$\rho_{\text{source}} = \text{tr}_{\text{target}}\left[\rho\right], \tag{3.71}$$

which, from Eq. (3.70), returns the master equation

$$\frac{\mathrm{d}\rho_{\text{source}}}{\mathrm{d}t} = -i\omega_s[s^\dagger s,\rho_{\text{source}}] - i[\mathcal{E}_{\text{current}}e^{-i\omega_s t}s^\dagger + \mathcal{E}^*_{\text{current}}e^{i\omega_s t}s,\rho_{\text{source}}] \tag{3.72}$$

$$+ \kappa_s\left(2s\rho_{\text{source}}s^\dagger - s^\dagger s\rho_{\text{source}} - \rho_{\text{source}}s^\dagger s\right), \tag{3.73}$$

with steady-state solution

$$\rho^{ss}_{\text{source}} = |\alpha_s e^{-i\omega_s t}\rangle\langle\alpha_s e^{-i\omega_s t}|, \quad \alpha_s = -i\frac{\mathcal{E}_{\text{current}}}{\kappa_s}. \tag{3.74}$$

We see here that the classical driving current maintains the source mode in a coherent state, oscillating with amplitude α_s at frequency ω_s. The cascaded system master equation, Eq. (3.70), then has a factorised solution of the form

$$\rho(t) = \rho^{ss}_{\text{source}}\rho_{\text{target}}(t), \tag{3.75}$$

where

$$\begin{aligned}\frac{\mathrm{d}\rho_{\text{target}}}{\mathrm{d}t} &= -i\omega_a[a^\dagger a,\rho_{\text{target}}] - 2\sqrt{\kappa_s\kappa_a}[\alpha_s e^{-i\omega_s t}a^\dagger - \alpha_s^* e^{i\omega_s t}a,\rho_{\text{target}}]\\ &\quad + \kappa_a\left(2a\rho_{\text{target}}a^\dagger - a^\dagger a\rho_{\text{target}} - \rho_{\text{target}}a^\dagger a\right).\end{aligned} \tag{3.76}$$

Equation (3.76) can be solved by a coherent state, $|\alpha_a(t)\rangle$, i.e., by substituting the ansatz $\rho_{\text{target}}(t) = |\alpha_a(t)\rangle\langle\alpha_a(t)|$. With the coherent state expressed in terms of the displacement

operator, as in Eq. (2.70), we obtain for the left-hand side:

$$\begin{aligned}\text{L.H.S} = &\frac{\mathrm{d}\alpha_a(t)}{\mathrm{d}t} a^\dagger \left|\alpha_a(t)\right\rangle \left\langle\alpha_a(t)\right| + \frac{\mathrm{d}\alpha_a^*(t)}{\mathrm{d}t} \left|\alpha_a(t)\right\rangle \left\langle\alpha_a(t)\right| a \\ &- \left[\alpha_a(t)\frac{\mathrm{d}\alpha_a^*(t)}{\mathrm{d}t} + \alpha_a^*(t)\frac{\mathrm{d}\alpha_a(t)}{\mathrm{d}t}\right] \left|\alpha_a(t)\right\rangle \left\langle\alpha_a(t)\right|, \end{aligned} \tag{3.77}$$

and, similarly, for the right-hand-side:

$$\begin{aligned}\text{R.H.S} = &\left[-\left(\kappa_a + i\omega_a\right)\alpha_a(t) - 2\sqrt{\kappa_a\kappa_s}\alpha_s e^{-i\omega_s t}\right] a^\dagger \left|\alpha_a(t)\right\rangle \left\langle\alpha_a(t)\right| \\ &+ \left[-\left(\kappa_a - i\omega_a\right)\alpha_a^*(t) - 2\sqrt{\kappa_a\kappa_s}\alpha_s^* e^{i\omega_s t}\right] \left|\alpha_a(t)\right\rangle \left\langle\alpha_a(t)\right| a \\ &+ \left[2\sqrt{\kappa_a\kappa_s}\alpha_s e^{-i\omega_s t}\alpha_a^*(t) + 2\sqrt{\kappa_a\kappa_s}\alpha_s^* e^{i\omega_s t}\alpha_a(t) + 2\kappa|\alpha_a(t)|^2\right] \left|\alpha_a(t)\right\rangle \left\langle\alpha_a(t)\right|. \end{aligned} \tag{3.78}$$

Comparing similar terms in Eqs. (3.77) and (3.78), we then see that Eq. (3.76) can indeed be solved by a coherent state, $|\alpha_a(t)\rangle$, where $\alpha_a(t)$ obeys the classical equation of motion

$$\frac{\mathrm{d}\alpha_a}{\mathrm{d}t} = -\left(\kappa_a + i\omega_a\right)\alpha_a - 2\sqrt{\kappa_s\kappa_a}\alpha_s e^{-i\omega_s t}. \tag{3.79}$$

4 Frequency Filtering Through Optical Cavities

We begin this chapter with a discussion of the most common type of frequency filtering device in optical – both classical and quantum – settings: the *Fabry-Pérot interferometer*, or cavity, named after Charles Fabry and Alfred Pérot. Using a transfer matrix method we derive simple expressions for the transmission spectrum of a Fabry-Pérot cavity, accounting for all possible modes that are supported. These spectra are then compared to those of a quantum optical model, where we allow for only a single supported mode.

Single-mode Fabry-Pérot cavities are relatively simple to implement as frequency filters in quantum optics, both experimentally and theoretically. This ease of use and effectiveness is one of the reasons why they are so widely used [78, 79]. Unfortunately the Lorentzian-shaped frequency response is not ideal when considering multi-frequency input sources due to the trade off between frequency isolation and temporal response. Lending inspiration from the ideal, yet unobtainable, box-filter, we introduce the novel filtering model that we will use throughout the thesis: the *multi-mode array filter*. We then calculate the temporal and frequency response of this filter model and compare them to that of a conventional single-mode cavity.

4.1 Single-Mode Cavities and Lorentzian Distributions

The transfer matrix method is an especially useful and powerful method for describing the propagation of fields through linear optical media [79]. Here we present a brief investigation of the transmission spectrum of a Fabry-Pérot cavity, comparing it to the derived transmission spectrum derived from a quantum optical model.

4.1.1 Transmission spectrum of a Fabry-Pérot cavity

The propagation of electromagnetic waves through a linear optical medium, or element, can be described using the *transfer matrix method*, where the left- and right-hand incoming and outgoing fields of the element are related via a transfer matrix,

$$\begin{pmatrix} E_1^{(\text{in})} \\ E_2^{(\text{out})} \end{pmatrix} = \mathcal{T} \begin{pmatrix} E_1^{(\text{out})} \\ E_2^{(\text{in})} \end{pmatrix}. \tag{4.1}$$

The transfer matrix for a system composed of multiple optical elements is given by the product of the transfer matrices of each of the components; for the Fabry-Pérot cavity, as depicted in Fig. 4.1, this is the product of the matrices for the two mirrors, M1 and M2, and the for free propagation over a length l between the two mirrors [80, 81]:

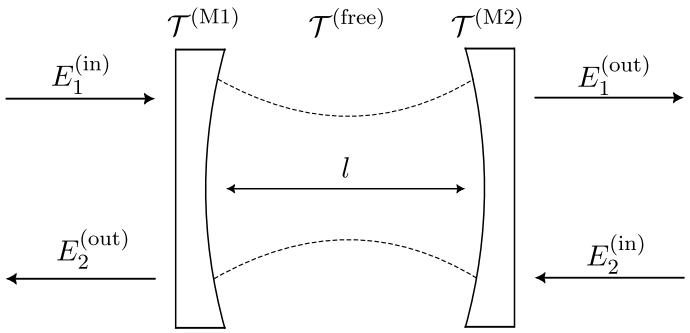

Figure 4.1: The Fabry-Pérot cavity consists of two partially reflecting mirrors, M1 and M2, separated by a distance of free-space, l. Here the left and right directional fields are labelled as E_1 and E_2 respectively, where the input and output fields are related by the transfer matrix, Eq. (4.2).

$$\begin{aligned}\mathcal{T}^{(\mathrm{FP})} &= \mathcal{T}^{(\mathrm{M1})}\mathcal{T}^{(\mathrm{free})}\mathcal{T}^{(\mathrm{M2})} \\ &= \frac{i}{\sqrt{T_1}}\begin{pmatrix} -1 & \sqrt{R_1} \\ -\sqrt{R_1} & T_1+R_1 \end{pmatrix} \times \begin{pmatrix} e^{-ikl}/\sqrt{\eta} & 0 \\ 0 & \sqrt{\eta}e^{ikl} \end{pmatrix} \times \frac{i}{\sqrt{T_2}}\begin{pmatrix} -1 & \sqrt{R_2} \\ -\sqrt{R_2} & T_2+R_2 \end{pmatrix} \\ &= \frac{e^{-ikl}}{\sqrt{\eta T_1 T_2}}\begin{pmatrix} 1-e^{2ikl}\eta\sqrt{R_1R_2} & -\sqrt{R_2}+e^{2ikl}\eta\sqrt{R_1}\,(T_2+R_2) \\ \sqrt{R_1}-e^{2ikl}\eta\sqrt{R_2}\,(T_1+R_1) & -\eta\sqrt{R_1R_2}\,(T_1+R_1)\,(T_2+R_2) \end{pmatrix}, \end{aligned} \tag{4.2}$$

where R_j (T_j) is the reflectivity (transmittance) of mirror j, l is the propagation length of the cavity, η is the propagation efficiency inside the cavity, and $k = \omega/c$ is the wavenumber of the propagating wave with frequency ω and speed c. The frequency spacing between supported modes inside the cavity, known as the *free spectral range* (FSR), is defined by

$$\omega_{\mathrm{FSR}} = 2\pi \times \mathrm{FSR} = 2\pi\frac{c}{2l} = \frac{\pi c}{l}. \tag{4.3}$$

This allows us to write

$$e^{ikl} = e^{i\pi\frac{\omega}{\omega_{\mathrm{FSR}}}} = e^{i\pi\frac{\omega-\omega_c}{\omega_{\mathrm{FSR}}}}, \tag{4.4}$$

where we have introduced the cavity resonance frequency ω_c which satisfies

$$e^{-i\pi\frac{\omega_c}{\omega_{\mathrm{FSR}}}} = 1. \tag{4.5}$$

For the sake of simplicity, we ignore any intrinsic cavity loss, $\eta = 1$, and set the mirrors to be lossless and identical, so that $R_1 = R_2 = R$ and $T_1 = T_2 = 1 - R$. The transmission spectrum is then given by:

$$S_T^{(FP)} = \left|\frac{1}{\mathcal{T}_{11}^{(\mathrm{FP})}}\right|^2 = \frac{(1-R)^2}{1+R^2-2R\cos\left(2\pi\frac{\omega-\omega_c}{\omega_{\mathrm{FSR}}}\right)}. \tag{4.6}$$

We show Eq. (4.6) in Figs. 4.2 and 4.3 for a variety of different parameters. From Fig. 4.2 and Eq. (4.3) we see that, by increasing the length of the cavity, the FSR decreases and therefore the modes move closer in frequency space. An increase in length also shows a decrease in the linewidth of each mode. Figure 4.3 shows, for a fixed length, that by decreasing the reflectivities of the two mirrors, there is an increase in the linewidth, to the point that the responses of each

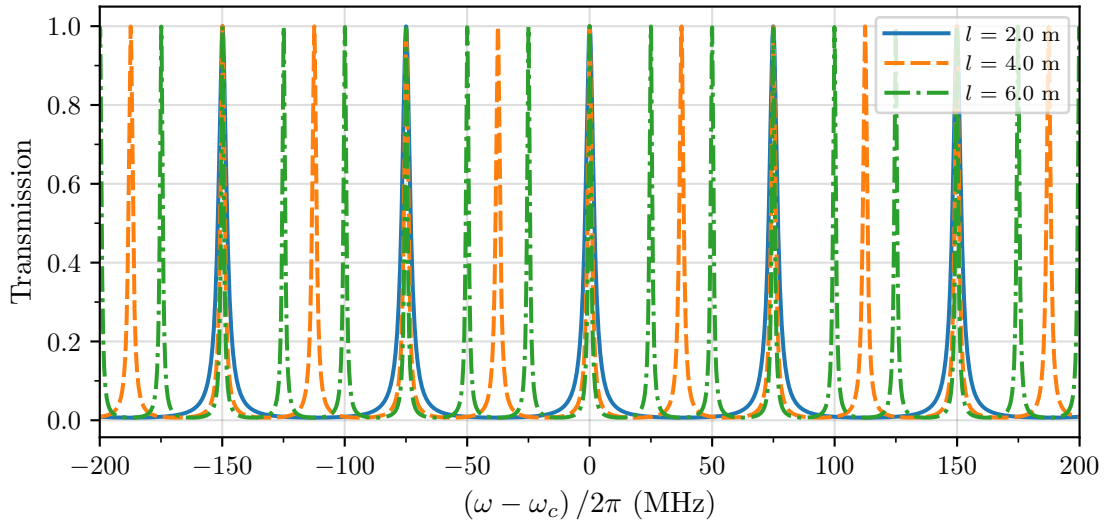

Figure 4.2: Transmission spectra of a Fabry-Pérot cavity with lengths: $l = 2$ m (blue, solid), $l = 4$ m (orange, dashed), and $l = 6$ m (green, dot-dash). The reflectivities of the two mirrors are fixed at $R = 0.85$.

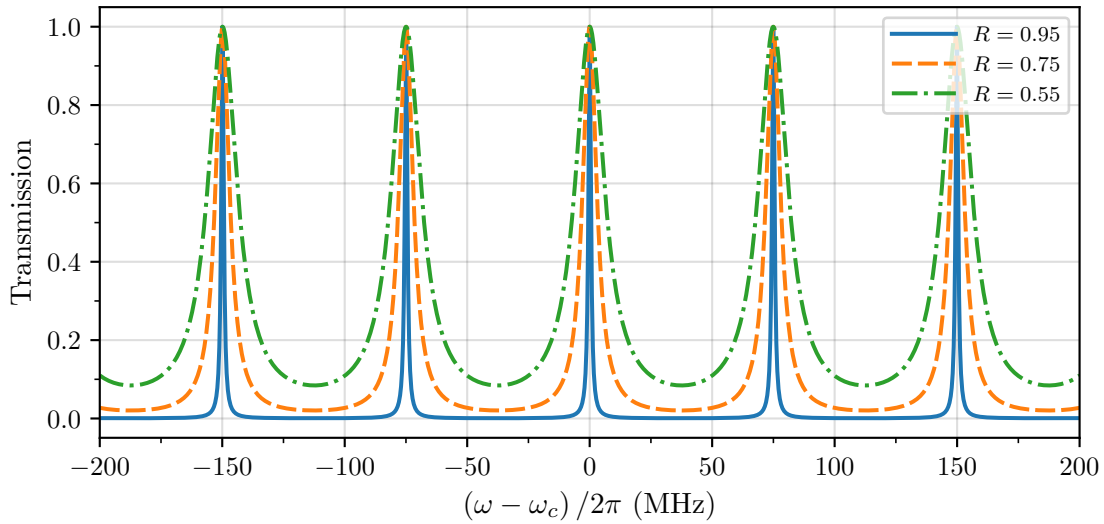

Figure 4.3: Transmission spectra of Fabry-Pérot cavity with reflectivities of the two mirrors: $R = 0.95$ (blue, solid), $R = 0.75$ (orange, dashed), and $R = 0.55$ (green, dot-dash). The length of the cavity is fixed at $l = 2$ m.

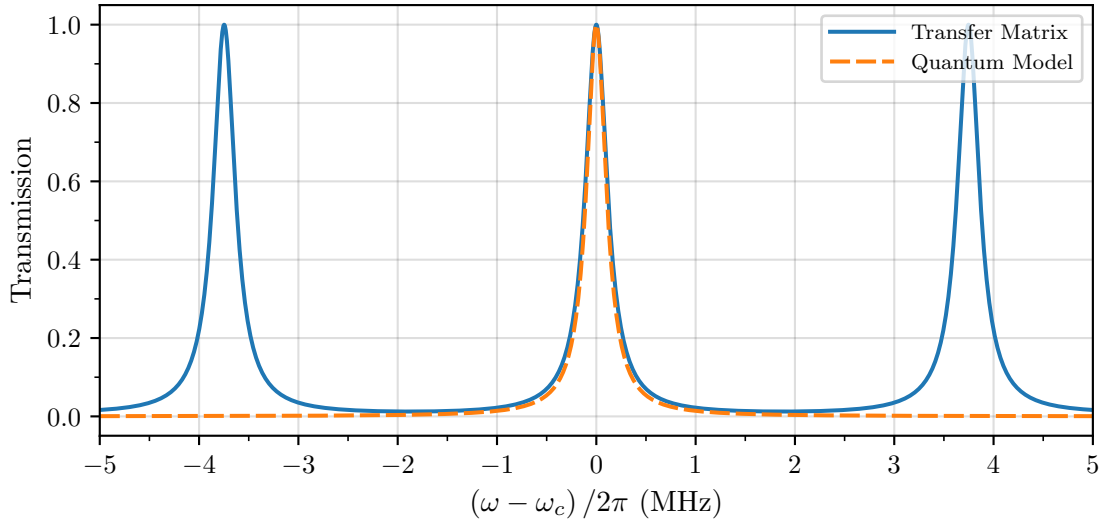

Figure 4.4: Transmission spectra of a single-mode filter using the transfer matrix method (blue, solid) and the quantum model (orange, dashed). For the transfer matrix method, Eq. (4.6), the parameters are $R = 0.8$ and $l = 40$ m. For the single-mode mode approximation, Eqs. (4.7) and (4.8), the total cavity decay rate is $\kappa_c/2\pi = 0.119$ MHz.

mode start to overlap. Allowing for multiple overlapping modes is not beneficial when applied to frequency filtering; with a frequency response that extends over all frequency space, any photon is able to pass through. We can, however, approximate a single-mode response from the Fabry-Pérot by making some simple assumptions: first, we assume the cavity to have a short length, increasing the FSR as in Fig. 4.2; secondly, we assume the reflectivities of both mirrors are high. In this limit where $1 - R \ll 1$, Eq. (4.6) reduces to

$$S_T^{(\mathrm{FP})}(\omega) = \frac{\kappa_c^2}{\kappa_c^2 + (\omega - \omega_c)^2}, \tag{4.7}$$

where

$$\kappa_c = \frac{\omega_{\mathrm{FSR}}}{2\pi}(1 - R), \tag{4.8}$$

is the total field decay rate for the cavity. As shown in Fig. 4.4, this approximation works well provided that the FSR of the cavity is large enough; we see that the single-mode approximation closely matches the Lorentzian distribution of the central mode from the transfer matrix approach. As we will see in the following section, Eq. (4.7) is comparable to the result obtained from the purely quantum optical approach of a single-mode cavity.

4.1.2 Quantum optical single-mode cavity

Through Eq. (4.7) we have shown that the single-mode approximation of a Fabry-Pérot cavity works well for isolated modes, however we now wish to take a quantum optical treatment. Following on from Eqs. (3.76) and (3.79), we model the scanning interferometer as a single-mode cavity. To demonstrate its frequency response we consider it to be driven by a frequency

dependent coherent driving field, with Hamiltonian

$$H_C = \hbar\omega_c a^\dagger a + i\hbar\left(\mathcal{E}_d e^{-i\omega t}a^\dagger - \mathcal{E}_d^* e^{i\omega t}a\right), \tag{4.9}$$

where ω_c is the tunable resonance frequency of the cavity mode and $\mathcal{E}_d$ is the coherent driving amplitude of the pump at frequency ω (from Eq. (3.76) we can take $\mathcal{E}_d = -2\alpha_s\sqrt{\kappa_s\kappa_a}$). The cavity also experiences photon loss at a rate 2κ, which can be described by the master equation

$$\frac{\mathrm{d}\rho}{\mathrm{d}t} = \frac{1}{i\hbar}[H_C, \rho] + \kappa\left(2a\rho a^\dagger - a^\dagger a\rho - \rho a^\dagger a\right). \tag{4.10}$$

Taking the cavity to initially be in the vacuum state, we recast Eq. (3.76) and write the equation of motion for the coherent state amplitude of the cavity field as

$$\frac{\mathrm{d}}{\mathrm{d}t}\alpha(t) = -\left(\kappa + i\omega_c\right)\alpha(t) + \mathcal{E}_d e^{-i\omega t}, \tag{4.11}$$

which has solution

$$\alpha(t) = \frac{\mathcal{E}_d e^{-i\omega t}}{\kappa - i\left(\omega - \omega_c\right)}\left(1 - e^{-\kappa t}e^{i(\omega-\omega_c)t}\right). \tag{4.12}$$

In the long time limit, $t \to \infty$, we find the cavity response as a function of drive frequency, ω, at fixed ω_c, is a Lorentzian shape with halfwidth κ,

$$|\alpha(\omega)|^2 = \frac{|\mathcal{E}_d|^2}{\kappa^2 + \left(\omega - \omega_c\right)^2}, \tag{4.13}$$

which, like Eq. (4.7), is a Lorentzian distribution. Here we arrive at the main issue with single-mode cavity filters and Lorentzian distributions for time-dependent photon correlations. Ultimately we aim for a filter which allows target photons to enter the cavity and be re-emitted immediately after. The bandwidth of the filter, however, is inversely proportional to the cavity lifetime, κ. A faster temporal response then requires a larger bandwidth, yet the tails of a Lorentzian distribution extend quite far from a target frequency. If our source system emits photons of frequencies spread over some range, these long tails may allow non-target frequencies to enter into the cavity. If we then decrease the bandwidth to reject non-target frequencies, the average lifetime of a photon inside the cavity increases and the filtered photon correlations will no longer be indicative of the true nature of the source system dynamics [39].

4.2 An Improved Filtering Model

Our ultimate goal is to develop a type of filter model that allows us to pick very specific frequencies from a general source system and calculate photon correlations. To do this we take inspiration from an ideal bandpass filter, i.e., the sinc filter. With its infinitely sharp frequency response cut-off, we can increase the bandwidth, and thus the temporal response, much more than a conventional Lorentzian filter while still maintaining good frequency isolation.

We begin this section with a brief discussion on sinc filters and their limitations. We then introduce the novel model used in this thesis, the *multi-mode array filter*, and investigate its temporal and frequency responses.

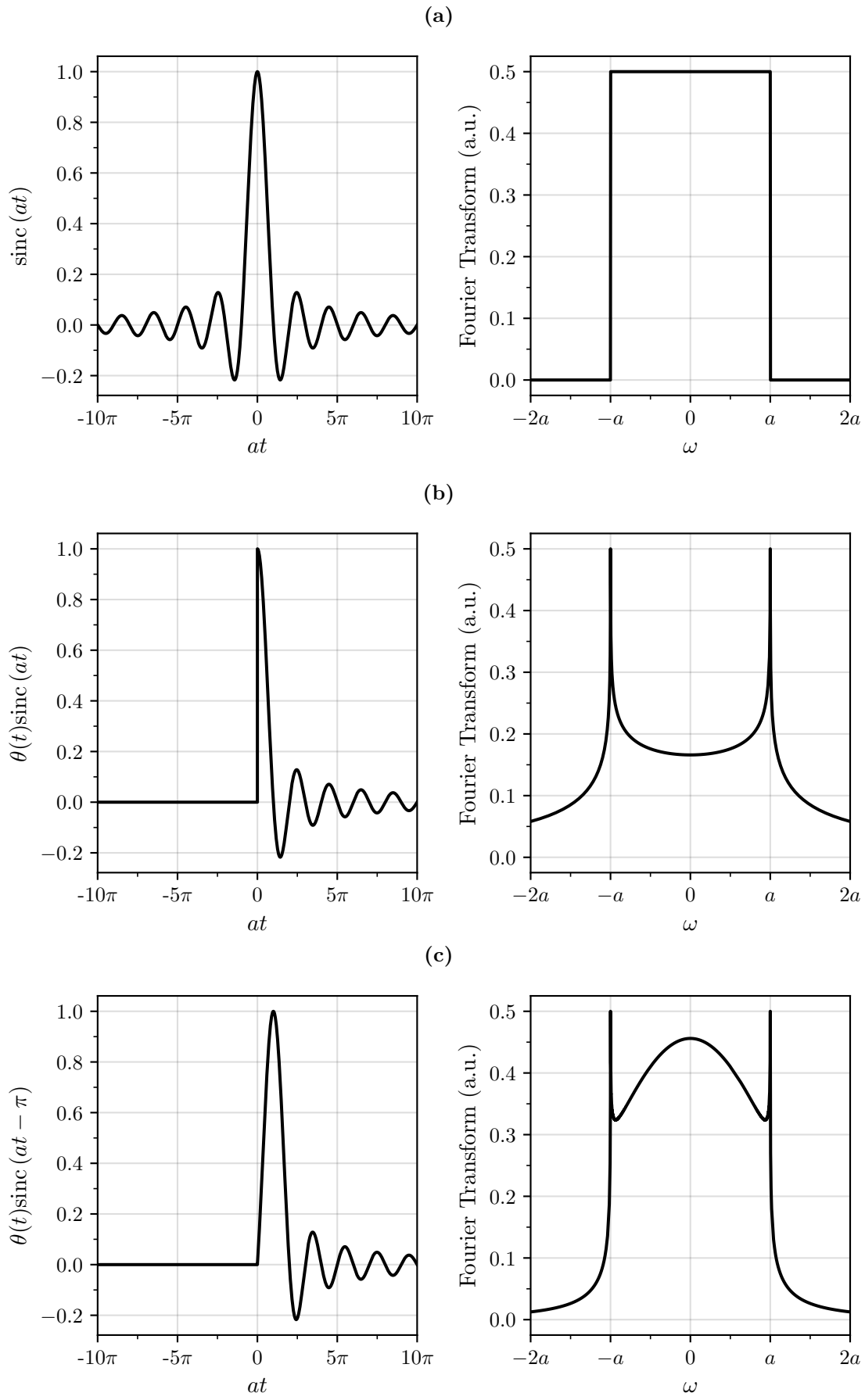

Figure 4.5: Time series and Fast-Fourier Transform (FFT) of a complete sinc function (a), positive-side sinc function (b), and a positive-side sinc function with a π phase delay (c).

4.2.1 The sinc function and ideal filters

In the realm of frequency filtering an ideal bandpass filter is one which allows complete transmission over a certain frequency range and complete attenuation outside. One such model is the sinc filter – also known as the rectangle filter – which results from the Fourier transform of the sinc function in the time domain:

$$\mathcal{F}\left[\mathrm{sinc}\left(at\right)\right] = \frac{a}{2\pi}\int_{-\infty}^{\infty}\frac{\sin\left(at\right)}{at}e^{i\omega t}\mathrm{d}t = \begin{cases} 0 & a < |\omega| \\ \frac{1}{4} & |\omega| = a \\ \frac{1}{2} & |\omega| < a \end{cases}. \tag{4.14}$$

We see from this equation, and in Fig. 4.5a, that by increasing the width of the intervals in the sinc response we also increase the width of the frequency response.

Unfortunately, perfect sinc filters are *non-causal filters*, and are physically impossible to realise. Unlike *causal filters*, which only use past and present inputs to produce a response, the sinc filter also includes negative times; the filter responds to an impulse before it has arrived, violating the principles of causality and time invariance (see Ref. [82], Chapter 11). We can consider a physically realisable causal filter by neglecting the negative time response, with $\theta(t)\mathrm{sinc}\left(at\right)$, where

$$\theta(t) = \begin{cases} 0 & t \leq 0 \\ 1 & 0 < t \end{cases} \tag{4.15}$$

is the *Heaviside step function*. In dropping half of the temporal response, we see in Fig. 4.5b that the frequency response, as calculated from the Fourier transform, has drastically changed. The introduced artefacts still show a semblance of the original rectangular "width", yet the sharp frequency cut-off has been completely lost, and there is now a low dip in the centre of the frequency response.

Fortunately, we can recover the rectangular nature by introducing a phase modulation. Shifting the centre of the temporal response to the right, we regain more of the initial sinc function. In Fig. 4.5c we introduce a π-phase delay, with response $\theta(t)\mathrm{sinc}\left(at-\pi\right)$. The Fourier transform of this shows a much sharper cut-off than non-delayed response, Fig. 4.5b, and the central peak has been restored. We can increase the phase modulation even further, recovering much more of the sinc function, leading to an even more rectangular frequency distribution. Unfortunately, a greater phase modulation also results in a greater temporal delay. As we are ultimately interested in calculating photon correlations from filtered sources, we need to minimise the temporal delay of our filter as much as possible. We will see in the following sections what impact the size of this delay has on the filter response, and how much delay we can introduce without affecting the performance of the filter.

4.2.2 A novel approach: Multi-mode array filtering

It is no simple feat to develop a new cavity model that does not have a non-Lorentzian frequency response, as we have shown this is an innate property of Fabry-Pérot cavities. We therefore propose a model where we couple the output of a system of interest into an *array of*

single-mode cavities, each with a small bandwidth, rather than a solitary cavity. At first glance, the smaller bandwidth of each individual cavity mode might appear to result in a poor temporal resolution of the filter as a whole, nevertheless we will see in the following sections that this is not the case.

The proposed model consists of $2N+1$ cavity modes, where the resonance frequency of each mode is slightly detuned from a central frequency ω_c. To achieve equal coupling, we pass the input field through an array of mirrors with increasing reflectivity, as shown in Fig. 4.6, where the reflected field couples an equal amplitude into each individual cavity mode. We therefore extend the Hamiltonian, Eq. (4.9), as

$$H = \hbar \sum_{j=-N}^{N} \omega_j a_j^\dagger a_j + i\hbar \sum_{j=-N}^{N} \left(\mathcal{E}_j e^{-i\omega t} a_j^\dagger - \mathcal{E}_j^* e^{i\omega t} a_j \right), \tag{4.16}$$

where N is the number of cavity modes either side of the central mode, $a_j^\dagger$ (a_j) is the photon creation (annihilation) operator for the j^{th} filter mode,

$$\omega_j = \omega_c + j\delta\omega \tag{4.17}$$

is the resonance frequency of the j^{th} filter mode, with mode frequency spacing $\delta\omega$, and

$$\mathcal{E}_j = \frac{\mathcal{E}_d}{\sqrt{2N+1}} e^{imj\pi/N} \tag{4.18}$$

is the mode-dependent driving amplitude. Note here that a mode dependent phase modulation is applied to each filter mode with the exponential term in Eq. (4.18), where m sets the size of the introduced delay.

The output of each filter mode is directed into individual detectors, allowing us to write the master equation as

$$\frac{\mathrm{d}\rho}{\mathrm{d}t} = \frac{1}{i\hbar}[H, \rho] + \kappa \sum_{j=-N}^{N} \left(2a_j \rho a_j^\dagger - a_j^\dagger a_j \rho - \rho a_j^\dagger a_j \right), \tag{4.19}$$

where, as before, 2κ is the total cavity decay rate for each mode.

4.2.3 Temporal response to an impulse

Before we assess the frequency response of this proposed model, we will first investigate its temporal response to an impulse. As with the single-mode cavity, we calculate the coherent state amplitude of the cavity field, however, we replace the continuous driving in Eq. (4.16) with an impulse driving term. The equation of motion for the field amplitude for the j^{th} filter mode is then

$$\frac{\mathrm{d}}{\mathrm{d}t}\alpha_j(t) = -\left(\kappa + i\omega_j\right)\alpha_j(t) + \mathcal{E}_j\delta(t), \tag{4.20}$$

where $\delta(t)$ is the *Dirac delta-function*. Equation (4.20) has solution

$$\alpha_j(t) = \mathcal{E}_j e^{-(\kappa+i\omega_j)t}\theta(t), \tag{4.21}$$

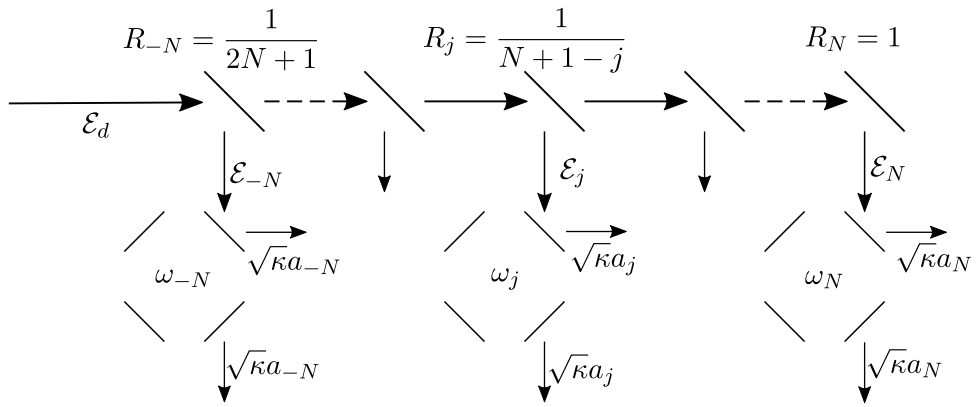

Figure 4.6: Schematic of coherently driven multi-mode array filter model. The input field is evenly split into each individual two-sided cavity mode, where a mode-dependent phase modulation is applied. To achieve the equal coupling of the input fluorescence, the input field is passed through an array of beam splitters with increasing intensity reflectivity coefficients.

where $\theta(t)$ is the Heaviside step function, as defined in Eq. (4.15). To find the total response of the array filter we add the mode amplitudes together, and consider the *collective field amplitude*:

$$A(t) = \frac{1}{\sqrt{2N+1}} \sum_{j=-N}^{N} \alpha_j(t). \tag{4.22}$$

Assuming a large number of closely-spaced modes, we can convert the summation over modes into an integral. We then find the collective field amplitude to be:

$$\begin{aligned} A(t) \simeq \frac{1}{\sqrt{2N+1}} \int_{-N}^{N} \alpha(j,t)\mathrm{d}j &= \int_{-N}^{N} \frac{\mathcal{E}_d}{2N+1} e^{ijm\pi/N} e^{-[\kappa+i(\omega_c+j\delta\omega)]t}\theta(t)\mathrm{d}j \\ &= \frac{\mathcal{E}_d}{2N+1}\theta(t)e^{-(\kappa+i\omega_c)t} \times \int_{-N}^{N} e^{-i(N\delta\omega t - m\pi)j/N}\mathrm{d}j \\ &= \frac{N\mathcal{E}_d}{2N+1}\theta(t)e^{-(\kappa+i\omega_c)t} \times \frac{e^{i(N\delta\omega t-m\pi)} - e^{-i(N\delta\omega t-m\pi)}}{i\left(N\delta\omega t - m\pi\right)} \\ &= \frac{N\mathcal{E}_d}{2N+1}\theta(t)e^{-(\kappa+i\omega_c)t} \times \frac{2\sin\left(N\delta\omega t - m\pi\right)}{\left(N\delta\omega t - m\pi\right)} \\ &= \frac{2N\mathcal{E}_d}{2N+1}\theta(t)e^{-(\kappa+i\omega_c)t}\mathrm{sinc}\left(N\delta\omega t - m\pi\right). \end{aligned} \tag{4.23}$$

We see here that this proposed model behaves as we expect from a sinc-response filter. When compared with Eq. (4.14), the halfwidth of the filter is given by the span of modes in Eq. (4.17), $N\delta\omega$. We also see a similarity with the positive-sided and shifted sinc response in Fig. (4.5c), where the causality is enforced by the Heaviside step function and the temporal delay of $m\pi$ arises from the mode-dependent coupling, Eq. (4.18).

Ignoring the normalisation term and the Heaviside step-function, there is one important difference in Eq. (4.23) when compared to the ideal sinc response: the exponential decay and oscillating term $e^{-(\kappa+i\omega_c)t}$. The oscillatory term, $e^{-i\omega_c t}$, simply centres the response in frequency space at ω_c, as we see with the single-mode cavity in Eq. (4.12). The cavity decay term, however, can have a much more significant effect on the filter's response. This is shown in Fig. 4.7, where

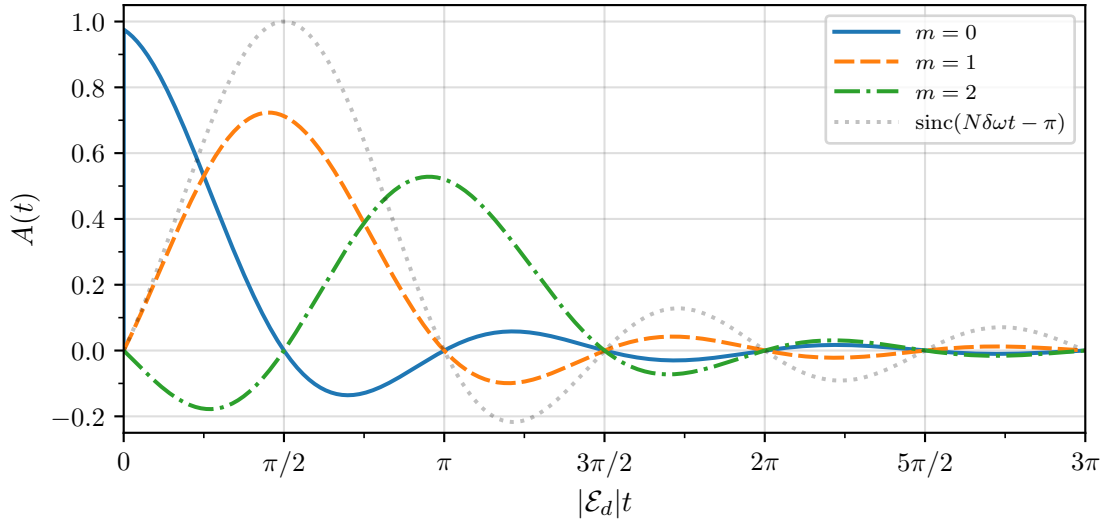

Figure 4.7: Normalised field amplitude response to an impulse driving, Eq. (4.23), with $m = 0$ (blue, solid), $m = 1$ (orange, dashed), and $m = 2$ (green, dot-dash). Also shown is pure sinc term of Eq. (4.23) (grey, dotted), showing the effect the decay has on the temporal response. The other parameters are $N = 20, \delta\omega/|\mathcal{E}_d| = 0.1, \kappa/|\mathcal{E}_d| = 0.2, \omega_c/|\mathcal{E}_d| = 0.0$.

the response for the phase-shifted multi-mode array filter, in orange, is plotted against the sinc term in Eq. (4.23), with $m = 1$. The cavity decay causes the response, and thus the peaks, to decay with regard to the pure sinc term, an effect which becomes more noticeable for larger κ. We are able to mitigate this affect, and thus achieve a response closer to a pure sinc function, by ensuring the decay of each cavity mode is much smaller than the effective halfwidth of the array filter, $\kappa \ll N\delta\omega$. We will see in the following section, however, that this is not without its limits.

4.2.4 Cavity response in frequency space

The sinc-like response due to an instantaneous driving impulse is promising, yet it is not enough to tell the entire story of the filter. To see whether this new model has a much sharper frequency cut-off than a standard Lorentzian, we must return to the case of a continuous drive and investigate the response of the filter in frequency space. With the same approach that led to Eq. (4.13), we replace the delta-function in Eq. (4.20) with a continuous driving term, at frequency ω, so that the rate equation for the cavity field amplitude of the j^{th} filter mode becomes

$$\frac{\mathrm{d}}{\mathrm{d}t}\alpha_j(t) = -\left(\kappa + i\omega_j\right)\alpha_j(t) + \mathcal{E}_j e^{-i\omega t}, \tag{4.24}$$

which has a solution in the long-time limit similar to Eq. (4.12),

$$\alpha_j(\omega) = \frac{\mathcal{E}_j e^{-i\omega t}}{\kappa - i\left(\omega - \omega_j\right)}. \tag{4.25}$$

Following the same approach as for Eq. (4.23), we find the frequency response of the filtering system is the total sum of the field amplitudes of all modes:

$$A(\omega) = \frac{1}{\sqrt{2N+1}} \sum_{j=-N}^{N} \alpha_j(\omega). \tag{4.26}$$

The solution, Eq. (4.12), is more complex than Eq. (4.23) due to the dependence on the mode number, j, in both the denominator and in the exponential phase modulation in $\mathcal{E}_j$, Eq. (4.18), hence it is difficult to derive a general analytic expression for the frequency response. We can remove the mode dependency in the numerator in the case where $m = 0$, that is, when there is no phase modulation. As before, we may then replace the sum over modes with an integral to find the collective field amplitude as:

$$\begin{aligned} A(\omega) &\simeq \int_{-N}^{N} \frac{\mathcal{E}_d e^{-i\omega t}}{2N+1} \frac{1}{\kappa - i\left(\omega - \omega_c - j\delta\omega\right)} \mathrm{d}j \\ &= \frac{\mathcal{E}_d e^{-i\omega t}}{2N+1} \int_{-N}^{N} \frac{1}{\kappa - i\left(\omega - \omega_c\right) + ij\delta\omega} \mathrm{d}j \\ &= \frac{-ie^{-i\omega t}}{2N+1} \frac{\mathcal{E}_d}{\delta\omega} \Big[\log\left[\kappa - i\left(\omega - \omega_c - j\delta\omega\right)\right] \Big]_{-N}^{N} \\ &= \frac{-ie^{-i\omega t}}{2N+1} \frac{\mathcal{E}_d}{\delta\omega} \log\left[\frac{\kappa - i\left(\omega - \omega_N\right)}{\kappa - i\left(\omega - \omega_{-N}\right)} \right], \end{aligned} \tag{4.27}$$

where $\omega_{\pm N}$ are given by Eq. (4.17). The cavity frequency response is, therefore,

$$|A(\omega)|^2 = \frac{|\mathcal{E}_d|^2}{\delta\omega^2 \left(2N+1\right)^2} \log\left[\frac{\kappa + i\left(\omega - \omega_N\right)}{\kappa + i\left(\omega - \omega_{-N}\right)} \right] \log\left[\frac{\kappa - i\left(\omega - \omega_N\right)}{\kappa - i\left(\omega - \omega_{-N}\right)} \right], \tag{4.28}$$

from which we see the effective width of the filter in the $\omega - \omega_{\pm N}$ terms.

Using Eq. (4.28), we plot, in Fig. 4.8a, the frequency response of the multi-mode array filter for a range of effective halfwidths: $N\delta\omega/|\mathcal{E}_d| = 1, 2$, and 4. With our aim of creating a frequency filter that is more effective than a single-mode Lorentzian, we also compare these responses with a Lorentzian of halfwidth $\kappa/|\mathcal{E}_d| = 1$. Without shifting the temporal response of the filter, the multi-mode responses resemble that of the response in Fig. 4.5b; there is a slow decay in the frequency cut-off and we see the characteristic "bunny-ear" peaks at $\omega_{\pm N}$.

Knowing that we can better approximate a box-like response by introducing a phase modulation we show numerical calculations, using Eq. (4.26) for $m = 1$ and $m = 2$, in Figs. 4.8b and 4.8c, respectively. Figure 4.8b shows an immediate improvement over the $m = 0$ case. The "dip" in the response of the central frequencies has been removed and there is a much sharper frequency cut-off, even for the larger halfwidth of $N\delta\omega/|\mathcal{E}_d| = 4$.

There is, however, a limit to the applied modulation. For $m = 2$ (Fig. 4.8c) we see that the frequency response still has as sharp a cut-off as with the $m = 1$ case, yet there is a large dip in the centre. As mentioned in Section 4.2.1, any increase in the phase modulation also increases the delay in the temporal response; a major disadvantage when calculating temporal photon correlations.

The results of Fig. 4.8 are promising as it shows that we can increase the bandwidth of

(a) Zero phase modulation ($m = 0$).

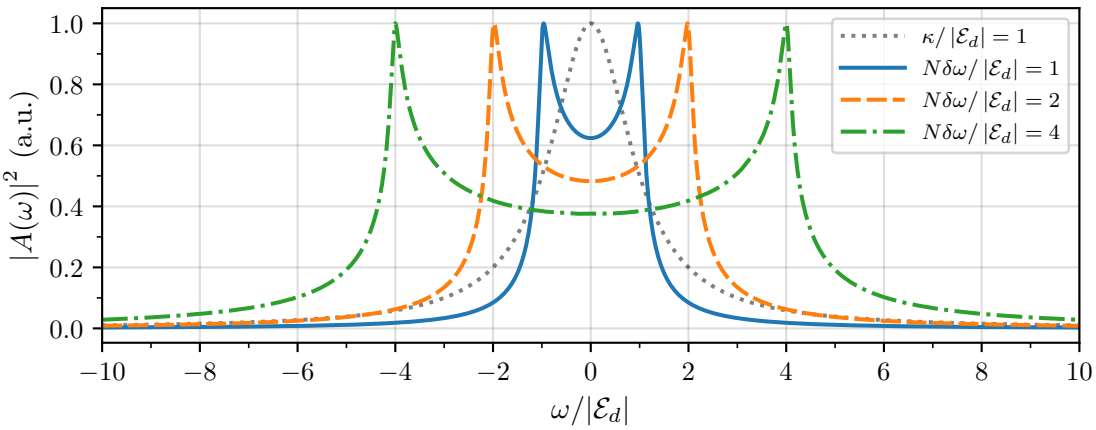

(b) π-phase modulation ($m = 1$).

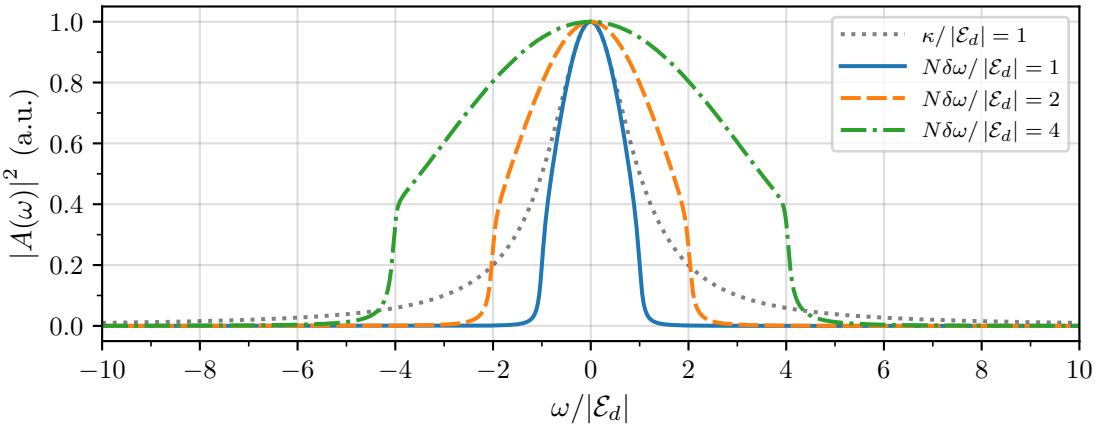

(c) 2π-phase modulation ($m = 2$).

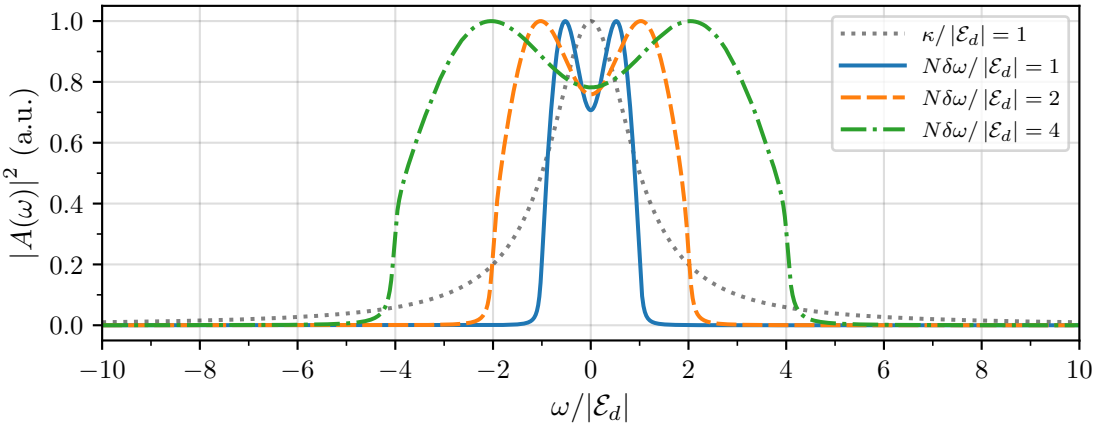

Figure 4.8: Normalised frequency response of a single-mode with $\kappa/|\mathcal{E}_d| = 1$ (grey, dots) and multi-mode array filter with no phase modulation, (a), and π-phase modulation ($m = 1$), (b), and 2π-phase modulation ($m = 2$), (c), with $N\delta\omega/|\mathcal{E}_d| = 1$ (blue, solid), $N\delta\omega/|\mathcal{E}_d| = 2$ (orange, dashed), and $N\delta\omega/|\mathcal{E}_d| = 4$ (green, dot-dash). The other parameters are $N = 80, \omega_c/|\mathcal{E}_d| = 0.0$, and, for the multi-mode array filter, $\kappa/|\mathcal{E}_d| = 0.07$.

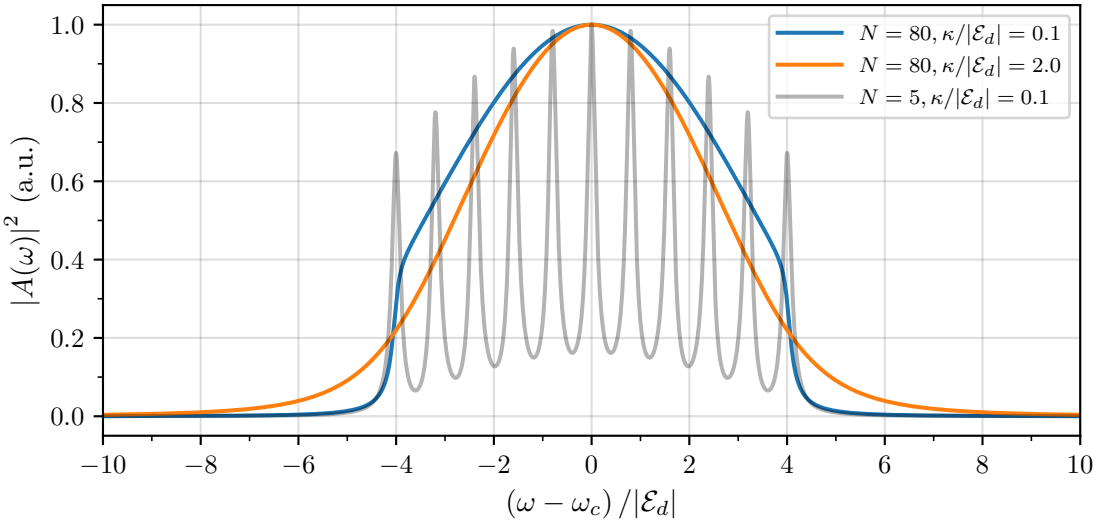

Figure 4.9: Frequency response comparison for a set bandwidth, $N\delta\omega/|\mathcal{E}_d| = 4$ for three sets of values: $N = 80, \delta\omega/|\mathcal{E}_d| = 0.05$ with $\kappa/|\mathcal{E}_d| = 0.1$ (blue) and $\kappa/|\mathcal{E}_d| = 2$ (orange), and $N = 5, \delta\omega/|\mathcal{E}_d| = 0.8$ with $\kappa/|\mathcal{E}_d = 0.05$ (grey). The other parameters are $N = 80, \delta\omega/|\mathcal{E}_d| = 0.05, m = 1$, and $\omega_c/|\mathcal{E}_d| = 0$.

our filter further than a Lorentzian, without sacrificing frequency isolation. This is important for two reasons: firstly, the wider bandwidth also improves the temporal response of the filter, allowing for more accurate photon correlation calculations; secondly, if the spectral distribution of the input light is Lorentzian, as it is for the systems we consider in this thesis, the filter must be able to envelope as much of the spectral shape in frequency space as possible, while still being able to reject any non target frequencies. If the filter bandwidth is too narrow compared to the natural linewidth of the input light – and, thus, the lifetime of the cavity is much longer than timescale of the source – the dynamics of the source system are now averaged over the lifetime of the filter. The filtered photon correlations may no longer be indicative of the true photon statistics of the source photons. We shall see this later with the two-level atom, in what has been called the "thermalisation of the source" [83], a phenomenon first discussed by Nienhuis in 1993 (see Ref. [39]).

From the impulse response of the filter, Eq. (4.23), we can expect to see a more rectangular frequency response for smaller κ. If κ is too small with respect to the mode spacing, $\delta\omega$, then there will be minimal overlap between each cavity mode and the collective response resembles that of an array of individual modes. This is depicted in Fig. 4.9, as the grey, curve. By increasing the number of modes, and thus decreasing the mode spacing, we can then allow for much smaller values of κ, giving a much sharper frequency response, as we see in blue. If κ is too large, however, the rectangular shape is replaced by a rounder, longer decaying response, as shown by the orange curve in Fig. 4.9. For this thesis, then, we will consider a large number of modes and, set the cavity mode width to $\kappa = 2.5\delta\omega$. The larger the value of N, the smaller the mode spacing becomes, and thus we will also have a narrow cavity mode width.

Part II

Resonance Fluorescence

5 The Dressed States of The Mollow Triplet

We now move our focus to the first system of interest: the *resonantly driven two-level atom*. The two-level atom provides an excellent scenario with which to test the multi-mode array filter due to its relative simplicity and its long studied history. Early work, such as that of Mollow [1, 2], showed that, upon strong coherent driving, the power spectrum of the fluorescence splits intro three components, yielding the spectrum now known as the "Mollow triplet" [3, 84]. Later work by Tannoudji and others [4, 85–87] showed that this splitting phenomenon is due to transitions amongst the atom's "dressed states", a result of the atom interacting with a strong quantised electromagnetic field. This work, so early on in the field of quantum optics, led to a "greatly renewed interest in the details of the interaction between light and resonant atomic systems" [6].

Around the time Mollow's papers were published, there were also investigations into the quantum nature of the light emitted from a two-level atom. By studying the photon correlations, it was shown that the two-level atom exhibits another purely quantum effect, namely *antibunching* [9–11], where photons are emitted individually.

In this chapter we present a summary of the theory of the resonantly driven two-level atom. We will first derive a mathematical model for investigating the two-level atom, following a similar method that lead to the Jaynes Cummings model in 1963 [88], culminating in the *optical Bloch equations*: a set of equations that allow us to easily calculate the evolution of this specific system. We then introduce the *atomic dressed states*, which gives us an intuitive description of the structure of the atomic spectrum. Following this we introduce the idea of *second-order coherence*, which is an integral quantity of interest in this thesis. Finally, we consider the system in the dressed-state picture and take the *secular approximation*, allowing us to derive ideal second-order correlation functions for each of the separate frequency components of the Mollow triplet. This will be our baseline for comparing the effectiveness of the multi-mode array filter in the following chapter.

5.1 Two-Level Atom Interacting with the Quantised Radiation Field

We begin by deriving a mathematical description of a two-level atom and its coupling to the quantised electromagnetic field. Following the method as described by Loudon (Ref. [89], Section 4.8), we make two important approximations: the *dipole* and *rotating wave* approximations.

5.1.1 Atom-field Hamiltonian: Dipole interaction for a pseudo-spin system

The Hamiltonian of an atom interacting with the transverse component of the electromagnetic field is given by

$$H = H_F + H_A + H_I, \tag{5.1}$$

where H_F is the Hamiltonian describing the free field, given by Eq. (2.51), and

$$H_A = \sum_{l=1}^{N} \hbar\omega_l \left|l\right\rangle \left\langle l\right| \tag{5.2}$$

is the free-energy Hamiltonian for a generalised N-level atom, with atomic states $|l\rangle$ and corresponding eigenfrequencies ω_l. In general the interaction between the electromagnetic field and the atom consists of many multipolar expansion terms, however when we compare the magnitude of these interaction terms we find that the electric-dipole interaction is dominant (Ref. [90], p. 132). We can assume that the wavelength of the electromagnetic field is much larger than the size of the atom, and hence assume that the field is constant over the dimensions of the atom. We then expand the spatial dependence of the electric field, Eq. (2.56), as

$$e^{i\boldsymbol{k}\cdot\boldsymbol{r}} = e^{i\boldsymbol{k}\cdot\boldsymbol{r}_0} e^{i\boldsymbol{k}\cdot(\boldsymbol{r}-\boldsymbol{r}_0)} = e^{i\boldsymbol{k}\cdot\boldsymbol{r}_0}\left[1 + i\boldsymbol{k}\cdot(\boldsymbol{r}-\boldsymbol{r}_0) + \mathcal{O}\left(\left|\boldsymbol{k}\cdot(\boldsymbol{r}-\boldsymbol{r}_0)\right|^2\right)\right]. \tag{5.3}$$

Retaining only the first term, we therefore make the *dipole approximation* and neglect all terms but the electric-dipole interaction so that the interaction Hamiltonian is

$$H_I = -\boldsymbol{D}\cdot\boldsymbol{E}(\boldsymbol{r}_0), \tag{5.4}$$

where $\boldsymbol{E}$ is the electric field at the position of the atomic nucleus, $\boldsymbol{r}_0$, given by Eq. (2.55), and

$$\boldsymbol{D} = \sum_{l,m=1}^{N} \left|l\right\rangle \left\langle l\right| e\left(\boldsymbol{r}-\boldsymbol{r}_0\right) \left|m\right\rangle \left\langle m\right| = \sum_{l,m=1}^{N} \boldsymbol{d}_{lm} \left|l\right\rangle \left\langle m\right| \tag{5.5}$$

is the dipole operator, with e the charge of an electron, $\boldsymbol{r}$ the electron position operator, and dipole matrix element

$$\boldsymbol{d}_{lm} = \left\langle l\right| e\left(\boldsymbol{r}-\boldsymbol{r}_0\right) \left|m\right\rangle. \tag{5.6}$$

The *complete Hamiltonian for a generalised* N*-level atom interacting with the quantised electromagnetic field in the dipole approximation* is then:

$$H = \sum_{l=1}^{N} \hbar\omega_l \left|l\right\rangle \left\langle l\right| + \sum_{\boldsymbol{k},\lambda} \hbar\omega_{\boldsymbol{k}} r^{\dagger}_{\boldsymbol{k},\lambda} r_{\boldsymbol{k},\lambda} + \sum_{\boldsymbol{k},\lambda} \sum_{l,m=1}^{N} \hbar \left|l\right\rangle \left\langle m\right| \left[g^{lm}_{\boldsymbol{k},\lambda} r_{\boldsymbol{k},\lambda} + \left(g^{lm}_{\boldsymbol{k},\lambda}\right)^{*} r^{\dagger}_{\boldsymbol{k},\lambda}\right], \tag{5.7}$$

with coupling

$$g^{lm}_{\boldsymbol{k},\lambda} = -i\sqrt{\frac{\omega_{\boldsymbol{k}}}{2\hbar\epsilon_0 V}}\left(\boldsymbol{d}_{lm}\cdot\hat{\boldsymbol{e}}_{\boldsymbol{k},\lambda}\right) e^{i\boldsymbol{k}\cdot\boldsymbol{r}_0}. \tag{5.8}$$

For our simple case we consider an atom with only two states: a ground state $|g\rangle$ and an excited state $|e\rangle$, with respective eigenfrequencies ω_g and ω_e. The mechanics of a two-state

system can be described using the same tools as spin-half systems, and so we find it useful to treat the two-level atom as a *pseudo-spin* system. The atomic Hamiltonian, Eq. (5.2), can then be written as

$$\begin{aligned} H_A &= \hbar\omega_g \left|g\right\rangle \left\langle g\right| + \hbar\omega_e \left|e\right\rangle \left\langle e\right| \\ &= \frac{\hbar}{2}\left(\omega_g + \omega_e\right)\mathbb{1} + \frac{\hbar}{2}\left(\omega_e - \omega_g\right)\sigma_z, \end{aligned} \tag{5.9}$$

where

$$\sigma_z \equiv \left|e\right\rangle \left\langle e\right| - \left|g\right\rangle \left\langle g\right|. \tag{5.10}$$

We can eliminate the constant term in Eq. (5.9) by setting the zero of energy at the midpoint between the ground and excited states, and so write the Hamiltonian as

$$H_A = \hbar\frac{\omega_A}{2}\sigma_z, \quad \omega_A \equiv \omega_e - \omega_g. \tag{5.11}$$

We also introduce the *atomic raising and lowering operators*,

$$\sigma_+ = \left|e\right\rangle \left\langle g\right|, \quad \sigma_- = \left|g\right\rangle \left\langle e\right|, \tag{5.12}$$

which have commutation relations:

$$\left[\sigma_+, \sigma_-\right] = \sigma_z, \quad \left[\sigma_z, \sigma_\pm\right] = \pm 2\sigma_\pm. \tag{5.13}$$

The complete Hamiltonian, Eq. (5.7), for the two-level atom is then

$$\begin{aligned} H = \hbar\frac{\omega_A}{2}\sigma_z + \sum_{\boldsymbol{k},\lambda}\hbar\omega_{\boldsymbol{k}} r^\dagger_{\boldsymbol{k},\lambda} r_{\boldsymbol{k},\lambda} + \sum_{\boldsymbol{k},\lambda}\hbar\sigma_-\left(g_{\boldsymbol{k},\lambda} r_{\boldsymbol{k},\lambda} + g^*_{\boldsymbol{k},\lambda} r^\dagger_{\boldsymbol{k},\lambda}\right) \\ + \hbar\sigma_+\left(g_{\boldsymbol{k},\lambda} r_{\boldsymbol{k},\lambda} + g^*_{\boldsymbol{k},\lambda} r^\dagger_{\boldsymbol{k},\lambda}\right), \end{aligned} \tag{5.14}$$

where we have redefined the coupling constant, Eq. (5.8), as

$$g_{\boldsymbol{k},\lambda} = g^{ge}_{\boldsymbol{k},\lambda} = -i\sqrt{\frac{\omega_{\boldsymbol{k}}}{2\hbar\epsilon_0 V}}\left(\boldsymbol{d}_{ge}\cdot\hat{\boldsymbol{e}}_{\boldsymbol{k},\lambda}\right)e^{i\boldsymbol{k}\cdot\boldsymbol{r}_0}. \tag{5.15}$$

5.1.2 Rotating wave approximation and coherent driving

Equation (5.14) contains interaction terms on two different time scales. We ultimately aim to drop any rapidly oscillating terms, and thus make the *rotating wave approximation* by introducing the unitary evolution operator

$$\mathcal{U}(t) = e^{\frac{1}{i\hbar}(H_A + H_F)t} = e^{-i\omega_{\boldsymbol{k}} t r^\dagger_{\boldsymbol{k},\lambda} r_{\boldsymbol{k},\lambda}} e^{-i\frac{\omega_A t}{2}\sigma_z}. \tag{5.16}$$

The Hamiltonian in the interaction picture then becomes

$$\tilde{H}_I(t) = \mathcal{U}^\dagger(t) H_I \mathcal{U}(t) = \sum_{\boldsymbol{k},\lambda} \hbar\sigma_- \left(g_{\boldsymbol{k},\lambda} r_{\boldsymbol{k},\lambda} e^{-i\varpi_C t} + g^*_{\boldsymbol{k},\lambda} r^\dagger_{\boldsymbol{k},\lambda} e^{i\varpi_R t} \right) + \hbar\sigma_+ \left(g_{\boldsymbol{k},\lambda} r_{\boldsymbol{k},\lambda} e^{-i\varpi_R t} + g^*_{\boldsymbol{k},\lambda} r^\dagger_{\boldsymbol{k},\lambda} e^{i\varpi_C t} \right), \tag{5.17}$$

with the rotating and counter-rotating frequencies,

$$\varpi_R = \omega_{\boldsymbol{k}} - \omega_A, \quad \varpi_C = \omega_{\boldsymbol{k}} + \omega_A. \tag{5.18}$$

Over the shortest time scale of the system evolution, the rapidly oscillating terms with frequencies ϖ_C will average to zero. The rotating wave approximation consists in neglecting these counter-rotating terms, leaving the slower rotating terms with frequency ϖ_R. After transforming back into the Schrödinger picture we obtain the complete Hamiltonian for a two-level atom interacting with the electric field in the dipole and rotating wave approximations:

$$H = \hbar\frac{\omega_A}{2}\sigma_z + \sum_{\boldsymbol{k},\lambda} \hbar\omega_{\boldsymbol{k}} r^\dagger_{\boldsymbol{k},\lambda} r_{\boldsymbol{k},\lambda} + \sum_{\boldsymbol{k},\lambda} \hbar \left(g^*_{\boldsymbol{k},\lambda}\sigma_- r^\dagger_{\boldsymbol{k},\lambda} + g_{\boldsymbol{k},\lambda}\sigma_+ r_{\boldsymbol{k},\lambda} \right). \tag{5.19}$$

As the focus of this thesis is filtering the fluorescence of driven quantum systems, we therefore assume the atom is pumped at resonance by a coherent driving laser of frequency ω_A. This can be accounted for by taking all but one mode of the electric field in the vacuum state, and a single mode, $\boldsymbol{k}$, with single polarisation to be in a highly populated coherent state $|\beta e^{-i\omega_A t}\rangle$, with field amplitude β. We therefore replace the annihilation and creation operators in Eq. (5.19) with complex amplitudes (see Ref. [90], p. 139):

$$r_{\boldsymbol{k}} \to \beta e^{-i\omega_A t}, \quad r^\dagger_{\boldsymbol{k}} \to \beta^* e^{i\omega_A t}. \tag{5.20}$$

Dropping the constant energy and vacuum terms, we are now left with the time-dependent Hamiltonian

$$H = \hbar\frac{\omega_A}{2}\sigma_z + \hbar\frac{\Omega}{2}\left(\sigma_- e^{i\omega_A t} + \sigma_+ e^{-i\omega_A t}\right), \tag{5.21}$$

where, adopting a phase convention, we have defined the driving amplitude, also known as the *Rabi frequency*, as a real value with

$$\Omega \equiv 2|g_{\boldsymbol{k},\lambda}\beta|. \tag{5.22}$$

5.1.3 Master equation for spontaneous emission

Energy loss in a two-level atom can occur via spontaneous emission which can be treated using a master equation approach. We may follow a similar method as with Eq. (3.26), however there are some key differences. The photons emitted via spontaneous emission can be in any direction in three-dimensional space, hence the summations over the reservoir mode in Eqs. (3.22) now involve a summation over wavevector directions, $\boldsymbol{k}$, and polarisations, λ. The pseudo spin operators also have different commutation relations than the bosonic operators. With these differences in mind, we follow through the same procedure as before to obtain the

master equation for a radiatively damped two-level atom (see Ref. [75], Section 2.2.1 for details):

$$\frac{\mathrm{d}\rho}{\mathrm{d}t} = \frac{1}{i\hbar}[H_A, \rho] + \frac{\gamma}{2}\Big(2\sigma_-\rho\sigma_+ - \sigma_+\sigma_-\rho - \rho\sigma_+\sigma_-\Big), \tag{5.23}$$

where γ is the atomic excited state decay rate.

While the Hamiltonian, Eq. (5.21), contains time-dependent terms, we may transform into the interaction picture to eliminate the time dependence and the master equation still holds. Hence we may replace the Hamiltonian in Eq. (5.23) with the time-independent form,

$$H_A = \hbar\frac{\Omega}{2}\left(\sigma_- + \sigma_+\right). \tag{5.24}$$

5.1.4 Optical Bloch equations

Expanding the density operator for the two-level atom explicitly in terms of the atomic states,

$$\rho = \rho_{gg}\left|g\right\rangle\left\langle g\right| + \rho_{ge}\left|g\right\rangle\left\langle e\right| + \rho_{eg}\left|e\right\rangle\left\langle g\right| + \rho_{ee}\left|e\right\rangle\left\langle e\right|, \tag{5.25}$$

we see a correspondence between the density operator matrix elements and the averages of the pseudo-spin operators: $\langle\sigma_z\rangle = \rho_{ee} - \rho_{gg}$, $\langle\sigma_+\rangle = \rho_{ge}$, and $\langle\sigma_-\rangle = \rho_{eg}$. The master equation, Eq. (5.23), can then be rewritten in terms of the operator averages:

$$\frac{\mathrm{d}}{\mathrm{d}t}\langle\sigma_-\rangle = -\frac{\gamma}{2}\langle\sigma_-\rangle + i\frac{\Omega}{2}\langle\sigma_z\rangle, \tag{5.26a}$$

$$\frac{\mathrm{d}}{\mathrm{d}t}\langle\sigma_+\rangle = -\frac{\gamma}{2}\langle\sigma_+\rangle - i\frac{\Omega}{2}\langle\sigma_z\rangle, \tag{5.26b}$$

$$\frac{\mathrm{d}}{\mathrm{d}t}\langle\sigma_z\rangle = i\Omega\langle\sigma_-\rangle - i\Omega\langle\sigma_+\rangle - \gamma\left(\langle\sigma_z\rangle + 1\right), \tag{5.26c}$$

or, in matrix form,

$$\frac{\mathrm{d}}{\mathrm{d}t}\langle\boldsymbol{\sigma}\rangle = \boldsymbol{M}^{(\sigma)}\langle\boldsymbol{\sigma}\rangle + \boldsymbol{B}, \tag{5.27}$$

where

$$\langle\boldsymbol{\sigma}\rangle = \begin{pmatrix}\langle\sigma_-\rangle\\ \langle\sigma_+\rangle\\ \langle\sigma_z\rangle\end{pmatrix}, \quad \boldsymbol{B} = \begin{pmatrix}0\\ 0\\ -\gamma\end{pmatrix}, \quad \boldsymbol{M}^{(\sigma)} = \begin{pmatrix}-\frac{\gamma}{2} & 0 & i\frac{\Omega}{2}\\ 0 & -\frac{\gamma}{2} & -i\frac{\Omega}{2}\\ i\Omega & -i\Omega & -\gamma\end{pmatrix}. \tag{5.28}$$

These equations, also known as the *optical Bloch equations* due to their relation to the equations for a spin-half system in a magnetic field [91], provide a concise and simple method for calculating appropriate quantities, such as the population inversion of the atom. They are also very useful when considering two-time correlation functions – as we will see in the following sections – owing to the direct implementation of the quantum regression equations, as in Eqs. (3.46) and (3.47).

Another useful aspect of using the operator moment equations is the ease with which the steady-state moments can be calculated. For matrix based differential equations, such as Eq. (5.27), the steady-state vector can be found with a simple matrix inversion:

$$\langle\boldsymbol{\sigma}\rangle_{ss} = \lim_{t\to\infty}\langle\boldsymbol{\sigma}(t)\rangle = -\left[\boldsymbol{M}^{(\boldsymbol{\sigma})}\right]^{-1}\boldsymbol{B}, \tag{5.29}$$

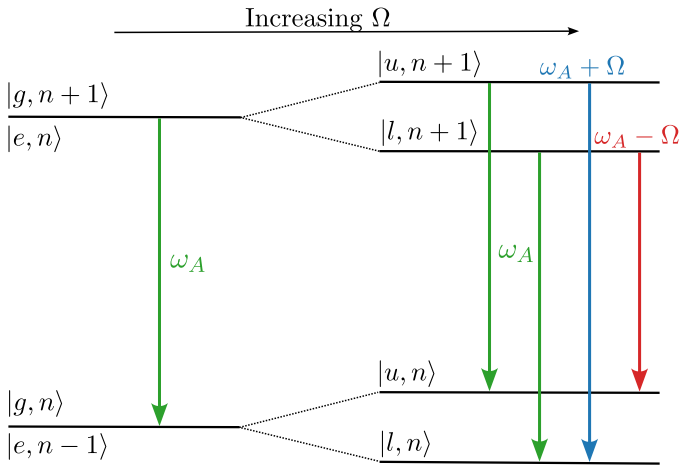

Figure 5.1: Eigenstates of the uncoupled atom-field Hamiltonian, Eq. (5.19). For weak driving, there is a degeneracy in the energy levels of the uncoupled atom-field system. As the driving strength is increased, this degeneracy is lifted allowing for more transitions.

which, in this case, gives a steady-state solution,

$$\langle \boldsymbol{\sigma} \rangle_{ss} = \begin{pmatrix} \langle \sigma_- \rangle_{ss} \\ \langle \sigma_+ \rangle_{ss} \\ \langle \sigma_z \rangle_{ss} \end{pmatrix} = \frac{1}{\gamma^2 + 2\Omega^2} \begin{pmatrix} -i\gamma\Omega \\ i\gamma\Omega \\ -\gamma^2 \end{pmatrix}. \tag{5.30}$$

5.1.5 Dressed states

The bare atomic states, $|g\rangle$ and $|e\rangle$, are eigenstates of the bare Hamiltonian, Eq. (5.11), yet they are not eigenstates of the full Hamiltonian, Eq. (5.24), when coherent driving is introduced. If we write the Hamiltonian in matrix form we can then diagonalise it to find the eigenstates and corresponding eigenenergies:

$$H_A |u\rangle = +\hbar\frac{\Omega}{2} |u\rangle, \quad |u\rangle = \frac{1}{\sqrt{2}}\Big(|e\rangle + |g\rangle \Big), \tag{5.31a}$$

$$H_A |l\rangle = -\hbar\frac{\Omega}{2} |l\rangle, \quad |l\rangle = \frac{1}{\sqrt{2}}\Big(|e\rangle - |g\rangle \Big). \tag{5.31b}$$

These eigenstates – also known as the atomic *dressed states* – are a direct result of the interaction of the atomic field with a quantised electromagnetic field. Briefly returning to the uncoupled atom-field Hamiltonian, Eq. (5.19), we see there is a degeneracy in the $|g, n\rangle$ and $|e, n-1\rangle$ states for low driving amplitudes, as shown on the left-hand side of Fig. 5.1. As the driving amplitude is increased, this degeneracy is lifted and we see a splitting of the dressed-state energies. We have, however, assumed the field to be in a highly populated coherent state, hence the Fock state hierarchy is not resolvable. Therefore we drop the Fock state labelling in Eqs. 5.31, even though we have kept them in Fig. 5.1.

Later on in this chapter we will move into a *secular approximation* by rewriting our atomic operators, Eqs. (5.10) and (5.12), in terms of these dressed states. This allows us to derive analytical expressions for the first- and second-order correlation functions, as defined in the following sections, for each of the possible dressed state transitions in the limit of very strong

driving, $\Omega \gg \gamma$. These results will then act as a benchmark to evaluate the effectiveness of the single-mode and multi-mode array filters.

5.2 Fluorescence Spectrum of the Two-Level Atom

The dressed state picture may tell us what frequencies we expect to be emitted by the atom, but it does not tell us the entire story. Here we will investigate the fluorescence, or power, spectrum of the atom. To do so, we must first introduce the *first-order correlation function*, a quantity which tells us how correlated an electric field is at two different times. Then, using the *Wiener-Khinchin* theorem, we present the *coherent* and *incoherent* spectra of the emitted light.

5.2.1 First-order coherence

We introduce the general *first-order correlation function*,

$$G^{(1)}(\boldsymbol{r}, t; \boldsymbol{r}', t') = \langle \boldsymbol{E}^{(-)}(\boldsymbol{r}, t) \boldsymbol{E}^{(+)}(\boldsymbol{r}', t') \rangle, \tag{5.32}$$

which quantifies the correlation of the electric field at two different points, $\boldsymbol{r}$ and $\boldsymbol{r}'$, and at two different times, t and t' (see Ref. [78], p. 221). In this thesis we are only interested in the *temporal coherence*, that is we consider a solitary point detector, where $\boldsymbol{r} = \boldsymbol{r}'$, such that only the temporal dependence remains. Defining the time delay variable $\tau \equiv t - t'$, we introduce the *normalised first-order temporal correlation function*:

$$g^{(1)}(\tau) = \frac{\langle \boldsymbol{E}^{(-)}(t) \boldsymbol{E}^{(+)}(t+\tau) \rangle}{\sqrt{\langle \boldsymbol{E}^{(-)}(t) \boldsymbol{E}^{(+)}(t) \rangle \langle \boldsymbol{E}^{(-)}(t+\tau) \boldsymbol{E}^{(+)}(t+\tau) \rangle}}, \tag{5.33}$$

which is bounded by the range

$$|g^{(1)}(\tau)| \leq 1. \tag{5.34}$$

If the field is completely coherent then $|g^{(1)}(\tau)| = 1$ for all τ, whereas the field becomes completely uncorrelated as $\tau \to \infty$, $g^{(1)}(\tau \to \infty) \to 0$ (see Ref. [92], p. 73).

5.2.2 The Mollow triplet

Following on from Section 3.1.4 – Eqs. (3.32 - 3.34) in particular – we may rewrite the generalised correlation function, Eq. (5.33), entirely in terms of the atomic operators, σ_+ and σ_-. Similar to the steps involved for calculating the master equation, the summation of reservoir modes now includes a summation over wavevectors and polarisations. Following the method as outlined by Carmichael (Ref. [75], Section 2.3.1), we indeed find:

$$\boldsymbol{E}^{(+)}(\boldsymbol{r}, t) = \boldsymbol{E}_s^{(+)}(\boldsymbol{r}, t) \propto \sigma_-(t - r/c), \tag{5.35}$$

where, with the reservoir in thermal equilibrium at zero temperature, the free field makes no contribution to the normal-ordered correlation functions. We therefore introduce the *normalised*

first-order correlation function for a resonantly driven two-level atom:

$$g^{(1)}(t,\tau) = \frac{\langle \sigma_+(t)\sigma_-(t+\tau)\rangle}{\sqrt{\langle \sigma_+\sigma_-(t)\rangle\langle \sigma_+\sigma_-(t+\tau)\rangle}}, \tag{5.36}$$

or, in the steady-state limit,

$$g^{(1)}_{ss}(\tau) = \lim_{t\to\infty} g^{(1)}(t,\tau) = \frac{\langle \sigma_+(0)\sigma_-(\tau)\rangle_{ss}}{\langle \sigma_+\sigma_-\rangle_{ss}}. \tag{5.37}$$

As mentioned in Section 3.2, the power spectrum of the field can be calculated from the Fourier transform of the first-order correlation function, which is a form of the *Wiener-Khinchin* theorem [93, 94]:

$$S(\omega) = \frac{1}{2\pi}\int_{-\infty}^{\infty} e^{i\omega\tau} g^{(1)}_{ss}(\tau)\mathrm{d}\tau. \tag{5.38}$$

In the steady state there exists quantum fluctuations described by the operators (Ref. [75], Section 2.3.4):

$$\Delta\sigma_\pm = \sigma_\pm - \langle\sigma_\pm\rangle_{ss}, \tag{5.39a}$$

$$\Delta\sigma_z = \sigma_z - \langle\sigma_z\rangle_{ss}. \tag{5.39b}$$

We therefore decompose the power spectrum, as defined by Eq. (5.38), into *coherent* and *incoherent* components, corresponding to the elastic and inelastic scattering of light from the atom (Ref. [73], pp. 207-208):

$$S(\omega) = S_{\mathrm{coh}}(\omega) + S_{\mathrm{inc}}(\omega), \tag{5.40}$$

where

$$S_{\mathrm{coh}}(\omega) = \frac{1}{2\pi}\frac{1}{\langle\sigma_+\sigma_-\rangle_{ss}}\int_{-\infty}^{\infty} e^{i\omega\tau}\langle\sigma_+\rangle_{ss}\langle\sigma_-\rangle_{ss}\mathrm{d}\tau, \tag{5.41a}$$

$$S_{\mathrm{inc}}(\omega) = \frac{1}{2\pi}\frac{1}{\langle\sigma_+\sigma_-\rangle_{ss}}\int_{-\infty}^{\infty} e^{i\omega\tau}\langle\Delta\sigma_+(0)\Delta\sigma_-(\tau)\rangle_{ss}\mathrm{d}\tau. \tag{5.41b}$$

We find that the ratio of the coherent and incoherent intensities is

$$\frac{I_{\mathrm{inc}}}{I_{\mathrm{coh}}} = \frac{\langle\Delta\sigma_+\Delta\sigma_-\rangle_{ss}}{\langle\sigma_+\rangle_{ss}\langle\sigma_-\rangle_{ss}} = \frac{2\Omega^2}{\gamma^2}, \tag{5.42}$$

hence for weak driving, $\Omega \ll \gamma$, coherent scattering dominates, and for strong driving, $\Omega \gg \gamma$, incoherent scattering dominates.

We plot the first-order correlation, Eq. (5.37), in Fig. 5.2 in the weak and strong driving regimes, for $\Omega/\gamma = 0.01$, and $\Omega/\gamma = 5$. In the weak driving limit, there is a small effect of the weak Rabi frequency in the short time-scale ($\tau \ll \gamma$), yet in the later times it decays exponentially. In the strong driving regime we see a frequency term occurring, known as *Rabi oscillations*; the atomic population is oscillating between the excited and ground states.

For the two-level atom the first-order correlation function is entirely real, resulting in a symmetric power spectrum. We see this in Fig. 5.3, where the incoherent power spectrum of the correlation functions in Fig. 5.2 are calculated. For the weak drive regime, the atomic spectrum is Lorentzian, situated at the atomic frequency, ω_A, and with fullwidth γ. As the

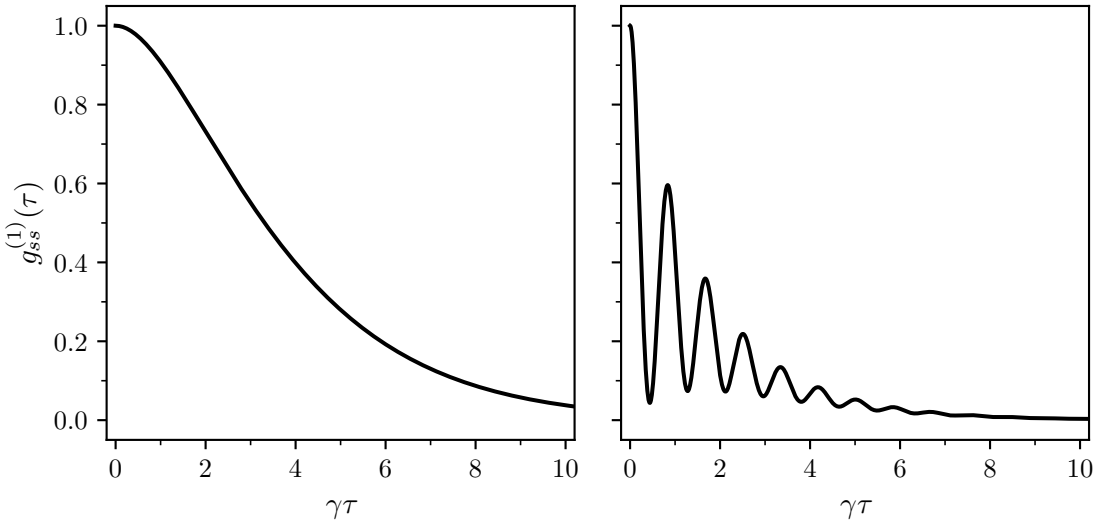

Figure 5.2: Normalised first-order correlation function, $g^{(1)}_{ss}(\tau)$ for the driven two-level atom for $\Omega/\gamma = 0.1$ (left) and $\Omega/\gamma = 7.5$ (right). When driven on resonance, the correlation function is entirely real and hence the spectra will be symmetrical.

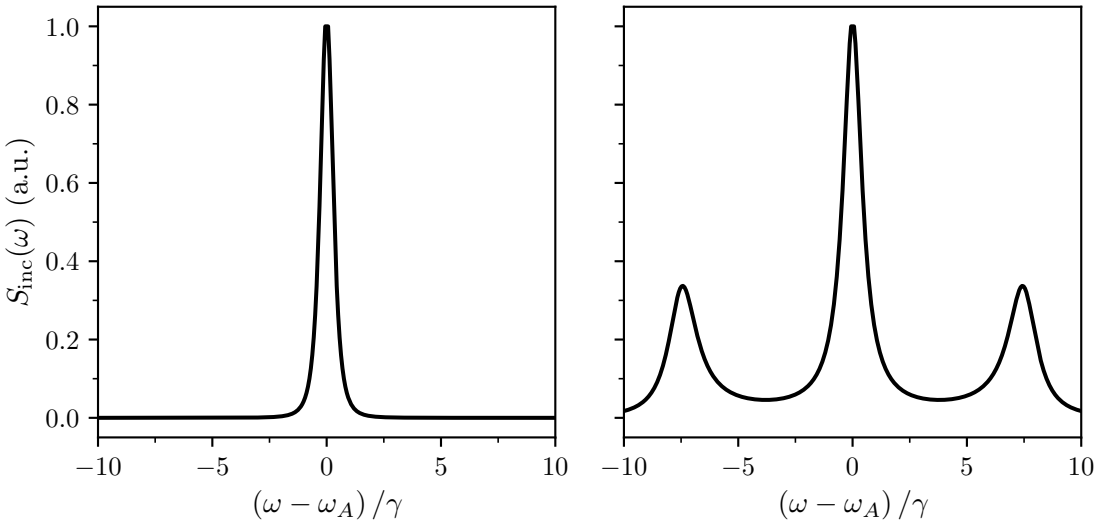

Figure 5.3: Incoherent power spectra of the driven two-level atom for $\Omega/\gamma = 0.1\gamma$ (left) and $\Omega/\gamma = 7.5$ (right), calculated by taking the Fourier transform of the correlation functions shown in Fig. 5.2.

drive strength is increased, side peaks emerge at $\omega_A \pm \Omega$, giving shape to the well known Mollow triplet [1, 2]. These side-peaks are a direct result of transitions amongst the atom's dressed states [4], Eqs. (5.31), as illustrated in Fig. 5.1.

5.3 Photon Correlations and Antibunching

In this section we will introduce the *second-order correlation function*, the concept of *second-order coherence* and what it means for light to be "bunched" and "antibunched".

5.3.1 Second-order coherence

The second-order correlation function is a measure of the fluctuations in the intensity of a field (Ref. [78], p. 229), and is defined classically as

$$g^{(2)}(t,\tau) = \frac{\langle I(t)I(t+\tau)\rangle}{\langle I(t)\rangle\langle I(t+\tau)\rangle}, \tag{5.43}$$

where $I(t)$ is the intensity of the field at time t. If we consider a statistically stationary classical source, such that $\langle I(t)\rangle = \langle I(t+\tau)\rangle = \langle I\rangle$, then Eq. (5.43) can be written as

$$\begin{aligned} g^{(2)}(\tau) &= \frac{\langle I\rangle^2 + \langle I\rangle\langle \Delta I(t)\rangle + \langle I\rangle\langle \Delta I(t+\tau)\rangle + \langle \Delta I(t)\Delta I(t+\tau)\rangle}{\langle I\rangle^2} \\ &= 1 + \frac{\langle \Delta I(t)\Delta I(t+\tau)\rangle}{\langle I\rangle^2}, \end{aligned} \tag{5.44}$$

where we have introduced the field fluctuation, $\Delta I(t) = I(t) - \langle I\rangle$, as in Eq. (5.39). We note here that the fluctuation $\langle \Delta I(t)\rangle = \langle \Delta I(t+\tau)\rangle = 0$ by definition. Equation (5.44) shows two distinct properties: firstly, in the long time limit, $\tau \to \infty$, the intensity fluctuations become completely uncorrelated with

$$g^{(2)}(\tau \to \infty) = 1; \tag{5.45}$$

and secondly, for zero time delay the correlation is bounded by

$$g^{(2)}(\tau = 0) = \frac{\langle I^2\rangle}{\langle I\rangle^2} \geq 1. \tag{5.46}$$

One of the first distinctly quantum optical experiments was the Hanbury Brown and Twiss experiment [95–97], though it was initially motivated by stellar interferometry. This experiment investigated the intensity correlations of light emitted from distant stars by splitting the light through a 50:50 beam splitter and correlating the time between detections in each arm, as depicted in Fig. 5.4a. While the technology has changed since the original Hanbury Brown and Twiss papers, the principle of correlating light with two detectors has remained and forms the basis of this work.

If the field is in a coherent state, the correlation function is unity for all time, $g^{(2)}(\tau) = 1$. In the case of thermal light there are larger fluctuations in the intensity, resulting in an increased

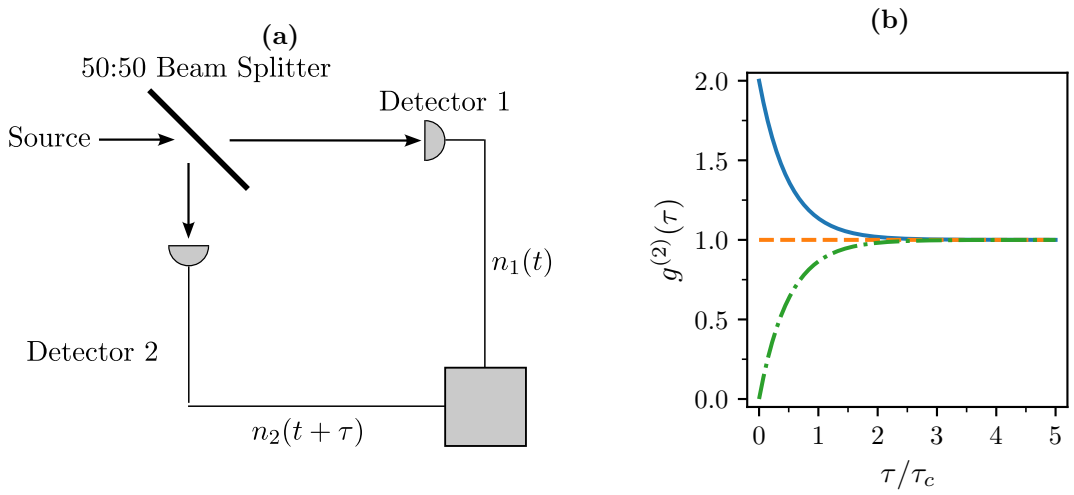

Figure 5.4: Schematic of a Hanbury Brown and Twiss device (a) and the $g^{(2)}(\tau)$ functions (b) for bunched (blue, solid), coherent (orange, dashed), and antibunched (green, dot-dash) light.

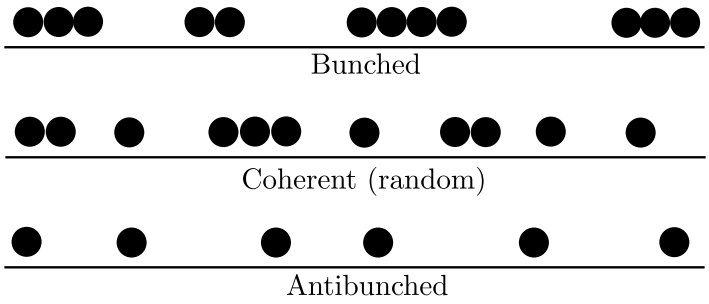

Figure 5.5: Temporal distribution of photon detector "clicks" for bunched, coherent, and antibunched light.

initial correlation, with (Ref. [73], p. 40)

$$g^{(2)}(\tau = 0) = 1 + |g^{(1)}(\tau = 0)|^2 = 2. \tag{5.47}$$

From this result we see that there is a high probability for detecting a photon at detector 2 *at the same time* a photon is detected at the first detector. From here we can make two important distinctions: *bunched light*, where photons are detected in clusters, with $g^{(2)}(0) > 1$; and *coherent light*, where photons are detected at random intervals, with $g^{(2)}(0) = 1$. These two classes of photon statistics are represented in Figs. 5.4b and 5.5, as well as the third classification which we will introduce in the following section.

5.3.2 Antibunching

We return now to familiar quantum notation, and introduce the quantum mechanical second-order correlation function for a stationary field, as first discussed by Glauber in 1963 [8]:

$$g^{(2)}(t,\tau) = \frac{\langle E^{(-)}(t)E^{(-)}(t+\tau)E^{(+)}(t+\tau)E^{(+)}(t)\rangle}{\langle E^{(-)}E^{(+)}(t)\rangle\langle E^{(-)}E^{(+)}(t+\tau)\rangle}. \tag{5.48}$$

As with the first-order correlation function, we may write this in terms of the source operators for the field scattered by the two-level atom, which, in the steady-state limit, is:

$$g^{(2)}_{ss}(\tau) = \lim_{t\to\infty} g^{(2)}(t,\tau) = \frac{\langle \sigma_+(0)\sigma_+\sigma_-(\tau)\sigma_-(0)\rangle_{ss}}{\langle \sigma_+\sigma_-\rangle^2_{ss}}. \tag{5.49}$$

From the optical Bloch equations, Eqs. (5.26), we may derive an analytic solution (see Ref. [75], Section 2.3.5 for details),

$$g^{(2)}(\tau) = 1 - e^{-\frac{3\gamma}{4}\tau}\left[\cosh(\delta\tau) + \frac{3\gamma}{4\delta}\sinh(\delta\tau)\right], \tag{5.50}$$

where

$$\delta = \sqrt{\left(\frac{\gamma}{4}\right)^2 - \Omega^2}. \tag{5.51}$$

From Eq. (5.50) we see that this correlation has an initial value of zero, which is impossible for a classical source. This entirely quantum effect gives rise to the third classification of photon statistics that we consider: *antibunching* [9, 12, 98]. In the case of this driven two-level system, the atom can only store a single quantum of energy and must be excited again before emitting another photon, hence only single-photon emissions occur. In Fig. 5.6, we plot the normalised second-order correlation function for the two-level atom in the weak and low driving regimes. For weak driving, as the atom emits a photon, the state population slowly returns back to its steady state. For stronger driving, the atomic state oscillates between the ground and excited states. As with the first-order correlation function, we again see this in the atomic photon correlations.

It has also been shown that, in the weak driving regime, antibunching is a result of the generation of squeezed resonance fluorescence [99, 100]. This has been proven again in the recent experimental works of Hanschke et al. [35] and Phillips et al. [34].

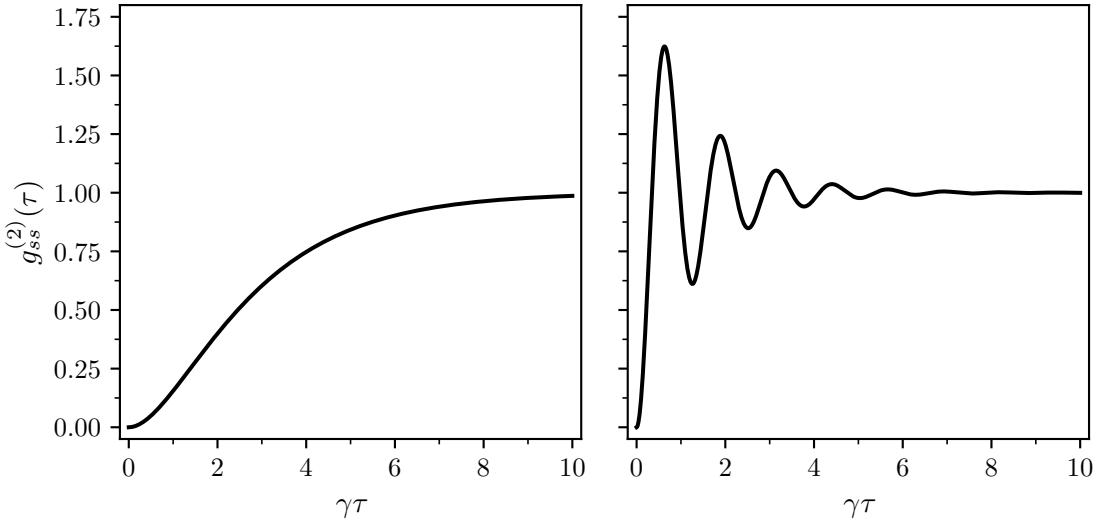

Figure 5.6: Normalised second-order correlation function, $g^{(2)}_{ss}(\tau)$ of the driven two-level atom for $\Omega/\gamma = 0.1$ (left) and $\Omega/\gamma = 5$ (right).

5.4 Dressed State Correlation Functions

In this section we will examine the evolution of the two-level atom in terms of the dressed states by making the *secular approximation* [23]. We may rewrite the original master equation in terms of dressed state operators, giving us separate decay terms for each of the possible dressed state transitions: $|u\rangle \to |u\rangle$ and $|l\rangle \to |l\rangle$; $|u\rangle \to |l\rangle$; and $|l\rangle \to |u\rangle$. With this expanded master equation, we then derive first- and second-order correlation functions for each of the dressed-state transitions, giving us ideal benchmarks with which to compare our frequency filtered correlations in the following chapter.

5.4.1 Dressed state optical Bloch equations

Assuming the atom is strongly driven, with $\Omega \gg \gamma$, and side-peaks in the Mollow spectrum are sufficiently separated in frequency space, we may then make a secular approximation and rewrite the evolution of the system, Eq. (5.23), in terms of dressed-state operators. Rearranging Eqs. (5.31), we write the bare atomic states in terms of the dressed states:

$$|g\rangle = \frac{1}{\sqrt{2}}\Big(|u\rangle + |l\rangle\Big), \quad |e\rangle = \frac{1}{\sqrt{2}}\Big(|u\rangle - |l\rangle\Big). \tag{5.52}$$

This allows us to rewrite the atomic raising and lowering operators, Eq. (5.12), as

$$\sigma_{\pm} = \frac{1}{2}\Big(|u\rangle\langle u| - |l\rangle\langle l|\Big) \mp \frac{1}{2}\Big(|u\rangle\langle l| - |l\rangle\langle u|\Big). \tag{5.53}$$

We then transform into a rotating frame with unitary evolution operator

$$\mathcal{U}(t) = e^{\frac{1}{i\hbar}H_A t}, \tag{5.54}$$

and hence the Lindblad master equation becomes

$$\frac{\mathrm{d}\tilde{\rho}}{\mathrm{d}t} = \frac{\gamma}{2}\Big(2\tilde{\sigma}_-(t)\tilde{\rho}(t)\tilde{\sigma}_+(t) - \tilde{\sigma}_+(t)\tilde{\sigma}_-(t)\tilde{\rho}(t) - \tilde{\rho}(t)\tilde{\sigma}_+(t)\tilde{\sigma}_-(t)\Big), \tag{5.55}$$

with density operator

$$\tilde{\rho}(t) = \mathcal{U}^\dagger\tilde{\rho}(t)\mathcal{U}(t), \tag{5.56}$$

and decay operators

$$\tilde{\sigma}_\pm(t) = \mathcal{U}^\dagger(t)\tilde{\sigma}_\pm(t)\mathcal{U}(t) = \frac{1}{2}\Big(\,|u\rangle\langle u| - |l\rangle\langle l|\,\Big) \mp \frac{1}{2}\Big(e^{i\Omega t}\,|u\rangle\langle l| - e^{-i\Omega t}\,|l\rangle\langle u|\,\Big), \tag{5.57}$$

Expanding the decay operators in the dressed state representation, we then make the secular approximation by dropping any rapidly oscillating terms so that the master equation in the interaction picture now becomes

$$\begin{aligned}\frac{\mathrm{d}\tilde{\rho}}{\mathrm{d}t} = {}& \frac{\gamma}{8}\Big(2\,|u\rangle\langle u|\,\tilde{\rho}(t)\,|u\rangle\langle u| - |u\rangle\langle u|\,\tilde{\rho}(t) - \tilde{\rho}(t)\,|u\rangle\langle u|\,\Big)\\ &+ \frac{\gamma}{8}\Big(2\,|l\rangle\langle l|\,\tilde{\rho}(t)\,|l\rangle\langle l| - |l\rangle\langle l|\,\tilde{\rho}(t) - \tilde{\rho}(t)\,|l\rangle\langle l|\,\Big)\\ &+ \frac{\gamma}{8}\Big(2\,|u\rangle\langle l|\,\tilde{\rho}(t)\,|l\rangle\langle u| - |l\rangle\langle l|\,\tilde{\rho}(t) - \tilde{\rho}(t)\,|l\rangle\langle l|\,\Big)\\ &+ \frac{\gamma}{8}\Big(2\,|l\rangle\langle u|\,\tilde{\rho}(t)\,|u\rangle\langle l| - |u\rangle\langle u|\,\tilde{\rho}(t) - \tilde{\rho}(t)\,|u\rangle\langle u|\,\Big)\\ &- \frac{\gamma}{8}\Big(\,|u\rangle\langle u|\,\tilde{\rho}(t)\,|l\rangle\langle l| + |l\rangle\langle l|\,\tilde{\rho}(t)\,|u\rangle\langle u|\,\Big).\end{aligned} \tag{5.58}$$

Transforming back out of the interaction picture, we introduce the *dressed-state operators for a driven two-level atom*,

$$\sigma_-^D = |l\rangle\langle u|\,, \quad \sigma_+^D = |u\rangle\langle l|\,, \quad \sigma_z^D = |u\rangle\langle u| - |l\rangle\langle l|\,, \tag{5.59}$$

and write the master equation in the secular approximation:

$$\begin{aligned}\frac{\mathrm{d}\rho}{\mathrm{d}t} = -i\frac{\Omega}{2}[\sigma_z^D, \rho] &+ \frac{\gamma}{8}\Big(2\sigma_-^D\rho\sigma_+^D - \sigma_+^D\sigma_-^D\rho - \rho\sigma_+^D\sigma_-^D\Big)\\ &+ \frac{\gamma}{8}\Big(2\sigma_+^D\rho\sigma_-^D - \sigma_-^D\sigma_+^D\rho - \rho\sigma_-^D\sigma_+^D\Big)\\ &+ \frac{\gamma}{4}\Big(\sigma_z^D\rho\sigma_z^D - \rho\Big).\end{aligned} \tag{5.60}$$

Here we can identify three main processes: a decay from the dressed state $|u\rangle$ to the state $|l\rangle$; a decay from the state $|l\rangle$ to the state $|u\rangle$; and, from the last term in Eq. (5.60), an atomic dressed state "dephasing", which does not change the dressed state populations.

From Eq. (5.60) we may write coupled moment equations for the dressed-state "spin" operators, resulting in a set of equations similar to the optical Bloch equations, Eqs. (5.26), but now decoupled from each other:

$$\frac{\mathrm{d}}{\mathrm{d}t}\langle\sigma_-^D\rangle = -\left(\frac{3\gamma}{4} + i\Omega\right)\langle\sigma_-^D\rangle, \tag{5.61a}$$

$$\frac{\mathrm{d}}{\mathrm{d}t}\langle\sigma_+^D\rangle = -\left(\frac{3\gamma}{4} + i\Omega\right)\langle\sigma_-^D\rangle, \tag{5.61b}$$

$$\frac{\mathrm{d}}{\mathrm{d}t}\langle\sigma_z^D\rangle = -\frac{\gamma}{2}\langle\sigma_z^D\rangle. \tag{5.61c}$$

These have simple solutions:

$$\langle\sigma_-^D(t)\rangle = \langle\sigma_-^D(0)\rangle e^{-\left(\frac{3\gamma}{4}+i\Omega\right)t}, \tag{5.62a}$$

$$\langle\sigma_+^D(t)\rangle = \langle\sigma_+^D(0)\rangle e^{-\left(\frac{3\gamma}{4}-i\Omega\right)t}, \tag{5.62b}$$

$$\langle\sigma_z^D(t)\rangle = \langle\sigma_z^D(0)\rangle e^{-\frac{\gamma}{2}t}. \tag{5.62c}$$

5.4.2 First-order correlation functions in the secular approximation

In this strong driving limit, we expect each peak of the Mollow triplet, Fig. 5.3, to be well separated resulting in three distinct Lorentzians. Each peak is then linked to of the dressed state operators: the left-peak is the result of the transition $|l\rangle \to |u\rangle$ with operator σ_+^D; the central peak is a result of the degenerate transitions $|u\rangle \to |u\rangle$ and $|l\rangle \to |l\rangle$ which we may associate with the dephasing term, σ_z^D; and the right-peak is a result of the transition $|u\rangle \to |l\rangle$ with operator σ_-^D.

With these three operators and the quantum regression equations, Eqs. (3.47), we may derive first-order correlation functions for each of these three dressed-state transitions:

$$g^{(1)}_{\text{centre}}(\tau) = \frac{\langle\sigma_z^D(0)\sigma_z^D(\tau)\rangle}{\langle\sigma_z^D\sigma_z^D\rangle_{ss}} = e^{-\frac{\gamma}{2}\tau}, \tag{5.63a}$$

$$g^{(1)}_{\text{left}}(\tau) = \frac{\langle\sigma_-^D(0)\sigma_+^D(\tau)\rangle}{\langle\sigma_-^D\sigma_+^D\rangle_{ss}} = e^{-\left(\frac{3\gamma}{4}-i\Omega\right)\tau}, \tag{5.63b}$$

$$g^{(1)}_{\text{right}}(\tau) = \frac{\langle\sigma_+^D(0)\sigma_-^D(\tau)\rangle}{\langle\sigma_+^D\sigma_-^D\rangle_{ss}} = e^{-\left(\frac{3\gamma}{4}+i\Omega\right)\tau}. \tag{5.63c}$$

Taking the Fourier transforms of these three correlation functions, we see there are indeed three distinct peaks,

$$S_{\text{centre}}(\omega) = \frac{1}{2\pi}\frac{\gamma}{(\gamma/2)^2 + \omega^2}, \tag{5.64a}$$

$$S_{\text{left}}(\omega) = \frac{1}{2\pi}\frac{3\gamma/2}{(3\gamma/4)^2 + (\omega+\Omega)^2}, \tag{5.64b}$$

$$S_{\text{right}}(\omega) = \frac{1}{2\pi}\frac{3\gamma/2}{(3\gamma/4)^2 + (\omega-\Omega)^2}, \tag{5.64c}$$

that is, the central peak is a Lorentzian with half-width $\gamma/2$, and the side-peaks are Lorentzians with half-width $3\gamma/4$, situated at $\omega = \pm\Omega$.

5.4.3 Second-order correlation functions in the secular approximation

We follow the same procedure now for the second-order auto-correlation functions for each frequency component. In the complete picture we know that the light emitted from the atom is completely antibunched. When looking at each component individually, however, we see a

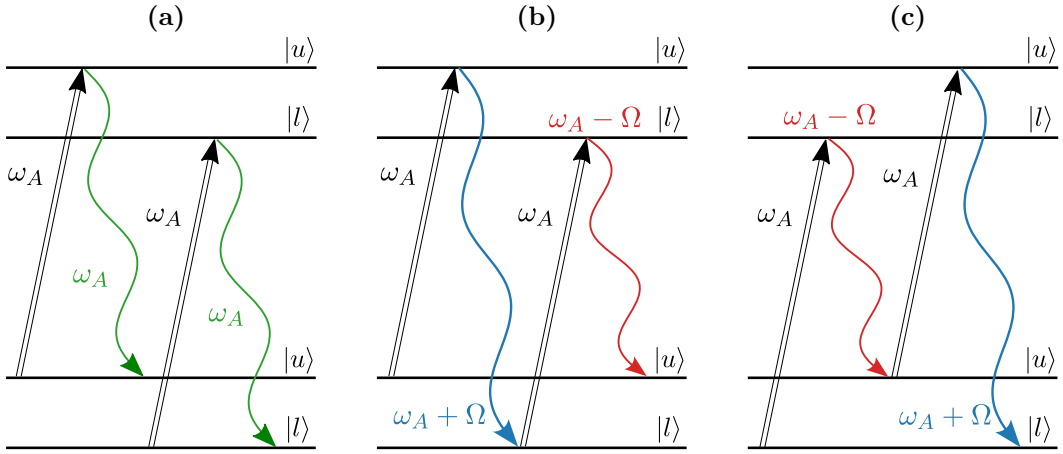

Figure 5.7: Photon emissions from the atomic dressed states and their orderings for (a) central peak photons, (b) a left-peak photon followed by a right-peak photon, and (c) a right-peak photon followed by a left-peak photon.

difference. For the central peak photons, due to the degenerate dressed state transitions, the light is entirely second-order coherent, with auto-correlation function

$$g^{(2)}_{\text{centre}}(\tau) = \frac{\langle \sigma_z^D(0)\sigma_z^D\sigma_z^D(\tau)\sigma_z^D(0)\rangle}{\langle \sigma_z^D\sigma_z^D\rangle^2_{ss}} = 1. \tag{5.65}$$

Left- and right-peak photons exhibit behaviour similar to the two-level atom, in that the light from these transitions is also antibunched, as can be seen in the auto-correlation functions:

$$\begin{aligned} g^{(2)}_{\text{left}}(\tau) &= \frac{\langle \sigma_-^D(0)\sigma_-^D\sigma_+^D(\tau)\sigma_+^D(0)\rangle}{\langle \sigma_-^D\sigma_+^D\rangle^2_{ss}} \\ &= \frac{1}{2}\frac{1}{\langle \sigma_-^D\sigma_+^D\rangle_{ss}} - \frac{1}{2}\frac{\langle \sigma_-^D(0)\sigma_z^D(\tau)\sigma_+^D(0)\rangle}{\langle \sigma_-^D\sigma_+^D\rangle^2_{ss}} \\ &= 1 - 2\langle \sigma_-^D\sigma_z^D\sigma_+^D\rangle_{ss} e^{-\frac{\gamma}{2}\tau} \\ &= 1 - e^{-\frac{\gamma}{2}\tau}, \end{aligned} \tag{5.66a}$$

and

$$g^{(2)}_{\text{right}}(\tau) = \frac{\langle \sigma_+^D(0)\sigma_+^D\sigma_-^D(\tau)\sigma_-^D(0)\rangle}{\langle \sigma_+^D\sigma_-^D\rangle^2_{ss}} = 1 - e^{-\frac{\gamma}{2}\tau}. \tag{5.66b}$$

While the auto-correlation tells us the conditional likelihood of detecting an emission from a transition some time τ after a first detection, the cross-correlation allows us to look at two different transitions. As an example, if we consider detecting a left-peak photon at $\tau = 0$, we see there is an increased probability of detecting a right-peak photon at the same time, with cross-correlation function

$$g^{(2)}_{\text{left}\to\text{right}}(\tau) = \frac{\langle \sigma_+^D(0)\sigma_-^D\sigma_+^D(\tau)\sigma_-^D(0)\rangle}{\langle \sigma_+^D\sigma_-^D\rangle_{ss}\langle \sigma_-^D\sigma_+^D\rangle_{ss}} = 1 + e^{-\frac{\gamma}{2}\tau} = g^{(2)}_{\text{right}\to\text{left}}(\tau). \tag{5.67}$$

This is to be expected as, shown in Fig. 5.7, the ordering of the dressed transitions must conserve the total energy of the photons absorbed from the driving field.

Similarly, for a side-peak to central-peak correlation function, for example the right-peak, we have second-order coherence, with

$$g^{(2)}_{\text{right}\to\text{centre}}(\tau) = \frac{\langle \sigma_+^D(0)\sigma_z^D\sigma_z^D(\tau)\sigma_-^D(0)\rangle_{ss}}{\langle \sigma_+^D\sigma_-^D\rangle_{ss}\langle \sigma_z^D\sigma_z^D\rangle_{ss}} = 1. \tag{5.68}$$

While the equations in this section have been derived in the secular approximation, in the next chapter we will attempt to recover the same results using a frequency filter approach. As previously mentioned, Eqs. (5.65 - 5.67) will then be used to compare with the calculated frequency filtered photon correlations.

6 Multi-Mode Frequency Filtered Mollow Triplet

Historically, there has been great interest in measuring and calculating photon correlations from the driven two-level atom; of particular interest are photon correlations from each component of the Mollow triplet [14, 15, 19, 24, 27]. With the recent developments in quantum dot technology, there has also been a surge in interest in frequency-filtered photon correlations of the Mollow triplet [34, 35, 38, 101, 102], due to their use as single-photon sources, generators of two-photon pulses, as well as entangled photons [103–107], all of which have applications in quantum computing and cryptography.

Much of the research has used either tunable single-mode cavities as the frequency filter, or the technique developed by del Valle et al. [43], which employs N tunable two-level atoms. Both methods, however, still result in Lorentzian profile filters being used. The standard approach, then, considers the case where the side-peaks of the Mollow triplet are well separated, i.e., $\Omega \gg \gamma$. This approach works well for the two-level atom, but cannot be guaranteed for any general system. We therefore wish to demonstrate the effectiveness of the multi-mode array filter in the case where the side-peaks are separated, but not extremely so.

The focus of this chapter is to use the resonantly driven two-level atom as a "test scenario" for the multi-mode array filter. With the long studied history of the Mollow triplet – and the derived ideal correlation functions, Eqs. (5.65) - (5.67) – we can explore the effect that different filtering parameters have on the effectiveness of the filter, much like in Chapter 4.

We begin this chapter by introducing the mathematical model upon which we base our calculations. This model extends the open cascaded system theory in Section 3.3 to include the two-level atom and the multi-mode array filter. We then calculate the frequency-filtered incoherent power spectra of the single-mode and multi-mode array filters, comparing them both against the unfiltered Mollow triplet. We then move towards the main quantity of interest of this thesis: *frequency-filtered photon correlations*. We calculate and compare both auto- and cross-correlation functions, highlighting the superior performance of the multi-mode array filter, relative to the single-mode Lorentzian filter.

6.1 Frequency Filtering Model for Resonance Fluorescence

Having already introduced the multi-mode array filter and the concepts behind the resonantly driven two-level atom, we now apply the cascaded open quantum systems theory to these two systems.

6.1.1 Hamiltonian and master equation

To model the frequency filtering of the two-level atom, we treat the atom as the source subsystem of a cascaded open system. In particular, the atomic fluorescence is assumed to be uniformly distributed amongst, or cascaded evenly into, all of the cavities of the multi-mode

array filter. We therefore start with the general cascaded system's Hamiltonian, Eq. (3.66), and replace the source system with the driven atomic Hamiltonian, Eq. (5.24), and the target subsystem with the multi-mode array, Eq. (4.16). Summing over the cavity modes, the total Hamiltonian for our atom-filter cascaded system is then (in a frame rotating at the atomic transition frequency):

$$H = \hbar\frac{\Omega}{2}\left(\sigma_- + \sigma_+\right) + \hbar\sum_{j=-N}^{N}\Delta\omega_j a_j^\dagger a_j + \frac{i\hbar}{2}\sum_{j=-N}^{N}\left(\mathcal{E}_j^* a_j\sigma_+ - \mathcal{E}_j a_j^\dagger\sigma_-\right), \tag{6.1}$$

where

$$\Delta\omega_j = (\omega_0 + j\delta\omega) - \omega_A \tag{6.2}$$

is the frequency detuning of the j^{th} mode from atomic resonance, with mode frequency spacing $\delta\omega$, and

$$\mathcal{E}_j = \sqrt{\frac{\gamma\kappa}{2N+1}}e^{imj\pi/N} \tag{6.3}$$

is the mode-dependent coupling, as in Eq. (4.18).

The atomic resonance fluorescence is evenly coupled into an array of $2N+1$ tunable single-mode cavities, as depicted in Fig. 6.1a. We model each mode with two lossy mirrors, both with loss rates $\kappa/2$, resulting in two separate decay channels: reflection of the input field and transmission from the cavity mode through the first mirror is directed towards one photon detector, while transmission through the cavity mode is directed towards another photon detector (see Fig. 6.1b). We therefore expand the cascaded systems master equation, Eq. (3.68), to allow for both decay channels, i.e.,

$$\begin{aligned}\frac{\mathrm{d}\rho}{\mathrm{d}t} = \frac{1}{i\hbar}[H,\rho] &+ \frac{\kappa}{2}\sum_{j=-N}^{N}\left(2a_j\rho a_j^\dagger - a_j^\dagger a_j\rho - \rho a_j^\dagger a_j\right)\\ &+ \frac{1}{2}\left(2C_j\rho C_j^\dagger - C_j^\dagger C_j\rho - \rho C_j^\dagger C_j\right),\end{aligned} \tag{6.4}$$

with cascaded decay operator:

$$C_j = \sqrt{\frac{\gamma}{2N+1}}e^{imj\pi/N}\sigma_- + \sqrt{\kappa}a_j. \tag{6.5}$$

We may expand out each of the terms in Eq. (6.4) to give us a less compact, yet more intuitive master equation,

$$\begin{aligned}\frac{\mathrm{d}\rho}{\mathrm{d}t} = &-i\frac{\Omega}{2}[\sigma_+ + \sigma_-,\rho] + \frac{\gamma}{2}\left(2\sigma_-\rho\sigma_+ - \sigma_+\sigma_-\rho - \rho\sigma_+\sigma_-\right)\\ &- i\sum_{j=-N}^{N}\Delta\omega_j[a_j^\dagger a_j,\rho] + \kappa\sum_{j=-N}^{N}\left(2a_j\rho a_j^\dagger - a_j^\dagger a_j\rho - \rho a_j^\dagger a_j\right)\\ &- \sum_{j=-N}^{N}\mathcal{E}_j\left(a_j^\dagger\sigma_-\rho - \sigma_-\rho a_j^\dagger\right) - \sum_{j=-N}^{N}\mathcal{E}_j^*\left(\rho\sigma_+ a_j - a_j\rho\sigma_+\right).\end{aligned} \tag{6.6}$$

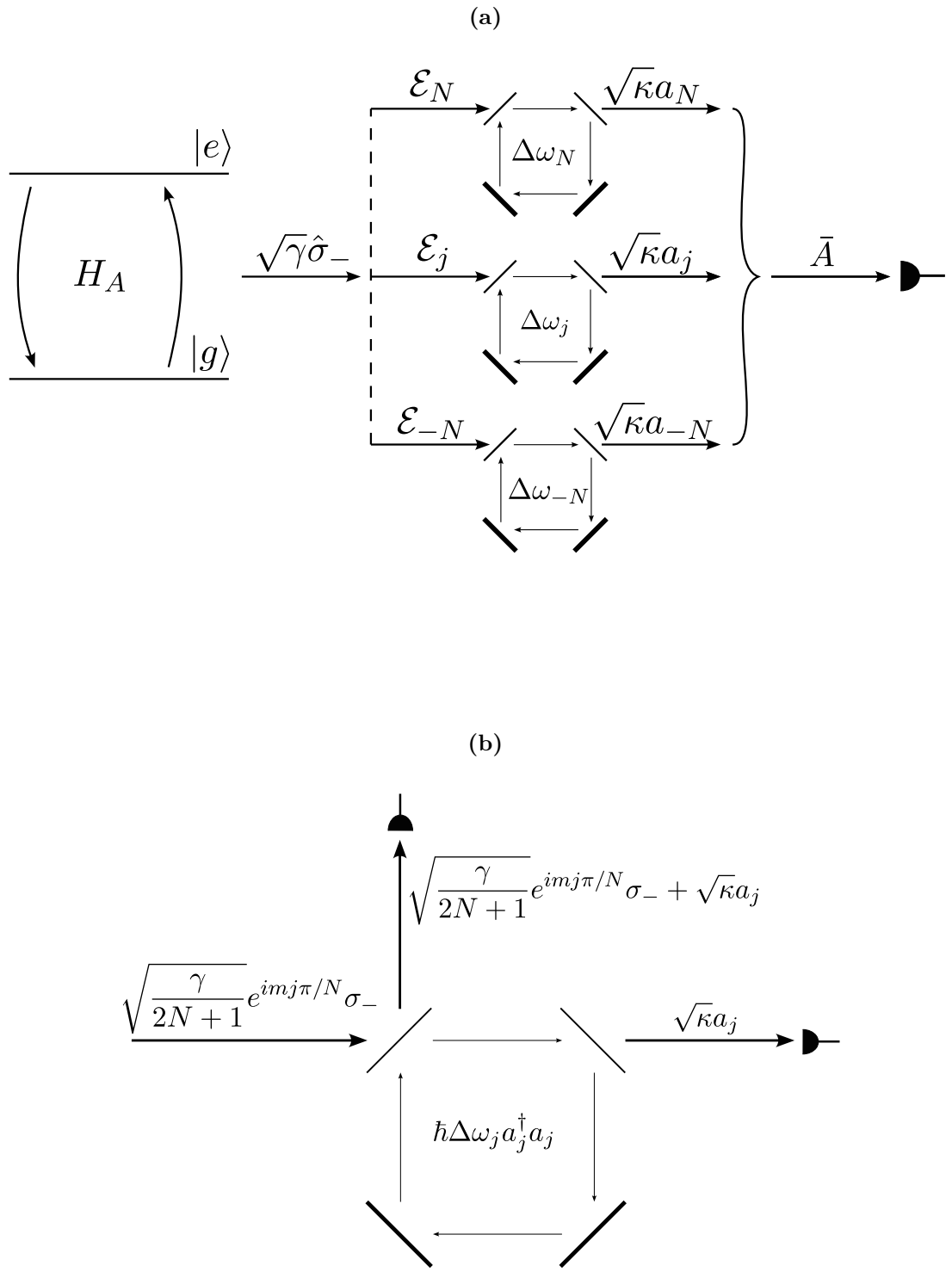

Figure 6.1: Full schematic of the multi-mode filtered two-level atom (a) with detail of the decay channels of the j^{th} cavity (b). The phase-shifted fluorescence is sent into a ring cavity with two perfectly reflecting mirrors at the bottom. The reflection (and transmission) from the input mirror and the transmission from the output mirror are sent to separate detectors. As we are interested in frequency-filtered correlations, our results only focus on the transmission channel.

6.1.2 Density operator and moment equation calculations

In order to calculate the frequency-filtered correlations from the multi-mode array filter, we take the total output field, Eq. (3.34), to be the sum of the output fields of all of the cavity modes,

$$E^{(+)}_{\text{source}}(z,t) = \sum_{j=-N}^{N} \sqrt{\frac{\hbar\omega_j}{2\epsilon_0 Ac}}\sqrt{2\kappa}a_j(t-z/c). \tag{6.7}$$

With frequencies in the optical range (THz), we may assume that the total width of the filter, $2N\delta\omega$, is much smaller than the central frequency, ω_0. We may then replace the ω_j with ω_0, so that the total field is proportional to the sum over all mode annihilation operators,

$$E^{(+)}_{\text{source}}(z,t) \propto \bar{A}(t-z/c) \tag{6.8}$$

where

$$\bar{A} = \frac{A}{\sqrt{2N+1}}, \quad A = \sum_{j=-N}^{N} a_j, \tag{6.9}$$

is the *collective mode annihilation operator*, the quantum mechanical analogue of Eq. (4.22). We then define the *normalised second-order correlation function for the multi-mode frequency filter*,

$$g^{(2)}_{\text{filtered}}(\tau) = \frac{\langle A^\dagger(0)A^\dagger A(\tau)A(0)\rangle_{ss}}{\langle A^\dagger A\rangle^2_{ss}}. \tag{6.10}$$

Using only the master equation, Eq. (6.6), and the appropriate form of the quantum regression equations, Eq. (3.45), we can numerically calculate solutions to this second-order correlation function. There are, however, some difficulties to this method. Firstly, the Hilbert, or Fock, space of single-mode cavities is infinitely large, and one must make a truncation at some point to be able to perform any calculations. For this specific method of filtering we allow for a large number of cavities modes, each with their own Fock space. Even by truncating each individual cavity mode to a maximum of only two photons, the dimensions of the total Hilbert space, and thus the density operator, grows rapidly. The calculations then prove to be extremely demanding, such that we were limited to the case of $N = 20$ on our current computer hardware.

Fortunately there is a much more efficient method which allows for these same calculations to be performed in seconds. Instead of calculating the two-time correlation functions through the master equation and density operator, we instead use a series of operator moment equations. Expanding the numerator of Eq. (6.10) as

$$\langle A^\dagger(0)A^\dagger A(\tau)A(0)\rangle = \sum_{j,k=-N}^{N} \langle A^\dagger(0)a_j^\dagger a_k(\tau)A(0)\rangle, \tag{6.11}$$

we see that this two-time correlation function has initial condition

$$\langle A^\dagger(0)a_j^\dagger a_k(\tau=0)A(0)\rangle = \langle A^\dagger a_j^\dagger a_k A\rangle_{ss} = \sum_{l,m=-N}^{N} \langle a_l^\dagger a_j^\dagger a_k a_m\rangle_{ss}. \tag{6.12}$$

From the quantum regression equations, Eq. (3.47b) in particular, to calculate Eq. (6.11) we

need to solve the equation of motion for the operator average $\langle a_j^\dagger a_k\rangle$. With the master equation, Eq. (6.6), we make use of Eq. (2.22) and the cyclic property of the trace,

$$\mathrm{tr}\left[XYZ\right] = \mathrm{tr}\left[ZXY\right] = \mathrm{tr}\left[YZX\right], \tag{6.13}$$

to find that the expectation of the operator $a_j^\dagger a_k$ evolves as:

$$\begin{aligned}
\frac{\mathrm{d}}{\mathrm{d}t}\langle a_j^\dagger a_k\rangle = \mathrm{tr}\Big\{&-i\Delta\omega_j a_j^\dagger a_k\left(a_j^\dagger a_j\rho - \rho a_j^\dagger a_j\right) - i\Delta\omega_k a_j^\dagger a_k\left(a_k^\dagger a_k\rho - \rho a_k^\dagger a_k\right)\\
&+\kappa a_j^\dagger a_k\left(2a_j\rho a_j^\dagger - a_j^\dagger a_j\rho - \rho a_j^\dagger a_j\right) + \kappa a_j^\dagger a_k\left(2a_k\rho a_k^\dagger - a_k^\dagger a_k\rho - \rho a_k^\dagger a_k\right)\\
&-\mathcal{E}_j^* a_j^\dagger a_k\left(\rho\sigma_+ a_j - a_j\rho\sigma_+\right) - \mathcal{E}_k a_j^\dagger a_k\left(a_k^\dagger\sigma_- \rho - \sigma_-\rho a_k^\dagger\right)\Big\}\\
= \mathrm{tr}\Big\{&-i\Delta\omega_j a_j^\dagger\left(a_j^\dagger a_j - a_j a_j^\dagger\right)a_k\rho - i\Delta\omega_j a_j^\dagger\left(a_k a_k^\dagger - a_k^\dagger a_k\right)a_k\rho\\
&+\kappa a_j^\dagger\left(a_j^\dagger a_j - a_j a_j^\dagger\right)a_k\rho + \kappa a_j^\dagger\left(a_k^\dagger a_k - a_k a_k^\dagger\right)a_k\rho\\
&-\mathcal{E}_j^*\left(a_j a_j^\dagger - a_j^\dagger a_j\right)a_k\sigma_+\rho - \mathcal{E}_k a_j^\dagger\left(a_k a_k^\dagger - a_k^\dagger a_k\right)\sigma_-\rho\Big\}\\
= -&\left[2\kappa - i\left(\Delta\omega_j - \Delta\omega_k\right)\right]\langle a_j^\dagger a_k\rangle - \mathcal{E}_j^*\langle a_k\sigma_+\rangle - \mathcal{E}_k\langle a_j^\dagger\sigma_-\rangle.
\end{aligned} \tag{6.14}$$

This operator moment is dependent only on itself and the two moments $\langle a_k\sigma_+\rangle$ and $\langle a_j^\dagger\sigma_-\rangle$. Following the same procedure, we find that these operator moments evolve as:

$$\frac{\mathrm{d}}{\mathrm{d}t}\langle a_j\sigma_-\rangle = -\left(\frac{\gamma}{2} + \kappa + i\Delta\omega_j\right)\langle a_j\sigma_-\rangle + i\frac{\Omega}{2}\langle a_j\sigma_z\rangle, \tag{6.15a}$$

$$\frac{\mathrm{d}}{\mathrm{d}t}\langle a_j\sigma_+\rangle = -\left(\frac{\gamma}{2} + \kappa + i\Delta\omega_j\right)\langle a_j\sigma_+\rangle - i\frac{\Omega}{2}\langle a_j\sigma_z\rangle - \frac{1}{2}\mathcal{E}_j\left(\langle\sigma_z\rangle + 1\right), \tag{6.15b}$$

$$\frac{\mathrm{d}}{\mathrm{d}t}\langle a_j\sigma_z\rangle = i\Omega\langle a_j\sigma_-\rangle - i\Omega\langle a_j\sigma_+\rangle - \gamma\langle a_j\sigma_z\rangle - \gamma\langle a_j\rangle + \mathcal{E}_j\langle\sigma_-\rangle. \tag{6.15c}$$

Here we see a familiar structure appearing, namely the optical Bloch equations, Eqs. (5.26) and (5.27). From the structure of these equations, we can then arrange Eqs. (6.15) in matrix form,

$$\frac{\mathrm{d}}{\mathrm{d}t}\begin{pmatrix}\langle a_j\sigma_-\rangle\\ \langle a_j\sigma_+\rangle\\ \langle a_j\sigma_z\rangle\end{pmatrix} = \left[\boldsymbol{M}^{(\sigma)} - \left(\kappa + i\Delta\omega_j\right)\mathbb{1}\right]\begin{pmatrix}\langle a_j\sigma_-\rangle\\ \langle a_j\sigma_+\rangle\\ \langle a_j\sigma_z\rangle\end{pmatrix} + \begin{pmatrix}0\\ -\frac{1}{2}\mathcal{E}_j\left(\langle\sigma_z\rangle + 1\right)\\ -\gamma\langle a_j\rangle + \mathcal{E}_j\langle\sigma_-\rangle\end{pmatrix}, \tag{6.16}$$

where $\boldsymbol{M}^{(\sigma)}$ is the evolution matrix of the optical Bloch equations, Eq. (5.28), and $\mathbb{1}$ is the unit matrix. As with Eq. (6.14), these moment equations are also only dependent on lower order terms. To calculate $\langle a_j^\dagger a_k\rangle$ we only need six sets of equations:

$$\frac{\mathrm{d}}{\mathrm{d}t}\langle\boldsymbol{\sigma}\rangle = \boldsymbol{M}^{(\boldsymbol{\sigma})}\langle\boldsymbol{\sigma}\rangle + \begin{pmatrix}0\\0\\-\gamma\end{pmatrix}, \tag{6.17a}$$

$$\frac{\mathrm{d}}{\mathrm{d}t}\langle a_j\rangle = -\left(\kappa + i\Delta\omega_j\right)\langle a_j\rangle - \mathcal{E}_j\langle\sigma_-\rangle, \tag{6.17b}$$

$$\frac{\mathrm{d}}{\mathrm{d}t}\langle a_j^\dagger\rangle = -\left(\kappa - i\Delta\omega_j\right)\langle a_j\rangle - \mathcal{E}_j^*\langle\sigma_+\rangle, \tag{6.17c}$$

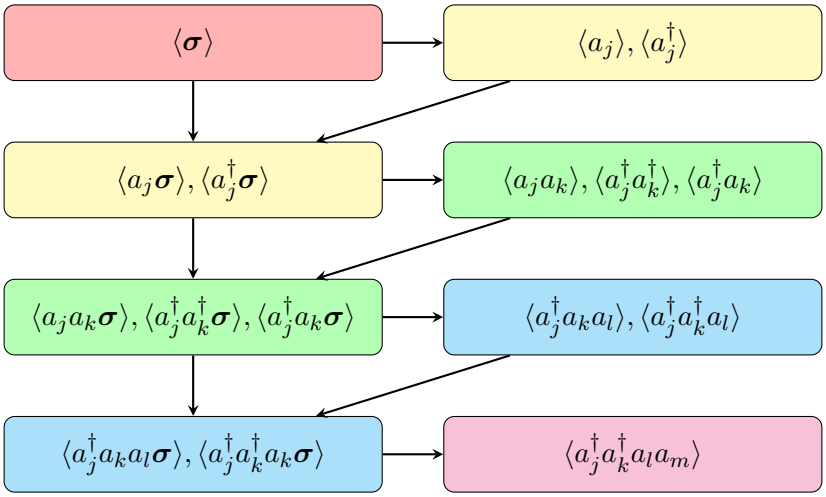

Figure 6.2: The operator moments couple in a cascaded scheme, where lower-order moments can be solved independently from the higher-order moments. The highlighted colours indicate the order of which these equations can be solved, due to the number of filter mode operators, while the arrows indicate the coupling into higher-order modes.

$$\frac{\mathrm{d}}{\mathrm{d}t}\langle a_j \boldsymbol{\sigma}\rangle = \left[\boldsymbol{M}^{(\sigma)} - (\kappa + i\Delta\omega_j)\,\mathbb{1}\right]\langle a_j \boldsymbol{\sigma}\rangle + \begin{pmatrix} 0 \\ -\frac{1}{2}\mathcal{E}_j\left(\langle\sigma_z\rangle + 1\right) \\ -\gamma\langle a_j\rangle + \mathcal{E}_j\langle\sigma_-\rangle \end{pmatrix}, \tag{6.17d}$$

$$\frac{\mathrm{d}}{\mathrm{d}t}\langle a_j^\dagger \boldsymbol{\sigma}\rangle = \left[\boldsymbol{M}^{(\sigma)} - (\kappa - i\Delta\omega_j)\,\mathbb{1}\right]\langle a_j^\dagger \boldsymbol{\sigma}\rangle + \begin{pmatrix} -\frac{1}{2}\mathcal{E}_j^*\left(\langle\sigma_z\rangle + 1\right) \\ 0 \\ -\gamma\langle a_j^\dagger\rangle + \mathcal{E}_j^*\langle\sigma_+\rangle \end{pmatrix}, \tag{6.17e}$$

$$\frac{\mathrm{d}}{\mathrm{d}t}\langle a_j^\dagger a_k\rangle = -\left[2\kappa - i\left(\Delta\omega_j - \Delta\omega_k\right)\right]\langle a_j^\dagger a_k\rangle - \mathcal{E}_j^*\langle a_k\sigma_+\rangle - \mathcal{E}_k\langle a_j^\dagger\sigma_-\rangle. \tag{6.17f}$$

The unidirectional coupling of the atomic fluorescence into the filter modes introduces a simple structure into the coupled moment equations; higher-order operator moments are entirely dependent on lower-order moments. If we instead consider a bidirectional coupling, like that of the Jaynes-Cummings Hamiltonian, we would be unable to derive a closed set of equations, with second-order operator moments appearing in even the optical Bloch equations. This simple structure then provides a very efficient method to calculate them, both numerically and analytically – if one so desires. As there is no influence of the filter cavity modes on the evolution of the atom, the optical Bloch equations are the source of all of the dynamics of the system, and can easily be solved as a 3×3 matrix system. The structure of the coupling, seen in Eqs. (6.17), continues through all combinations of atomic and cavity mode operators. We depict this coupling in order of calculations in Fig. 6.2, up to the fourth-order moment, $\langle a_j^\dagger a_k^\dagger a_l a_m\rangle$.

In Appendix A we present the complete set of coupled moment equations, up to fourth-order, as needed to calculate the frequency-filtered spectra and photon correlations in the following sections. To calculate the steady-state correlations presented in the following sections, we first need to calculate the moment equation steady states. Routines written in `Fortan90` compute these steady states using `LAPACK` matrix inversion routines [108]. With the initial conditions calculated, the time dependence is then numerically integrated using the Runge-Kutta 4^{th} Order

method [109, 110]. Unless otherwise stated, a time step of $\gamma \mathrm{d}t = 10^{-3}$ was chosen such that numerical errors were minimised, without increasing computational time unnecessarily.

6.2 Frequency Filtered Power Spectrum

Now that we have introduced the explicit model for the frequency-filtered two-level atom, we can now calculate the correlation functions of interest. Before we calculate any second-order correlation functions, we will first investigate the filtered power spectrum of the atomic fluorescence.

As previously discussed, the fluorescence is largely coherent and monochromatic in the weak-driving regime, and thus we are more interested in the strong driving regime. Thus, we choose a driving strength such that the sidebands of the Mollow triplet are separated enough to be distinguishable, yet close enough that we will see an improvement of the multi-mode array filter. As mentioned in the opening of this chapter, we wish to test the filter against the simpler case of a two-level atom first, and then move towards systems where the emitted frequencies may not be so well separated. Therefore, for the following sections we set $\Omega/\gamma = 5\pi$.

6.2.1 Frequency-filtered first-order correlation function

Following on from Eqs. (5.37) and (6.10), the normalised first-order correlation function for the multi-mode array filter in the steady-state limit is

$$g^{(1)}_{\text{filtered}}(\tau) = \frac{\langle A^\dagger(\tau)A(0)\rangle_{ss}}{\langle A^\dagger A\rangle_{ss}}, \tag{6.18}$$

where

$$\langle A^\dagger(\tau)A(0)\rangle_{ss} = \sum_{j=-N}^{N} \langle a_j^\dagger(\tau)A(0)\rangle_{ss}. \tag{6.19}$$

Decomposing the filtered power spectrum into coherent and incoherent scattering components, the frequency-filtered incoherent power spectrum is then given by

$$S_{\text{inc}}(\omega) = \frac{1}{2\pi}\frac{1}{\langle A^\dagger A\rangle_{ss}} \int_{-\infty}^{\infty} e^{i\omega\tau} \sum_{j=-N}^{N} \langle \Delta a_j^\dagger(\tau)\Delta A(0)\rangle_{ss}\mathrm{d}\tau. \tag{6.20}$$

As this is a first-order correlation function, we are able to solve for the time dependence by solving only two sets of equations, Eqs. (6.17a) and (6.17c) (See Section A.2 for the explicit correlation function equations to solve). The Bloch equations are a simple 3×3 set of coupled equations, and thus can easily be solved analytically; therefore, we are also able to derive an analytic expression for the correlation function, Eq. (6.19). The *first-order correlation function for the multi-mode filtered two-level atom* is then (see Appendix B for details):

$$\langle \Delta a_j^\dagger(\tau)\Delta A(0)\rangle_{ss} = \frac{\mathcal{E}_j^* C^{(1)}}{\frac{\gamma}{2} - (\kappa - i\Delta\omega_j)} e^{-\frac{\gamma}{2}\tau} + \frac{\mathcal{E}_j^* C^{(2)}}{\frac{3\gamma}{4} + \delta - (\kappa - i\Delta\omega_j)} e^{-\left(\frac{3\gamma}{4}+\delta\right)\tau}$$

$$+\frac{\mathcal{E}_j^* C^{(3)}}{\frac{3\gamma}{4}-\delta-(\kappa-i\Delta\omega_j)}e^{-\left(\frac{3\gamma}{4}-\delta\right)\tau}+C_j^{(4)}e^{-(\kappa-i\Delta\omega_j)\tau}, \tag{6.21}$$

where δ is defined by Eq. (5.51), and the coefficients are

$$C^{(1)}=\frac{1}{2}\sum_{k=-N}^{N}\Big(\langle\Delta\sigma_-\Delta a_k\rangle_{ss}+\langle\Delta\sigma_+\Delta a_k\rangle_{ss}\Big), \tag{6.22a}$$

$$C^{(2)}=\frac{1}{4\delta}\sum_{k=-N}^{N}\left[\frac{\gamma-4\delta}{4}\Big(\langle\Delta\sigma_-\Delta a_k\rangle_{ss}-\langle\Delta\sigma_+\Delta a_k\rangle_{ss}\Big)+i\Omega\langle\Delta\sigma_z\Delta a_k\rangle_{ss}\right], \tag{6.22b}$$

$$C^{(3)}=\frac{-1}{4\delta}\sum_{k=-N}^{N}\left[\frac{\gamma+4\delta}{4}\Big(\langle\Delta\sigma_-\Delta a_k\rangle_{ss}-\langle\Delta\sigma_+\Delta a_k\rangle_{ss}\Big)+i\Omega\langle\Delta\sigma_z\Delta a_k\rangle_{ss}\right], \tag{6.22c}$$

$$\begin{aligned}C_j^{(4)}=\sum_{k=-N}^{N}\Bigg[&\langle\Delta a_j^\dagger\Delta a_k\rangle_{ss}-\frac{\mathcal{E}_j^* C^{(1)}}{\frac{\gamma}{2}-(\kappa-i\Delta\omega_j)}-\frac{\mathcal{E}_j^* C^{(2)}}{\frac{3\gamma}{4}+\delta-(\kappa-i\Delta\omega_j)}\\&-\frac{\mathcal{E}_j^* C^{(3)}}{\frac{3\gamma}{4}-\delta-(\kappa-i\Delta\omega_j)}\Bigg],\end{aligned} \tag{6.22d}$$

with

$$\langle\Delta X\Delta Y\rangle_{ss}=\langle XY\rangle_{ss}-\langle X\rangle_{ss}\langle Y\rangle_{ss}. \tag{6.23}$$

While we have not given explicit expressions for the steady-state moments, and thus we cannot give a complete expression for the incoherent power spectrum, we can see four important frequency terms in Eq. (6.21): $e^{-\gamma\tau/2}$ corresponds to the central peak of the Mollow triplet; $e^{-(3\gamma/4\pm\delta)\tau}$ correspond to the left- and right-side peak; and $e^{-(\kappa-i\Delta\omega_j)\tau}$ corresponds directly to the output field of the j^{th} filter mode. As we encountered in the derivation of the frequency response, Eq. (4.27), a complete analytic expression for Eq. (6.19) is too difficult to derive.

6.2.2 Filtering out non-target peaks

Using Eq. (6.21), with numerically obtained steady states, we calculate the incoherent power spectrum of the multi-mode array filter for increasing halfwidths; κ for the single-mode filter, $N=0$, and $N\delta\omega$ for the multi-mode array, $N>0$. Following on from Section 4.2.4, we choose a large number of modes, $N=80$, and set the mode halfwidth to $\kappa=2.5\delta\omega$, such that the frequency response of the multi-mode array filter has a sharp cut-off. In the following section, however, we will more closely investigate the effects of the filter parameters.

We first look at the response of a standard single-mode cavity filter in Fig. 6.3, for increasing values of $\kappa/\gamma=1,2,4,8$, and 16. With the filter resonant with the central peak, Fig. 6.3a, and the right peak, Fig. 6.3b, we see two distinct features of the single-mode filtering. Firstly, when the bandwidth is too small compared to the linewidth of the target fluorescence – γ for the central peak and 1.5γ for the side-peaks – the output resonances become too narrow; that is, narrower than the natural linewidths. This can be seen more clearly in Fig. 6.3a for the two narrow bandwidths, $\kappa/\gamma=1$ (blue) and $\kappa/\gamma=2$ (orange). Secondly, as the bandwidth of the filter *increases*, the filter becomes unable to distinguish between target and non-target frequencies. As discussed earlier, in the limit $\kappa\to\infty$, the "filtered" output field tends towards

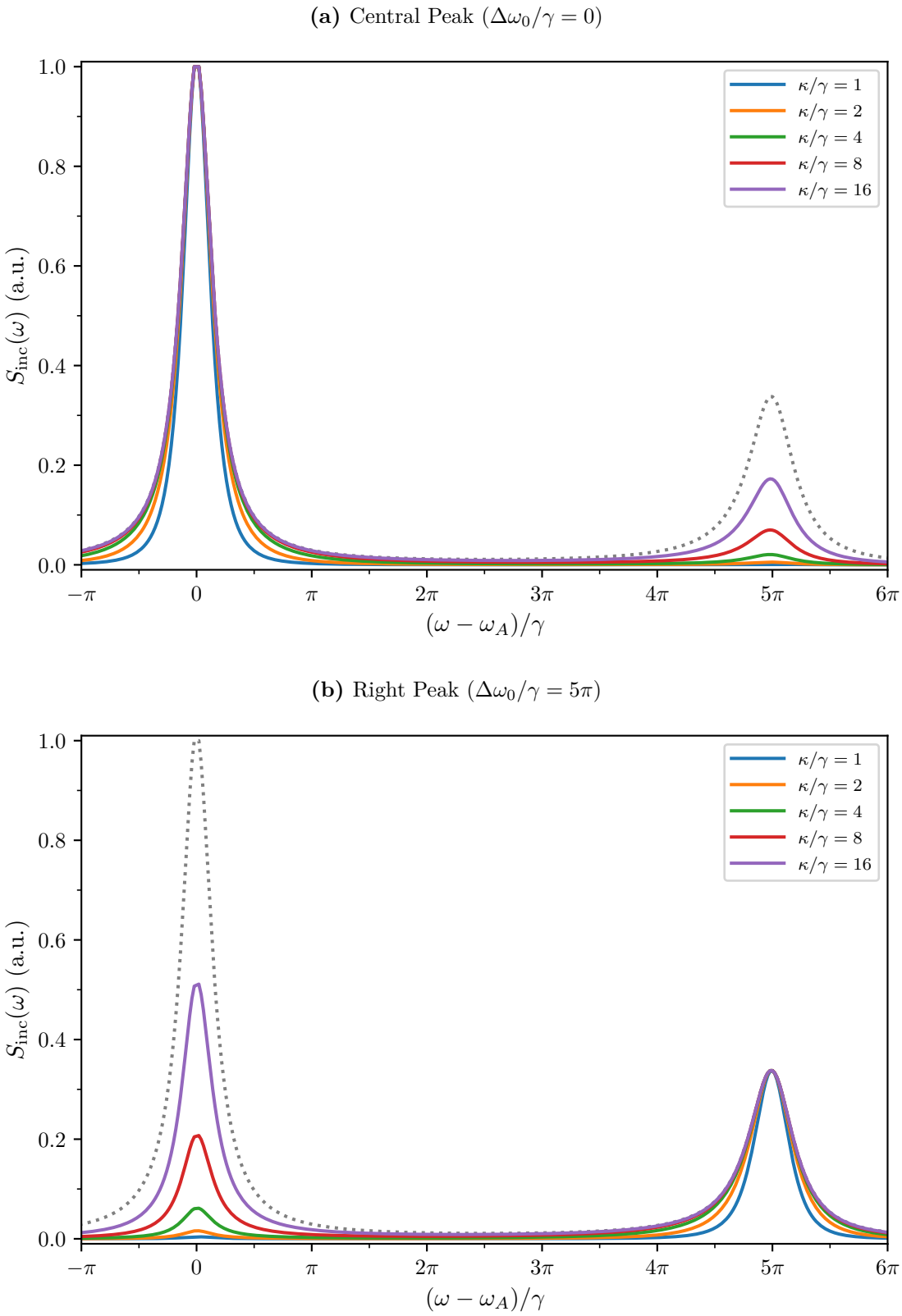

Figure 6.3: Frequency-filtered incoherent power spectrum, Eq. (6.20), of a single-mode filter ($N = 0$), for a range of increasing halfwidths, κ. The filter resonance is tuned to the central peak (a) and the right peak (b) of the Mollow triplet, which is also plotted as a comparison (grey, dotted). The driving amplitude is $\Omega/\gamma = 5\pi$.

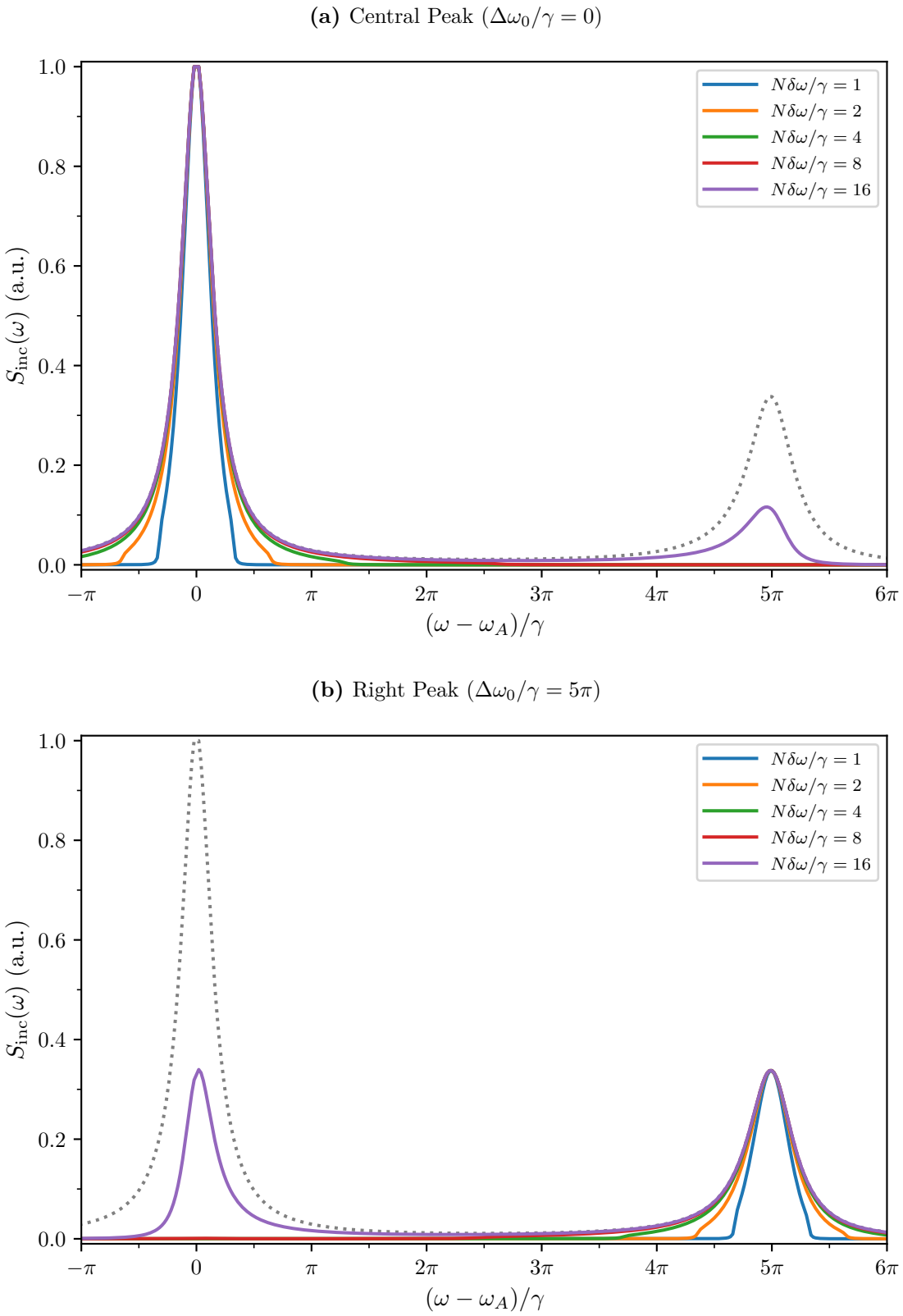

Figure 6.4: Frequency-filtered incoherent power spectrum, Eq. (6.20), of a multi-mode array filter ($N = 80$), for a range of increasing halfwidths, $N\delta\omega$. The filter resonance is tuned to the central peak (a) and the right peak (b) of the Mollow triplet, which is also plotted as a comparison (grey, dotted). The other parameters are $\Omega/\gamma = 5\pi, \kappa = 2.5\delta\omega, m = 1$.

the input field, as the filter cavity allows any frequency to pass through. We see this clearly in Fig. 6.3b, where the filter is centred on the right peak ($\Delta\omega_0 = \Omega$), yet there is an emerging central peak as the bandwidth increases.

Turning our attention to the multi-mode array filter, Fig. 6.4, we can already see a remarkable improvement in its ability to isolate frequencies when compared to the single-mode Lorentzian filter. Compared to the halfwidths shown in Fig. 6.3, the multi-mode array filter is able to effectively isolate the target peak for all but the largest halfwidth, $N\delta\omega/\gamma = 16$. The single-mode filter, however, still shows evidence of other peaks for a halfwidth as small as 2γ, as can be seen by the orange curve in Fig. 6.3.

Looking at smaller bandwidths, we see a different story. As the filter bandwidth decreases, and the frequency isolation improves, the multi-mode array filter rejects even more non-target light. When the filter halfwidth is equal to the atomic linewidth, $\kappa = \gamma$ and $N\delta\omega = \gamma$ (the blue curve in Figs. 6.3 and 6.4, respectively), we see that the spectral shape is much thinner than the bare atomic resonance. The multi-mode array filter is now rejecting frequencies that make up the target peak, therefore we expect the filter field to no longer be completely representative of the target transitions.

6.3 Second-Order Auto-Correlation Function

Figures 6.3 and 6.4 show exactly what we expected from the multi-mode array filter, that is, the multi-mode array filter is able to isolate frequencies much more effectively than a single-mode filter. Having shown this in the frequency domain, we now move into the time domain and towards the main quantity of interest for this thesis: *frequency-filtered photon correlations*.

In this section we present calculations of the filtered second-order correlation function, Eq. (6.10), for a variety of different parameters, with the goal of finding a regime that results in correlation functions as close to the secular approximations as possible. Unlike the previous section, we do not have an analytic expression to work with. We therefore present numerical calculations of the second-order correlation functions.

6.3.1 Fine tuning the multi-mode array filter

There are three important aspects of the multi-mode array filter that affect its performance: the effective halfwidth, $N\delta\omega$; the size of the phase modulation, m; and the relationship between the number of modes, N, and the width of each individual mode, κ.

We have already discussed the effect of the relationship between the cavity mode width and the number of modes in Section 4.2.4. We therefore consider, for the multi-mode array filter, a large number of modes, $N = 80$, with a cavity mode width $\kappa = 2.5\delta\omega$, where the mode spacing, $\delta\omega$, depends on the chosen effective halfwidth. In this section, then, we will discuss the effects of the halfwidths and the phase modulation on the filtered photon correlations.

Varying the halfwidth

In Figs. 6.5 and 6.6, we plot sets of correlation functions for increasing filter halfwidths of the single-mode and multi-mode filters, respectively. Similar to the filtered power spectra,

(a) Central Peak ($\Delta\omega_0/\gamma = 0$)

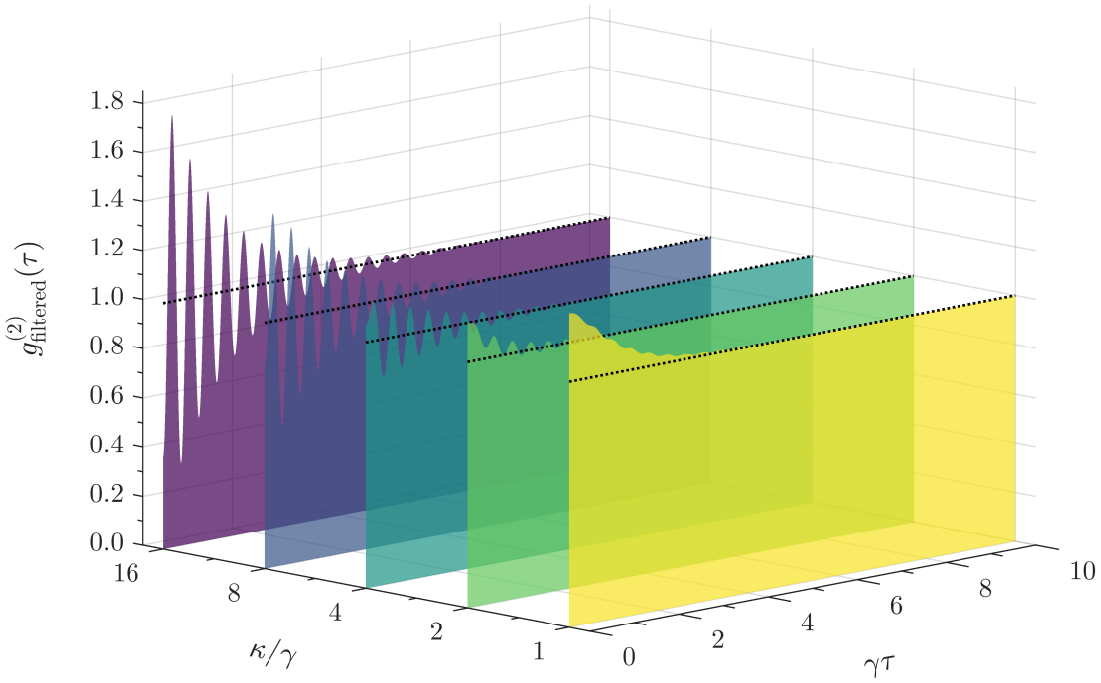

(b) Right Peak ($\Delta\omega_0/\gamma = 5\pi$)

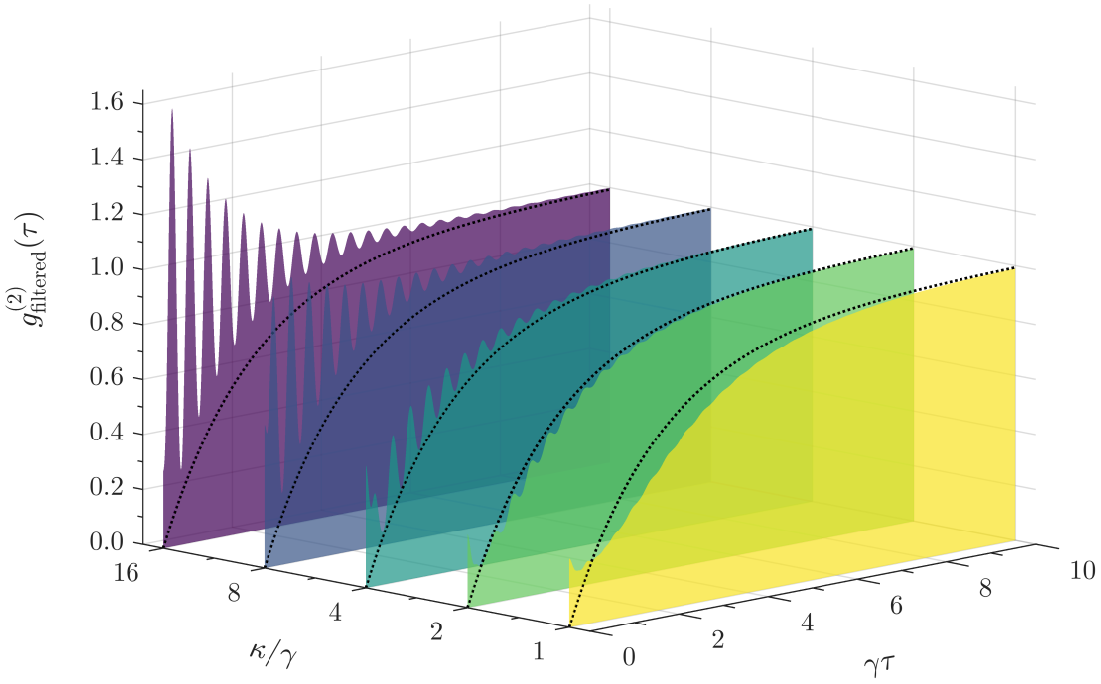

Figure 6.5: Frequency-filtered $g^{(2)}(\tau)$ of a single-mode filter ($N = 0$), for a range of increasing halfwidths, κ. The filter resonance is tuned to the central peak (a) and the right peak (b) of the Mollow triplet, with comparisons against the auto-correlation functions derived in the secular approximation (black, dotted), Eq. (5.65) (a) and Eq. (5.66b) (b). The driving amplitude is $\Omega/\gamma = 5\pi$.

(a) Central Peak ($\Delta\omega_0/\gamma = 0$)

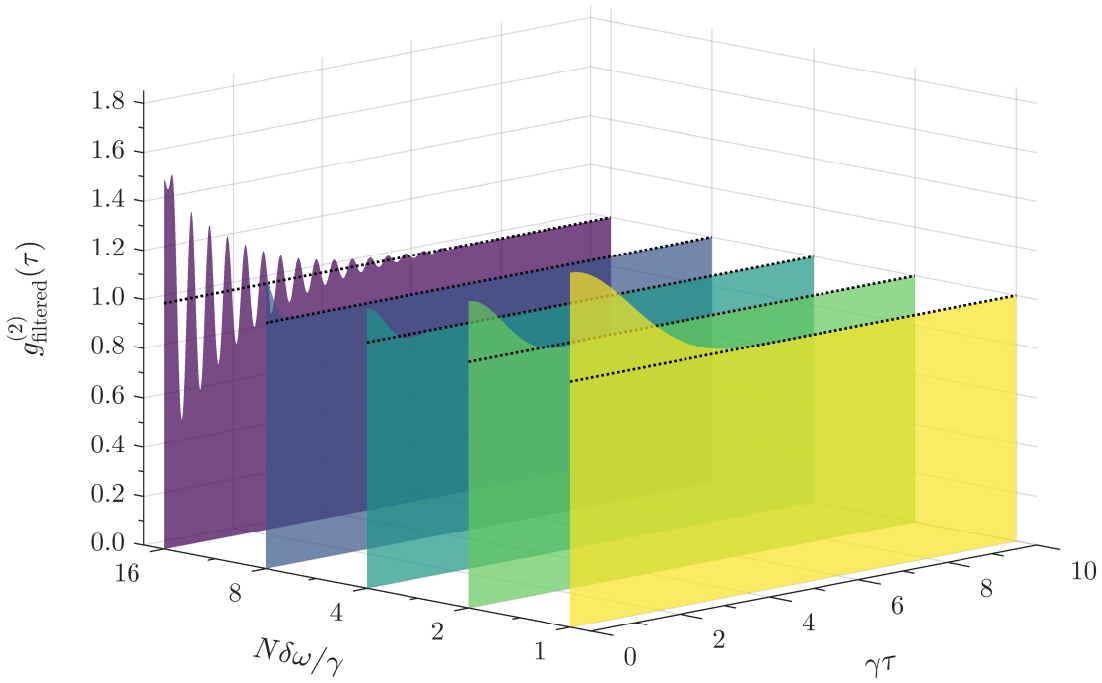

(b) Right Peak ($\Delta\omega_0/\gamma = 5\pi$)

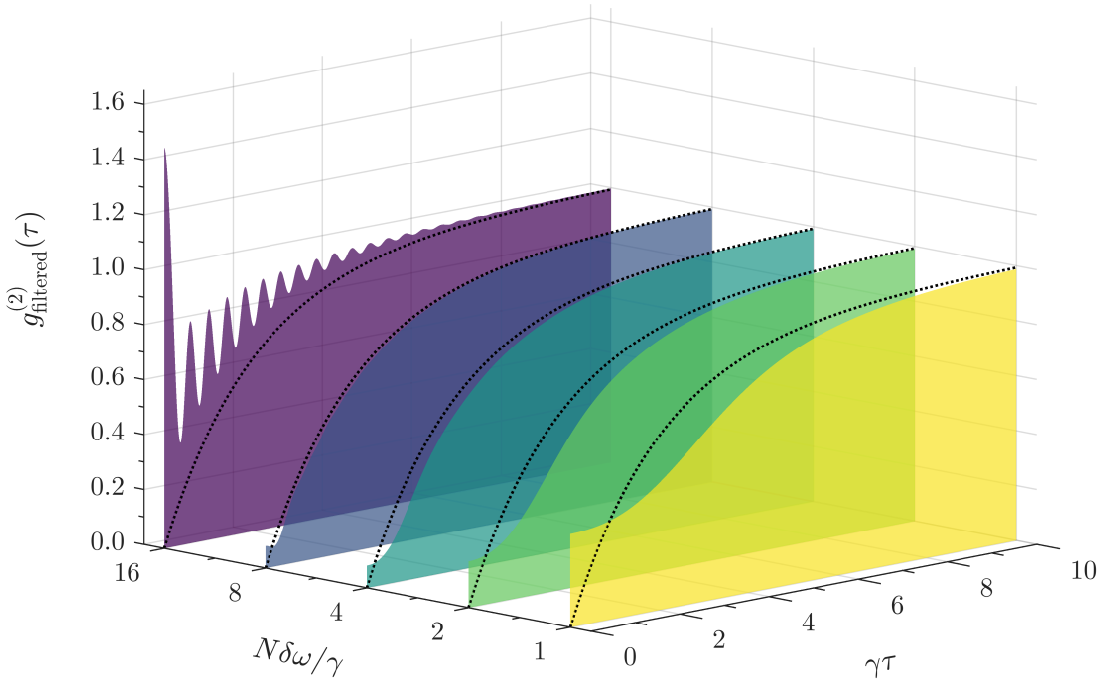

Figure 6.6: Frequency-filtered $g^{(2)}(\tau)$ of the multi-mode array filter ($N = 80$), for a range of increasing filter halfwidths, $N\delta\omega$. The filter resonance is tuned to the central peak (a) and the right peak (b) of the Mollow triplet, with comparisons against the auto-correlation functions derived in the secular approximation (black, dotted), Eq. (5.65) (a) and Eq. (5.66b) (b). The other parameters are $\Omega/\gamma = 5\pi, m = 1$, and $\kappa = 2.5\delta\omega$.

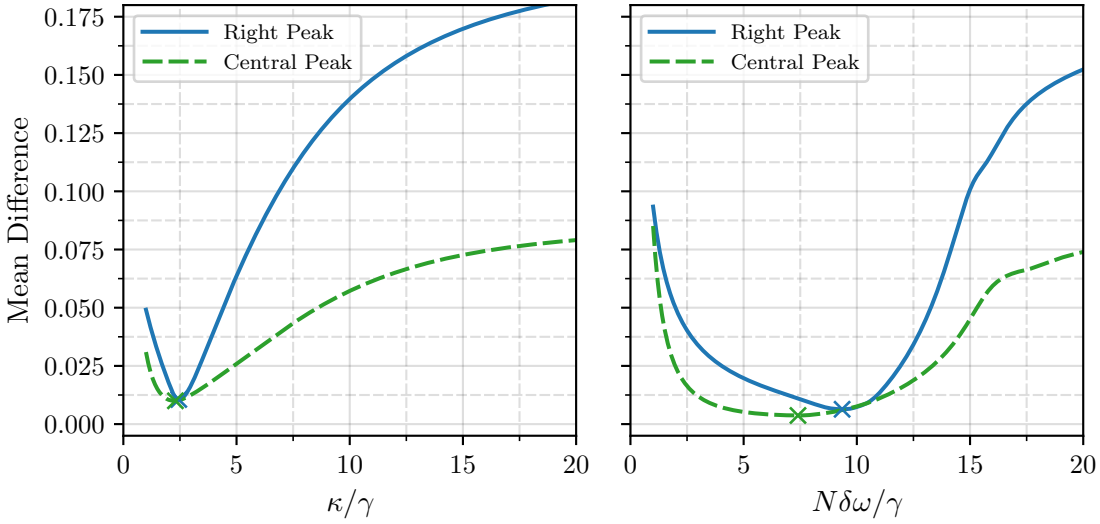

Figure 6.7: Mean absolute difference, Eq. (6.24), between the dressed state correlation functions and the single-mode (left) and multi-mode (right) filtered correlation functions of the right (blue, solid), $\Delta\omega_0/\gamma = 5\pi$, and central (green, dashed), $\Delta\omega_0/\gamma = 0$, filtered peaks. The driving amplitude is $\Omega/\gamma = 5\pi$, and the multi-mode array parameters are $N = 80, m = 1, \kappa = 2.5\delta\omega$. The correlation functions were calculated to a maximum time of $\gamma\tau = 10$.

we see an immediate improvement in the multi-mode array filter over the single-mode filter in terms of its ability to isolate frequencies. For the smaller filter halfwidths of the single-mode filter, there are still oscillations visible in the correlations of the central- and right-filtered peaks, Figs. 6.5a and 6.5b, respectively. These oscillations, at the Rabi frequency Ω, are indicative of the poor frequency isolation of the single-mode filter. Again, the multi-mode array filter fares much better in isolating frequencies of interest, with more evidence in Fig. 6.6. Only for the largest halfwidth shown, $N\delta\omega/\gamma = 16$, are there visible oscillations, which is to be expected with a full bandwidth that encompasses the entire Mollow triplet.

When comparing the filtered correlation functions with the ideal dressed state functions (black, dashed curves), Eqs. (5.65) and (5.66b), we see that both filter setups produce filtered photon correlations that follow the dressed state functions closely, with the multi-mode array filter producing more accurate results. We can quantify this by considering the mean difference between the filtered photon correlations and the dressed state correlations,

$$\text{Mean Difference} = \overline{|g^{(2)}_{\text{dressed}}(\tau) - g^{(2)}_{\text{filtered}}(\tau)|}. \tag{6.24}$$

To calculate the mean difference, the correlation functions were calculated up to a maximum time of $\gamma\tau = 10$. Except for the smallest of filter halfwidths, as we will discuss later, this is ample time for the correlations to tend closely to their steady state. As we are calculating the *normalised* second-order correlation functions, they will always tend to unity in the limit $\tau \to \infty$, and thus we do not need to calculate for longer times to compare mean differences.

Figure 6.7 shows this difference for the single- and multi-mode filters, when resonant with photons of the central and right peaks, for a range of filter halfwidths. In the small halfwidth, $\kappa/\gamma, N\delta\omega/\gamma < 1$, and large halfwidth, $\kappa/\gamma, N\delta\omega/\gamma > 10$, regimes, the filtered correlation func-

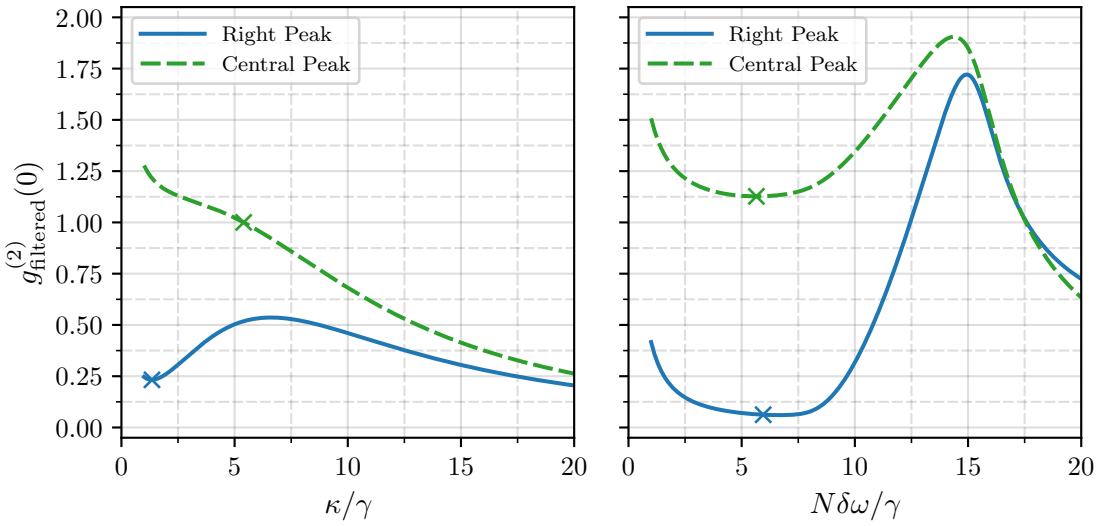

Figure 6.8: Initial correlation value of the single-mode (left) and multi-mode (right) filtered correlation functions of the right (blue, solid), $\Delta\omega_0/\gamma = 5\pi$, and central (green, dashed), $\Delta\omega_0/\gamma = 0$, filtered peaks. The driving amplitude is $\Omega/\gamma = 5\pi$, and the multi-mode array parameters are $N = 80, m = 1, \kappa = 2.5\delta\omega$.

tions deviate greatly from those derived in the secular approximation. In the intermediate regime, however, the multi-mode filtered photon correlations deviate much less than the single-mode. The markers in Fig. 6.7 indicate the halfwidth at which the lowest mean difference occurs; for the single-mode filter this occurs at $\kappa/\gamma = 2.4$, where the mean difference is ≈ 0.01 for both filtered peaks. This is only a narrow range as, for larger halfwidths, the Lorentzian filter allows even more bare atomic fluorescence to pass through, thus giving strong Rabi oscillations. For the multi-mode array filter, there is a much wider range of acceptable halfwidths due to the almost rectangular frequency response. Not only is the mean difference in the intermediate halfwidth range lower for the multi-mode array filter – 0.004–0.006 for the filtered central and right peak, respectively – but the smallest difference occurs at a much wider halfwidth – $N\delta\omega/\gamma = 7.5$ and 9.5 for the filtered central and right peak, respectively.

There is another important metric with which to measure the filter's ability, namely, the initial value of the correlation function; definitions for bunched, coherent, and antibunched light all arise from the initial correlation value. For the smaller halfwidths, we saw that the filtered spectra were much narrower than the bare atomic Lorentzian. We see a similar effect in the time domain, too, where the behaviour of the filtered correlation functions diverges from the dressed state correlation functions – see Fig. 6.8. This is more noticeable with the multi-mode array filter where, for the central peak, and $N\delta\omega/\gamma = 1.0$ (the yellow curve in Fig. 6.6a), the initial correlation value has increased when compared to the correlation function for $N\delta\omega/\gamma = 2.0$. Similarly, for the right peak (Fig. 6.6b), the initial value is also higher. The effect that narrow linewidths have on the filtered correlation functions will be discussed in the following section.

As with Fig. 6.7, markers indicate the halfwidth – in the intermediate range – where the initial correlation value is closest to that of the secular approximation: $g^{(2)}(0) = 1$ for the central peak and $g^{(2)}(0) = 0$ for the right peak. For the single-mode array, the closest value

when resonant with the right peak is $g^{(2)}_{\text{filtered}}(0) \approx 0.25$ at $\kappa/\gamma \approx 1.4$; and $g^{(2)}_{\text{filtered}}(0) \approx 1.0$ at $\kappa/\gamma \approx 5.5$ for the central peak. While the initial value for the central peak seems promising for the single-mode filter, we know that a halfwidth of 5.5 is already too large, given the visible Rabi oscillations for $\kappa/\gamma = 4.0$ in Fig. 6.5a. The multi-mode array filter, however, has initial values that lie much closer to the secular approximation. For the right peak, $g^{(2)}_{\text{filtered}}(0) = 0.0632$ for $N\delta\omega/\gamma = 5.95$, and for the central peak, $g^{(2)}_{\text{filtered}}(0) = 1.1270$ for $N\delta\omega/\gamma = 5.4$.

Again, as the halfwidth increases even further, and the filtered correlation function approaches that of the direct atomic fluorescence, the initial value tends towards zero, i.e., perfect antibunching. While this may seem agreeable when filtering the right peak, we know that this indicates different underlying mechanics than with the dressed state picture.

Unfortunately we cannot pick a single multi-mode array halfwidth that will give optimal results for *both* the initial correlation value and the overall trend. For a more accurate overall correlation, a slightly larger halfwidth is more favourable, as the transitory behaviour of the filter's temporal response decays faster for larger halfwidths. For a more accurate initial value, a slightly narrower halfwidth is preferable as it allows for more precise frequency isolation. We will therefore consider the two regimes, and motivations, separately.

Varying the phase modulation

So far we have only really considered a maximum phase modulation of π, with $m = 1$. From the characteristics of the sinc function, Fig. 4.5, and the frequency response of the multi-mode array filter, Fig. 4.8, we expect $m = 1$ to be an optimal value. If $m < 1$, the tails of the frequency response extend too far; if $m > 1$, we introduce a large temporal delay, as well as a dip in the centre of the frequency response.

Figure 6.10 shows the mean difference and $g^{(2)}_{\text{filtered}}(0)$ for a range of phase modulations. Here the effective halfwidths have been chosen such that the mean difference or initial value have been optimised for the given driving amplitude, $\Omega/\gamma = 5\pi$. If there is no phase modulation, $m = 0$, we see large deviations in both the overall behaviour and the initial value. This can also be seen in Fig. 6.9, where we plot the temporal evolution of the filtered correlation function. It is only when the phase modulation increases, and thus the frequency response becomes more rectangular, that the filtered correlation functions approach the ideal dressed state functions.

The closest initial correlation value for both resonance cases lies at exactly $m = 1$, with $g^{(2)}_{\text{filtered}}(0) = 1.12696$ and 0.06215 for the central and right peaks, respectively. There is, however, a slight difference when considering the overall mean difference. When resonant with the right peak, the smallest mean difference is ≈ 0.0056 for $m = 0.8$, while for $m = 1$ the mean difference is ≈ 0.0064. This is only a small improvement in the overall mean difference, especially when compared to the closer initial value for $m = 1$. We will therefore consider a phase modulation of $m = 1$, as we have done thus far.

Frequency isolated photon correlations

Having now discussed the various parameter regimes of the multi-mode array, we now make a final comparison of the frequency-filtered photon correlations between the single-mode Lorentzian filter and the multi-mode array filter. We do note that the parameters chosen are

(a) Central Peak ($\Delta\omega_0/\gamma = 0$)

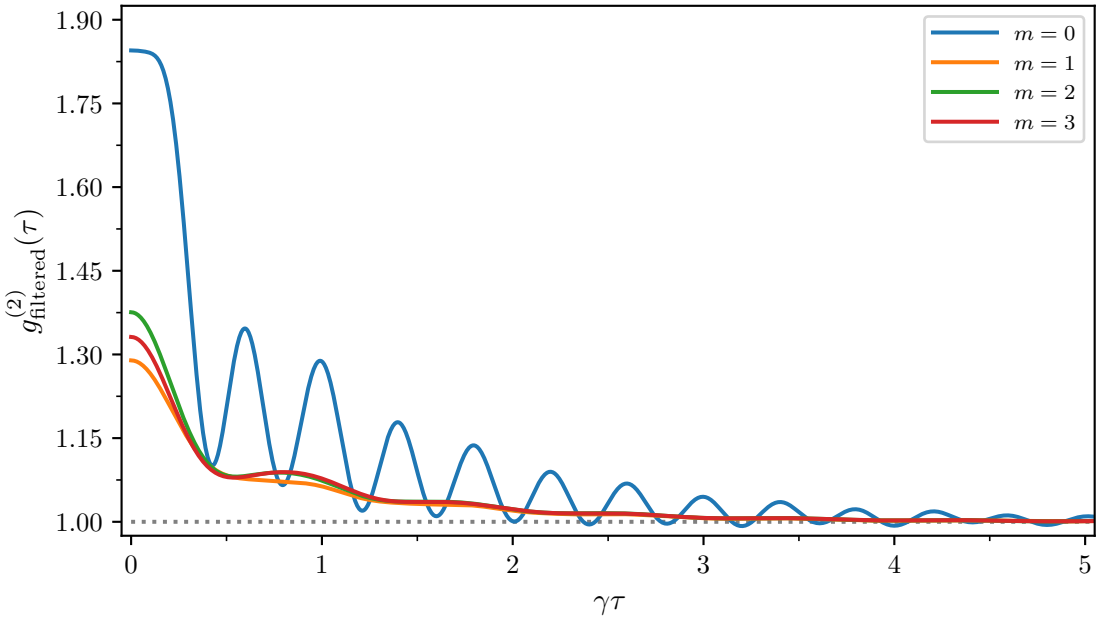

(b) Right Peak ($\Delta\omega_0/\gamma = 5\pi$)

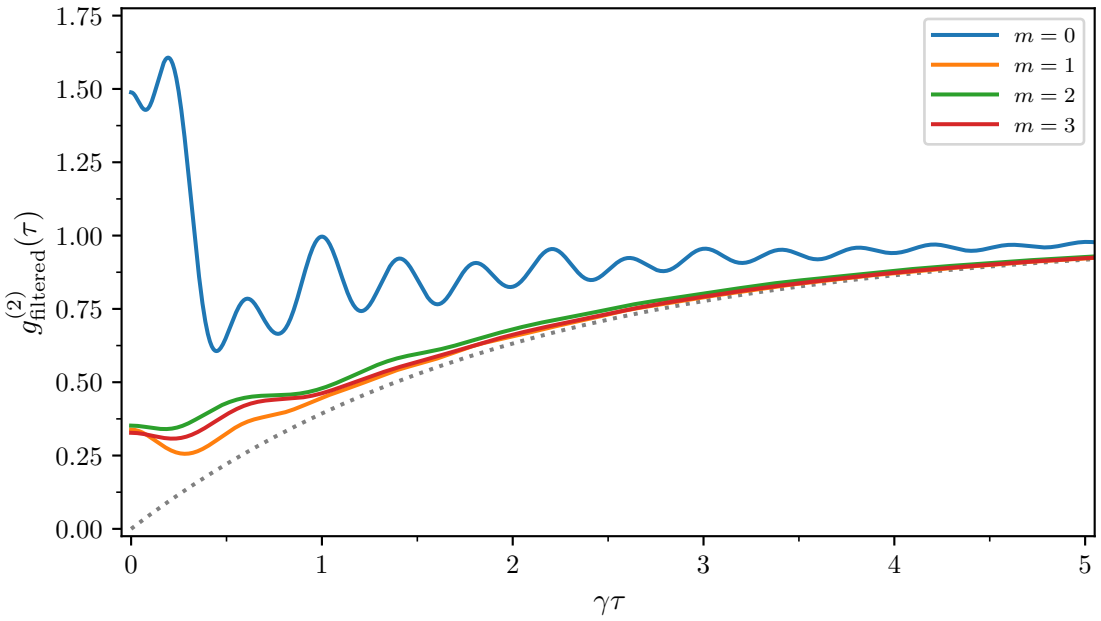

Figure 6.9: Multi-mode filtered correlation function for a few different values of m, for the filtered central peak (a) and right peak (b). The filtered correlations are compared against the dressed state correlation functions (grey, dotted), Eqs. (5.65) (a) and (5.66b) (b). The other parameters are $\Omega/\gamma = 5\pi, N = 80, \kappa = 2.5\delta\omega$.

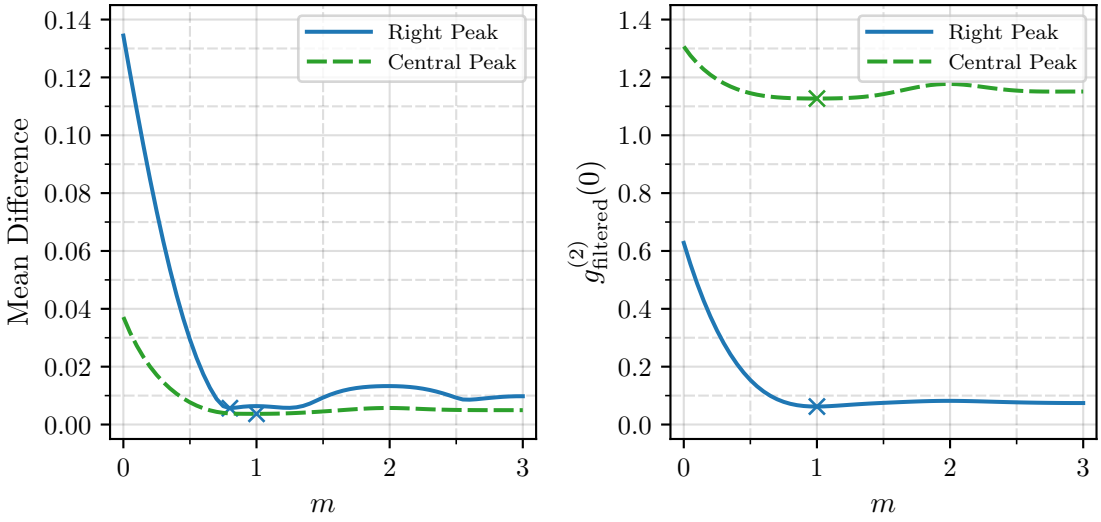

Figure 6.10: Mean difference between the filtered and dressed state correlation functions (left) and initial correlation value (right) for different values of phase modulation. The filter is resonant with the right (blue, solid), $\Delta\omega_0/\gamma = 5\pi$, and central (green, dashed), $\Delta\omega_0/\gamma = 0$, peaks. For the central peak, the filter halfwidths are $N\delta\omega/\gamma = 7.4$ (left) and $N\delta\omega/\gamma = 5.65$ (right). For the right peak, the filter halfwidths are $N\delta\omega/\gamma = 9.35$ (left) and $N\delta\omega/\gamma = 5.95$ (right). The other parameters are $\Omega/\gamma = 5\pi, N = 80, \kappa = 2.5\delta\omega$.

effective for the given sideband splitting, or driving amplitude. With that in mind we present correlation functions, in Fig. 6.11, calculated with halfwidths that result in a more accurate overall result: $\kappa/\gamma = 2.5$ for the single-mode filter, and $N\delta\omega/\gamma = 7.4$ and 9.35 for the multi-mode array filter when resonant with the central and right peaks, respectively.

As previously mentioned, we have set the driving amplitude as $\Omega/\gamma = 5\pi$ such that the sidebands of the Mollow triplet are separated enough to distinguish them, but still in the limit where the long-reaching tails of a Lorentzian filter will have a noticeable effect.

Considering first a suitable bandwidth for the single-mode filter, the top figures of Figs. 6.11a and 6.11b, we see that the single-mode filtered correlations do follow the trend of the dressed state correlation functions. Unfortunately for the single-mode filter, the orange dashed curve, we still do see quite visible Rabi oscillations, indicative of its poor ability to isolate target frequencies. For the same halfwidth, the multi-mode array filter produces a much smoother filtered correlation function, yet the frequency response is still too narrow to capture most of the target peak. The initial transitory behaviour of the single-mode filter also takes much longer to settle.

Increasing the halfwidth to $N\delta\omega/\gamma = 7.4$ for the central peak, and 9.35 for the right peak, we see an immediate improvement in the multi-mode filtered photon correlations. Non-target photons have been almost completely rejected, with only very small amplitude oscillations visible, and the initial transitory behaviour decays quickly.

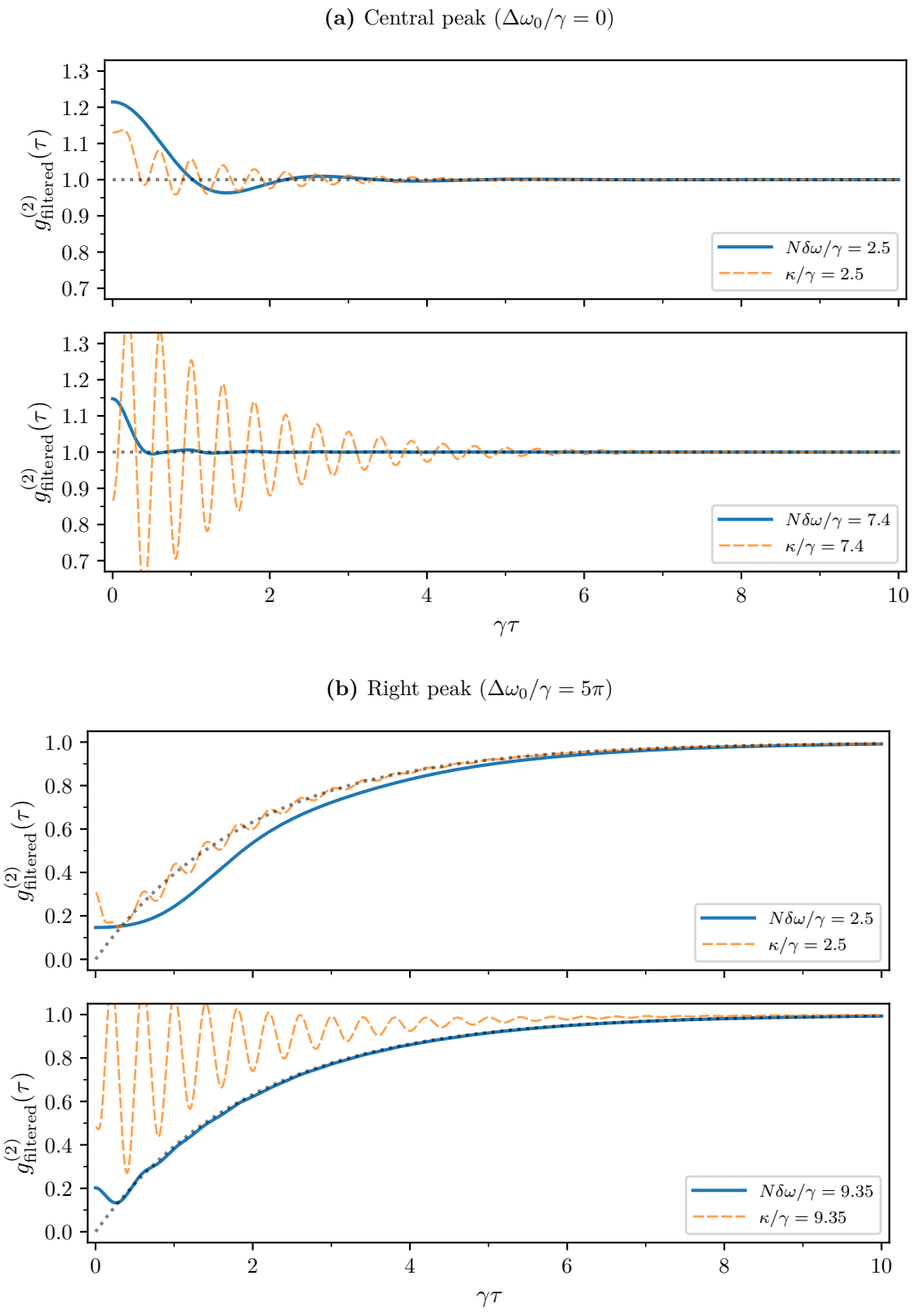

Figure 6.11: Frequency-filtered photon correlations of the central (a) and right (b) peaks for the single- (orange, dashed) and multi-mode array (blue, solid) filters. The filtered correlations are compared against the dressed state correlation functions (grey, dotted), Eqs. (5.65) (a) and (5.66b) (b). Halfwidths have been chosen to give a more accurate overall correlation function. The other parameters are $\Omega/\gamma = 5\pi, N = 80, \kappa = 2.5\delta\omega$

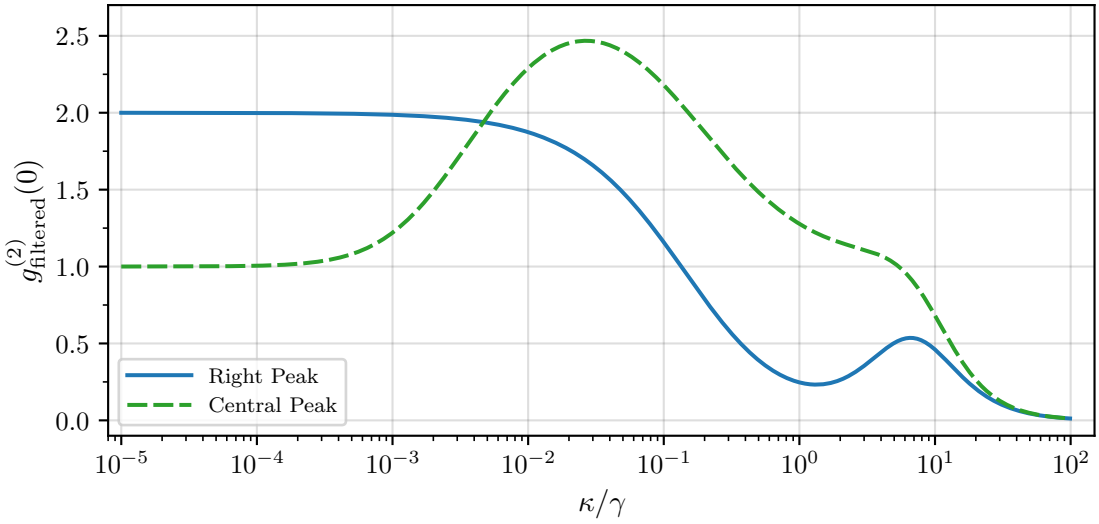

Figure 6.12: Initial value of the filtered correlation function, $g^{(2)}_{\text{filtered}}(0)$, for the single-mode filter ($N = 0$) when resonant with the right (blue, solid) and central (green, dashed) peak. The driving amplitude is $\Omega/\gamma = 5\pi$.

6.3.2 Filtering within the peak

In the previous section we established that, as the filter halfwidth increases, more of the atomic fluorescence passes through the filter and the filtered photon correlations tend towards the bare atomic correlations. There is, then, some intermediate halfwidth where the filter is able to isolate a target peak, such that the filtered correlations closely capture the expected behaviour as derived in the secular approximation. We could see in Figs. 6.7 and 6.8, however, that smaller halfwidths – smaller than the bare atomic linewidth – caused the correlation functions to evolve into something different.

In Fig. 6.12 we show the initial value of the filtered correlation function, $g^{(2)}_{\text{filtered}}(\tau = 0)$, when resonant with the central (the blue, solid curve) and the right peak (the orange, dashed curve), with varying filter halfwidth. Even with the single-mode filter, we can see drastic changes in the correlation functions as the filter halfwidth decreases. These results agree with those discussed by Carreño et al. [83] and Gonzalez et al. [46, 48] for the strongly driven two-level atom. Similar results have been also found recently in the weak driving regime (see Refs. [34, 35]). With the extension of the multi-mode array filter, we can, in fact, reveal even richer correlations due to the improved frequency isolation. From here on, then, we will discuss these correlations from the context of the multi-mode array filter, for which the corresponding results are shown in Fig. 6.13.

We highlight five filter halfwidths in Fig. 6.13 corresponding to different regions of photon correlations: $N\delta\omega/\gamma = 100.0$ (i), 14.5 (ii), 5.68 (iii), 0.0685 (iv), and 0.00001 (v). We plot the temporal correlation functions of the central peak for these halfwidths in Fig. 6.14. Starting with the largest halfwidth in region (i), the filtered photon correlations are almost perfectly antibunched, as there is almost no suppression of the atomic fluorescence for such an extreme filter width.

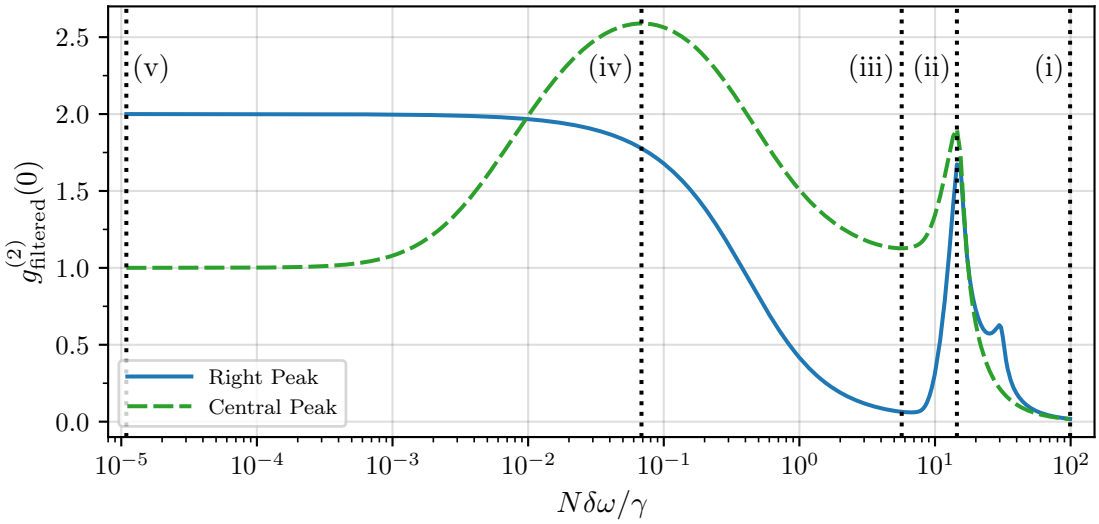

Figure 6.13: Initial value of the filtered correlation function, $g^{(2)}_{\text{filtered}}(0)$, for the multi-mode array filter when resonant with the right (blue, solid) and central (green, dashed) peak. The other parameters are $\Omega/\gamma = 5\pi, N = 80, m = 1, \kappa = 2.5\delta\omega$.

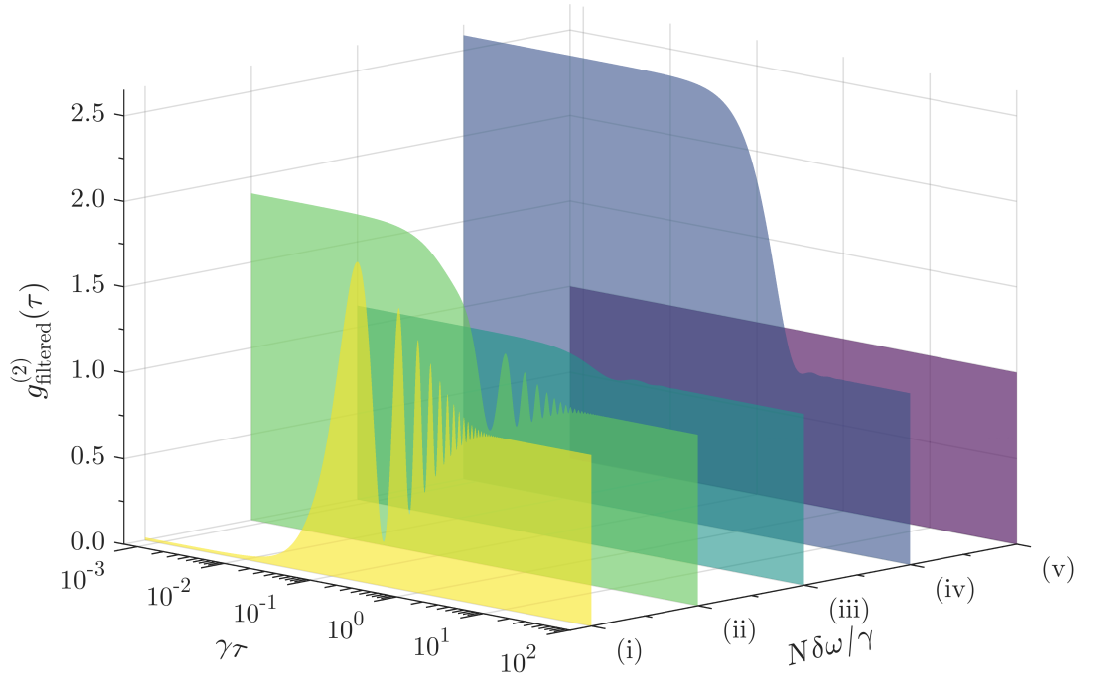

Figure 6.14: Frequency-filtered photon correlations of the central peak, $\Delta\omega_0/\gamma = 0.0$, for the regions of interest highlighted in Fig. 6.13. The halfwidths are $N\delta\omega/\gamma = 100$ (i), 14.5 (ii), 5.68 (iii), 0.0685 (iv), and 0.00001 (v). The other parameters are $\Omega/\gamma = 5\pi, N = 80, m = 1$, and $\kappa = 2.5\delta\omega$.

Skipping to region (v), the smallest halfwidth at $N\delta\omega/\gamma = 10^{-5}$, we see two very different correlations for the central and right peak. Firstly, for the filtered central peak, we see that the filtered correlation function is entirely second-order coherent, with $g^{(2)}_{\text{filtered}}(\tau) \approx 1$ in the purple curve in Fig. 6.14. As the filter width becomes smaller and smaller, more and more of the incoherent scattering is filtered out. The filter halfwidth then approaches that of the coherent driving laser, which can be reasonably modelled as a Dirac delta function. For the filtered right peak, as the filter halfwidth becomes increasingly smaller, the initial value tends towards $g^{(2)}_{\text{filtered}}(0) \approx 2$ (Fig. 6.13, orange dashed curve). From the perspective of the filter, the incoming field – which is entirely Lorentzian – becomes broader and broader. This effect, known as the 'thermalisation" of the source field [39, 41, 46], results in photon correlations resembling those of a broadband thermal field, i.e.,

$$g^{(2)}_{\text{filtered}}(\tau) = 1 + e^{-2N\delta\omega\tau}. \tag{6.25}$$

In region (ii), the filter halfwidth is approximately the same as the spacings between the sidebands, $N\delta\omega \approx \Omega$. When the filter is resonant with the central peak, the filter just encompasses all three peaks of the Mollow triplet; when resonant with the right peak, the filter suppresses the left sideband. This emerging peak in the initial value, $g^{(2)}_{\text{filtered}}(0)$, indicates a region of strong bunching, and is only possible when filtered with a near rectangular filter. This increase in bunching has in fact been reported by Kamide et al. in their study of frequency filtering using the "eigenvalue decomposition method" [57]. In this study, Kamide et al. calculated frequency-filtered correlation functions for Lorentzian, Gaussian, and pure rectangular filters. For the ideal rectangular filter, this peak occurs when the halfwidth is exactly equal to the splitting, Ω. In this region, the filter is able to detect cascaded emissions from the dressed states, e.g., $|u\rangle \to |u\rangle \to |l\rangle$ or $|l\rangle \to |l\rangle \to |u\rangle$. Hence, the probability of detecting two photons at zero time delay is increased, giving a higher initial correlation. The oscillations are still visible in the temporal evolution, as seen in the green curve in Fig. 6.14, however, due to the filter allowing multiple frequencies to pass through. When the filter is resonant with the right peak, we see this happening at two halfwidths, $N\delta\omega \approx \Omega$ and 2Ω, simply because the spacing between the right and central peaks is Ω, and the spacing between the right and left peaks is 2Ω.

The correlation functions in region (iii) are no different from what we saw in the previous section. For a halfwidth of $N\delta\omega/\gamma = 5.68$, the filter is able to reasonably isolate the target peaks, and hence the auto-correlation functions resemble that of the dressed state correlations derived in the secular approximation.

Finally, in region (iv), we see a large increase in the initial value, but only for the filtered central peak. Before discussing how the filtered correlation functions change, however, it will be helpful to first discuss how the intensities of the coherent and incoherent scattering of the filter change with decreasing halfwidth. From Eq. (5.42), the ratio of the intensity of the incoherent scattering and the coherent scattering from the multi-mode array filter is given by

$$\frac{I_{\text{inc}}}{I_{\text{coh}}} = \frac{\langle \Delta A^\dagger \Delta A \rangle_{ss}}{\langle A^\dagger \rangle_{ss} \langle A \rangle_{ss}} = \frac{\langle A^\dagger A \rangle_{ss}}{\langle A^\dagger \rangle_{ss} \langle A \rangle_{ss}} - 1, \tag{6.26}$$

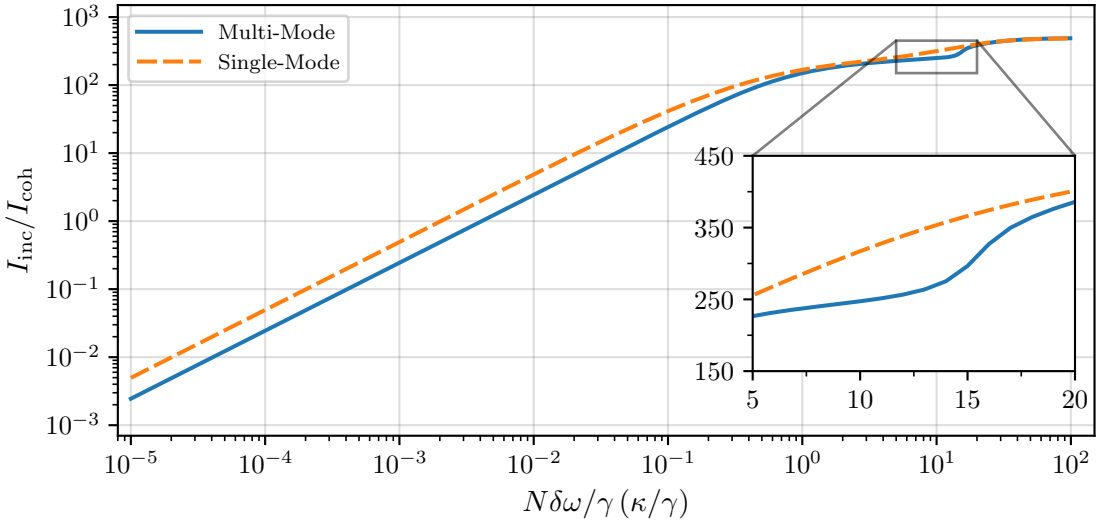

Figure 6.15: Intensity ratio of the filtered coherent and incoherent spectra for the multi-mode (blue, solid), with $N = 80, \kappa = 2.5\delta\omega$, and the single-mode (orange, dashed) filter, when resonant with the central peak, $\Delta\omega_0/\gamma = 0$. The inset is zoomed in on the region where $N\delta\omega \approx \Omega$, where there is a clear deviation between the multi-mode and single-mode intensity ratios. The single-mode ratio is calculated from Eq. (6.27), while the multi-mode ratio is numerically calculated from the steady-state equations. The driving amplitude is $\Omega/\gamma = 5\pi$.

which, for the single-mode filter resonant with the central peak, is

$$\frac{I_{\mathrm{inc}}}{I_{\mathrm{coh}}} = \frac{\gamma^2 + 2\Omega^2}{\gamma + 2\kappa} \frac{2\kappa\Omega^2 + (\gamma+\kappa)(\gamma+2\kappa)^2}{2\Omega^2 + (\gamma+\kappa)(\gamma+2\kappa)} - 1. \tag{6.27}$$

Figure 6.15 shows the intensity ratio for the multi-mode (blue, solid) and the single-mode (orange, dashed) filter, when resonant with the central peak. When the halfwidth of the filter is approximately in region (iii), we see that the intensity of the coherent scattering starts to dominate. Here, then, the interference between the two possible decay paths, $|u\rangle \to |u\rangle$ and $|l\rangle \to |l\rangle$, no longer holds, and thus the expected bunching of two possible transitions can be detected [17, 83]. Figure 6.15 also shows a deviation in the intensity ratio for the multi-mode array filter from the single-mode filter when $N\delta\omega, \kappa \approx \Omega$.

6.4 Second-Order Cross-Correlation Function

Now we take the filtered frequency system one step further and introduce a *second* filter. Tuning this second filter to a different transition allows us to *cross-correlate* two photons of different frequencies.

6.4.1 A new Hamiltonian and master equation

To achieve this two-filter coupling, we can pass the atomic fluorescence through a 50:50 beam splitter, with one arm coupling into the first filter, mode A, and the other arm into the second filter, mode B. The Hamiltonian and master equation describing this system is essentially the

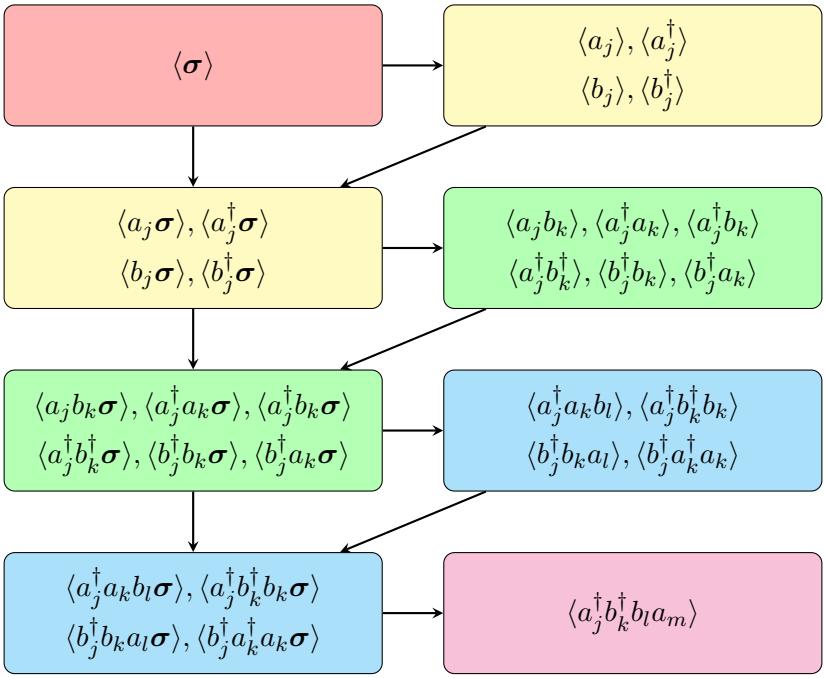

Figure 6.16: The operator moments couple in a cascaded scheme, where lower-order moments can be solved independently from the higher-order moments.

same as Eqs. (6.1) and (6.4), but with an extra coupling term. We then have the Hamiltonian

$$H = \hbar\frac{\Omega}{2}\left(\sigma_- + \sigma_+\right) + \hbar\sum_{j=-N}^{N}\Delta\omega_j^{(a)}a_j^\dagger a_j + \frac{i\hbar}{2}\sum_{j=-N}^{N}\left(\mathcal{E}_j^{(a)*}a_j\sigma_+ - \mathcal{E}_j^{(a)}a_j^\dagger\sigma_-\right) + \hbar\sum_{j=-N}^{N}\Delta\omega_j^{(b)}b_j^\dagger b_j + \frac{i\hbar}{2}\sum_{j=-N}^{N}\left(\mathcal{E}_j^{(b)*}b_j\sigma_+ - \mathcal{E}_j^{(b)}b_j^\dagger\sigma_-\right), \tag{6.28}$$

where

$$\Delta\omega_j^{(a)} = \left(\omega_0^{(a)} + j\delta\omega_a\right) - \omega_A, \quad \Delta\omega_j^{(b)} = \left(\omega_0^{(b)} + j\delta\omega_b\right) - \omega_A, \tag{6.29}$$

are the frequency detunings, and

$$\mathcal{E}_j^{(a)} = \sqrt{\frac{\gamma\kappa_a/2}{2N+1}}e^{imj\pi/N}, \quad \mathcal{E}_j^{(b)} = \sqrt{\frac{\gamma\kappa_b/2}{2N+1}}e^{imj\pi/N}, \tag{6.30}$$

are the mode-dependent couplings, for filters A and B, respectively. We note here that, different to Eq. (6.6), there is a factor of $1/2$ due to the 50:50 splitting of the atomic fluorescence. Similarly, the master equation is

$$\frac{\mathrm{d}\rho}{\mathrm{d}t} = \frac{1}{i\hbar}[H,\rho] + \frac{\kappa_a}{2}\sum_{j=-N}^{N}\left(2a_j\rho a_j^\dagger - a_j^\dagger a_j\rho - \rho a_j^\dagger a_j\right) + \frac{1}{2}\sum_{j=-N}^{N}\left(2C_j^{(a)}\rho C_j^{(a)\dagger} - C_j^{(a)\dagger}C_j^{(a)}\rho - \rho C_j^{(a)\dagger}C_j^{(a)}\right)$$

$$+\frac{\kappa_b}{2}\sum_{j=-N}^{N}\left(2b_j\rho b_j^\dagger - b_j^\dagger b_j\rho - \rho b_j^\dagger b_j\right)$$
$$+\frac{1}{2}\sum_{j=-N}^{N}\left(2C_j^{(b)}\rho C_j^{(b)\dagger} - C_j^{(b)\dagger}C_j^{(b)}\rho - \rho C_j^{(b)\dagger}C_j^{(b)}\right), \tag{6.31}$$

with cascaded decay operators:

$$C_j^{(a)} = \sqrt{\frac{\gamma/2}{2N+1}}e^{imj\pi/N}\sigma_- + \sqrt{\kappa_a}a_j, \quad C_j^{(b)} = \sqrt{\frac{\gamma/2}{2N+1}}e^{imj\pi/N}\sigma_- + \sqrt{\kappa_b}b_j. \tag{6.32}$$

For this two-filter system, we wish to correlate photons emitted from a mode, B, some time τ after detection of an emission from mode A. We therefore introduce the *frequency-filtered second-order cross-correlation function*:

$$g^{(2)}_{\text{cross}}(\tau) = \frac{\langle A^\dagger(0)B^\dagger B(\tau)A(0)\rangle_{ss}}{\langle A^\dagger A\rangle_{ss}\langle B^\dagger B\rangle_{ss}}, \tag{6.33}$$

with

$$A = \sum_{j=-N}^{N} a_j, \quad B = \sum_{j=-N}^{N} b_j. \tag{6.34}$$

Just like with the single-filter system, we may derive a set of operator moment equations, allowing a simple and efficient method to calculate the second-order two-time correlation function,

$$\langle A^\dagger(0)B^\dagger B(\tau)A(0)\rangle_{ss} = \sum_{j,k=-N}^{N}\langle A^\dagger(0)b_j^\dagger b_k(\tau)A(0)\rangle_{ss}. \tag{6.35}$$

The complete set of coupled moment equations, which can be found in Appendix C, follow the exact same structure as with the single-filter system, albeit with a few more equations needed. This structure is also depicted as a flowchart in Fig. 6.16, with all the necessary operator moments.

As there are multiple frequencies which we can investigate, we find it easier to redefine Eq. (6.33) as

$$g^{(2)}(\alpha,0;\beta,\tau) = \frac{\langle A^\dagger(0)B^\dagger B(\tau)A(0)\rangle_{ss}}{\langle A^\dagger A\rangle_{ss}\langle B^\dagger B\rangle_{ss}}, \tag{6.36}$$

where α and β indicate the central resonance frequencies of filters A and B. For the two-level atom, the simple structure of the atomic spectrum allows us to consider two identical filters. We will therefore set $\kappa_a = \kappa_b = \kappa$ and $\delta\omega_a = \delta\omega_b = \delta\omega$.

6.4.2 Photon-photon correlations of different transitions

The wider halfwidth of the filter gives a much faster temporal response, something we saw in the auto-correlation functions, Fig. 6.11. Due to the finite temporal response of a cavity filter, the cavity will inevitably have some effect on the output correlations [40, 41, 111]. A faster temporal response causes this effect to quickly decay, so that the filtered correlation function tends towards that of the secular approximation. We also saw that a wider filter halfwidth

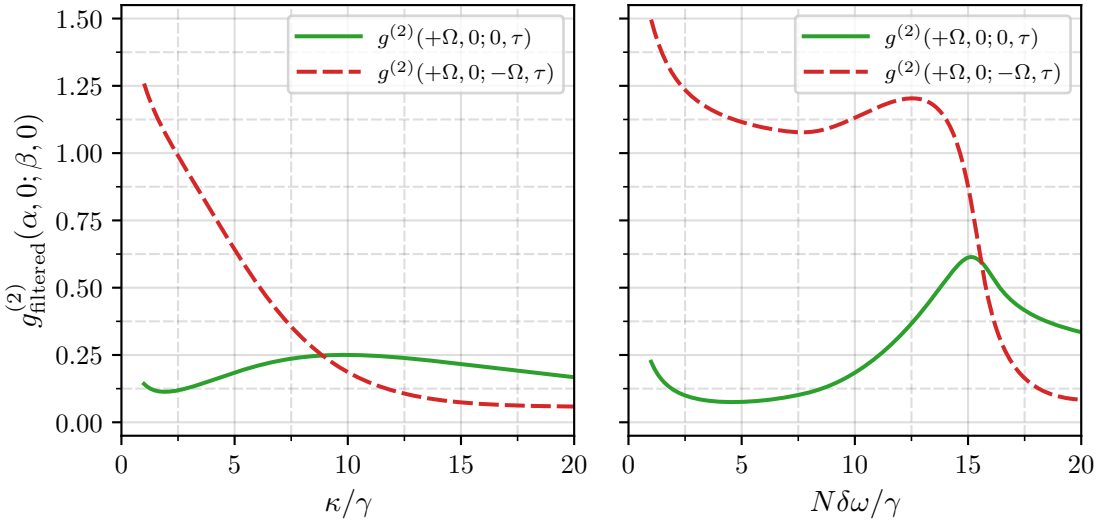

Figure 6.17: Initial cross-correlation value for the single- (left) and multi-mode array (right) filtered cross-correlations for right-to-central (green, solid) peak and left-to-right (red, dashed) peak detections.

resulted in a more accurate initial auto-correlation value, $g^{(2)}_{\text{filtered}}(0)$, up to the limit where the filter was unable to cleanly isolate the target frequency. Unfortunately this is not the case when considering frequency-filtered *cross*-correlations. Figure 6.17 shows the initial value of the right-to-central peak and right-to-left peak correlation functions. From the secular approximation, we expect the right-to-left peak cross-correlation to be perfectly bunched, with an initial value $g^{(2)}(+\Omega, 0; -\Omega, 0) = 2$; we also expect the right-to-central peak to be second-order coherent, with an initial value $g^{(2)}(+\Omega, 0; 0, 0) = 1$. As we see in Fig. 6.17, unlike the *auto*-correlation functions, the initial values are no longer indicative of the expected behaviour from the secular approximation.

That is, however, only true for the *long-time* behaviour. As discussed by Schrama et al. in 1992 (Section III in Ref. [26, 27]), there are short-time, $\tau \ll \gamma^{-1}$, and long-time, $\tau \gg \gamma^{-1}$, behaviours. In the long-time behaviour, the frequency-filtered correlation functions closely follow the dynamics derived in Section 5.4.3. We see this in the filtered correlation functions in Fig. 6.18, where, for $\tau > (N\delta\omega)^{-1}$, the filtered correlations closely follow the dressed state correlations (the grey dotted curve).

In the short-time behaviour, there are some more complicated dynamics occurring. For the right-to-central peak correlation, the left figure in Fig. 6.18, there are two different cascade decay pathways for the emission to occur: $|u\rangle \to |l\rangle \to |l\rangle$ and $|u\rangle \to |u\rangle \to |l\rangle$. With the first pathway a side peak photon is detected first, and in the second pathway a central peak photon is detected first. While these pathways correspond to two separate correlation functions, $g^{(2)}(+\Omega, 0; 0, \tau)$ and $g^{(2)}(0, 0; +\Omega, \tau)$, they are both transitions starting in the upper state $|u\rangle$ and ending in the lower state $|l\rangle$, for different time orderings. At zero time delay, both time orderings contribute equally to the initial correlation value and, in fact, cancel each other out,

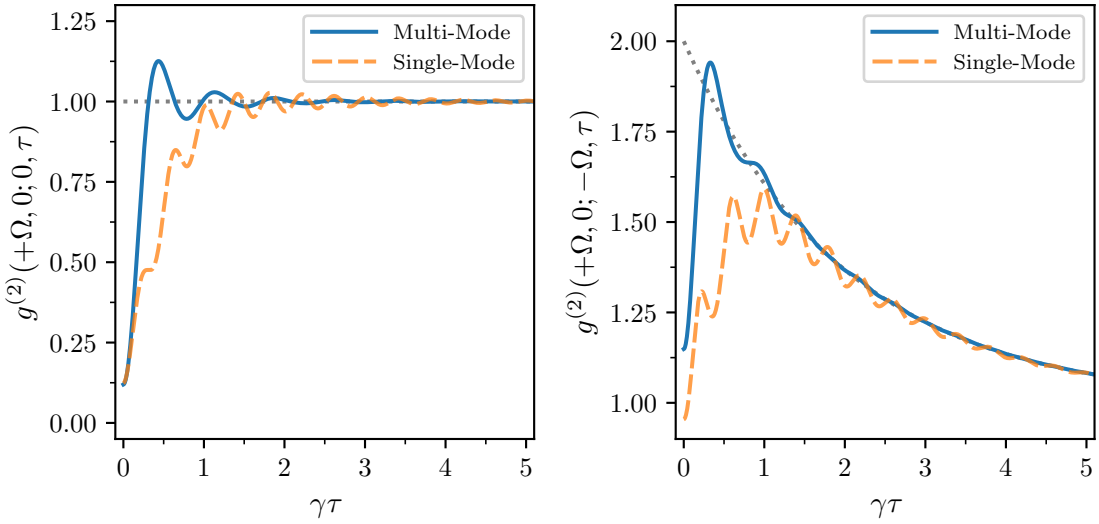

Figure 6.18: Multi-mode (blue, solid) and single-mode (orange, dashed) filtered cross-correlation function for the right-to-centre peak transitions (left) and the right-to-left peak transitions (right), compared against Eq. (5.68) and (5.66) (grey, dotted), respectively. The other parameters are $\Omega/\gamma = 5\pi, N = 80, \kappa = 2.5\delta\omega$, and $m = 1$.

which, from Eqs. (38) and (39) in Ref. [27], results in

$$g^{(2)}(+\Omega, 0; 0, \tau) = \left(1 - e^{-K\tau}\right)^2 = g^{(2)}(0, 0; +\Omega, \tau), \tag{6.37}$$

where K is the halfwidth of the filter system [27] – in our notation, κ for the single-mode filter and $N\delta\omega$ for the multi-mode array filter. We note here that Eq. 6.37 has been derived in the limit where the sidebands of the Mollow triplet are well separated, $\Omega \ggg \gamma$, such that each frequency can be ideally isolated. Similarly, for the side-peak to side-peak cross-correlations, $g^{(2)}(+\Omega, 0; -\Omega, \tau)$ and $g^{(2)}(-\Omega, 0; +\Omega, \tau)$, there is interference between the two different time orderings, and the bunching is diminished. The resulting short-time behaviour, from Eq. (40) in Ref. [26, 27], is

$$g^{(2)}(\pm\Omega, 0; \mp\Omega, \tau) = e^{-\frac{\gamma}{2}\tau} - 1 + 2\left(1 - \frac{1}{2}e^{-K\tau}\right)^2 + \frac{1}{2}e^{-2K\tau}. \tag{6.38}$$

Figure 6.19 shows the single- and multi-mode filtered correlation functions for the two transitions. Comparing these results with the *updated* secular approximation correlation functions, Eqs. (6.37) and (6.38), we see a close match. We also see similar results in experimental works by Ulhaq et al., Shatokhin et al., and others [14, 15, 23, 29, 56, 102, 112]. Once again, the sharper frequency response cut-off of the multi-mode array filter allows a more effective frequency isolation over the single-mode filter, as seen by the diminished Rabi oscillations.

6.4.3 Cross-correlations outside the Mollow triplet peaks

We are not just limited to correlating photons from only the three peaks of the Mollow triplet; we can set the resonance of each filter to be any frequency. In doing so, we are able

(a) Right Peak to Central Peak ($\Delta\omega_0^{(a)}/\gamma = 5\pi, \Delta\omega_0^{(b)}/\gamma = 0$)

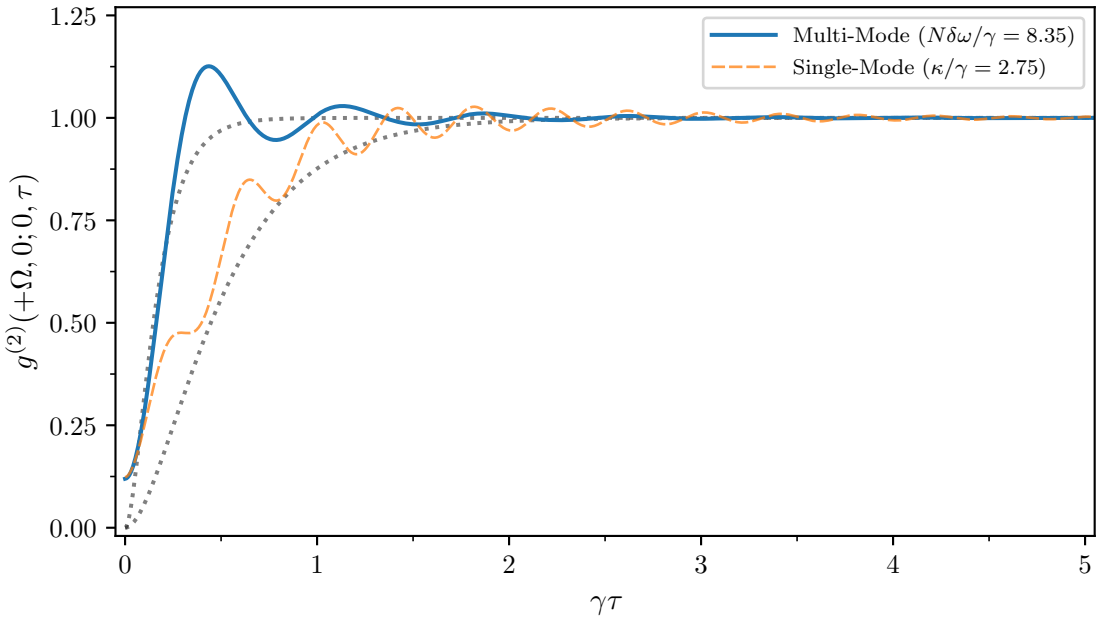

(b) Right Peak to Left Peak ($\Delta\omega_0^{(a)}/\gamma = 5\pi, \Delta\omega_0^{(b)}/\gamma = -5\pi$)

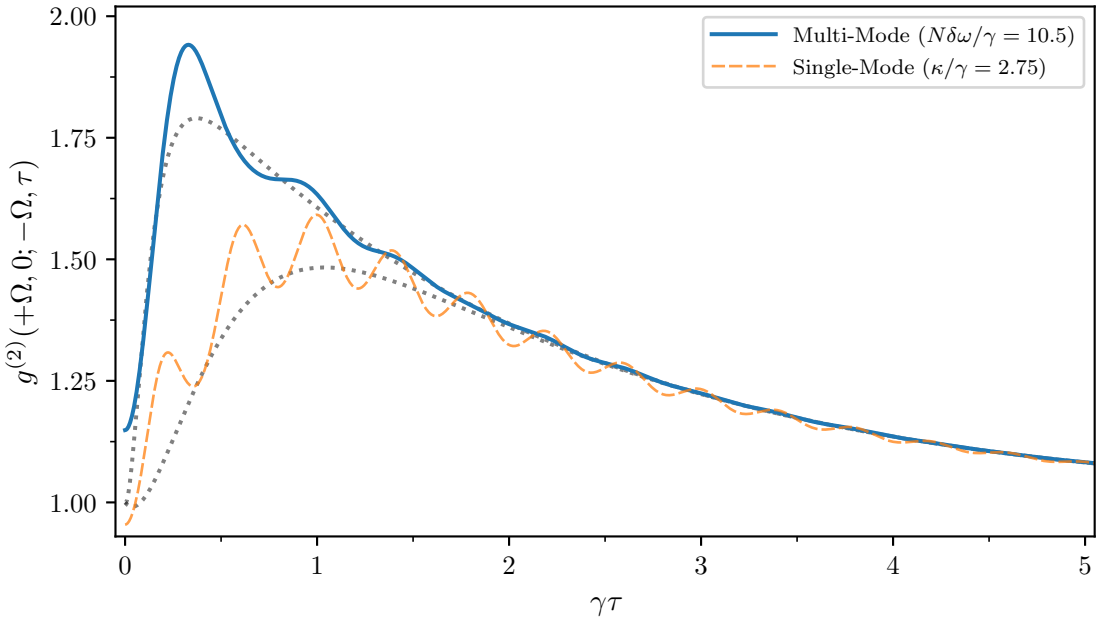

Figure 6.19: Multi-mode (blue, solid) and single-mode (orange, dashed) filtered cross-correlation function for the right-to-centre peak transitions (a) and the right-to-left peak transitions (b), compared against Eq. (6.37) and (6.38) (grey, dotted), respectively. The other parameters are $\Omega/\gamma = 5\pi, N = 80, \kappa = 2.5\delta\omega$, and $m = 1$.

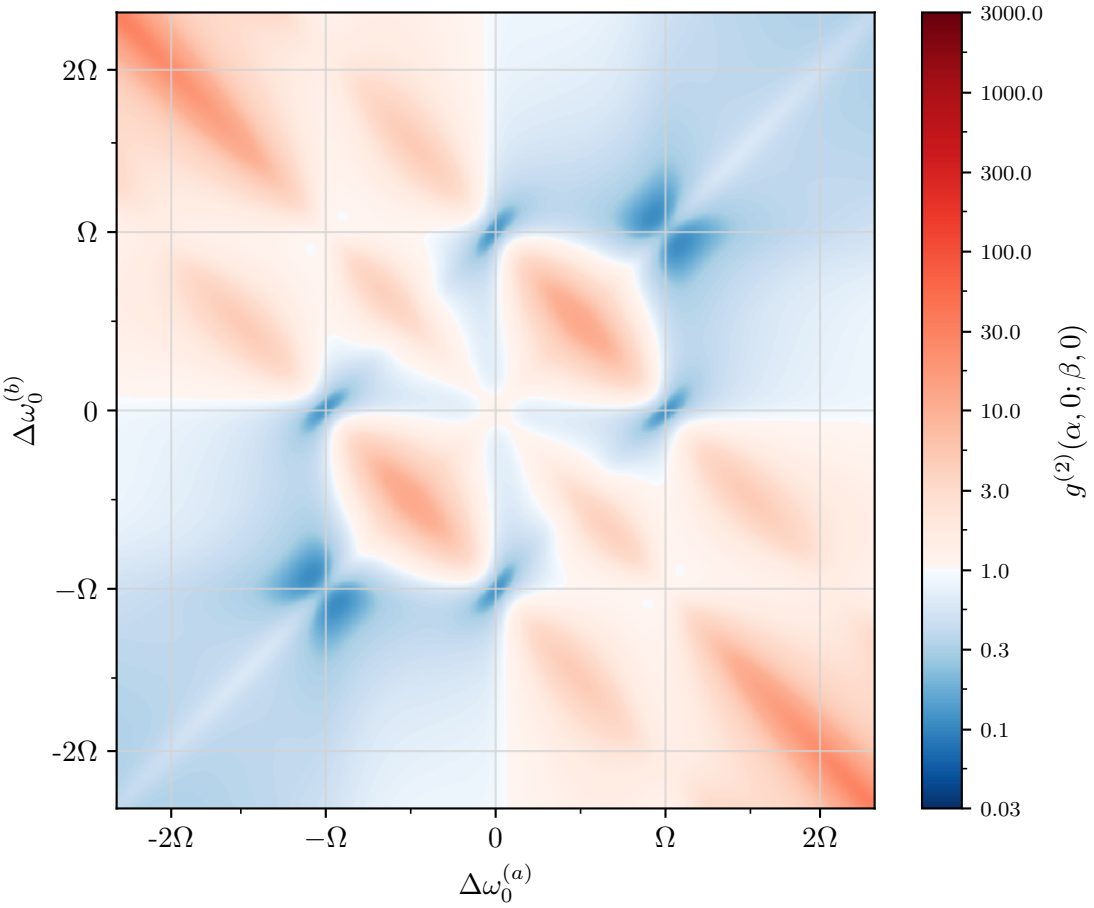

Figure 6.20: Scan of initial cross-correlation values for varying central frequencies of two single-mode filters. This figure is a reproduction of Fig. 1 in Ref. [102], using the model of this thesis. For this figure, blue corresponds to antibunching with $g^{(2)}(0) < 1$, red corresponds to bunching with $g^{(2)}(0) > 1$, and white corresponds to second-order coherence with $g^{(2)}(0) = 1$. The parameters are $\Omega/\gamma = 5\pi, N = 0$, and $\kappa/\gamma = 1.0$.

to uncover more interesting, and potentially useful, photon correlations. In Figs. 6.20 and 6.21 we depict a landscape of initial correlation values, by varying the central frequency of filters A and B of the single-mode and multi-mode array filters, respectively. Figure 6.20 in particular closely resembles results from recent work, both experimental and theoretical [46–48, 51, 102]. For this discussion, however, we will focus on the multi-mode filtered results, Fig. 6.21.

In the regions of auto-correlation surrounding each peak, $\Delta\omega_0^{(a)} \approx \Delta\omega_0^{(b)}$, we see the expected photon statistics; there are regions of strong antibunching, blue, surrounding the side peaks and near second-order coherence around the central peak. As expected, we also see the expected photon statistics surrounding the peaks in regions of cross-correlations; strong antibunching when targeting the central peak and either side peak, and second-order coherence for the left-to-right and right-to-left cross-correlations.

Things get interesting, however, when the filters are off resonant with the peaks. For the auto-correlation diagonal line, we see two regions of bunching in between the side peaks and the central peak. At the far edges of the cross-correlation, where $\Delta\omega_0^{(a)} = \pm 2\Omega$ and $\Delta\omega_0^{(b)} = \mp 2\Omega$,

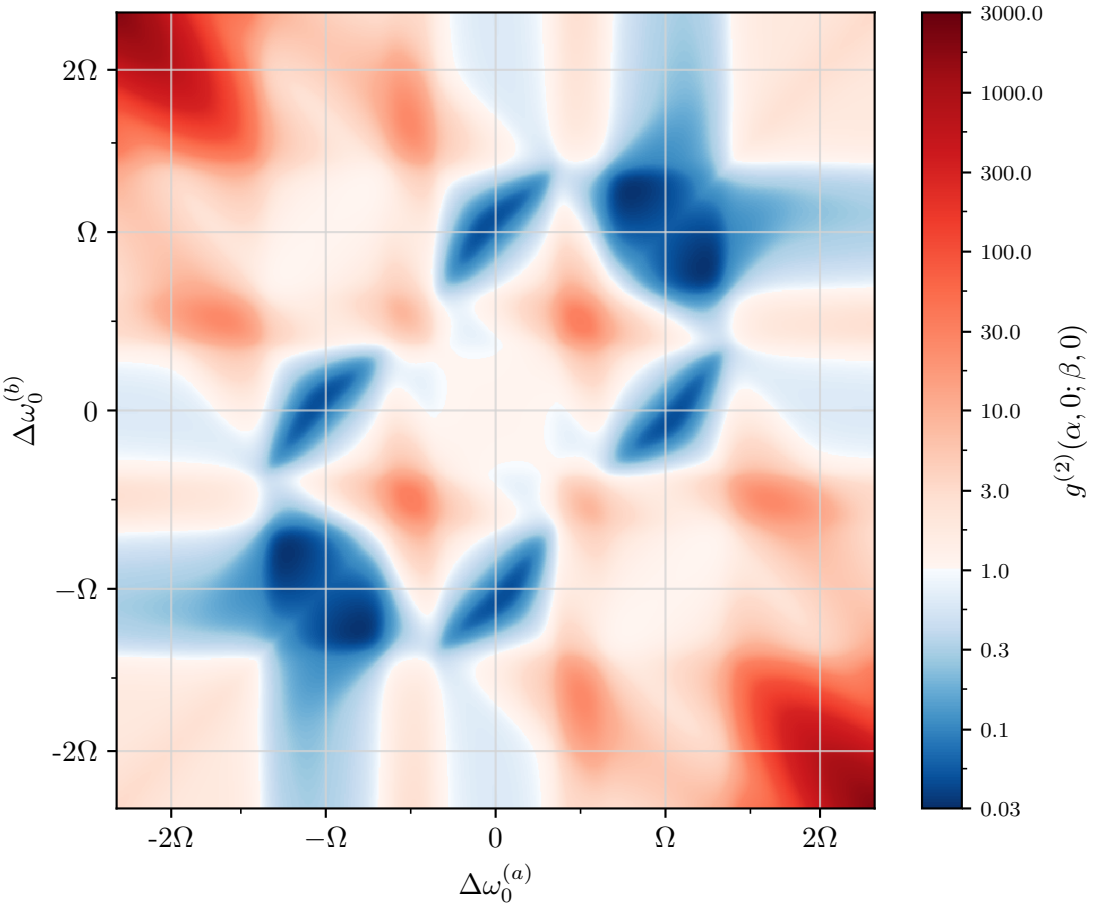

Figure 6.21: Scan of initial cross-correlation values for varying central frequencies of two multi-mode array filters. For this figure, blue corresponds to antibunching with $g^{(2)}(0) < 1$, red corresponds to bunching with $g^{(2)}(0) > 1$, and white corresponds to second-order coherence with $g^{(2)}(0) = 1$. The parameters are $\Omega/\gamma = 5\pi, N\delta\omega/\gamma = 6.3$ ($N = 80, \delta\omega/\gamma = 0.07875$), and $\kappa = 2.5\delta\omega$.

we also see extreme bunching, with initial correlation value of ≈ 2000. Why is it, then, that we see such intense bunching in these regions? There are two possible ways to explain this. The first possibility takes a more mathematical approach. When thinking of the power spectrum of the atomic fluorescence in these frequency ranges, we expect the field to be quite weak. When we couple the field into filters off resonant with the peaks, the weak field will result in a very low mean photon number inside each cavity, $\langle A^\dagger A\rangle_{ss}, \langle B^\dagger B\rangle_{ss} \ll 1$. Normalising by the product of the two mean photon numbers will drastically increase the initial value of the *normalised* correlation function.

The second approach considers a decay process known as the "leapfrog process" [30, 45, 46, 102]. This leapfrog process involves a simultaneous two-photon decay as two virtual photons, with halfway energy depicted by the dashed line in Fig. 6.22a. Figure 6.22a also shows the four possible two-photon decays that can occur: (i) $\omega_A + \Omega/2$ and $\omega_A - \Omega/2$, (ii) $\omega_A - \Omega/2$ and $\omega_A + \Omega/2$, and finally $\omega_A \pm \Omega/2$ and $\omega_A \pm \Omega/2$. We plot the auto- and cross-correlation functions, $g^{(2)}(+\Omega/2, 0; +\Omega/2, \tau)$ (blue solid curve) and $g^{(2)}(+\Omega/2, 0; 0, \tau)$ (orange dashed curve)

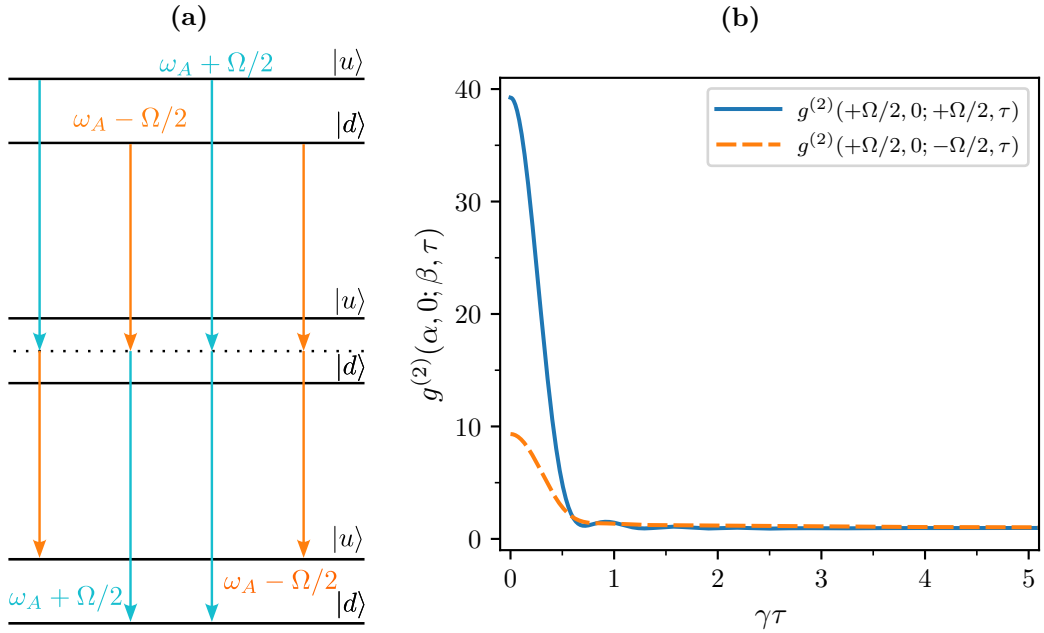

Figure 6.22: "Leapfrog" decay processes in the dressed state picture (a), and corresponding frequency-filtered cross-correlation functions (b). The processes labelled (i) and (ii) have an average frequency of ω_A, and correspond to the off-diagonal in Fig. 6.21. Processes (iii) and (iv) have average frequencies $\omega_A + \Omega/2$ and $\omega_A - \Omega/2$, respectively, and correspond to the diagonal. The parameters in (b) are $\Omega/\gamma = 5\pi, N\delta\omega/\gamma = 5.5$ ($N = 80, \delta\omega/\gamma = 0.07875$), and $\kappa = 2.5\delta\omega$.

in Fig. 6.22b, where we indeed see the strong bunching of the simultaneously emitted photons. The dynamics of these weak, yet experimentally measured [30], decay processes can only be detected by frequency filtering.

7 Two-Photon Resonance Fluorescence of a Three-Level Ladder-Type Atom

Where the Mollow triplet of the driven two-level atom was a relatively simple case to test the multi-mode array filter, we now turn our attention towards a slightly more complicated model: a three-level ladder-type atom. With the two-level atom, the frequency spacing between the sidebands was determined by the amplitude of the driving field; by simply increasing one parameter, we can separate the sidebands enough that the single-mode filter with a sufficiently large bandwidth will work well. This is not the case with the three-level ladder-type atom. The addition of an extra dipole transition complicates the dynamics of the system, especially with regards to the dressed states. The three-level ladder type atom offers a rich fluorescence spectrum consisting of up to seven separate frequencies, with different intensities and linewidths.

We begin this chapter by extending the model of the two-level atom, and introducing the model as used by Gasparinetti et al. [65, 66]. Initially interested in the three-level atom as a source of single photons due to the cascaded decay, it was found that, upon strong coherent excitation, the three-level atom can also produce strongly correlated bunches of photons [113–117]. With the model determined, we present a summary of some of the key results of Ngaha [118], i.e., the power spectrum and unfiltered photon correlations. Following Chapter 6, we then couple the emission from the three-level atom into the multi-mode array filter, and compare the frequency-filtered first- and second-order correlation functions against the single-mode filter. Finally, we introduce a second filter and compare the second-order cross-correlations. While the physical results will not differ greatly from those of Ngaha, we will see a remarkable improvement in the frequency isolation of the multi-mode array filter.

7.1 Modelling The Three-Level Atom

Here we briefly introduce the Hamiltonian and master equation of the radiatively damped three-level ladder-type atom, and derive expressions for the atomic dressed states when at two-photon resonance.

7.1.1 Time independent Hamiltonian

Following on from the description of the two-level atom, we extend our model to that of a three-level ladder type atom, with ground state $|g\rangle$, excited state $|f\rangle$, and intermediate state $|e\rangle$, with energies $\hbar\omega_g, \hbar\omega_f$, and $\hbar\omega_e$, respectively. With coherent driving of the $|g\rangle \leftrightarrow |e\rangle$ and $|e\rangle \leftrightarrow |f\rangle$ transitions, the Hamiltonian we consider is

$$H_A = \hbar\omega_g |g\rangle\langle g| + \hbar\omega_e |e\rangle\langle e| + \hbar\omega_f |f\rangle\langle f| + \hbar\frac{\Omega}{2}\left(|g\rangle\langle e| e^{i\omega_d t} + |e\rangle\langle g| e^{-i\omega_d t}\right) + \hbar\xi\frac{\Omega}{2}\left(|e\rangle\langle f| e^{i\omega_d t} + |f\rangle\langle e| e^{-i\omega_d t}\right), \tag{7.1}$$

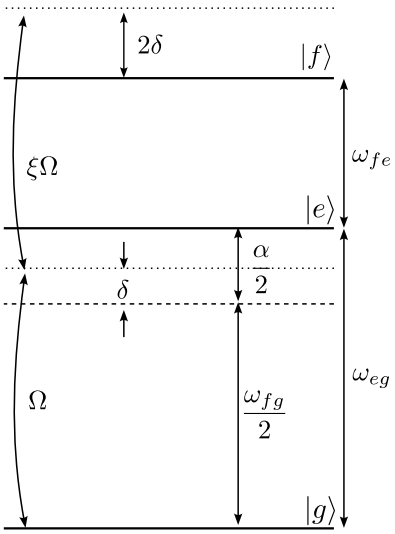

Figure 7.1: Energy level diagram of the three-level ladder-type atom. ω_{fg} is the two-photon resonance frequency, whereas ω_{eg} and ω_{fe} are the two single-photon resonances.

where

$$\xi = \frac{\boldsymbol{d}_{fe} \cdot \hat{\boldsymbol{e}}^*_{\boldsymbol{k},\lambda}}{\boldsymbol{d}_{eg} \cdot \hat{\boldsymbol{e}}^*_{\boldsymbol{k},\lambda}} \tag{7.2}$$

is the ratio of the dipole moments for the upper and lower dipole transitions, as defined by Eq. (5.6), and Ω is the coherent driving amplitude of the lower transition, Eq. (5.22). As with the two-level atom, we eliminate the time dependence in the Hamiltonian by transforming into a rotating frame. We thus obtain the *time-independent Hamiltonian for a driven three-level ladder-type atom*,

$$H_A = -\hbar\left(\frac{\alpha}{2} + \delta\right)|e\rangle\langle e| - 2\hbar\delta\,|f\rangle\langle f| + \hbar\frac{\Omega}{2}\left(\Sigma_+ + \Sigma_-\right), \tag{7.3}$$

where, following Gasparinetti et al. (Refs. [65, 66]),

$$\alpha = \omega_{fe} - \omega_{eg} \tag{7.4}$$

is the *anharmonicity* of the $|e\rangle \to |g\rangle$ and $|f\rangle \to |e\rangle$ transitions, with $\omega_{ij} = \omega_i - \omega_j$,

$$\delta = \omega_d - \frac{\omega_{fg}}{2} \tag{7.5}$$

is the *drive detuning from two-photon resonance*, and

$$\Sigma_- = |g\rangle\langle e| + \xi\,|e\rangle\langle f|, \quad \Sigma_+ = |e\rangle\langle g| + \xi\,|f\rangle\langle e| \tag{7.6}$$

are the *atomic lowering and raising operators*. We depict the structure and excitation of the three-level atom in Fig. 7.1.

If we wish to consider the case of two-photon resonance, with a cascaded decay from the $|f\rangle$ to $|g\rangle$, we must assume a large anharmonicity relative to the natural linewidth. If $|\alpha|$ is small, the atom can transition from the ground state $|g\rangle$ to the excited state $|f\rangle$ in two separate

absorption events, via the intermediate state $|e\rangle$. Here we are only interested in the case where this transition occurs via a simultaneous *two-photon* absorption, such that the intermediate level is only virtually populated.

7.1.2 Atomic moment equations for the three-level atom

To account for energy decay from the atom into the environment, we follow the same method by which we derived the master equation for the radiatively damped two-level atom, Eq. (5.23). We therefore extend that case to the three-level atom and consider the *master equation for the radiatively damped three-level ladder-type atom* [119, 120]:

$$\frac{\mathrm{d}\rho}{\mathrm{d}t} = \frac{1}{i\hbar}[H_A, \rho] + \frac{\Gamma}{2}\left(2\Sigma_-\rho\Sigma_+ - \Sigma_+\Sigma_-\rho - \rho\Sigma_+\Sigma_-\right), \tag{7.7}$$

where Γ is the population decay rate for the lower dipole, $\boldsymbol{d}_{eg}$, and Σ_- is, as before, the atomic lowering operator, Eq. (7.6).

Drawing even more inspiration from the two-level atom – the optical Bloch equations, in particular – we can derive a set of coupled operator moment equations for the three-level ladder-type atom:

$$\frac{\mathrm{d}}{\mathrm{d}t}\langle\boldsymbol{\Sigma}\rangle = \boldsymbol{M}\langle\boldsymbol{\Sigma}\rangle + \boldsymbol{B}, \tag{7.8}$$

with $(\sigma^{ii} = |i\rangle\langle i|, \sigma_-^{ij} = |j\rangle\langle i|, \sigma_+^{ij} = |i\rangle\langle j|)$

$$\langle\boldsymbol{\Sigma}\rangle = \begin{pmatrix} \langle\sigma^{gg}\rangle \\ \langle\sigma_-^{eg}\rangle \\ \langle\sigma_+^{eg}\rangle \\ \langle\sigma^{ee}\rangle \\ \langle\sigma_-^{fe}\rangle \\ \langle\sigma_+^{fe}\rangle \\ \langle\sigma_-^{fg}\rangle \\ \langle\sigma_+^{fg}\rangle \end{pmatrix}, \quad \boldsymbol{B} = \begin{pmatrix} 0 \\ 0 \\ 0 \\ \Gamma\xi^2 \\ i\xi\frac{\Omega}{2} \\ -i\xi\frac{\Omega}{2} \\ 0 \\ 0 \end{pmatrix}, \tag{7.9}$$

and

$$\boldsymbol{M}^{(\Sigma)} = \begin{pmatrix} 0 & -i\frac{\Omega}{2} & i\frac{\Omega}{2} & \Gamma & 0 & 0 & 0 & 0 \\ -i\frac{\Omega}{2} & -\left[\frac{\Gamma}{2}-i\left(\frac{\alpha}{2}+\delta\right)\right] & 0 & i\frac{\Omega}{2} & \Gamma\xi & 0 & -i\xi\frac{\Omega}{2} & 0 \\ i\frac{\Omega}{2} & 0 & -\left[\frac{\Gamma}{2}+i\left(\frac{\alpha}{2}+\delta\right)\right] & -i\frac{\Omega}{2} & 0 & \Gamma\xi & 0 & i\xi\frac{\Omega}{2} \\ -\Gamma\xi^2 & i\frac{\Omega}{2} & -i\frac{\Omega}{2} & -\Gamma(1+\xi^2) & -i\xi\frac{\Omega}{2} & i\xi\frac{\Omega}{2} & 0 & 0 \\ -i\xi\frac{\Omega}{2} & 0 & 0 & -i\xi\Omega & -\left[\frac{\Gamma}{2}(1+\xi^2)+i\left(\frac{\alpha}{2}-\delta\right)\right] & 0 & i\frac{\Omega}{2} & 0 \\ i\xi\frac{\Omega}{2} & 0 & 0 & i\xi\Omega & 0 & -\left[\frac{\Gamma}{2}(1+\xi^2)-i\left(\frac{\alpha}{2}-\delta\right)\right] & 0 & -i\frac{\Omega}{2} \\ 0 & -i\xi\frac{\Omega}{2} & 0 & 0 & i\frac{\Omega}{2} & 0 & -\left[\frac{\Gamma}{2}\xi^2-2i\delta\right] & 0 \\ 0 & 0 & i\xi\frac{\Omega}{2} & 0 & 0 & -i\frac{\Omega}{2} & 0 & -\left[\frac{\Gamma}{2}\xi^2+2i\delta\right] \end{pmatrix}. \tag{7.10}$$

Besides the obvious difference in the size of the evolution matrices – 3×3 for the two-level atom and 8×8 for the three-level atom – the structure of the atomic operator moment equations are the same. This matrix structure, then, allows for an easy implementation of the multi-mode array filter, just as it did with the two-level atom.

7.2 Atomic Fluorescence and Photon Correlations

Before investigating the frequency-filtered photon correlations from the fluorescence of the three-level atom, we will first discuss the *unfiltered case*. We start by introducing the dressed states of the three-level atom at two-photon resonance which, like the two-level atom, allows us to derive analytic expressions for the second-order correlation functions of each of the expected dressed state transitions. We then discuss the structure of the incoherent power spectrum, highlighting the rich dynamics that occur. Finally, we investigate the bunched nature of the atomic photon correlations.

While there is some interesting physics when considering off-resonance driving, $\delta \neq 0$, and for different dipole moment ratios, for this discussion we will stick to the case of two-photon resonance, with $\xi = 1$. For a discussion on the effects of the drive detuning and the dipole moment ratio, please refer to Ngaha [118].

7.2.1 The dressed states of the three-level atom

Diagonalising the Hamiltonian, Eq. (7.3), we find that the dressed state eigenfrequencies are solutions to the characteristic polynomial,

$$\omega_i^3 + \left(\frac{\alpha}{2} + 3\delta\right)\omega_i^2 + \left[(\alpha + 2\delta)\,\delta - \left(\frac{\Omega}{2}\right)^2\left(1+\xi^2\right)\right]\omega_i - 2\delta\left(\frac{\Omega}{2}\right)^2 = 0. \tag{7.11}$$

Cubic polynomials generally have complicated roots, therefore we simplify this equation by considering the special case of two-photon resonance. Setting $\delta = 0$, the three eigenfrequencies are:

$$\omega_m = 0, \tag{7.12a}$$

$$\omega_u = -\frac{\alpha}{4} + \sqrt{\left(\frac{\alpha}{4}\right)^2 + \left(\frac{\Omega}{2}\right)^2(1+\xi^2)}, \tag{7.12b}$$

$$\omega_l = -\frac{\alpha}{4} - \sqrt{\left(\frac{\alpha}{4}\right)^2 + \left(\frac{\Omega}{2}\right)^2(1+\xi^2)}, \tag{7.12c}$$

with corresponding eigenstates,

$$|m\rangle = \frac{1}{\sqrt{1+\xi^2}}\Big(\xi\,|g\rangle - |f\rangle\Big), \tag{7.13a}$$

$$|u\rangle = \frac{1}{\sqrt{4\omega_u^2 + \Omega^2\left(1+\xi^2\right)}}\Big(\Omega\,|g\rangle + 2\omega_u\,|e\rangle + \xi\Omega\,|f\rangle\Big), \tag{7.13b}$$

$$|l\rangle = \frac{1}{\sqrt{4\omega_l^2 + \Omega^2\left(1+\xi^2\right)}}\Big(\Omega\,|g\rangle + 2\omega_l\,|e\rangle + \xi\Omega\,|f\rangle\Big), \tag{7.13c}$$

such that

$$H_A\,|m\rangle = \hbar\omega_m\,|m\rangle\,, \quad H_A\,|u\rangle = \hbar\omega_u\,|u\rangle\,, \quad H_A\,|l\rangle = \hbar\omega_l\,|l\rangle\,. \tag{7.14}$$

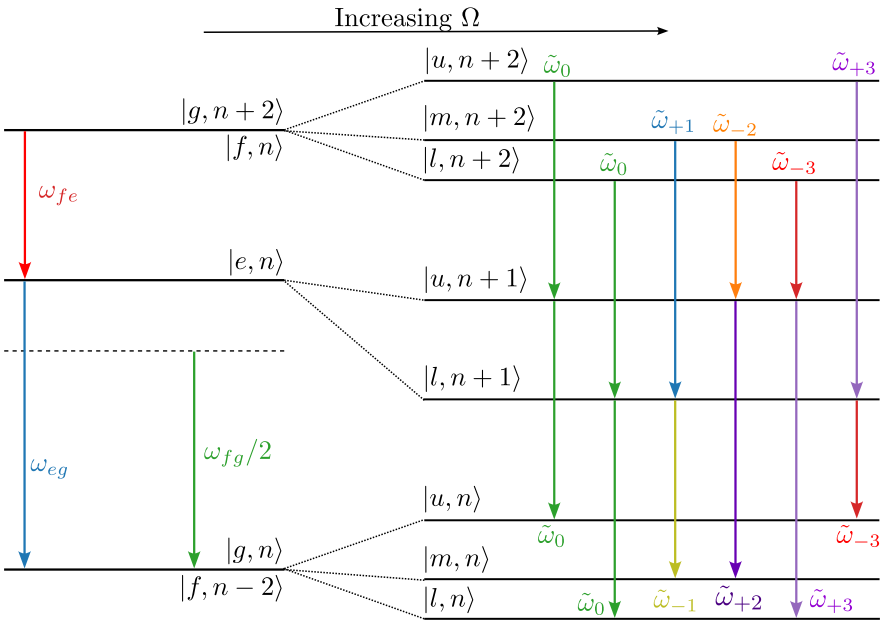

Figure 7.2: Energy level diagram of the dressed states of the three-level ladder-type atom at two-photon resonance ($\delta = 0$), with all possible transition paths shown.

These dressed states, as depicted in Fig. 7.2 with uncoupled atom-field states, open up several more decay channels than the two-level atom. We expect, in fact, seven different possible frequencies to appear in the fluorescence spectrum:

$$\tilde{\omega}_0 = \omega_d, \tag{7.15a}$$

$$\tilde{\omega}_{\pm 1} = \omega_d \pm (\omega_m - \omega_l)\,, \tag{7.15b}$$

$$\tilde{\omega}_{\pm 2} = \omega_d \pm (\omega_u - \omega_m)\,, \tag{7.15c}$$

$$\tilde{\omega}_{\pm 3} = \omega_d \pm (\omega_u - \omega_l)\,. \tag{7.15d}$$

While the dressed states of the three-level atom are more complex, we are still able to derive expressions for first- and second-order correlation functions in the *secular approximation* for the various different dressed state transitions. Assuming a large separation between the dressed state frequencies, in the limit $\Omega \gg \Gamma$, we derive moment equations for a set of dressed state operators ($\omega_{ij} = \omega_i - \omega_j$):

$$\frac{\mathrm{d}}{\mathrm{d}t}\langle\sigma_-^{um}\rangle = -\left(\frac{\Gamma_{um}}{2} + i\omega_{um}\right)\langle\sigma_-^{um}\rangle, \qquad \frac{\mathrm{d}}{\mathrm{d}t}\langle\sigma_+^{um}\rangle = -\left(\frac{\Gamma_{um}}{2} - i\omega_{um}\right)\langle\sigma_+^{um}\rangle, \tag{7.16a}$$

$$\frac{\mathrm{d}}{\mathrm{d}t}\langle\sigma_-^{ml}\rangle = -\left(\frac{\Gamma_{ml}}{2} + i\omega_{ml}\right)\langle\sigma_-^{ml}\rangle, \qquad \frac{\mathrm{d}}{\mathrm{d}t}\langle\sigma_+^{ml}\rangle = -\left(\frac{\Gamma_{ml}}{2} - i\omega_{ml}\right)\langle\sigma_+^{ml}\rangle, \tag{7.16b}$$

$$\frac{\mathrm{d}}{\mathrm{d}t}\langle\sigma_-^{ul}\rangle = -\left(\frac{\Gamma_{ul}}{2} + i\omega_{ul}\right)\langle\sigma_-^{ul}\rangle, \qquad \frac{\mathrm{d}}{\mathrm{d}t}\langle\sigma_+^{ul}\rangle = -\left(\frac{\Gamma_{ul}}{2} - i\omega_{ul}\right)\langle\sigma_+^{ul}\rangle, \tag{7.16c}$$

and

$$\frac{\mathrm{d}}{\mathrm{d}t}\begin{pmatrix}\langle\sigma_{mm}\rangle\\ \langle\sigma_{uu}\rangle\end{pmatrix} = \boldsymbol{M}\begin{pmatrix}\langle\sigma_{mm}\rangle\\ \langle\sigma_{uu}\rangle\end{pmatrix} + \boldsymbol{B}, \tag{7.17}$$

where

$$\sigma_{-}^{um} = |m\rangle\langle u|, \quad \sigma_{+}^{um} = |u\rangle\langle m|, \tag{7.18a}$$

$$\sigma_{-}^{ml} = |l\rangle\langle m|, \quad \sigma_{+}^{ml} = |m\rangle\langle l|, \tag{7.18b}$$

$$\sigma_{-}^{ul} = |l\rangle\langle u|, \quad \sigma_{+}^{ul} = |u\rangle\langle l|, \tag{7.18c}$$

$$\sigma_{mm} = |m\rangle\langle m|, \quad \sigma_{uu} = |u\rangle\langle u|, \tag{7.18d}$$

are the dressed state operators. For more details of the derivation, definitions of the decay rates, Γ_{ij}, and the evolution matrix and nonhomogeneous vector, $\boldsymbol{M}$ and $\boldsymbol{B}$, please refer to Appendix D.

Analytic expressions can easily be derived for the raising and lowering operators in Eq. (7.16), due to their uncoupled nature. The first-order correlation functions then resemble Eqs. (5.63), in that they are simple exponential functions. The resulting power spectra in the dressed state approximation, for all but the central frequency term, can derived be as Lorentzians.

Unfortunately, the dressed states and their corresponding frequencies for the three-level atom, Eqs. (7.13) and (7.12), are not simple expressions, even when considering two-photon resonance. We therefore generalise the second-order correlation function, by considering two dressed state transitions, labelled "1" and "2", with initial and final states labelled "i" and "f",

$$|1\rangle_i \longrightarrow |1\rangle_f, \quad |2\rangle_i \longrightarrow |2\rangle_f, \tag{7.19}$$

and corresponding dressed state operators, from Eqs. (7.18),

$$\sigma_1 = |1\rangle_{f\,i}\langle 1|, \quad \sigma_2 = |2\rangle_{f\,i}\langle 2|. \tag{7.20}$$

Using the quantum regression equations, Eq. (3.47b) in particular, the second-order two-time correlation function for the two dressed state transitions is then defined as

$$g^{(2)}_{\text{auto}}(\tau) = \frac{\langle \sigma_1^\dagger(0)\sigma_1^\dagger\sigma_1(\tau)\sigma_1(0)\rangle_{ss}}{\langle \sigma_1^\dagger\sigma_1\rangle^2_{ss}}, \tag{7.21}$$

or, for a general two-transition case,

$$g^{(2)}_{\text{cross}}(\tau) = \frac{\langle \sigma_1^\dagger(0)\sigma_2^\dagger\sigma_2(\tau)\sigma_1(0)\rangle_{ss}}{\langle \sigma_1^\dagger\sigma_1\rangle_{ss}\langle \sigma_2^\dagger\sigma_2\rangle_{ss}}. \tag{7.22}$$

As an example, we consider one of the dressed state transition frequencies, Eqs. (7.15), $\tilde{\omega}_{+1} = \omega_d + (\omega_m - \omega_l)$. This frequency is the result of the dressed state transition $|m\rangle \to |l\rangle$, with dressed state operator σ_-^{ml}. The normalised auto-correlation function for this dressed state transition is then given by

$$g^{(2)}_{\tilde{\omega}_{+1}}(\tau) = \frac{\langle \sigma_+^{ml}(0)\sigma_+^{ml}\sigma_-^{ml}(\tau)\sigma_-^{ml}(0)\rangle_{ss}}{\langle \sigma_+^{ml}\sigma_-^{ml}\rangle^2_{ss}}. \tag{7.23}$$

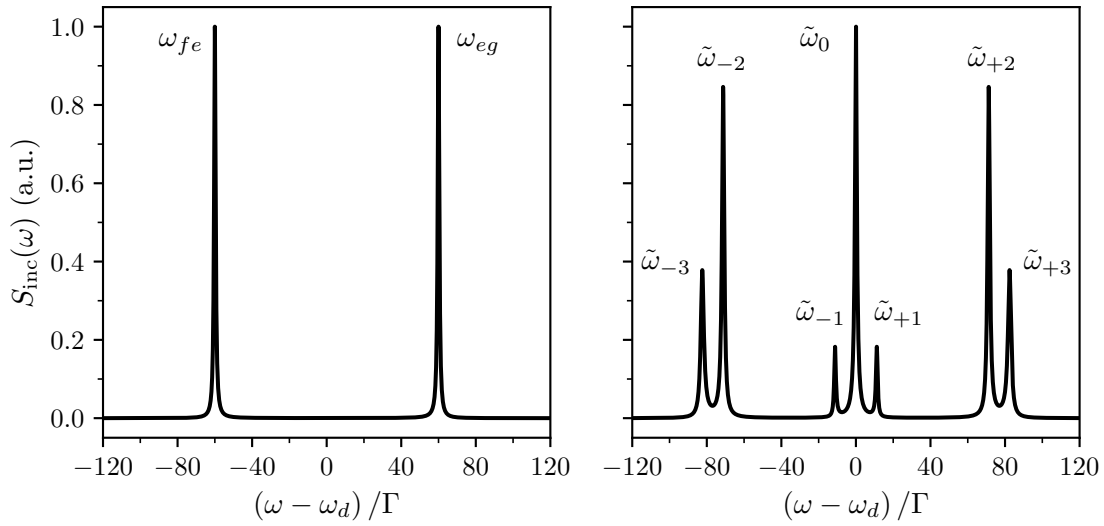

Figure 7.3: Incoherent power spectrum of the driven three-level atom for weak, $\Omega/\Gamma = 0.01$ (left), and strong driving, $\Omega/\Gamma = 40.0$ (right) strengths. The other parameters are $\alpha/\Gamma = -120.0, \delta/\Gamma = 0.0$, and $\xi = 1.0$.

For the other transition frequencies we have:

$$g^{(2)}_{\tilde{\omega}_0} = \frac{\langle \sigma_z^{ul}(0)\sigma_z^{ul}\sigma_z^{ul}(\tau)\sigma_z^{ul}(0)\rangle_{ss}}{\langle \sigma_z^{ul}\sigma_z^{ul}\rangle^2_{ss}}, \tag{7.24a}$$

$$g^{(2)}_{\tilde{\omega}_{+2}} = \frac{\langle \sigma_-^{um}(0)\sigma_-^{um}\sigma_+^{um}(\tau)\sigma_+^{um}(0)\rangle_{ss}}{\langle \sigma_-^{um}\sigma_+^{um}\rangle^2_{ss}}, \tag{7.24b}$$

$$g^{(2)}_{\tilde{\omega}_{+3}} = \frac{\langle \sigma_-^{ul}(0)\sigma_-^{ul}\sigma_+^{ul}(\tau)\sigma_+^{ul}(0)\rangle_{ss}}{\langle \sigma_-^{ul}\sigma_+^{ul}\rangle^2_{ss}} \tag{7.24c}$$

where $\sigma_z^{ul} = |u\rangle\langle u| - |l\rangle\langle l|$. These correlation functions can be computed numerically and, as in Chapter 6, will be what we compare against the frequency-filtered correlation functions.

7.2.2 Atomic fluorescence spectrum

We define the *normalised first-order correlation function for the three-level ladder-type atom* as

$$g^{(1)}_{ss}(\tau) = \frac{\langle \Sigma_+(0)\Sigma_-(\tau)\rangle_{ss}}{\langle \Sigma_+\Sigma_-\rangle_{ss}}, \tag{7.25}$$

such that the coherent and incoherent components of the power spectrum are:

$$S_{\mathrm{coh}}(\omega) = \frac{1}{2\pi}\frac{1}{\langle \Sigma_+\Sigma_-\rangle_{ss}}\int_{-\infty}^{\infty} e^{i\omega\tau}\langle\Sigma_+\rangle_{ss}\langle\Sigma_-\rangle_{ss}\mathrm{d}\tau, \tag{7.26a}$$

$$S_{\mathrm{inc}}(\omega) = \frac{1}{2\pi}\frac{1}{\langle \Sigma_+\Sigma_-\rangle_{ss}}\int_{-\infty}^{\infty} e^{i\omega\tau}\langle\Delta\Sigma_+(0)\Delta\Sigma_-(\tau)\rangle\mathrm{d}\tau. \tag{7.26b}$$

For weak driving amplitudes, $\Omega < \Gamma$, the dressed states of the atom are mostly degenerate. The only de-excitation path available to the atom, then, is via a *cascaded decay*; the first decay emission from $|f\rangle$ to $|e\rangle$ by emitting a photon of frequency ω_{fe}, followed by a decay from $|e\rangle$ to

$|g\rangle$ with a photon of frequency ω_{eg}. We see this in the power spectrum as two separate peaks at $\omega_d \pm \alpha/2$ in Fig. 7.3. As the drive detuning increases, the frequency separation between the two peaks will decrease. As the drive detuning approaches single-photon resonance, that is, the frequency of the drive field is resonant with the lower dipole transition, $\omega_d = \omega_{eg}$, the incoherent power spectrum will resemble that of the resonantly driven two-level atom.

As the driving strength increases, we see two structures appearing; these are shown for three different values of the dipole moment ratio, ξ, in Fig. 7.4. The two sidebands each shift away from the single-photon frequencies due to a Stark shifting of the energy levels [121, 122]. The single-photon peaks also split into doublets, and are separated by the dressed state frequency $|\omega_l|$. Meanwhile, a central triplet also emerges around the two-photon resonance frequency. This triplet is similar to the Mollow triplet, and can in fact be found in two-level atoms driven at two-photon resonance [123]. Each peak of the incoherent power spectrum is labelled with the appropriate frequency, Eqs. (7.15), in Fig. 7.3.

Figures 7.5a - 7.5c show the effect that different dipole moment ratios have on the structure of the incoherent power spectrum. When $\xi = 1$ there is an equal driving amplitude for both dipoles, as well as an equal decay rate. This is reflected in the completely symmetric incoherent power spectrum, Fig. 7.7b, where each pair of spectral peaks, $\tilde{\omega}_{\pm i}$, have the same height. When $\xi \neq 1$, the power spectrum becomes asymmetric, with certain peaks being suppressed. In Fig. 7.5a, $\xi = 0.5$, we see the left sideband of the central triplet is much smaller than the right sideband, with frequencies corresponding to the upper dipole transition. With a lower moment ratio, the driving amplitude and the decay rate of the upper dipole is weaker than the lower dipole transition. We can then expect to see fewer transitions originating from the upper dipole transition, and thus lower intensities for the respective peaks in the incoherent power spectrum.

7.2.3 Atomic photon correlations

Following on from the first-order correlation function, we introduce the *normalised second-order correlation function for the three-level atom*:

$$g^{(2)}_{ss}(\tau) = \frac{\langle \Sigma_+(0)\Sigma_+\Sigma_-(\tau)\Sigma_-(0)\rangle_{ss}}{\langle \Sigma_+\Sigma_-\rangle^2_{ss}}. \tag{7.27}$$

As we saw in Chapter 5, photons emitted from a two-level atom are always perfectly anti-bunched, due to the finite time between a photon being emitted and the atom being re-excited. For the three-level atom, the atomic lowering operator, Σ_-, is a combination of the lowering operators for the two dipoles that make up the three-level atom, therefore an emission detected by a photon detector, with the operator Σ_-, can be from either the $|f\rangle \to |e\rangle$ transition, or the $|e\rangle \to |g\rangle$ transition.

In the low driving regime, the cascaded decay that gives rise to the two distinct peaks in the power spectrum, in Fig. 7.3, results in strongly bunched photons. When a photon is emitted from the upper dipole, another photon must follow it for the atom to completely de-excite to the ground state. Thus, detecting a first photon at time $\tau = 0$, there is a much higher probability of detecting another photon immediately after. Decreasing the driving amplitude, as in Fig. 7.6, we see that the initial correlation value *increases*. For weaker and weaker driving amplitudes,

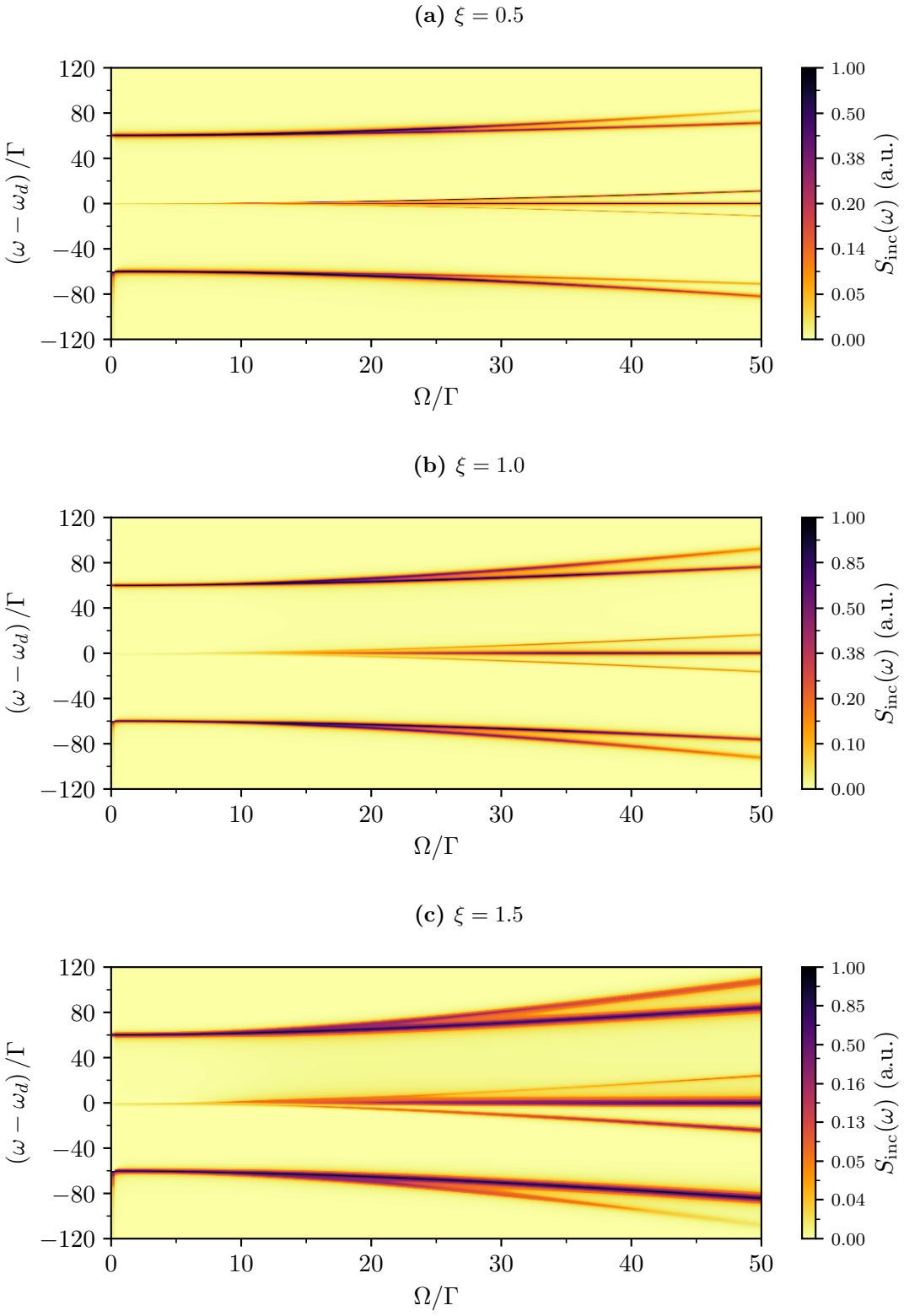

Figure 7.4: Normalised incoherent power spectrum of the three-level atom at two-photon resonance, $\delta = 0$, as a function of the driving amplitude, Ω, for $\xi = 0.5$ (a), $\xi = 1.0$ (b), and $\xi = 1.5$ (c). The anharmonicity is $\alpha/\Gamma = -120$.

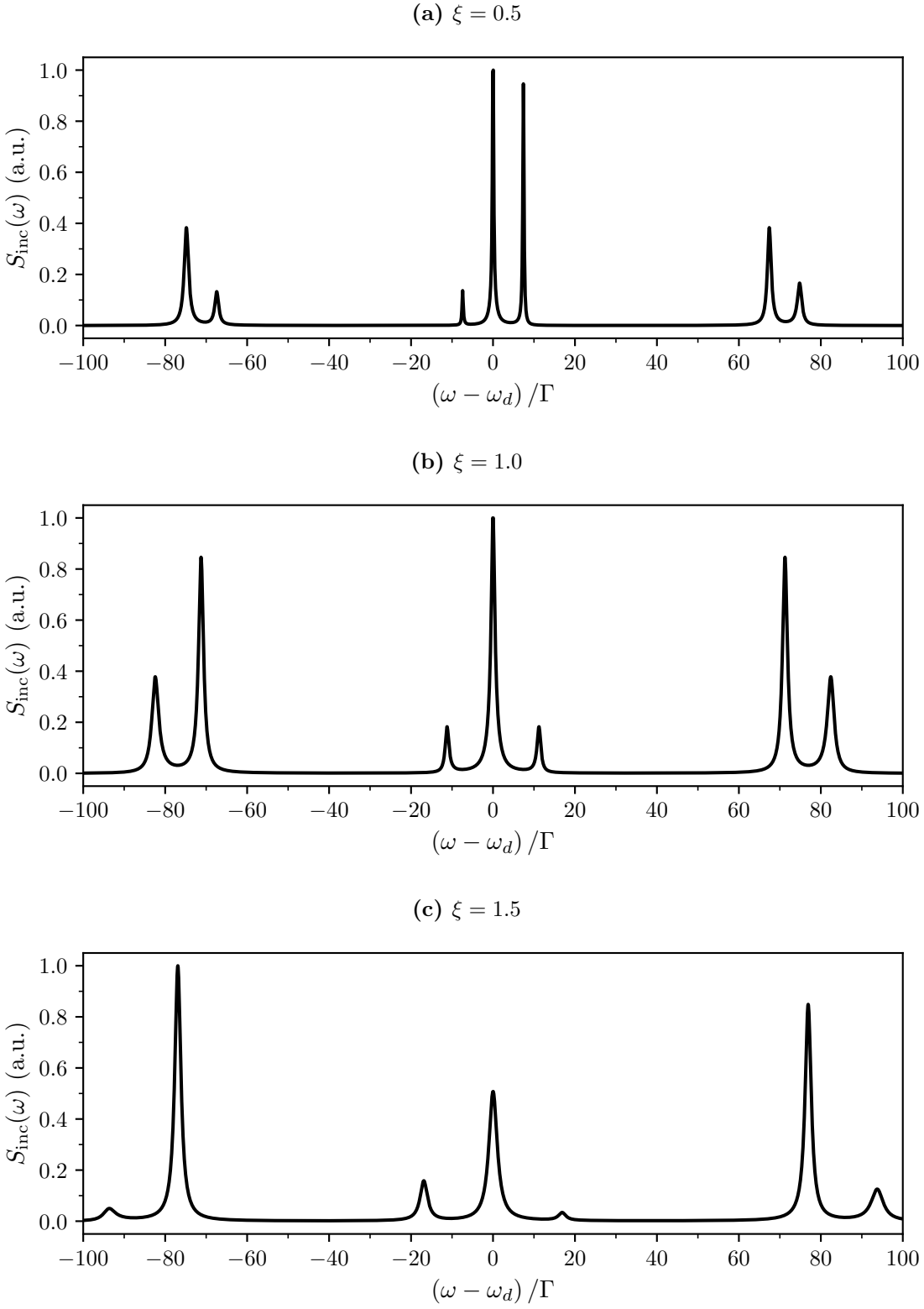

Figure 7.5: Normalised incoherent power spectrum of the three-level atom at two-photon resonance, $\delta/\Gamma = 0$, for $\xi = 0.5$ (a), $\xi = 1.0$ (b), and $\xi = 1.5$ (c). The other parameters are $\Omega/\Gamma = 40$ and $\alpha/\Gamma = -120$.

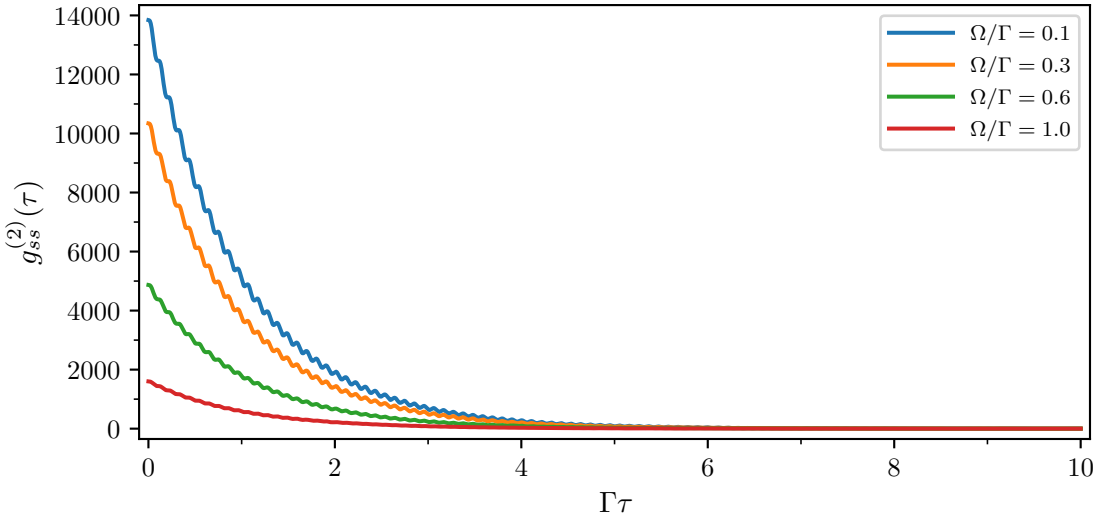

Figure 7.6: Unfiltered photon correlations, $g^{(2)}_{ss}(\tau)$, of the three-level atom at low driving amplitudes: $\Omega/\Gamma = 0.1$ (blue), 0.3 (orange), 0.6 (green), and 1.0 (red). The other parameters are $\alpha/\Gamma = -120.0, \delta/\Gamma = 0.0$, and $\xi = 1.0$.

two-photon absorption events become more and more infrequent, and thus the time between emissions grows. As a photon of frequency ω_{eg} will *always* follow a photon of frequency ω_{fe}, the "bunching" of the photon pairs becomes more distinct, hence a large initial value. There are also weak, yet visible, oscillations appearing in the correlation function with frequency $|\alpha|/2$ (Ref. [118], Section 6.2.1), due to the two different frequencies of photons detected.

Moving into the strong driving regime, specifically $\Omega/\Gamma = 40$, we see a considerable change in the nature of the photon correlations. Figure 7.7 shows the correlation functions for three values of the dipole moment ratio: $\xi = 0.5$, 1.0, and 1.5. Even in the strong driving regime, we still see the small oscillations, however they are of frequency $|\omega_d + \omega_u|$. There is also a much stronger component oscillating at the dressed state frequency $|\omega_d + \omega_l|$; this is the frequency separation between the sideband doublets and the sidebands of the central triplet. Another important distinction is that the time it takes for the correlations to decay to unity is dependent on ξ; for smaller values of ξ, the correlation functions take much longer to reach their steady state. This is to be expected as the rate at which the $|f\rangle$ state decays to $|e\rangle$ is $\xi^2\Gamma$, therefore a lower dipole moment ratio will result in a longer expected time between photons emitted from the upper dipole than the lower dipole.

The dipole moment ratio also appears to affect the initial correlation value. With a small dipole ratio, $\xi = 0.5$ in Fig. 7.7a, most of the steady-state atomic population will be in either the ground state $|g\rangle$ or the excited state $|f\rangle$. Hence, when a photon is detected at $\tau = 0$, the population will shift to the intermediate state, $|e\rangle$, which has a high probability of decay, resulting in bunched photons, $g^{(2)}(0) > 0$. We then see, as ξ increases in Figs. 7.7b and 7.7c, that the initial value decreases. In contrast to the lower dipole moment ratio, if $\xi > 1$, the atomic population will mostly be in the ground or intermediate states. Therefore, following a photon detection, the atom will likely be in the ground state, and thus there is a low probability for another detection to occur immediately, resulting in a lower initial correlation value.

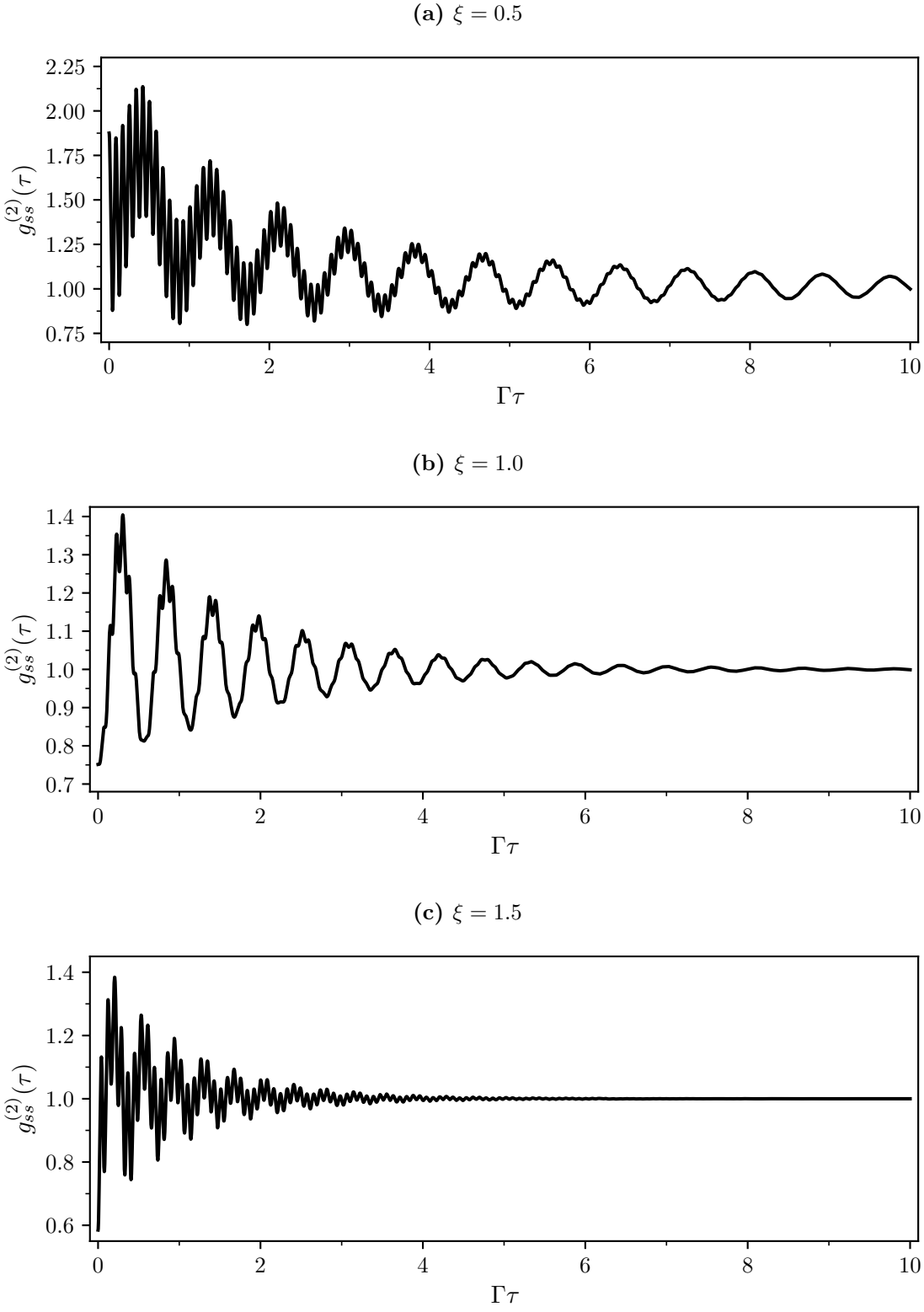

Figure 7.7: Second-order correlation functions of the three-level atom in the strong driving regime, $\Omega/\Gamma = 40$, for three dipole moment ratios: $\xi = 0.5$ (a), 1.0 (b), and 1.5(c). The other parameters are $\alpha/\Gamma = -120$ and $\delta/\Gamma = 0.0$

7.3 Multi-Mode Array Filtered Three-Level Atom Fluorescence

We have thus far summarised some of the key results that make the three-level ladder-type atom an interesting system. Following on from Chapter 6, we now investigate the atom through the lens of the multi-mode array filter. In doing so, we will demonstrate once again that the multi-mode array filter offers better performance than the single-mode Lorentzian filter, with regards to isolation of individual peaks in the fluorescence, while also verifying the dressed state picture for the three-level atom.

We therefore cascade the fluorescence emitted by the three-level atom into the multi-mode array filter, as described by the Hamiltonian is

$$\begin{aligned} H = &-\hbar\left(\frac{\alpha}{2}+\delta\right)|e\rangle\langle e| - 2\hbar\delta\,|f\rangle\langle f| + \hbar\frac{\Omega}{2}\left(\Sigma_- + \Sigma_+\right) \\ &+ \hbar\sum_{j=-N}^{N}\Delta\omega_j a_j^\dagger a_j + \frac{i\hbar}{2}\sum_{j=-N}^{N}\left(\mathcal{E}_j^* a_j\Sigma_+ - \mathcal{E}_j a_j^\dagger\Sigma_-\right), \end{aligned} \tag{7.28}$$

where

$$\Delta\omega_j = (\omega_0 + j\delta\omega) - \omega_d, \tag{7.29}$$

is the frequency detuning of the j^{th} mode from the atomic driving frequency, with mode frequency spacing $\delta\omega$, and

$$\mathcal{E}_j = \sqrt{\frac{\Gamma\kappa}{2N+1}}e^{imj\pi/N}, \tag{7.30}$$

is the mode-dependent coupling, as in Eq. (4.18). The master equation describing this system is then

$$\begin{aligned} \frac{\mathrm{d}\rho}{\mathrm{d}t} = &\frac{1}{i\hbar}[H,\rho] + \frac{\kappa}{2}\sum_{j=-N}^{N}\left(2a_j\rho a_j^\dagger - a_j^\dagger a_j\rho - \rho a_j^\dagger a_j\right) \\ &+ \frac{1}{2}\left(2C_j\rho C_j^\dagger - C_j^\dagger C_j\rho - \rho C_j^\dagger C_j\right), \end{aligned} \tag{7.31}$$

with cascaded decay operator:

$$C_j = \sqrt{\frac{\Gamma}{2N+1}}e^{imj\pi/N}\Sigma_- + \sqrt{\kappa}a_j. \tag{7.32}$$

We follow on from the two-level atom and derive a set of coupled moment equations for the coupled atom-filter mode operators. The structure of the coupling is the same as with the two-level atom, as shown in Fig. 6.2. Using these coupled moment equations, we numerically calculate the first- and second-order correlation functions for all results presented in this section. While not displayed here, all of the moment equations for the single-filter system, as well as the equations for solving the first- and second-order correlation functions, can be found in Appendix E.

Unless otherwise stated, the results presented in this section are calculated in the strong driving regime at two-photon resonance, with fixed parameters $\Omega/\Gamma = 40.0, \alpha/\Gamma = -120.0, \delta/\Gamma = 0.0$, and $\xi = 1.0$.

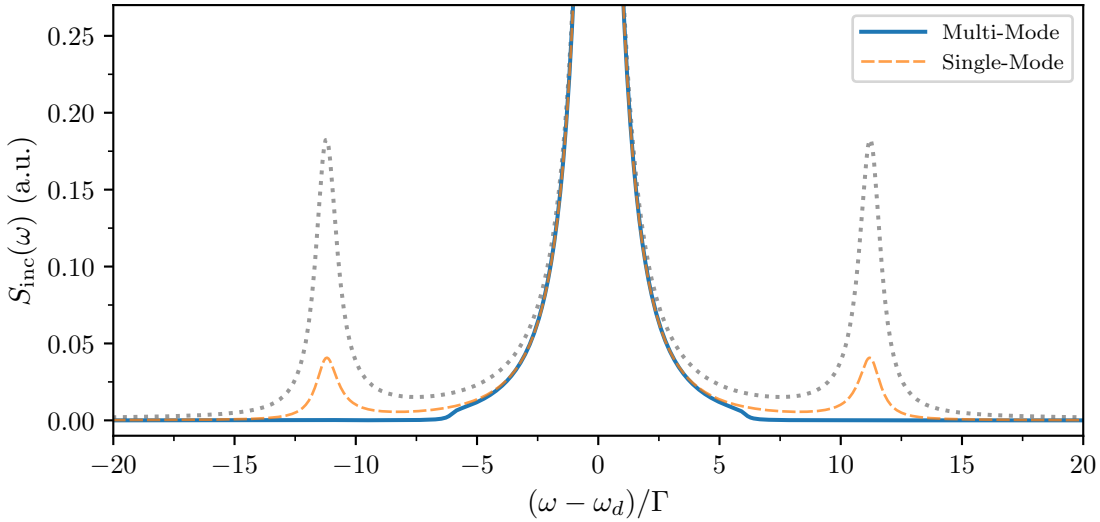

Figure 7.8: Frequency-filtered incoherent power spectrum of the central peak of the three-level atom, $\Delta\omega_0 = 0$, for the multi-mode array filter (blue, solid), with $N\delta\omega/\Gamma = 6.0$, and the single-mode filter (orange, dashed), with $\kappa/\Gamma = 6.0$. The filtered spectra are compared against the full atomic spectrum (grey, dotted). The multi-mode array filter parameters are $N = 80$ and $\kappa = 2.5\delta\omega$.

7.3.1 Frequency-filtered incoherent power spectrum

As in the previous chapter, the normalised first-order correlation function for the multi-mode array filtered three-level atom is

$$g^{(1)}_{\mathrm{filtered}}(\tau) = \frac{\langle A^\dagger(\tau)A(0)\rangle_{ss}}{\langle A^\dagger A\rangle_{ss}}, \tag{7.33}$$

and, using the definition of the quantum fluctuation operators, Eq. (5.39), the incoherent power spectrum of the filtered fluorescence is given by

$$S_{\mathrm{inc}}(\omega) = \frac{1}{2\pi}\frac{1}{\langle A^\dagger A\rangle_{ss}}\int_{-\infty}^{\infty} e^{i\omega\tau}\langle \Delta A^\dagger(\tau)\Delta A(0)\rangle_{ss}\mathrm{d}\tau. \tag{7.34}$$

Figures 7.3 - 7.5 have shown us that the unfiltered incoherent power spectrum of the three-level atom is much more complicated, and indeed more interesting, than the simple two-level atom. In the strong driving regime, the sideband doublets and the central triplet are well separated, yet the separation between each peak of the triplet and doublets is the dressed state frequency ω_l, Eq. (7.12c).

Figures 7.8 and 7.9 show comparisons of the frequency-filtered incoherent power spectra of the single- and multi-mode array filters when resonant with each of the seven peaks. The filter halfwidths for both the single- and multi-mode filters are chosen such that the fullwidth encompasses the entire peak of interest, and thus is set to $\kappa/\Gamma = 6$ for the single-mode filter, and $N\delta\omega/\Gamma = 6$ for the multi-mode filter, with $N = 80$ and $\delta\omega/\Gamma = 0.075$. For the chosen atomic parameters ($\Omega/\Gamma = 40, \alpha/\Gamma = -120, \delta/\Gamma = 0, \xi = 1$), the frequency separation of the split peaks is, from Eq. (7.12c), $\omega_l/\Gamma \approx 11$. This relatively close spacing results in some inevitable overlap

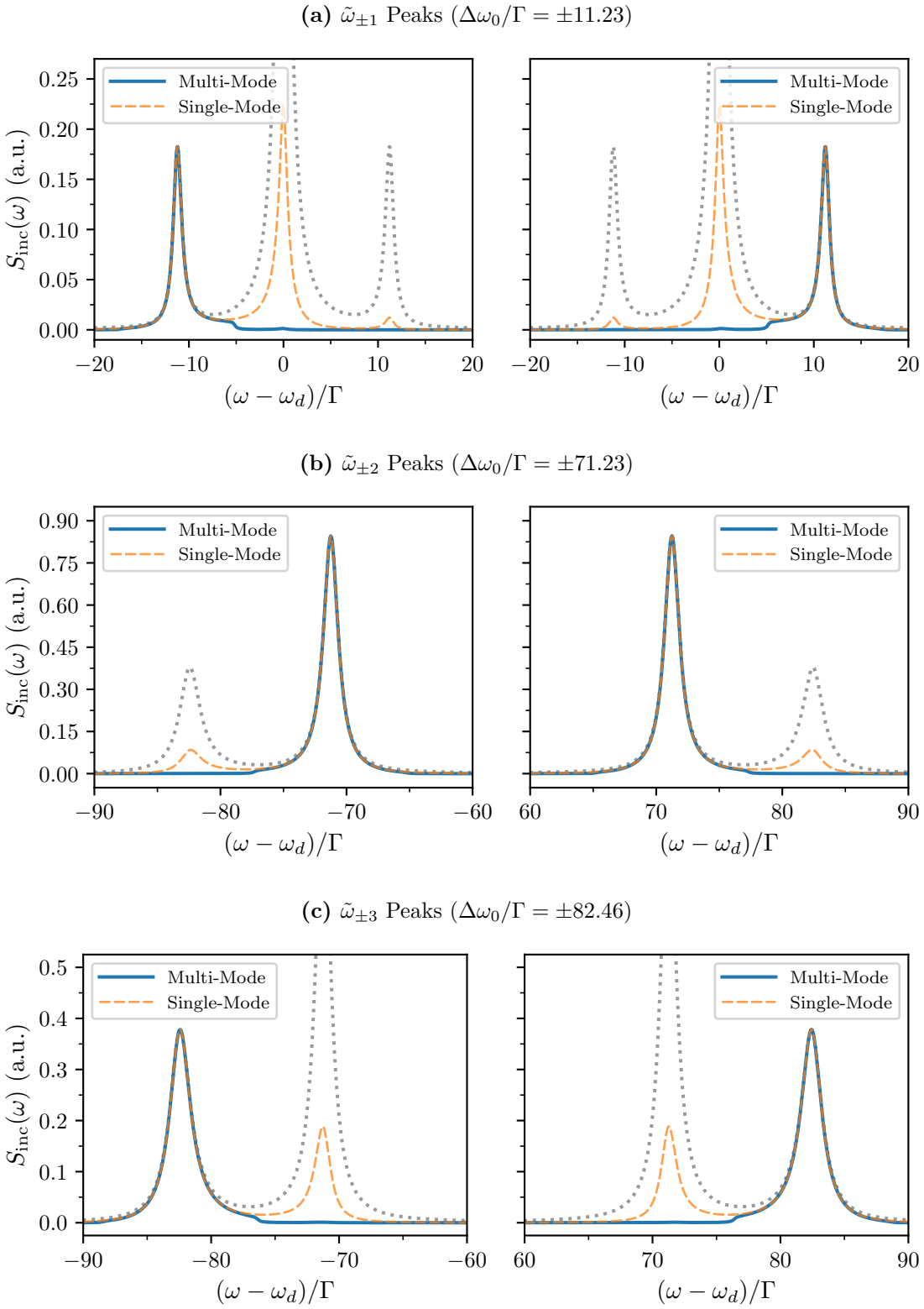

Figure 7.9: Frequency-filtered incoherent power spectrum of the side peaks of the three-level atom, $\Delta\omega_0 = \tilde{\omega}_{\pm1}$ (a), $\tilde{\omega}_{\pm2}$ (b), and $\tilde{\omega}_{\pm3}$ (c), for the multi-mode array filter (blue, solid), with $N\delta\omega/\Gamma = 6.0$, and the single-mode filter (orange, dashed), with $\kappa/\Gamma = 6.0$. The filtered spectra are compared against the full atomic spectrum (grey, dotted). The multi-mode array filter parameters are $N = 80$ and $\kappa = 2.5\delta\omega$.

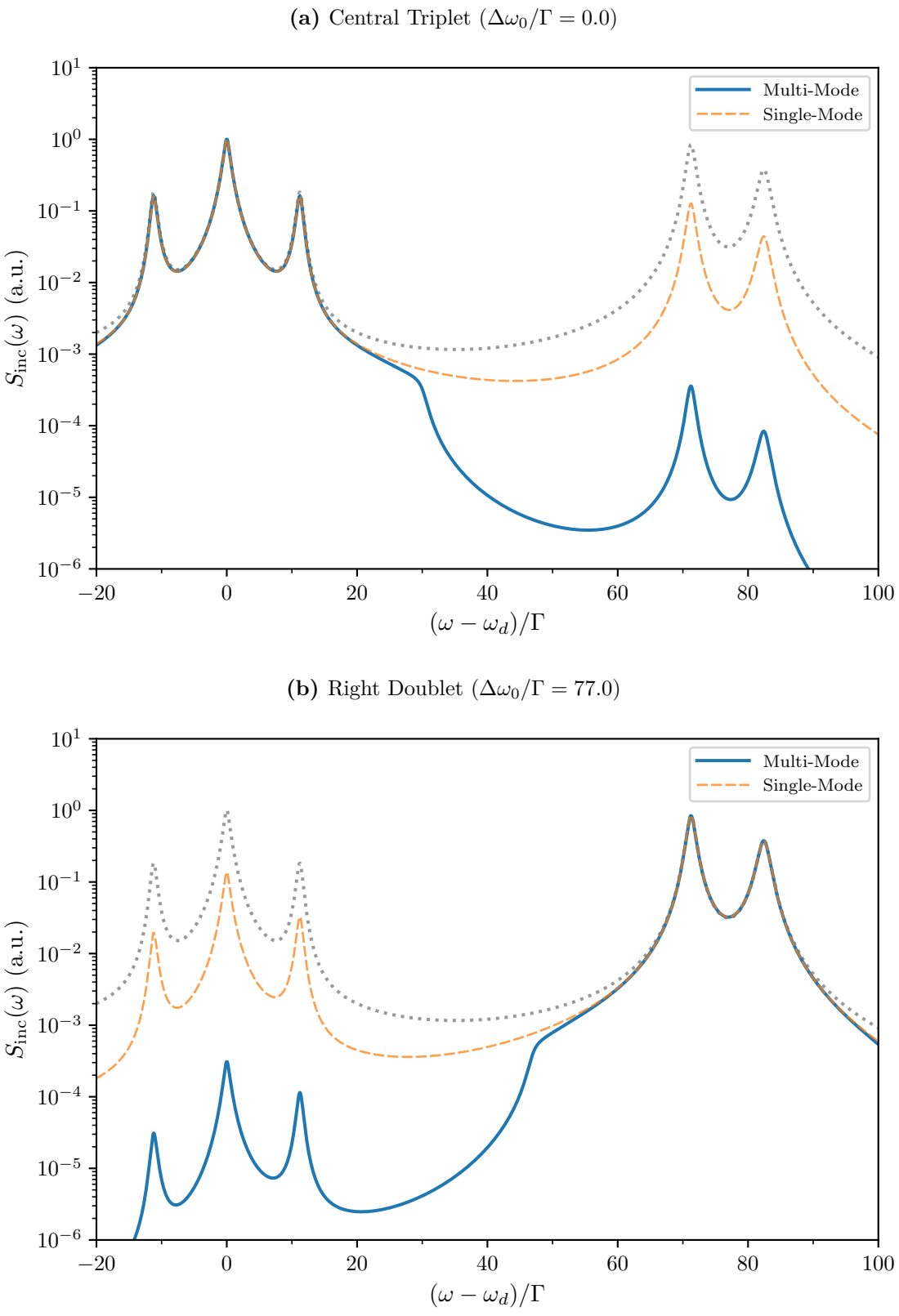

Figure 7.10: Frequency-filtered incoherent power spectrum of the central triplet, $\Delta\omega_0/\Gamma = 0.0$ (a), and right triplet, $\Delta\omega_0/\Gamma = 77.0$ (b), of the three-level atom for the multi-mode array filter (blue, solid), with $N\delta\omega/\Gamma = 30.0$, and the single-mode filter (orange, dashed), with $\kappa/\Gamma = 30.0$. The filtered spectra are compared against the full atomic spectrum (grey, dotted). The multi-mode array filter parameters are $N = 80$ and $\kappa = 2.5\delta\omega$.

between the peaks, making it difficult to isolate a target frequency entirely. We do see, however, the sharp cut-off in the frequency response of the multi-mode array filter playing an effective role in suppressing non target frequencies, just as we saw in Section 6.2.

The sharp frequency cut-off of the multi-mode array filter also allows us to correlate photons originating from the side doublets or the central triplet. To filter these frequency structures, we require a much larger filter halfwidth such that the entire doublet or triplet is enveloped by the frequency response. For a single-mode Lorentzian filter, larger filter halfwidths have even longer tails, easily allowing photons of other frequencies to enter. Figures 7.10a and 7.10b show the filtered incoherent spectra – on a logarithmic scale – when tuned to the central triplet and right doublet, respectively. For the respective spectral structure of interest, we see that both the single- and multi-mode filters accurately recreate the atomic spectrum. While the multi-mode array filter (blue) does not perfectly reject the other frequency peaks, the non target frequencies are approximately three orders of magnitude weaker than for the single-mode filter (orange, dashed). We also clearly see the sudden decrease in intensity of the multi-mode array filter around the filter halfwidth, $N\delta\omega/\Gamma = 30$.

7.3.2 Auto-correlations

We now look towards the frequency-filtered *second*-order correlation functions of the filtered three-level atom, where, as in Eq. (6.10), the second-order correlation function for the multi-mode array filter is

$$g^{(2)}_{\text{filtered}}(\tau) = \frac{\langle A^\dagger(0)A^\dagger A(\tau)A(0)\rangle_{ss}}{\langle A^\dagger A\rangle^2_{ss}}. \tag{7.35}$$

Given that the multi-mode array filter has a much sharper frequency response, we can allow for much wider halfwidths than the single-mode filter. We wish to present results comparing the optimal case for the single-mode filter against the optimal case for the multi-mode filter. Therefore, for the results presented in this section, we choose values of the filter halfwidth – κ/Γ for the single-mode and $N\delta\omega/\Gamma$ for the multi-mode array – such that resulting frequency-filtered auto-correlation closely matches the ideal dressed state correlation. The optimal filter halfwidths were chosen by investigating the mean difference between the filtered correlation functions and the dressed state correlation functions, Eq. (6.24), as we did for the two-level atom in Section 6.3.1, and choosing the halfwidth corresponding to the smallest mean difference.

Considering first the weak driving regime, with $\Omega/\Gamma = 5$, the atomic spectrum consists of two peaks, Fig. 7.3, corresponding to consecutive emissions from the upper and lower dipoles. We therefore expect each individual emission to be antibunched, for the same reason that the two-level atom is. With the large frequency separation of $|\alpha|$ between the two emission peaks, we set a large filter halfwidth for the multi-mode array filter. Figure 7.11 shows that these transitions are indeed antibunched, with an initial correlation value of 3.57×10^{-4} for the multi-mode array filter (blue), and 3.32×10^{-2} for the single-mode filter (orange, dashed).

Increasing the driving strength to $\Omega/\Gamma = 40$, we are now able to investigate the correlation functions of the dressed state transitions. From the dressed state picture, Fig. 7.2, we see the only cascaded decay of the same transition is for the central frequency, $\tilde{\omega}_0$, and thus we expect to see antibunched correlation functions for all side-peaks of the dressed state transitions. This

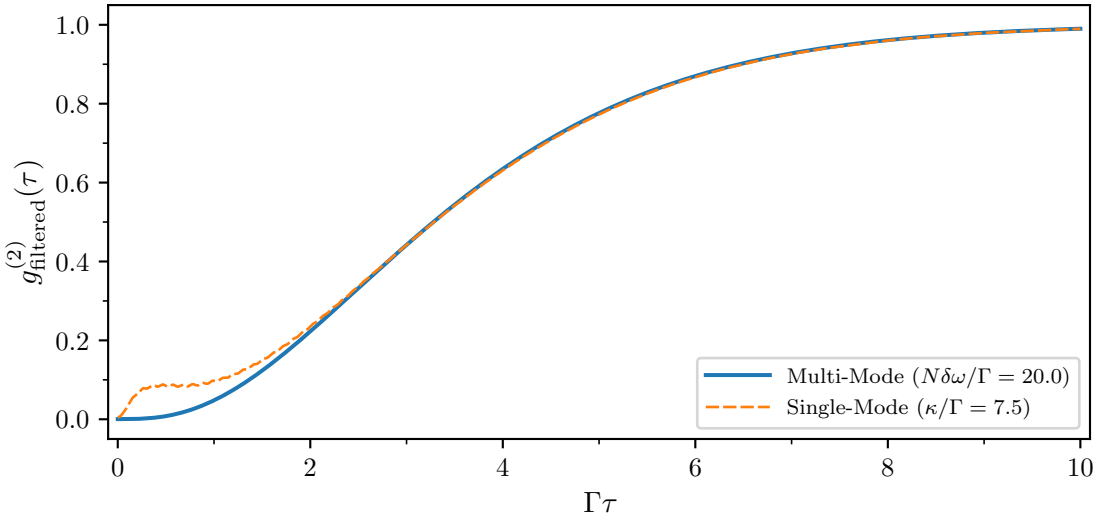

Figure 7.11: Frequency-filtered auto-correlation of the right peak, $\Delta\omega_0/\Gamma = 60$, of the three-level atom in the weak driving regime, $\Omega/\Gamma = 5$. The multi-mode array filter (blue, solid) has an effective halfwidth of $N\delta\omega/\Gamma = 20.0$, and the single-mode filter (orange, dashed) has an halfwidth of $\kappa/\Gamma = 1.0$. The other filter parameters are $N = 80, \delta\omega/\Gamma = 0.25, \kappa/\Gamma = 0.625$, and $m = 1$.

is reflected in the dressed state and the frequency-filtered correlation functions in Fig. 7.12, for each of the non-central peaks. Once again, the multi-mode array filter shows its improved frequency isolation over the single-mode filter where, in Figs. 7.12a - 7.12c, the faster oscillations have almost been entirely rejected by the multi-mode array filter.

In the two-level atom, interference between the two decay paths, $|u\rangle \to |u\rangle$ and $|d\rangle \to |d\rangle$, caused photons from the central peak of the Mollow triplet to be second-order coherent. For the three-level atom, however, the photons of the central peak appear to be bunched, as shown in Fig. 7.13a. From Fig. 7.2, any $|u\rangle \to |u\rangle$ or $|d\rangle \to |d\rangle$ transitions can be immediately followed by another. There are, however, two other possible decay paths available if starting in the upper dressed state $|u\rangle$: $|u\rangle \to |u\rangle \to |m\rangle$ and $|u\rangle \to |u\rangle \to |d\rangle$. These two pathways, as well as the interference between the $|u\rangle \to |u\rangle$ and $|d\rangle \to |d\rangle$ transitions, are most likely why the bunching for the filtered central peak is not very strong.

Looking now at the central triplet and the sideband doublets as a whole, we are able to calculate photon correlations from these structures more accurately using the multi-mode array filter, just as we filtered the spectrum in Fig. 7.10. In Figs. 7.13b and 7.13c, we compare the single- and multi-mode filtered correlation functions. We see, once again, that the multi-mode array filter is able to isolate the target frequencies more accurately; the faster oscillations visible in the single-mode filtered correlation functions (the orange curves) have been rejected by the multi-mode array filter. The slower oscillations seen in both is caused by the beating between the frequencies of the two or three peaks of the doublet or triplet, which is exactly the dressed state frequency $\omega_l/2\pi$.

We should note, however, that there are some key differences between the single-mode and multi-mode filtered results. In Fig. 7.12a, neither the single-mode or multi-mode filtered

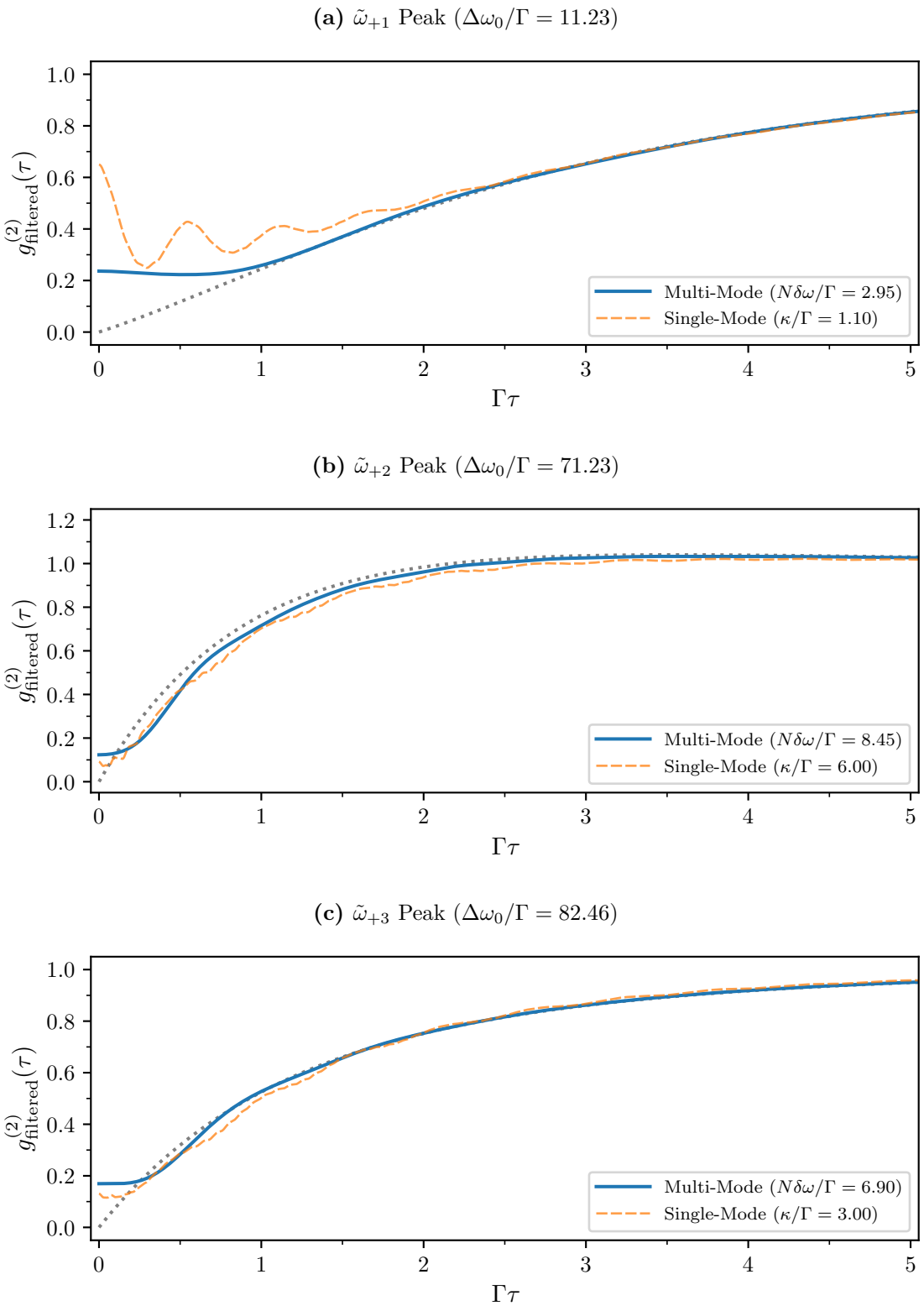

Figure 7.12: Frequency-filtered auto-correlation functions of the multi-mode (blue) and single-mode(orange) filtered first (a), second (b), and third (c) peak of the atomic spectrum, as labelled in Fig. 7.3. The frequency-filtered correlation functions are compared against the dressed-state correlation functions (grey, dotted). The other parameters are $\Omega/\Gamma = 40.0, N = 80, \delta\omega/\Gamma = 0.075, \kappa/\Gamma = 0.1875$, and, for the single-mode filter, $\kappa/\Gamma = 6.0$.

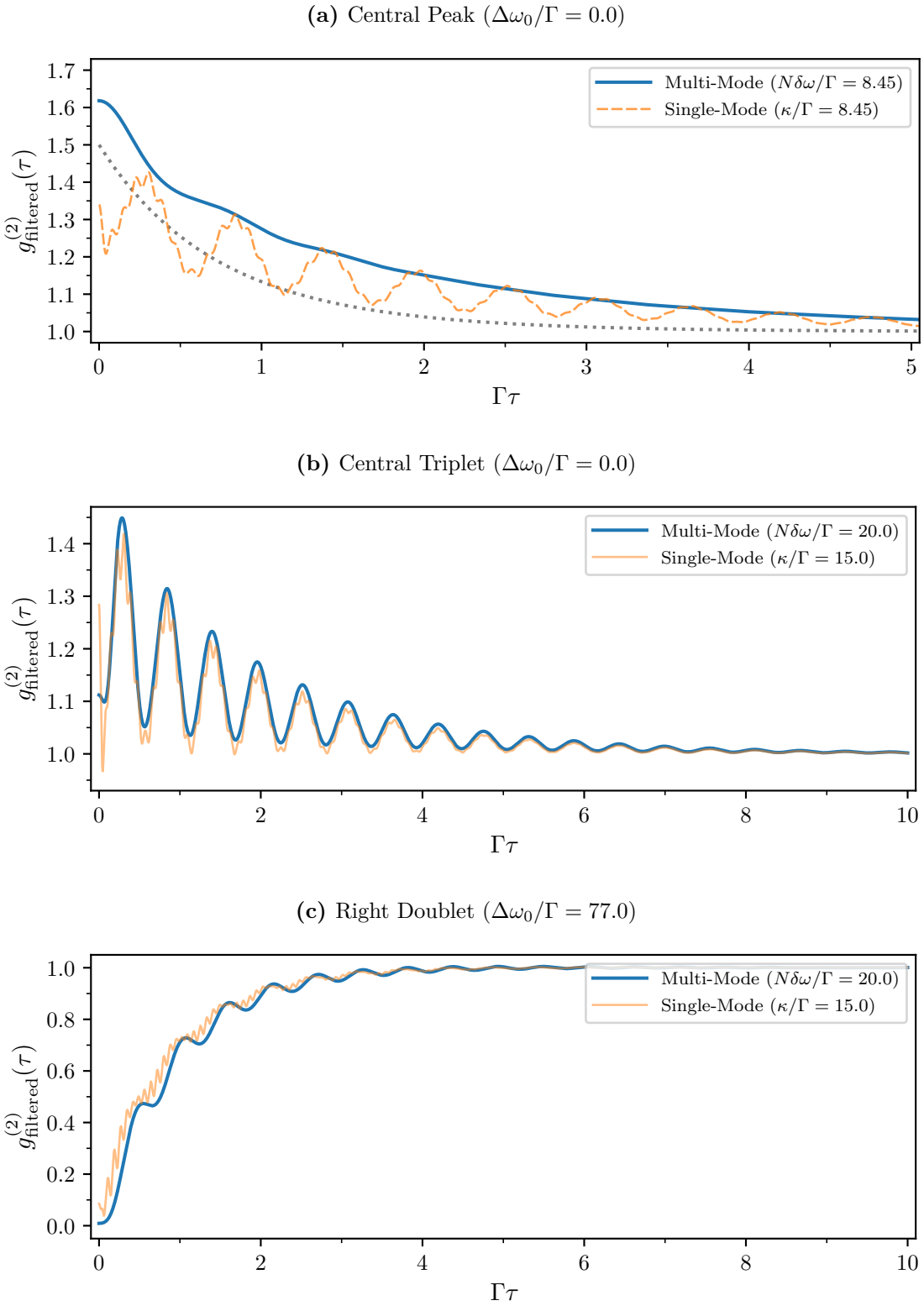

Figure 7.13: Frequency-filtered auto-correlation functions of the multi-mode (blue) and single-mode (orange) filtered central peak (a), central triplet (b), and right doublet (c) of the atomic spectrum. We compare the central filtered correlation function in (a) against the dressed state correlation function (grey, dotted). The other parameters are $N = 80$ and $m = 1$.

correlation functions match the dressed-state result particularly well. For the given atomic parameters, the target transitions, at frequency $\pm\omega_l \approx \pm 11.23$, are much weaker than the dominant central peak. Thus, it is difficult to completely filter out the central frequency. Figures 7.12b and 7.12c, on the other hand, show a better initial correlation value for the single-mode filter over the multi-mode array filter; for both peaks the single-mode filtered initial correlation value is slightly closer to zero. This is, however, due to the wider frequency response of the single-mode filter, such that both the $\tilde{\omega}_{\pm 2}$ and $\tilde{\omega}_{\pm 3}$ peaks are covered by the Lorentzian frequency response. As we saw in Fig. 7.13c, when detecting photons from either frequency, the resulting correlation function is nearly perfectly antibunched.

7.3.3 Cross-correlations of the transition peaks

To investigate the frequency-filtered cross-correlation functions, we once again split the atomic fluorescence evenly into two identical filters, as in Section 6.4, such that Hamiltonian is

$$\begin{aligned} H = &-\hbar\left(\frac{\alpha}{2}+\delta\right)|e\rangle\langle e| - 2\hbar\delta\,|f\rangle\langle f| + \hbar\frac{\Omega}{2}\left(\Sigma_- + \Sigma_+\right) \\ &+ \hbar\sum_{j=-N}^{N}\Delta\omega_j^{(a)}a_j^\dagger a_j + \frac{i\hbar}{2}\sum_{j=-N}^{N}\left(\mathcal{E}_j^{(a)*}a_j\Sigma_+ - \mathcal{E}_j^{(a)}a_j^\dagger\Sigma_-\right) \\ &+ \hbar\sum_{j=-N}^{N}\Delta\omega_j^{(b)}b_j^\dagger b_j + \frac{i\hbar}{2}\sum_{j=-N}^{N}\left(\mathcal{E}_j^{(b)*}b_j\Sigma_+ - \mathcal{E}_j^{(b)}b_j^\dagger\Sigma_-\right), \end{aligned} \tag{7.36}$$

where, as stated in Section 6.4,

$$\Delta\omega_j^{(a)} = \left(\omega_0^{(a)} + j\delta\omega^{(a)}\right) - \omega_d, \quad \Delta\omega_j^{(b)} = \left(\omega_0^{(b)} + j\delta\omega^{(b)}\right) - \omega_d, \tag{7.37}$$

are the frequency detunings, and

$$\mathcal{E}_j^{(a)} = \sqrt{\frac{\Gamma\kappa_a}{2\left(2N+1\right)}}e^{imj\pi/N}, \quad \mathcal{E}_j^{(b)} = \sqrt{\frac{\Gamma\kappa_b}{2\left(2N+1\right)}}e^{imj\pi/N}. \tag{7.38}$$

are the mode-dependent couplings, for filters A and B, respectively. The master equation for the two-filter three-level atom cascaded system is then

$$\begin{aligned} \frac{\mathrm{d}\rho}{\mathrm{d}t} = &\frac{1}{i\hbar}[H,\rho] + \frac{\kappa_a}{2}\sum_{j=-N}^{N}\left(2a_j\rho a_j^\dagger - a_j^\dagger a_j\rho - \rho a_j^\dagger a_j\right) \\ &+ \frac{1}{2}\left(2C_j^{(a)}\rho C_j^{(a)\dagger} - C_j^{(a)\dagger}C_j^{(a)}\rho - \rho C_j^{(a)\dagger}C_j^{(a)}\right) \\ &+ \frac{\kappa_b}{2}\sum_{j=-N}^{N}\left(2b_j\rho b_j^\dagger - b_j^\dagger b_j\rho - \rho b_j^\dagger b_j\right) \\ &+ \frac{1}{2}\left(2C_j^{(b)}\rho C_j^{(b)\dagger} - C_j^{(b)\dagger}C_j^{(b)}\rho - \rho C_j^{(b)\dagger}C_j^{(b)}\right), \end{aligned} \tag{7.39}$$

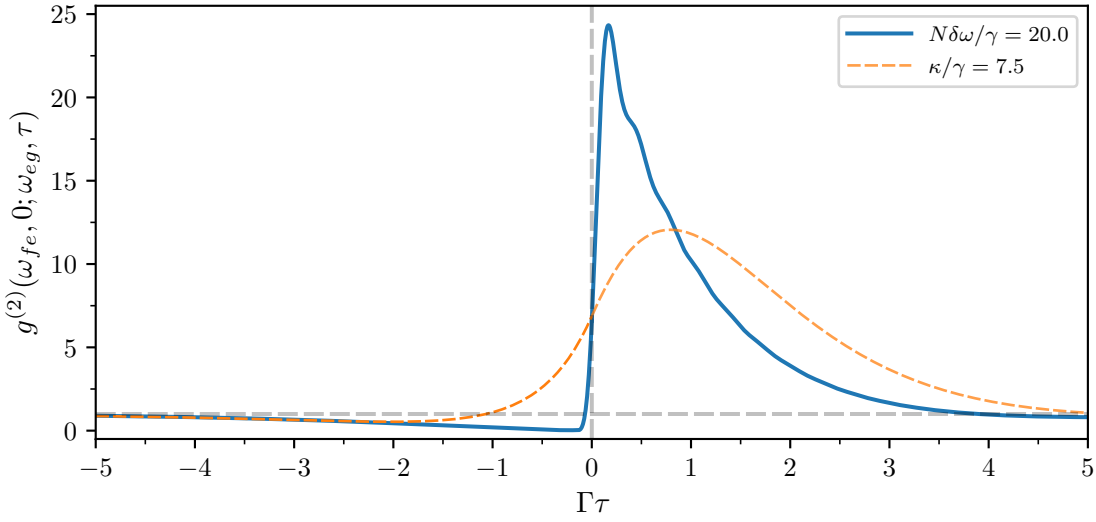

Figure 7.14: Frequency-filtered cross-correlation of the ω_{fe} and ω_{eg} peaks in the low driving limit, $\Omega/\Gamma = 5$. The horizontal dashed line indicates the stead-state $g^{(2)}(\tau \to \infty) = 1$. We treat both filters as identical, with $\delta\omega_a = \delta\omega_b = \delta\omega$ and $\kappa_a = \kappa_b = \kappa$. The other parameters are $N\delta\omega/\Gamma = 20, \kappa = 2.5\delta\omega, \Delta\omega_0^{(a)}/\Gamma = 60.0, \Delta\omega_0^{(b)}/\Gamma = -60.0$ and, for the single-mode filters, $\kappa_a/\Gamma = \kappa_b/\Gamma = 1$.

with cascaded decay operators:

$$C_j^{(a)} = \sqrt{\frac{\Gamma/2}{2N+1}} e^{imj\pi/N}\Sigma_- + \sqrt{\kappa_a}a_j, \quad C_j^{(b)} = \sqrt{\frac{\Gamma/2}{2N+1}} e^{imj\pi/N}\Sigma_- + \sqrt{\kappa_b}b_j. \tag{7.40}$$

Following the same moment equation method as before, we are able to easily solve for two-time cross-correlation functions. However, due to the increased complexity of the system, we no longer expect the second-order cross-correlation function to be symmetric in time. We therefore redefine the cross-correlation function, Eq. (6.36), as

$$g^{(2)}(\alpha, 0; \beta, \tau) = \frac{G^{(2)}(\alpha, 0; \beta, \tau)}{\langle A^\dagger A\rangle_{ss}\langle B^\dagger B\rangle_{ss}}, \tag{7.41}$$

with

$$G^{(2)}(\alpha, 0; \beta, \tau) = \begin{cases} \langle A^\dagger(0)B^\dagger B(\tau)A(0)\rangle_{ss} & 0 \le \tau \\ \langle B^\dagger(0)A^\dagger A(-\tau)B(0)\rangle_{ss} & \tau \le 0 \end{cases}, \tag{7.42}$$

where, as before, α and β indicate the central resonance frequencies of filters A and B. The complete set of moment equations needed to calculate the cross-correlation function for the two-filter system can be found in Appendix F.

For the results presented in this section, we choose filter halfwidths of the single- and multi-mode array filters such that, for a given target frequency, the *auto*-correlation is optimised, i.e., the filter halfwidth values from the previous section. This will give the largest filter halfwidth possible for isolating the target peak, with minimal contamination from other frequencies.

Starting with the weakly driven atom, we set the two filters, in Fig. 7.14, to be resonant with either ω_{fe} or ω_{eg}, the two bare atom transition frequencies. In Fig. 7.14 we first detect a photon

of frequency ω_{eg} and then detect a photon of frequency ω_{fe}, and for $\tau < 0$, we have the reverse. From the structure of the atom, Fig. 7.1, and the nature of the cascaded decay, we expect the atom to emit an ω_{eg} photon following an ω_{fe} photon and, in the filtered cross-correlation functions, this is exactly what we see. When the first filter is centred on ω_{eg}, we see strong anti-bunching in the short-time behaviour. Unfortunately, due to the higher dimensionality of the three-level atom, it is too difficult to derive expressions for the short-time behaviour of the filtered correlations, as could be done for the two-level atom [27]. We can, however, see that there are interferences between the two different time-orderings such that, for $\tau < 0$, the correlation functions are initially strongly bunched. Similarly, for $\tau > 0$, the strong bunching is initially diminished. While we do not have analytic expressions to compare with, these results match those seen experimentally by Gasparinetti et al. [65].

We have already seen that, in the strong driving regime, we expect to see seven different frequencies appearing in the power spectrum; this gives 49 possible arrangements of cross-correlations, including auto-correlations. We first look at cross-correlations between opposite peaks of the power spectrum, with $\Delta\omega_0^{(a)} = -\Delta\omega_0^{(b)}$. From the dressed state picture, Fig. 7.2, we expect photons from opposite peaks to be correlated such that the total energy is conserved. In Fig. 7.15 we cross-correlate photons from three transitions: $|m\rangle \to |l\rangle \to |m\rangle$ (Fig. 7.15a), $|m\rangle \to |u\rangle \to |m\rangle$ (Fig. 7.15b), and $|u\rangle \to |l\rangle \to |u\rangle$ (Fig. 7.15c). From the calculated dressed correlation functions – calculated using Eq. 7.22 – we indeed see that photons of opposite frequencies *should* be correlated. Just like the cross-correlated side-and-central peaks of the Mollow triplet, however, that bunching is reduced by approximately half due to the different time-orderings.

We now choose the resonance frequencies of our two filters to be completely different, i.e., correlating photons from different transitions altogether. In Fig. 7.16, each transition has been picked such that, in the dressed state picture, cascaded decay is possible in one direction, but impossible in the other direction. In Fig. 7.16a we target the $\tilde{\omega}_{+1}$ and $\tilde{\omega}_{-3}$ peaks. If detecting an $\tilde{\omega}_{+1}$ photon first, the expected dressed state decay path is $|m\rangle \to |l\rangle \to |u\rangle$ which, from Fig. 7.2, is an allowed transition. Decaying in the opposite direction, however, is impossible, as both transitions have different initial and final states states: $|l\rangle \to |u\rangle$ and $|m\rangle \to |l\rangle$. Similarly, for the other target frequencies in Fig. 7.16 we have: $\tilde{\omega}_0$ and $\tilde{\omega}_{-2}$ with respective transitions $|u\rangle \to |u\rangle$ and $|m\rangle \to |u\rangle$ (Fig. 7.16b); and $\tilde{\omega}_{+2}$ and $\tilde{\omega}_{+3}$ with respective transitions $|u\rangle \to |m\rangle$ and $|u\rangle \to |l\rangle$ (Fig. 7.16c).

The cross-correlations presented in Figs. 7.15 and 7.16 all show similar "short-time behaviour" to the two-level atom, as discussed in Section 6.4.2. Due to the increased complexity of the additional dipole transition of the three-level atom, there are no analytical expressions for the short-time behaviour with which can compare our results. We can, however, make qualitative comparisons based on the expected behaviour, as described by Schrama et al. [26, 27]. For the cross-correlations of opposite peaks, Fig. 7.15, we see a dip in the centre, at $\tau = 0$. This behaviour is most likely the same behaviour we saw with the cross-correlated side-peaks of the Mollow triplet, Fig. 6.19b, where the time-ordering of the two transitions cannot be determined by the two filters, and thus the correlation is diminished. For the cross-correlations in Figs. 7.16a and 7.16b, where there is strong correlation in one direction and anti-correlation

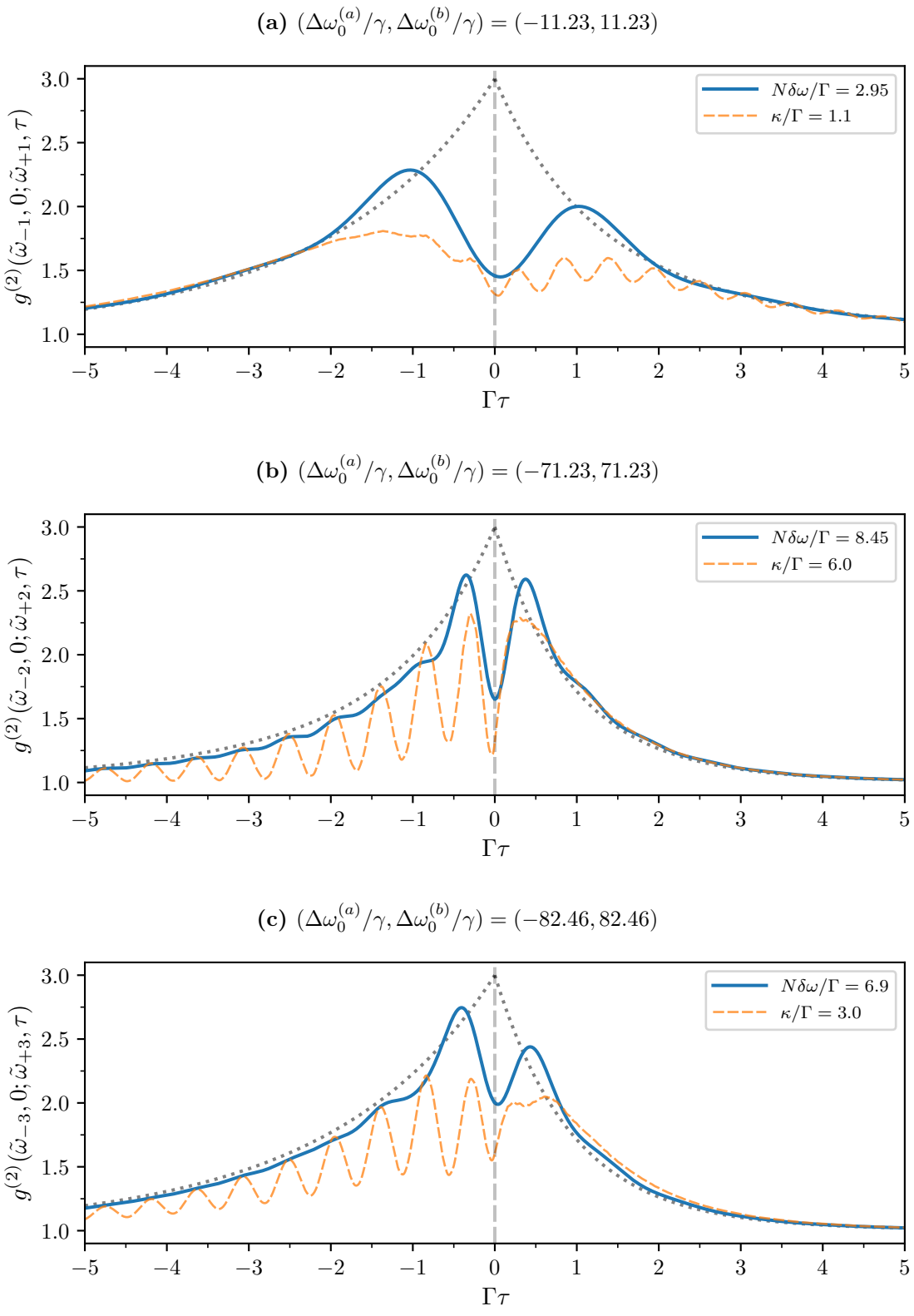

Figure 7.15: Frequency-filtered cross-correlations for opposite fluorescence peaks: $\tilde{\omega}_{\pm 1}$ (a, b), $\tilde{\omega}_{\pm 2}$ (c, d), and $\tilde{\omega}_{\pm 3}$ (e, f), in both directions. The correlations are filtered with the multi-mode array filter ($N = 80$) (blue, solid) and the single-mode filter (orange, dashed). The frequency-filtered correlation functions are compared against the dressed-state correlation functions (grey, dotted). We treat both filters as identical, with $\delta\omega_a = \delta\omega_b = \delta\omega$ and $\kappa_a = \kappa_b = \kappa$. For the multi-mode array filter, $\kappa = 2.5\delta\omega$ and $m = 1$.

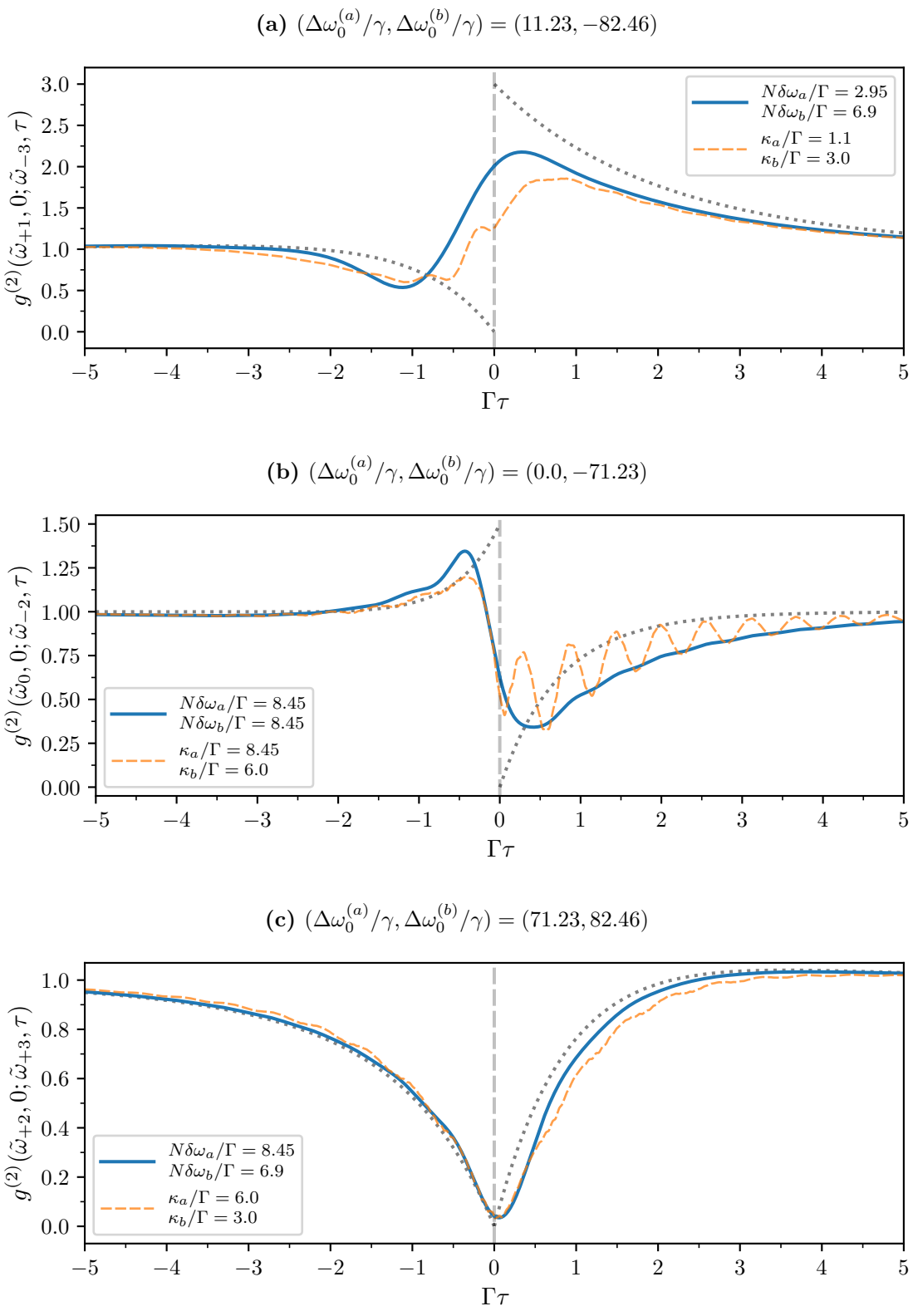

Figure 7.16: Frequency-filtered cross-correlations for different combinations of fluorescence peaks: $\tilde{\omega}_{+1}$ and $\tilde{\omega}_{-3}$ (a, b), $\tilde{\omega}_0$ and $\tilde{\omega}_{+3}$ (c, d), and $\tilde{\omega}_{+3}$ and $\tilde{\omega}_{-2}$ (e, f), in both directions. The correlations are filtered with the multi-mode array filter ($N = 80$) (blue, solid) and the single-mode filter (orange, dashed). The frequency-filtered correlation functions are compared against the dressed-state correlation functions (grey, dotted). For the multi-mode array filter, $\kappa_a/\delta\omega_a = \kappa_b/\delta\omega_b = 2.5$ and $m = 1$.

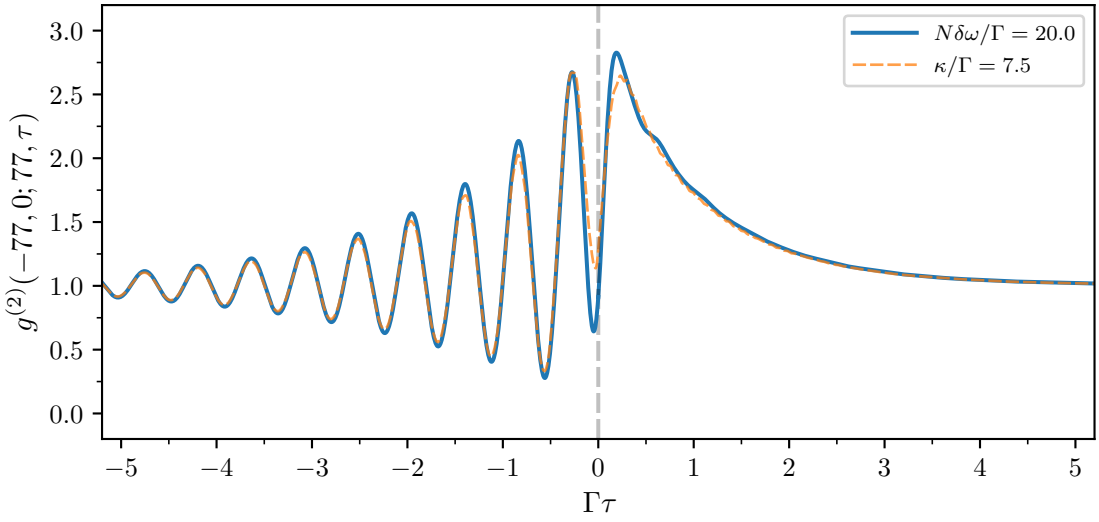

Figure 7.17: Frequency-filtered cross-correlation of the two side-doublets, with $\Delta\omega_0^{(a)}/\Gamma = 77.0$ and $\Delta\omega_0^{(b)}/\Gamma = -77.0$, for the multi-mode array filter (blue, solid) and the single-mode filter (orange, dashed). The other parameters are $N = 80, \kappa_a = 2.5\delta\omega_a, \kappa_b = 2.5\delta\omega_b$.

in the opposite, the initial *filtered* correlation appears to tend towards the midpoint

Interestingly, we see that some of these cross-correlations are not symmetrical. In fact, depending on the ordering of the photon detections, large oscillations appear in the cross-correlation; this is especially prominent for the single-mode filtered correlation functions for $\tau > 0$ in Figs. 7.15a and 7.16b, and for $\tau < 0$ in Figs. 7.15b and 7.15c. We notice that this generally occurs when the first conditional detection is of a photon of the *lower* transition of a cascaded decay. For example, for $\tau < 0$ in Fig. 7.15c, the first detected photon is of frequency $\tilde{\omega}_{+3}$ and the second photon is of frequency $\tilde{\omega}_{-3}$. From the dressed state picture, Fig. 7.2, the atom decays as $|l\rangle \to |u\rangle \to |l\rangle$; the first emission is a photon of frequency $\tilde{\omega}_{-3}$, followed by a photon of frequency $\tilde{\omega}_{+3}$. When detecting a lower photon first, $\tilde{\omega}_{+3}$, there is no guarantee that the atom will decay in the same pathway; this opens up the possibility of detecting a neighbouring frequency. Recalling that the frequency separation between the peaks of the side doublets, as well as the separation of the peaks in the central triplet, is the dressed state frequency ω_l, this could explain the large oscillations of frequency $\omega_l/2\pi$ in the asymmetrical cross-correlations.

In Fig. 7.17 we plot the cross-correlation function between the left and right side-doublets. Instead of choosing a smaller bandwidth such that only a single frequency is picked out, the multi-mode array filter encompasses both peaks. Seeing as both the multi-mode and single-mode filtered correlations appear closely matched, it seems likely that the second filter is detecting two possible transitions at the end of a cascaded decay. Fortunately, the improved frequency isolation of the multi-mode array filter allows for more precise frequency filtering, hence why the multi-mode filtered cross-correlation functions are in general much smoother than the single-mode filtered correlations when picking out a single frequency.

While this is most likely the reason for the asymmetry, we do note another potential explanation. Similar asymmetrical correlation functions, with large oscillations in one direction,

have been reported in the context of the "breakdown of detailed balance" [124–126]. In particular, Fig. 5 of Ref. [126] demonstrates the same asymmetry in the cross-correlations, where one arrangement of cross-correlations displays much larger oscillations. In this work, however, Marquina-Cruz et al. study the fluorescence of a three-level V-type atom, and the correlations in Fig. 5 are, in fact, amplitude-intensity correlation functions, $g^{(1.5)}(\tau)$. It could prove interesting to investigate these correlations in future work.

7.3.4 Cross-correlations outside of the transition peaks

We can also cross-correlate frequencies *outside* of the dressed state transition frequencies, just as we did for the two-level atom in Section 6.4.3. Along the auto-correlation diagonal, where $\Delta\omega_0^{(a)} = \Delta\omega_0^{(b)}$, we see regions of strong antibunching surrounding the six side-peaks. If we consider cross-correlations of frequencies far off resonance from any side-peak, say $\Delta\omega_0^{(a)}/\Gamma \approx -110.0$ and $\Delta\omega_0^{(b)}/\Gamma \approx -40.0$, we see that the resulting correlation function is approximately second-order coherent, with $g^{(2)}(0) \approx 1$. When the resonance of one of the filters is then shifted to a side-peak, the destructive interference in the time-orderings causes a decrease in the initial value. This is similar to the two-level atom when correlating photons from the central peak and one of the side-peaks.

We also see strong bunching along the off-diagonal; indicative of the two-photon "leapfrog" decay process discussed in Section 6.4.3. With the two-level atom, there were regions of strong correlations where the average frequency of the two photons were equal to ω_A and $\omega_A \pm \Omega$. With the seven different dressed state transition frequencies, we see regions of strong correlations where the average frequency is equal to $\omega_d \pm \tilde{\omega}_i$, where $i = 0, 1, 2, 3$.

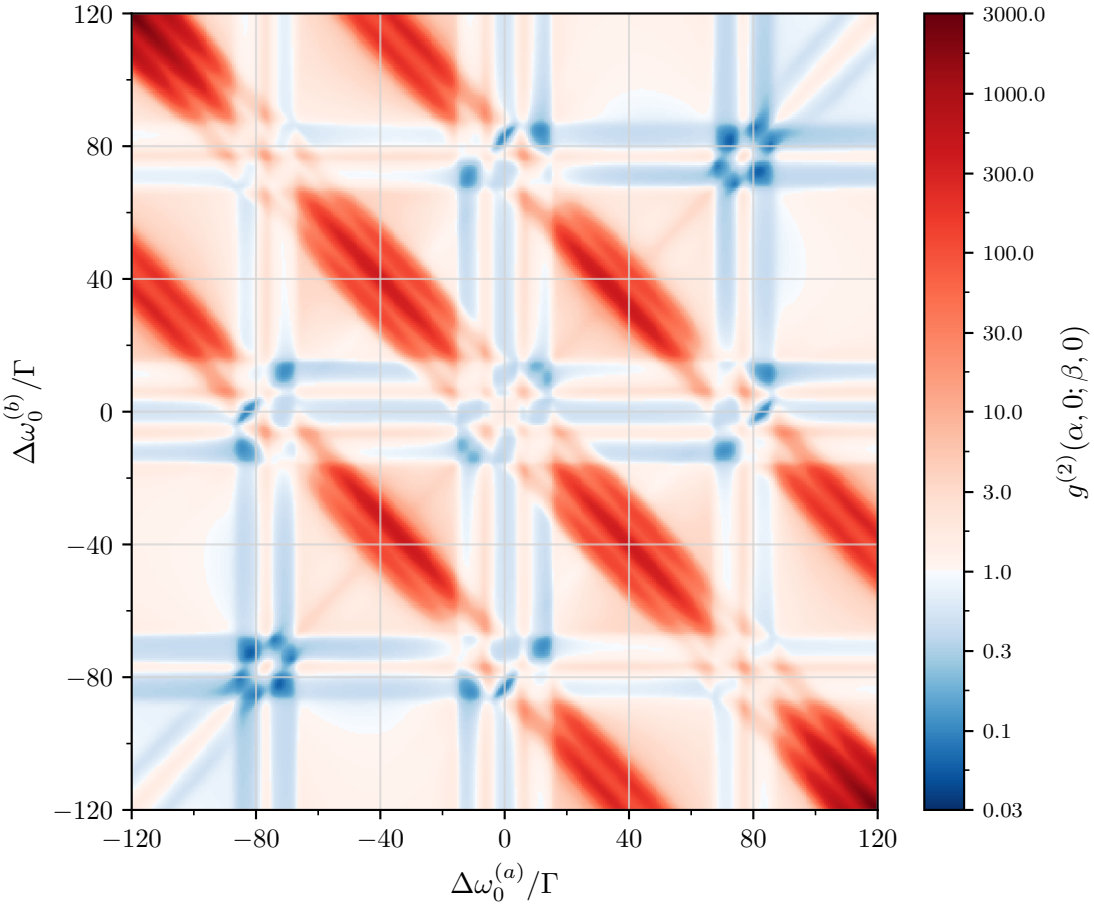

Figure 7.18: Scan of initial cross-correlation values for varying central frequencies of two multi-mode array filters. For this figure, blue corresponds to antibunching with $g^{(2)}(0) < 1$, red corresponds to bunching with $g^{(2)}(0) > 1$, and white corresponds to second-order coherence with $g^{(2)}(0) = 1$. The parameters are $N\delta\omega_a/\Gamma = N\delta\omega_b/\Gamma = 4.0$, and $\kappa_a/\delta\omega_a, \kappa_b/\delta\omega_b = 2.5$.

8 Conclusion

We will begin with a summary of topics and ideas introduced in this thesis. In the first part of this thesis, Part I Quantum Optics and Filtering, we focused on introducing some of the key concepts used throughout the thesis. In Chapter 2 we summarised key principles of quantum mechanics and, using these principles, quantised the electromagnetic field as a collection of harmonic oscillators. In Chapter 3 we then introduced a method for calculating quantities of lossy quantum systems. Using the *Markov* and *Born* approximations, we derived the *Lindblad master equation* for a damped harmonic oscillator. Using the Lindblad master equations, we then introduced the *quantum regression equations*, offering a simple method with which to calculate *first-* and *second-order correlation functions*. Finally, we introduced *quantum cascaded systems theory*, allowing us to model the output of one quantum system as the input of another quantum system.

In Chapter 4 we discussed the *Fabry-Pérot interferometer*, one of the most common methods of frequency filtering in a classical optical setting. By using the transfer matrix method, we derived an analytical expression for the transmission spectrum. In general, the Fabry-Pérot interferometer supports an infinite number of modes, and therefore frequencies. We therefore showed that, under the right conditions, the single-mode approximation, and thus the quantum model, of the Fabry-Pérot interferometer was valid. We then expanded the quantum model by allowing for an *array* of single-mode cavities, resulting in the novel method of this thesis: the *multi-mode array filter*. Under a delta-function impulse driving, we derived an analytic expression for the temporal response of the multi-mode array filter, Eq. (4.23), and found it to be a positive-sided sinc function. We then derived a semi-analytical expression for the frequency response of the filter under continuous driving. By choosing the correct set of parameters, we could tune the frequency response of the multi-mode array filter to approximate a rectangular filter. We compared the frequency response of the multi-mode array filter against that of a single-mode Lorentzian filter for a range of parameters, demonstrating that the multi-mode array filter can achieve much wider bandwidths, with a sharper response cut-off, than a single-mode filter.

In Part II Resonance Fluorescence, we then investigated two source systems that serve as test cases for the multi-mode array filter. Starting with Chapter 5, we introduced the first of these systems: the resonantly driven two-level atom. We began by deriving a mathematical model of the radiatively damped two-level atom interacting with a driving field in terms of the pseudo-spin *Pauli operators*. Using these operators we introduced the *optical Bloch equations*, providing a simple set of three coupled moment equations that allowed us to easily calculate any quantity of interest. We then derived expressions for the atomic dressed states, and showed that, when strongly driven, transitions amongst the dressed states resulted in a three-peaked fluorescence spectrum known as the *Mollow triplet*. We then introduced the *second-order correlation function* as the quantum mechanical analogue of intensity correlation functions, as well as the definitions

of *bunched* and *antibunched* light. Finally, we derived expressions for second-order correlations functions for each frequency component of the Mollow triplet in the *secular approximation*. These expressions would then be used to compare against the frequency-filtered correlation functions in Chapter 6.

Having laid the foundations of the first source system, we moved onto the main goal of the thesis: calculating *frequency-filtered photon-correlations*. By cascading the fluorescence into the multi-mode array filter, we ensured that the presence of the filter had no effect on the evolution of the atom. This allowed us to derive a closed system of coupled moment equations, up to the fourth-order in filter operators, resulting in an effective method for calculating filtered photon correlations. This proved extremely beneficial as the large dimensions of the atom-filter composite system made solving the master equation computationally difficult; the two-level atom, with excited and ground states $|e\rangle$ and $|g\rangle$, are coupled to $2N+1$ individual cavity modes, each with their own infinitely large Fock basis. Instead, we could obtain exact solutions for the operator averages without needing to truncate the Hilbert spaces. The lack of back-action of the filter on the evolution of the atom also provided a simple structure to the coupled moment equations, where higher-order terms were only dependent on lower-order terms. Calculations, both analytical and numerical, were therefore easier to perform.

Using the derived semi-analytical equation, Eqs. (6.21) and (6.22), we calculated frequency-filtered first-order correlations, and the subsequent frequency-filtered power spectra for the single- and multi-mode array filtered two-level atom. We compared the two filtering methods for varying halfwidth and demonstrated that the multi-mode array filter could reject non-target frequencies much more effectively than the standard single-mode filter. We then presented numerical calculations of frequency-filtered auto-correlations, when resonant with the central or right peak of the Mollow triplet. From the expressions derived in the secular approximation, we expect the ideal filtered correlation functions to be completely smooth. We saw that the multi-mode array filter produced much smoother correlation functions than the single-mode filter, once again owing to its improved frequency isolation. We compared the mean difference between the filtered and dressed-state correlation functions of the single- and multi-mode array filters for varying halfwidth and phase and showed that the multi-mode array filter produced more accurate filtered auto-correlations for larger filter bandwidths.

Due to the simplified computations of the moment equation method, we were able to easily introduce a second frequency filter in order to calculate frequency-filtered *cross*-correlations. We found, however, that the frequency-filtered cross-correlations did not accurately represent the correlation functions derived in the secular approximation. As it turns out, interferences between the time-orderings of the different transitions had a significant effect on the resulting correlation functions. We therefore compared the numerical results to expressions derived by Schrama et al. for the "short-time behaviour" [27]. The difference in the short-time behaviour and the dressed state correlation functions gave rise to interesting areas of correlations, as we saw in Section 6.4.3. By calculating the initial value of the cross-correlation function for varying frequency detunings, we found regions of strong correlations corresponding to "leapfrog decay" processes, i.e., simultaneous two-photon decay from the atom's dressed states. The multi-mode array filter showed more clearly defined regions of correlations due to its improved frequency

isolation.

Finally, in Chapter 7, we increased the complexity of the source subsystem and investigated the fluorescence of a three-level ladder-type atom driven at two-photon resonance. The addition of an extra dipole transition in the ladder structure resulted in a more intricate dressed state level structure. For a weak drive field, the fluorescence spectrum displayed two peaks, corresponding to transitions amongst the bare atomic states. When strongly driven, we saw the fluorescence spectrum split into seven distinct peaks; the two single-photon transition peaks split into doublets, and a central, Mollow-like triplet emerged. We derived expressions for the dressed states at two-photon resonance, and used them to derive semi-analytic expressions for dressed-state correlation functions in the secular approximation. Unfortunately, the increased complexity of the three-level atom limited our ability to derive explicit expressions for these correlation functions.

Operator moment equations were also derived for the three-level atom, which were governed by an eight-by-eight matrix. While this is larger than for the two-level atom, the structure of the atom-filter coupled moment equations was the same, thus we were again able to derive a complete set of moment equations for the filter operators. We then presented numerical calculations of frequency-filtered first- and second-order correlation functions for the filtered three-level atom. The varying heights of the seven transition peaks in the fluorescence spectrum made for a more trying example for the multi-mode array filter; particularly for the closely spaced peaks of the central triplet. It was shown, however, that the multi-mode array filter still made for a more accurate frequency filter. We then introduced a second frequency filter, and presented numerical results for frequency-filtered cross-correlations. Unlike the two-level atom driven at resonance, we do not expect cross-correlations of different transition frequencies to be symmetric about zero time delay. We therefore introduced the two-time correlation function for positive and negative time delay. When targeting opposite transition frequencies (with respect to the frequency of the driving laser), we found strong cross-correlations in close agreement with the long-time behaviour from the secular approximation. As the multi-mode array filter allows for larger filter halfwidths without compromising frequency isolation, we once again saw much smoother filtered correlation functions than the single-mode filtered results. Cross-correlation functions for different transition frequencies were presented, with the resulting long-time behaviour closely matching that of the secular approximation. While we do not have expressions for the short-time behaviour of the filtered correlations of the three-level atom, the results presented aligned with the underlying theory as discussed by Schrama et al. [27].

Following on from the two-level atom, the improved frequency response of the multi-mode array filter allowed us to uncover a rich landscape of interesting correlations for varying frequency detuning. Much like the two-level atom, there are various regions of strong correlations corresponding to two-photon leapfrog decays. The multi-mode array filter also allowed us to explain the large, asymmetrical oscillations present in some of the cross-correlation functions.

We have thus introduced, and investigated, an improved method for calculating frequency-filtered photon correlations with the multi-mode array filter. With both the two- and three-level atom, frequency-filtered power spectra and second-order correlation functions were compared against a standard Lorentzian filter with markedly improved results. This is due to the ap-

proximately rectangular frequency response of the multi-mode array filter, allowing for much larger filter bandwidths, and thus temporal response, without sacrificing frequency isolation. However, it is not necessarily a simple method to implement. A large number of modes N are required for the frequency response to better approximate a sinc filter, resulting in a very large Hilbert space. We were able to circumvent this issue by solving for the correlation functions with the moment equations, a novel approach on its own. For the two systems presented in this thesis, we were able to derive a closed set of moment equations that described the evolution of the source system. Unfortunately, not all systems can be described by a closed set of moment equations. Therefore a master equation approach is needed for such systems.

Finally, we have defined the construction of the multi-mode array filter with the goal of modelling a physically realisable system. The multi-mode array filter could be then realised in an experimental setting, offering an improved method for *measuring* frequency-filtered photon correlations. The improved frequency isolations means that the multi-mode array filter could potentially be more effective at isolating highly correlated photon pairs for use in interferometry, as in the work by Peiris et al. [32]. The box-type frequency response would also allow for more fluorescence to be captured by the filter, thus improving visibility of interference fringes.

Another system of interest that can produce interesting physics when frequency filtered is the *degenerate parametric amplifier*. This driven non-linear system produces correlated photon pairs, yet as a degenerate system the output spectrum is simply a single Lorentzian. By finely filtering photons from *within* the spectral shape, we can produce non-degenerate photons from a degenerate source. The sharper frequency response of the multi-mode array filter would allow for a much finer selection of entangled photons, and thus be worthwhile system for further exploration.

Appendices

A Moment Equations of the Two-Level Atom and Single Filter Cascaded System

Here we present all of the operator moment equations needed to calculate first- and second-order correlation functions for the multi-mode array filtered two-level atom. We first show the moment equations, as derived from Eq. (6.6). These are then followed by the coupled equations for both the filtered first- and second-order correlation functions.

The `Fortan90` code used to numerically calculate these equations can be found at the following Github repository: github.com/jnga773/multi-mode-filter.

A.1 Moment Equations

We write these coupled moment equations in matrix form, where we use the notation

$$\langle \boldsymbol{\sigma} \rangle = \begin{pmatrix} \langle \sigma_- \rangle \\ \langle \sigma_+ \rangle \\ \langle \sigma_z \rangle \end{pmatrix}, \quad \langle X\boldsymbol{\sigma} \rangle = \begin{pmatrix} \langle X\sigma_- \rangle \\ \langle X\sigma_+ \rangle \\ \langle X\sigma_z \rangle \end{pmatrix}. \tag{A.1}$$

A.1.1 Atomic Operator Moments

$$\frac{\mathrm{d}}{\mathrm{d}t}\langle \boldsymbol{\sigma} \rangle = \boldsymbol{M}\langle \boldsymbol{\sigma} \rangle + \begin{pmatrix} 0 \\ 0 \\ -\gamma \end{pmatrix}, \tag{A.2}$$

where

$$\boldsymbol{M}^{(\sigma)} = \begin{pmatrix} -\frac{\gamma}{2} & 0 & i\frac{\Omega}{2} \\ 0 & -\frac{\gamma}{2} & -i\frac{\Omega}{2} \\ i\Omega & -i\Omega & -\gamma \end{pmatrix}. \tag{A.3}$$

A.1.2 First-order: Filter

$$\frac{\mathrm{d}}{\mathrm{d}t}\langle a_j \rangle = -\left(\kappa + i\Delta\omega_j\right)\langle a_j \rangle - \mathcal{E}_j\langle \sigma_- \rangle, \tag{A.4a}$$

$$\frac{\mathrm{d}}{\mathrm{d}t}\langle a_j^\dagger \rangle = -\left(\kappa - i\Delta\omega_j\right)\langle a_j^\dagger \rangle - \mathcal{E}_j^*\langle \sigma_+ \rangle. \tag{A.4b}$$

A.1.3 First-order: Filter / Atom

$$\frac{\mathrm{d}}{\mathrm{d}t}\langle a_j\boldsymbol{\sigma}\rangle = \boldsymbol{M}_j^{(a)}\langle a_j\boldsymbol{\sigma}\rangle + \begin{pmatrix} 0 \\ -\frac{1}{2}\mathcal{E}_j\left(\langle\sigma_z\rangle + 1\right) \\ -\gamma\langle a_j\rangle + \mathcal{E}_j\langle\sigma_-\rangle \end{pmatrix}, \tag{A.5a}$$

$$\frac{\mathrm{d}}{\mathrm{d}t}\langle a_j^\dagger\boldsymbol{\sigma}\rangle = \boldsymbol{M}_j^{(a^\dagger)}\langle a_j\boldsymbol{\sigma}\rangle + \begin{pmatrix} -\frac{1}{2}\mathcal{E}_j^*\left(\langle\sigma_z\rangle + 1\right) \\ 0 \\ -\gamma\langle a_j^\dagger\rangle + \mathcal{E}_j^*\langle\sigma_+\rangle \end{pmatrix}, \tag{A.5b}$$

with

$$\boldsymbol{M}_j^{(a)} = \boldsymbol{M}^{(\sigma)} - (\kappa + i\Delta\omega_j)\,\mathbb{1}, \tag{A.6a}$$

$$\boldsymbol{M}_j^{(a^\dagger)} = \boldsymbol{M}^{(\sigma)} - (\kappa - i\Delta\omega_j)\,\mathbb{1}. \tag{A.6b}$$

A.1.4 Second-order: Filter

$$\frac{\mathrm{d}}{\mathrm{d}t}\langle a_j a_k\rangle = -\left[2\kappa + i\left(\Delta\omega_j + \Delta\omega_k\right)\right]\langle a_j a_k\rangle - \mathcal{E}_j\langle a_k\sigma_-\rangle - \mathcal{E}_k\langle a_j\sigma_-\rangle, \tag{A.7a}$$

$$\frac{\mathrm{d}}{\mathrm{d}t}\langle a_j^\dagger a_k\rangle = -\left[2\kappa - i\left(\Delta\omega_j - \Delta\omega_k\right)\right]\langle a_j^\dagger a_k\rangle - \mathcal{E}_j^*\langle a_k\sigma_+\rangle - \mathcal{E}_k\langle a_j^\dagger\sigma_-\rangle, \tag{A.7b}$$

$$\frac{\mathrm{d}}{\mathrm{d}t}\langle a_j^\dagger a_k^\dagger\rangle = -\left[2\kappa - i\left(\Delta\omega_j + \Delta\omega_k\right)\right]\langle a_j^\dagger a_k^\dagger\rangle - \mathcal{E}_j^*\langle a_k^\dagger\sigma_+\rangle - \mathcal{E}_k^*\langle a_j^\dagger\sigma_+\rangle. \tag{A.7c}$$

A.1.5 Second-order: Filter / Atom

$$\frac{\mathrm{d}}{\mathrm{d}t}\langle a_j a_k\boldsymbol{\sigma}\rangle = \boldsymbol{M}_{jk}^{(a^2)}\langle a_j a_k\boldsymbol{\sigma}\rangle + \begin{pmatrix} 0 \\ -\frac{1}{2}\mathcal{E}_j\left(\langle a_k\sigma_z\rangle + \langle a_k\rangle\right) - \frac{1}{2}\mathcal{E}_k\left(\langle a_j\sigma_z\rangle + \langle a_j\rangle\right) \\ -\gamma\langle a_j a_k\rangle + \mathcal{E}_j\langle a_k\sigma_-\rangle + \mathcal{E}_k a_j\sigma_-\rangle \end{pmatrix}, \tag{A.8a}$$

$$\frac{\mathrm{d}}{\mathrm{d}t}\langle a_j^\dagger a_k\boldsymbol{\sigma}\rangle = \boldsymbol{M}_{jk}^{(a^\dagger a)}\langle a_j^\dagger a_k\boldsymbol{\sigma}\rangle + \begin{pmatrix} -\frac{1}{2}\mathcal{E}_j^*\langle a_k\sigma_+\rangle \\ -\frac{1}{2}\mathcal{E}_k\langle a_j^\dagger\sigma_-\rangle \\ -\gamma\langle a_j^\dagger a_k\rangle + \mathcal{E}_j^*\langle a_k\sigma_+\rangle + \mathcal{E}_k a_j^\dagger\sigma_-\rangle \end{pmatrix}, \tag{A.8b}$$

$$\frac{\mathrm{d}}{\mathrm{d}t}\langle a_j^\dagger a_k^\dagger\boldsymbol{\sigma}\rangle = \boldsymbol{M}_{jk}^{(a^{\dagger 2})}\langle a_j^\dagger a_k^\dagger\boldsymbol{\sigma}\rangle + \begin{pmatrix} -\frac{1}{2}\mathcal{E}_j^*\left(\langle a_k^\dagger\sigma_z\rangle + \langle a_k^\dagger\rangle\right) - \frac{1}{2}\mathcal{E}_k^*\left(\langle a_j^\dagger\sigma_z\rangle + \langle a_j^\dagger\rangle\right) \\ 0 \\ -\gamma\langle a_j^\dagger a_k^\dagger\rangle + \mathcal{E}_j^*\langle a_k^\dagger\sigma_+\rangle + \mathcal{E}_k^* a_j^\dagger\sigma_+\rangle \end{pmatrix}, \tag{A.8c}$$

with

$$\boldsymbol{M}_{jk}^{(a^2)} = \boldsymbol{M}^{(\sigma)} - \left[2\kappa + i\left(\Delta\omega_j + \Delta\omega_k\right)\right]\mathbb{1}, \tag{A.9a}$$

$$\boldsymbol{M}_{jk}^{(a^\dagger a)} = \boldsymbol{M}^{(\sigma)} - \left[2\kappa - i\left(\Delta\omega_j - \Delta\omega_k\right)\right]\mathbb{1}, \tag{A.9b}$$

$$\boldsymbol{M}_{jk}^{(a^{\dagger 2})} = \boldsymbol{M}^{(\sigma)} - \left[2\kappa - i\left(\Delta\omega_j + \Delta\omega_k\right)\right]\mathbb{1}. \tag{A.9c}$$

A.1.6 Third-order: Filter

$$\begin{aligned}\frac{\mathrm{d}}{\mathrm{d}t}\langle a_j^\dagger a_k a_l\rangle =& -\left[3\kappa - i\left(\Delta\omega_j - \Delta\omega_k - \Delta\omega_l\right)\right]\langle a_j^\dagger a_k a_l\rangle \\ & - \mathcal{E}_j^*\langle a_k a_l \sigma_+\rangle - \mathcal{E}_k\langle a_j^\dagger a_l \sigma_-\rangle - \mathcal{E}_l\langle a_j^\dagger a_k \sigma_-\rangle, \qquad \text{(A.10a)}\\ \frac{\mathrm{d}}{\mathrm{d}t}\langle a_j^\dagger a_k^\dagger a_l\rangle =& -\left[3\kappa - i\left(\Delta\omega_j + \Delta\omega_k - \Delta\omega_l\right)\right]\langle a_j^\dagger a_k^\dagger a_l\rangle \\ & - \mathcal{E}_j^*\langle a_k^\dagger a_l \sigma_+\rangle - \mathcal{E}_k^*\langle a_j^\dagger a_l \sigma_+\rangle - \mathcal{E}_l\langle a_j^\dagger a_k^\dagger \sigma_-\rangle. \qquad \text{(A.10b)}\end{aligned}$$

A.1.7 Third-order: Filter / Atom

$$\begin{aligned}\frac{\mathrm{d}}{\mathrm{d}t}\langle a_j^\dagger a_k a_l \boldsymbol{\sigma}\rangle =& \boldsymbol{M}_{jkl}^{(a^\dagger a^2)}\langle a_j^\dagger a_k a_l \boldsymbol{\sigma}\rangle \\ & + \begin{pmatrix} -\frac{1}{2}\mathcal{E}_j^*\left(\langle a_k a_l \sigma_z\rangle + \langle a_k a_l\rangle\right) \\ -\frac{1}{2}\mathcal{E}_k\left(\langle a_j^\dagger a_l \sigma_z\rangle + \langle a_j^\dagger a_l\rangle\right) - \frac{1}{2}\mathcal{E}_l\left(\langle a_j^\dagger a_k \sigma_z\rangle + \langle a_j^\dagger a_k\rangle\right) \\ -\gamma\langle a_j^\dagger a_k a_l\rangle + \mathcal{E}_j^*\langle a_k l \sigma_+\rangle + \mathcal{E}_k\langle a_j^\dagger a_l \sigma_-\rangle + \mathcal{E}_l\langle a_j^\dagger a_k \sigma_-\rangle \end{pmatrix}, \qquad \text{(A.11a)}\\ \frac{\mathrm{d}}{\mathrm{d}t}\langle a_j^\dagger a_k^\dagger a_l \boldsymbol{\sigma}\rangle =& \boldsymbol{M}_{jkl}^{(a^{\dagger 2} a)}\langle a_j^\dagger a_k^\dagger a_l \boldsymbol{\sigma}\rangle \\ & + \begin{pmatrix} -\frac{1}{2}\mathcal{E}_j^*\left(\langle a_k^\dagger a_l \sigma_z\rangle + \langle a_k^\dagger a_l\rangle\right) - \frac{1}{2}\mathcal{E}_k^*\left(\langle a_j^\dagger a_l \sigma_z\rangle + \langle a_j^\dagger a_l\rangle\right) \\ -\frac{1}{2}\mathcal{E}_l\left(\langle a_j^\dagger a_k^\dagger \sigma_z\rangle + \langle a_j^\dagger a_k^\dagger\rangle\right) \\ -\gamma\langle a_j^\dagger a_k^\dagger a_l\rangle + \mathcal{E}_j^*\langle a_k^\dagger l \sigma_+\rangle + \mathcal{E}_k^*\langle a_j^\dagger a_l \sigma_+\rangle + \mathcal{E}_l\langle a_j^\dagger a_k^\dagger \sigma_-\rangle \end{pmatrix}, \qquad \text{(A.11b)}\end{aligned}$$

with

$$\begin{aligned}\boldsymbol{M}_{jkl}^{(a^\dagger a^2)} &= \boldsymbol{M}^{(\sigma)} - \left[3\kappa - i\left(\Delta\omega_j - \Delta\omega_k - \Delta\omega_l\right)\right]\mathbb{1}, \qquad \text{(A.12a)}\\ \boldsymbol{M}_{jkl}^{(a^{\dagger 2} a)} &= \boldsymbol{M}^{(\sigma)} - \left[3\kappa - i\left(\Delta\omega_j + \Delta\omega_k - \Delta\omega_l\right)\right]\mathbb{1}. \qquad \text{(A.12b)}\end{aligned}$$

A.1.8 Fourth-order: Filter

$$\begin{aligned}\frac{\mathrm{d}}{\mathrm{d}t}\langle a_j^\dagger a_k^\dagger a_l a_m\rangle =& -\left[4\kappa - i\left(\Delta\omega_j + \Delta\omega_k\right) + i\left(\Delta\omega_l + \Delta\omega_m\right)\right]\langle a_j^\dagger a_k^\dagger a_l a_m\rangle \\ & - \mathcal{E}_j^*\langle a_k^\dagger a_l a_m \sigma_+\rangle - \mathcal{E}_k^*\langle a_j^\dagger a_l m \sigma_+\rangle \\ & - \mathcal{E}_l\langle a_j^\dagger a_k^\dagger a_m \sigma_-\rangle - \mathcal{E}_k\langle a_j^\dagger a_k^\dagger a_l \sigma_-\rangle. \qquad \text{(A.13)}\end{aligned}$$

A.2 Filtered First-Order Correlation Function

The first-order correlation function for the filtered output field is given by

$$G^{(1)}(t,\tau) = \langle A^\dagger(t+\tau)A(t)\rangle = \sum_{j=-N}^{N} \langle a_j^\dagger(t+\tau)A(t)\rangle. \tag{A.14}$$

We use the quantum regression equations to solve for this with the following moment equations:

$$\frac{\mathrm{d}}{\mathrm{d}\tau}\langle \boldsymbol{\sigma}(t+\tau)A(t)\rangle = \boldsymbol{M}^{(\sigma)}\langle \boldsymbol{\sigma}(t+\tau)A(t)\rangle + \begin{pmatrix} 0 \\ 0 \\ -\gamma\langle A(t)\rangle \end{pmatrix}, \tag{A.15a}$$

and

$$\frac{\mathrm{d}}{\mathrm{d}\tau}\langle a_j^\dagger(t+\tau)A(t)\rangle = -\left(\kappa - i\Delta\omega_j\right)\langle a_j^\dagger A(t)\rangle - \mathcal{E}_j^*\langle \sigma_+(t+\tau)A(t)\rangle. \tag{A.15b}$$

We solve these differential equations with the initial conditions at $\tau = 0$,

$$\langle \boldsymbol{\sigma}A(t)\rangle = \sum_{k=-N}^{N} \langle a_k \boldsymbol{\sigma}(t)\rangle, \tag{A.16a}$$

$$\langle a_j^\dagger A(t)\rangle = \sum_{k=-N}^{N} \langle a_j^\dagger a_k(t)\rangle. \tag{A.16b}$$

A.3 Filtered Second-Order Correlation Function

The second-order correlation function for the filtered output field is given by

$$G^{(2)}(t,\tau) = \langle A^\dagger(t)A^\dagger A(t+\tau)A(t)\rangle = \sum_{j,k=-N}^{N} \langle A^\dagger(t)a_k^\dagger a_l(t+\tau)A(t)\rangle. \tag{A.17}$$

We use the quantum regression equations to solve for this with the following moment equations:

$$\frac{\mathrm{d}}{\mathrm{d}\tau}\langle A^\dagger(t)\boldsymbol{\sigma}(t+\tau)A(t)\rangle = \boldsymbol{M}^{(\sigma)}\langle A^\dagger(t)\boldsymbol{\sigma}(t+\tau)A(t)\rangle + \begin{pmatrix} 0 \\ 0 \\ -\gamma\langle A^\dagger A(t)\rangle \end{pmatrix}, \tag{A.18a}$$

and

$$\frac{\mathrm{d}}{\mathrm{d}\tau}\langle A^\dagger(t)a_j(t+\tau)A(t)\rangle = -\left(\kappa + i\Delta\omega_j\right)\langle A^\dagger(t)a_j A(t)\rangle - \mathcal{E}_j\langle A^\dagger(t)\sigma_-(t+\tau)A(t)\rangle, \tag{A.18b}$$

$$\frac{\mathrm{d}}{\mathrm{d}\tau}\langle A^\dagger(t)a_j^\dagger(t+\tau)A(t)\rangle = -\left(\kappa - i\Delta\omega_j\right)\langle A^\dagger(t)a_j^\dagger A(t)\rangle - \mathcal{E}_j^*\langle A^\dagger(t)\sigma_+(t+\tau)A(t)\rangle, \tag{A.18c}$$

and

$$\frac{\mathrm{d}}{\mathrm{d}\tau}\langle A^\dagger(t)a_j\boldsymbol{\sigma}(t+\tau)A(t)\rangle = \boldsymbol{M}_j^{(a)}\langle A^\dagger(t)a_j\boldsymbol{\sigma}(t+\tau)A(t)\rangle + \begin{pmatrix} 0 \\ -\frac{1}{2}\mathcal{E}_j\left(\langle A^\dagger(t)\sigma_z(t+\tau)A(t)\rangle + \langle A^\dagger A(t)\rangle\right) \\ -\gamma\langle A^\dagger(t)a_j(t+\tau)A(t)\rangle + \mathcal{E}_j\langle A^\dagger(t)\sigma_-(t+\tau)A(t)\rangle \end{pmatrix}, \tag{A.18d}$$

$$\frac{\mathrm{d}}{\mathrm{d}\tau}\langle A^\dagger(t)a_j^\dagger\boldsymbol{\sigma}(t+\tau)A(t)\rangle = \boldsymbol{M}_j^{(a^\dagger)}\langle A^\dagger(t)a_j\boldsymbol{\sigma}(t+\tau)A(t)\rangle + \begin{pmatrix} -\frac{1}{2}\mathcal{E}_j^*\left(\langle A^\dagger(t)\sigma_z(t+\tau)A(t)\rangle + \langle A^\dagger A(t)\rangle\right) \\ 0 \\ -\gamma\langle A^\dagger(t)a_j^\dagger(t+\tau)A(t)\rangle + \mathcal{E}_j^*\langle A^\dagger(t)\sigma_+(t+\tau)A(t)\rangle \end{pmatrix}, \tag{A.18e}$$

and

$$\begin{aligned}\frac{\mathrm{d}}{\mathrm{d}\tau}\langle A^\dagger(t)a_j^\dagger a_k(t+\tau)A(t)\rangle = &-\left[2\kappa - i\left(\Delta\omega_j - \Delta\omega_k\right)\right]\langle A^\dagger(t)a_j^\dagger a_k(t+\tau)A(t)\rangle \\ &- \mathcal{E}_j^*\langle A^\dagger(t)a_k\sigma_+(t+\tau)A(t)\rangle \\ &- \mathcal{E}_k\langle A^\dagger(t)a_j^\dagger\sigma_-(t+\tau)A(t)\rangle.\end{aligned} \tag{A.18f}$$

We solve these differential equations with the initial conditions at $\tau = 0$,

$$\langle A^\dagger\boldsymbol{\sigma}A(t)\rangle = \sum_{j,m=-N}^{N}\langle a_j^\dagger a_m\boldsymbol{\sigma}(t)\rangle, \tag{A.19a}$$

$$\langle A^\dagger a_k^\dagger A(t)\rangle = \sum_{j,m=-N}^{N}\langle a_j^\dagger a_k^\dagger a_m(t)\rangle, \tag{A.19b}$$

$$\langle A^\dagger a_l A(t)\rangle = \sum_{j,m=-N}^{N}\langle a_j^\dagger a_l a_m(t)\rangle, \tag{A.19c}$$

$$\langle A^\dagger a_k^\dagger\boldsymbol{\sigma}A(t)\rangle = \sum_{j,m=-N}^{N}\langle a_j^\dagger a_k^\dagger a_m\boldsymbol{\sigma}(t)\rangle, \tag{A.19d}$$

$$\langle A^\dagger a_l\boldsymbol{\sigma}A(t)\rangle = \sum_{j,m=-N}^{N}\langle a_j^\dagger a_l a_m\boldsymbol{\sigma}(t)\rangle, \tag{A.19e}$$

$$\langle A^\dagger a_k^\dagger a_l A(t)\rangle = \sum_{j,m=-N}^{N}\langle a_j^\dagger a_k^\dagger a_l a_m(t)\rangle. \tag{A.19f}$$

B Derivation of Equation (6.21)

While we can numerically calculate the frequency-filtered first-order correlation function from the two-time correlation functions, Eqs. (A.15), we will instead work from the original moment equations, Eqs. (6.17a) and (6.17c), and derive expressions in terms of the initial conditions and steady states of the moment equations.

B.1 Analytic Solutions to The Moment Equations

Restating Eqs. (5.27) and (5.28), the Bloch equations in matrix form are

$$\frac{\mathrm{d}}{\mathrm{d}t}\langle\boldsymbol{\sigma}\rangle = \boldsymbol{M}^{(\sigma)}\langle\boldsymbol{\sigma}\rangle + \boldsymbol{B}, \tag{B.1}$$

where

$$\langle\boldsymbol{\sigma}\rangle = \begin{pmatrix}\langle\sigma_-\rangle\\ \langle\sigma_+\rangle\\ \langle\sigma_z\rangle\end{pmatrix}, \quad \boldsymbol{B} = \begin{pmatrix}0\\0\\-\gamma\end{pmatrix}, \quad \boldsymbol{M}^{(\sigma)} = \begin{pmatrix}-\frac{\gamma}{2} & 0 & i\frac{\Omega}{2}\\ 0 & -\frac{\gamma}{2} & -i\frac{\Omega}{2}\\ i\Omega & -i\Omega & -\gamma\end{pmatrix}. \tag{B.2}$$

B.1.1 General solution to the homogeneous equation

The general solution for the homogeneous equation ($\boldsymbol{B} = 0$) is given by

$$\boldsymbol{A}_c(t) = C_1 e^{\lambda_1 t}\boldsymbol{v}_1 + C_2 e^{\lambda_2 t}\boldsymbol{v}_2 + C_3 e^{\lambda_3 t}\boldsymbol{v}_3. \tag{B.3}$$

We then have to find the eigenvalues and eigenvectors of the matrix $\boldsymbol{M}^{(\boldsymbol{\sigma})}$ which are

$$\lambda_0 = -\frac{\gamma}{2}, \quad \boldsymbol{v}_1 = \begin{pmatrix}1\\1\\0\end{pmatrix}, \tag{B.4a}$$

$$\lambda_\pm = -\left(\frac{3\gamma}{4} \pm \delta\right), \quad \boldsymbol{v}_2 = \frac{1}{\gamma \pm 4\delta}\begin{pmatrix}-2i\Omega,\\ 2i\Omega\\ \gamma \pm 4\delta\end{pmatrix}, \tag{B.4b}$$

where

$$\delta = \sqrt{\left(\frac{\gamma}{4}\right)^2 - \Omega^2}. \tag{B.5}$$

The general solution is then

$$\begin{pmatrix}\langle\sigma_-(t)\rangle\\ \langle\sigma+(t)\rangle\\ \langle\sigma z(t)\rangle\end{pmatrix}_c = C^{(1)}e^{-\frac{\gamma}{2}t}\begin{pmatrix}1\\1\\0\end{pmatrix} + C^{(2)}e^{-\left(\frac{3\gamma}{4}+\delta\right)t}\begin{pmatrix}\frac{-2i\Omega}{\gamma+4\delta},\\ \frac{2i\Omega}{\gamma+4\delta},\\ 1\end{pmatrix} + C^{(3)}e^{-\left(\frac{3\gamma}{4}-\delta\right)t}\begin{pmatrix}\frac{-2i\Omega}{\gamma-4\delta},\\ \frac{2i\Omega}{\gamma-4\delta},\\ 1\end{pmatrix}. \tag{B.6}$$

B.1.2 Particular solution to the nonhomogenous equation

Using variation of parameters, it can be shown for that the matrix, $\boldsymbol{X}(t)$, will be a solution to the differential equation

$$\frac{\mathrm{d}}{\mathrm{d}t}\boldsymbol{X}(t) = \boldsymbol{M}\boldsymbol{X}(t). \tag{B.7}$$

We then assume we can find a particular solution of the form

$$\boldsymbol{A}_P(t) = \boldsymbol{X}(t)\boldsymbol{v}(t), \tag{B.8}$$

where

$$\boldsymbol{v}(t) = \int \boldsymbol{X}^{-1}(t)\boldsymbol{B}(t)\mathrm{d}t. \tag{B.9}$$

For the Bloch equations, we find the matrix to be

$$\boldsymbol{X}(t) = \begin{pmatrix} e^{-\frac{\gamma}{2}t} & \frac{-2i\Omega}{\gamma+4\delta}e^{-\left(\frac{3\gamma}{4}+\delta\right)t} & \frac{-2i\Omega}{\gamma-4\delta}e^{-\left(\frac{3\gamma}{4}-\delta\right)t} \\ e^{-\frac{\gamma}{2}t} & \frac{2i\Omega}{\gamma+4\delta}e^{-\left(\frac{3\gamma}{4}+\delta\right)t} & \frac{2i\Omega}{\gamma-4\delta}e^{-\left(\frac{3\gamma}{4}-\delta\right)t} \\ 0 & e^{-\left(\frac{3\gamma}{4}+\delta\right)t} & e^{-\left(\frac{3\gamma}{4}-\delta\right)t} \end{pmatrix}, \tag{B.10}$$

which has inverse

$$\boldsymbol{X}^{-1}(t) = \begin{pmatrix} \frac{1}{2}e^{\frac{\gamma}{2}t} & \frac{1}{2}e^{\frac{\gamma}{2}t} & 0 \\ \frac{-i(\gamma+4\delta)(\gamma-4\delta)}{32\delta\Omega}e^{\left(\frac{3\gamma}{4}+\delta\right)t} & \frac{i(\gamma+4\delta)(\gamma-4\delta)}{32\delta\Omega}e^{\left(\frac{3\gamma}{4}+\delta\right)t} & \frac{\gamma+4\delta}{8\delta}e^{\left(\frac{3\gamma}{4}+\delta\right)t} \\ \frac{i(\gamma+4\delta)(\gamma-4\delta)}{32\delta\Omega}e^{\left(\frac{3\gamma}{4}-\delta\right)t} & \frac{-i(\gamma+4\delta)(\gamma-4\delta)}{32\delta\Omega}e^{\left(\frac{3\gamma}{4}-\delta\right)t} & -\frac{\gamma-4\delta}{8\delta}e^{\left(\frac{3\gamma}{4}-\delta\right)t}. \end{pmatrix} \tag{B.11}$$

Then

$$\boldsymbol{X}^{-1}(t)\boldsymbol{B}(t) = \begin{pmatrix} 0 \\ -\frac{\gamma(\gamma+4\delta)}{8\delta}e^{\left(\frac{3\gamma}{4}+\delta\right)t} \\ \frac{\gamma(\gamma-4\delta)}{8\delta}e^{\left(\frac{3\gamma}{4}-\delta\right)t} \end{pmatrix} \tag{B.12}$$

and

$$\boldsymbol{v}(t) = \int \boldsymbol{X}^{-1}(t)\boldsymbol{B}(t)\mathrm{d}t = \int \begin{pmatrix} 0 \\ -\frac{\gamma(\gamma+4\delta)}{8\delta}e^{\left(\frac{3\gamma}{4}+\delta\right)t} \\ \frac{\gamma(\gamma-4\delta)}{8\delta}e^{\left(\frac{3\gamma}{4}-\delta\right)t} \end{pmatrix} \mathrm{d}t = \begin{pmatrix} 0 \\ -\frac{\gamma(\gamma+4\delta)}{2\delta(3\gamma+4\delta)}e^{\left(\frac{3\gamma}{4}+\delta\right)t} \\ \frac{\gamma(\gamma-4\delta)}{2\delta(3\gamma-4\delta)}e^{\left(\frac{3\gamma}{4}-\delta\right)t} \end{pmatrix}. \tag{B.13}$$

Hence the particular solution is

$$\boldsymbol{A}_P(t) = \boldsymbol{X}(t)\boldsymbol{v}(t) = \begin{pmatrix} \frac{-8i\gamma\Omega}{9\gamma^2-16\delta^2} \\ \frac{8i\gamma\Omega}{9\gamma^2-16\delta^2} \\ \frac{-8\gamma^2}{9\gamma^2-16\delta^2} \end{pmatrix}, \tag{B.14}$$

which simplifies to

$$\boldsymbol{A}_P(t) = \frac{1}{\gamma^2 + 2\Omega^2}\begin{pmatrix} -i\gamma\Omega \\ i\gamma\Omega \\ -\gamma^2 \end{pmatrix} = \langle \boldsymbol{\sigma} \rangle_{ss}. \tag{B.15}$$

B.1.3 General solution to the Bloch equations

The total solution to the Bloch equations is then

$$\langle \boldsymbol{\sigma}(t) \rangle = C^{(1)} e^{-\frac{\gamma}{2}t}\begin{pmatrix} 1 \\ 1 \\ 0 \end{pmatrix} + C^{(2)} e^{-\left(\frac{3\gamma}{4}+\delta\right)t}\begin{pmatrix} -1 \\ 1 \\ \frac{\gamma+4\delta}{2i\Omega} \end{pmatrix} + C^{(3)} e^{-\left(\frac{3\gamma}{4}-\delta\right)t}\begin{pmatrix} -1 \\ 1 \\ \frac{\gamma-4\delta}{2i\Omega} \end{pmatrix} + \langle \boldsymbol{\sigma} \rangle_{ss}. \tag{B.16}$$

With initial conditions,

$$\langle \boldsymbol{\sigma}(t=0) \rangle = \begin{pmatrix} \langle \sigma_-(0) \rangle \\ \langle \sigma_+(0) \rangle \\ \langle \sigma_z(0) \rangle \end{pmatrix}, \tag{B.17}$$

we rearrange Eq. (B.16) to solve for the coefficients,

$$C^{(1)} = \frac{1}{2}\Big(\langle \sigma_-(0) \rangle + \langle \sigma_+(0) \rangle \Big), \tag{B.18a}$$

$$C^{(2)} = \frac{1}{4\delta}\left[\frac{\gamma - 4\delta}{4}\Big(\langle \sigma_-(0) \rangle - \langle \sigma_+(0) \rangle \Big) + i\Omega \langle \sigma_z(0) \rangle \right], \tag{B.18b}$$

$$C^{(3)} = \frac{-1}{4\delta}\left[\frac{\gamma + 4\delta}{4}\Big(\langle \sigma_-(0) \rangle - \langle \sigma_+(0) \rangle \Big) + i\Omega \langle \sigma_z(0) \rangle \right]. \tag{B.18c}$$

B.1.4 Analytic solution of the photon creation operator

For the j^{th} mode, the operator average for the photon creation operator evolves as

$$\frac{\mathrm{d}}{\mathrm{d}t}\langle a_j^\dagger \rangle = -\left(\kappa - i\Delta\omega_j\right)\langle a_j^\dagger \rangle - \mathcal{E}_j^* \langle \sigma_+ \rangle, \tag{B.19}$$

where, from Eqs. (B.16) and (B.18),

$$\langle \sigma_+(t) \rangle = C^{(1)} e^{-\frac{\gamma}{2}t} + 2i\Omega C^{(2)} e^{-\left(\frac{3\gamma}{4}+\delta\right)t} + 2i\Omega C^{(3)} e^{-\left(\frac{3\gamma}{4}-\delta\right)t} + \langle \sigma_+ \rangle_{ss}. \tag{B.20}$$

Using the integrating factor method,

$$\begin{aligned} \langle a_j^\dagger(t) \rangle e^{-(\kappa - i\Delta\omega_j)t} &= -\int \mathcal{E}_j^* e^{(\kappa - i\Delta\omega_j)t'} \langle \sigma_+(t') \rangle \mathrm{d}t' \\ &= \int \Bigg[-\mathcal{E}_j^* C^{(1)} e^{-\left(\frac{\gamma}{2} - \kappa + i\Delta\omega_j\right)t'} - \mathcal{E}_j^* C^{(2)} e^{-\left(\frac{3\gamma}{4}+\delta-\kappa+i\Delta\omega_j\right)t'} \\ &\qquad -\mathcal{E}_j^* C^{(3)} e^{-\left(\frac{3\gamma}{4}-\delta-\kappa+i\Delta\omega_j\right)t'} - \mathcal{E}_j^* \langle \sigma_+ \rangle_{ss} e^{(\kappa - i\Delta\omega_j)t'} \Bigg] \mathrm{d}t', \end{aligned} \tag{B.21}$$

we find Eq. (B.19) has solution

$$\langle a_j^\dagger(t)\rangle = \frac{\mathcal{E}_j^* C^{(1)}}{\frac{\gamma}{2}-(\kappa-i\Delta\omega_j)}e^{-\frac{\gamma}{2}t} + \frac{\mathcal{E}_j^* C^{(2)}}{\frac{3\gamma}{4}+\delta-(\kappa-i\Delta\omega_j)}e^{-\left(\frac{3\gamma}{4}+\delta\right)t} + \frac{\mathcal{E}_j^* C^{(3)}}{\frac{3\gamma}{4}-\delta-(\kappa-i\Delta\omega_j)}e^{-\left(\frac{3\gamma}{4}-\delta\right)t} + C_j^{(4)}e^{-(\kappa-i\Delta\omega_j)t} + \langle a_j^\dagger\rangle_{ss}, \tag{B.22}$$

where

$$\langle a_j^\dagger\rangle_{ss} = \frac{-\mathcal{E}_j^*\langle\sigma_+\rangle_{ss}}{\kappa-i\Delta\omega_j} = \frac{-i\gamma\Omega\mathcal{E}_j^*}{(\gamma^2+2\Omega^2)(\kappa-i\Delta\omega_j)}. \tag{B.23}$$

B.2 Steady State Solutions

Here we present a brief summary of the steady states needed to calculate Eqs. (6.22).

B.2.1 First-order moments

We have already derived the steady states for the Bloch equations and the first-order cavity mode operator, $\langle a_j^\dagger\rangle_{ss}$. For the sake of clarity, we present them here again:

$$\langle\sigma_-\rangle_{ss} = \frac{-i\gamma\Omega}{\gamma^2+2\Omega^2}, \tag{B.24a}$$

$$\langle\sigma_+\rangle_{ss} = \frac{i\gamma\Omega}{\gamma^2+2\Omega^2}, \tag{B.24b}$$

$$\langle\sigma_z\rangle_{ss} = \frac{-\gamma^2}{\gamma^2+2\Omega^2}, \tag{B.24c}$$

$$\langle a_j\rangle_{ss} = \frac{i\gamma\Omega\mathcal{E}_j}{(\gamma^2+2\Omega^2)(\kappa+i\Delta\omega_j)}, \tag{B.24d}$$

$$\langle a_j^\dagger\rangle_{ss} = \frac{-i\gamma\Omega\mathcal{E}_j^*}{(\gamma^2+2\Omega^2)(\kappa-i\Delta\omega_j)}. \tag{B.24e}$$

B.2.2 First-order: Filter / Atom

Using the method of matrix inversion to calculate the steady state,

$$\frac{\mathrm{d}}{\mathrm{d}t}\langle\boldsymbol{A}\rangle = \boldsymbol{M}\boldsymbol{A}+\boldsymbol{B} \Longrightarrow \langle\boldsymbol{A}\rangle_{ss} = \boldsymbol{M}^{-1}\boldsymbol{B}, \tag{B.25}$$

we may calculate the steady state moments of

$$\langle a_j\boldsymbol{\sigma}\rangle_{ss} = \begin{pmatrix}\langle a_j\sigma_-\rangle_{ss}\\ \langle a_j\sigma_+\rangle_{ss}\\ \langle a_j\sigma_z\rangle_{ss}\end{pmatrix}. \tag{B.26}$$

From Eq. (A.5a), we have the evolution matrix,

$$\boldsymbol{M}^{(a\boldsymbol{\sigma})} = \begin{pmatrix} -\left(\frac{\gamma}{2}+\kappa+i\Delta\omega_j\right) & 0 & i\frac{\Omega}{2} \\ 0 & -\left(\frac{\gamma}{2}+\kappa+i\Delta\omega_j\right) & -i\frac{\Omega}{2} \\ i\Omega & -i\Omega & -\left(\gamma+\kappa+i\Delta\omega_j\right) \end{pmatrix}, \tag{B.27}$$

and nonhomogenous vector

$$\boldsymbol{B}^{(a\boldsymbol{\sigma})} = \begin{pmatrix} 0 \\ -\frac{1}{2}\mathcal{E}_j\left(\langle\sigma_z\rangle_{ss}+1\right) \\ -\gamma\langle a_j\rangle_{ss}+\mathcal{E}_j\langle\sigma_-\rangle_{ss} \end{pmatrix} = \frac{-\Omega\mathcal{E}_j}{\gamma^2+2\Omega^2}\begin{pmatrix} 0 \\ \Omega \\ \frac{i\gamma(\gamma+\kappa+i\Delta\omega_j)}{\kappa+i\Delta\omega_j} \end{pmatrix}. \tag{B.28}$$

Multiplying the inverse of the evolution matrix with this vector, we have

$$\langle a_k\sigma_+\rangle_{ss} = \frac{-\Omega^2\mathcal{E}_k\left[\Omega^2+2\left(\frac{\gamma}{2}+\kappa+i\Delta\omega_k\right)^2+\gamma\left(2+\frac{\gamma}{\kappa+i\Delta\omega_k}\right)\left(\frac{\gamma}{2}+\kappa+i\Delta\omega_k\right)\right]}{\left(\frac{\gamma}{2}+\kappa+i\Delta\omega_k\right)\left(\gamma^2+2\Omega^2\right)\left[2\Omega^2+2\left(\frac{\gamma}{2}+\kappa+i\Delta\omega_k\right)^2+\gamma\left(\frac{\gamma}{2}+\kappa+i\Delta\omega_k\right)\right]}. \tag{B.29}$$

We then have

$$\langle a_j^\dagger\sigma_-\rangle_{ss} = \frac{-\Omega^2\mathcal{E}_j^*\left[\Omega^2+2\left(\frac{\gamma}{2}+\kappa-i\Delta\omega_j\right)^2+\gamma\left(2+\frac{\gamma}{\kappa-i\Delta\omega_j}\right)\left(\frac{\gamma}{2}+\kappa-i\Delta\omega_j\right)\right]}{\left(\frac{\gamma}{2}+\kappa-i\Delta\omega_j\right)\left(\gamma^2+2\Omega^2\right)\left[2\Omega^2+2\left(\frac{\gamma}{2}+\kappa-i\Delta\omega_j\right)^2+\gamma\left(\frac{\gamma}{2}+\kappa-i\Delta\omega_j\right)\right]}. \tag{B.30}$$

B.2.3 Second-order: Filter

Rearranging the moment equation, Eq. (A.7b), we find

$$\langle a_j^\dagger a_k\rangle_{ss} = \frac{-\mathcal{E}_j^*\langle a_k\sigma_+\rangle_{ss}-\mathcal{E}_k\langle a_j^\dagger\sigma_-\rangle_{ss}}{2\kappa-i\left(\Delta\omega_j-\Delta\omega_k\right)}. \tag{B.31}$$

C Moment Equations of the Two-Level Atom and Two-Filter Cascaded System

Here we present all of the operator moment equations needed to calculate second-order cross-correlation functions for the two-filter, multi-mode array filtered two-level atom. We first show the moment equations, as derived from Eq. (6.31). These are then followed by the coupled equations for the second-order cross-correlation functions.

The `Fortan90` code used to numerically calculate these equations can be found at the following Github repository: github.com/jnga773/multi-mode-filter.

C.1 Moment Equations

We write these coupled moment equations in matrix form, where we use the notation

$$\langle \boldsymbol{\sigma} \rangle = \begin{pmatrix} \langle \sigma_- \rangle \\ \langle \sigma_+ \rangle \\ \langle \sigma_z \rangle \end{pmatrix}, \quad \langle X\boldsymbol{\sigma} \rangle = \begin{pmatrix} \langle X\sigma_- \rangle \\ \langle X\sigma_+ \rangle \\ \langle X\sigma_z \rangle \end{pmatrix}. \tag{C.1}$$

C.1.1 Atomic Operator Moments

$$\frac{\mathrm{d}}{\mathrm{d}t}\langle \boldsymbol{\sigma} \rangle = \boldsymbol{M}\langle \boldsymbol{\sigma} \rangle + \begin{pmatrix} 0 \\ 0 \\ -\gamma \end{pmatrix}, \tag{C.2}$$

where

$$\boldsymbol{M}^{(\sigma)} = \begin{pmatrix} -\frac{\gamma}{2} & 0 & i\frac{\Omega}{2} \\ 0 & -\frac{\gamma}{2} & -i\frac{\Omega}{2} \\ i\Omega & -i\Omega & -\gamma \end{pmatrix}. \tag{C.3}$$

C.1.2 First-order: Filter

$$\frac{\mathrm{d}}{\mathrm{d}t}\langle a_j \rangle = -\left(\kappa_a + i\Delta\omega_j^{(a)}\right)\langle a_j \rangle - \mathcal{E}_j^{(a)}\langle \sigma_- \rangle, \tag{C.4a}$$

$$\frac{\mathrm{d}}{\mathrm{d}t}\langle a_j^\dagger \rangle = -\left(\kappa_a - i\Delta\omega_j^{(a)}\right)\langle a_j^\dagger \rangle - \mathcal{E}_j^{(a)*}\langle \sigma_+ \rangle. \tag{C.4b}$$

$$\frac{\mathrm{d}}{\mathrm{d}t}\langle b_j \rangle = -\left(\kappa_b + i\Delta\omega_j^{(b)}\right)\langle b_j \rangle - \mathcal{E}_j^{(b)}\langle \sigma_- \rangle, \tag{C.4c}$$

$$\frac{\mathrm{d}}{\mathrm{d}t}\langle b_j^\dagger \rangle = -\left(\kappa_b - i\Delta\omega_j^{(b)}\right)\langle b_j^\dagger \rangle - \mathcal{E}_j^{(b)*}\langle \sigma_+ \rangle. \tag{C.4d}$$

C.1.3 First-order: Filter / Atom

$$\frac{\mathrm{d}}{\mathrm{d}t}\langle a_j\boldsymbol{\sigma}\rangle = \boldsymbol{M}_j^{(a)}\langle a_j\boldsymbol{\sigma}\rangle + \begin{pmatrix} 0 \\ -\frac{1}{2}\mathcal{E}_j^{(a)}\left(\langle\sigma_z\rangle + 1\right) \\ -\gamma\langle a_j\rangle + \mathcal{E}_j^{(a)}\langle\sigma_-\rangle \end{pmatrix}, \tag{C.5a}$$

$$\frac{\mathrm{d}}{\mathrm{d}t}\langle a_j^\dagger\boldsymbol{\sigma}\rangle = \boldsymbol{M}_j^{(a^\dagger)}\langle a_j\boldsymbol{\sigma}\rangle + \begin{pmatrix} -\frac{1}{2}\mathcal{E}_j^{(a)^*}\left(\langle\sigma_z\rangle + 1\right) \\ 0 \\ -\gamma\langle a_j^\dagger\rangle + \mathcal{E}_j^{(a)^*}\langle\sigma_+\rangle \end{pmatrix}, \tag{C.5b}$$

$$\frac{\mathrm{d}}{\mathrm{d}t}\langle b_j\boldsymbol{\sigma}\rangle = \boldsymbol{M}_j^{(b)}\langle b_j\boldsymbol{\sigma}\rangle + \begin{pmatrix} 0 \\ -\frac{1}{2}\mathcal{E}_j^{(b)}\left(\langle\sigma_z\rangle + 1\right) \\ -\gamma\langle b_j\rangle + \mathcal{E}_j^{(b)}\langle\sigma_-\rangle \end{pmatrix}, \tag{C.5c}$$

$$\frac{\mathrm{d}}{\mathrm{d}t}\langle b_j^\dagger\boldsymbol{\sigma}\rangle = \boldsymbol{M}_j^{(b^\dagger)}\langle b_j\boldsymbol{\sigma}\rangle + \begin{pmatrix} -\frac{1}{2}\mathcal{E}_j^{(b)^*}\left(\langle\sigma_z\rangle + 1\right) \\ 0 \\ -\gamma\langle a_j^\dagger\rangle + \mathcal{E}_j^{(b)^*}\langle\sigma_+\rangle \end{pmatrix}, \tag{C.5d}$$

with

$$\boldsymbol{M}_j^{(a)} = \boldsymbol{M}^{(\sigma)} - \left(\kappa_a + i\Delta\omega_j^{(a)}\right)\mathbb{1}, \tag{C.6a}$$

$$\boldsymbol{M}_j^{(a^\dagger)} = \boldsymbol{M}^{(\sigma)} - \left(\kappa_a - i\Delta\omega_j^{(a)}\right)\mathbb{1}, \tag{C.6b}$$

$$\boldsymbol{M}_j^{(b)} = \boldsymbol{M}^{(\sigma)} - \left(\kappa_b + i\Delta\omega_j^{(b)}\right)\mathbb{1}, \tag{C.6c}$$

$$\boldsymbol{M}_j^{(b^\dagger)} = \boldsymbol{M}^{(\sigma)} - \left(\kappa_b - i\Delta\omega_j^{(b)}\right)\mathbb{1}. \tag{C.6d}$$

C.1.4 Second-order: Filter

$$\frac{\mathrm{d}}{\mathrm{d}t}\langle a_j b_k\rangle = -\left[\kappa_a + \kappa_b + i\left(\Delta\omega_j^{(a)} + \Delta\omega_k^{(b)}\right)\right]\langle a_j b_k\rangle - \mathcal{E}_j^{(a)}\langle b_k\sigma_-\rangle - \mathcal{E}_k^{(b)}\langle a_j\sigma_-\rangle, \tag{C.7a}$$

$$\frac{\mathrm{d}}{\mathrm{d}t}\langle a_j^\dagger b_k^\dagger\rangle = -\left[\kappa_a + \kappa_b - i\left(\Delta\omega_j^{(a)} + \Delta\omega_k^{(b)}\right)\right]\langle a_j^\dagger b_k^\dagger\rangle - \mathcal{E}_j^{(a)^*}\langle b_k^\dagger\sigma_+\rangle - \mathcal{E}_k^{(b)^*}\langle a_j^\dagger\sigma_+\rangle, \tag{C.7b}$$

$$\frac{\mathrm{d}}{\mathrm{d}t}\langle a_j^\dagger a_k\rangle = -\left[2\kappa_a - i\left(\Delta\omega_j^{(a)} - \Delta\omega_k^{(a)}\right)\right]\langle a_j^\dagger a_k\rangle - \mathcal{E}_j^{(a)^*}\langle a_k\sigma_+\rangle - \mathcal{E}_k^{(a)}\langle a_j^\dagger\sigma_-\rangle, \tag{C.7c}$$

$$\frac{\mathrm{d}}{\mathrm{d}t}\langle b_j^\dagger b_k\rangle = -\left[2\kappa_b - i\left(\Delta\omega_j^{(b)} - \Delta\omega_k^{(b)}\right)\right]\langle b_j^\dagger b_k\rangle - \mathcal{E}_j^{(b)^*}\langle b_k\sigma_+\rangle - \mathcal{E}_k^{(b)}\langle b_j^\dagger\sigma_-\rangle, \tag{C.7d}$$

$$\frac{\mathrm{d}}{\mathrm{d}t}\langle a_j^\dagger b_k\rangle = -\left[\kappa_a + \kappa_b - i\left(\Delta\omega_j^{(a)} - \Delta\omega_k^{(b)}\right)\right]\langle a_j^\dagger b_k\rangle - \mathcal{E}_j^{(a)^*}\langle b_k\sigma_+\rangle - \mathcal{E}_k^{(b)}\langle a_j^\dagger\sigma_-\rangle, \tag{C.7e}$$

$$\frac{\mathrm{d}}{\mathrm{d}t}\langle b_j^\dagger a_k\rangle = -\left[\kappa_a + \kappa_b - i\left(\Delta\omega_j^{(b)} - \Delta\omega_k^{(a)}\right)\right]\langle b_j^\dagger a_k\rangle - \mathcal{E}_j^{(b)^*}\langle a_k\sigma_+\rangle - \mathcal{E}_k^{(a)}\langle b_j^\dagger\sigma_-\rangle. \tag{C.7f}$$

C.1.5 Second-order: Filter / Atom

$$\frac{\mathrm{d}}{\mathrm{d}t}\langle a_j b_k \boldsymbol{\sigma}\rangle = \boldsymbol{M}_{jk}^{(ab)}\langle a_j b_k \boldsymbol{\sigma}\rangle + \begin{pmatrix} 0 \\ -\frac{1}{2}\mathcal{E}_j^{(a)}\left(\langle b_k\sigma_z\rangle + \langle b_k\rangle\right) - \frac{1}{2}\mathcal{E}_k\left(\langle a_j\sigma_z\rangle + \langle a_j\rangle\right) \\ -\gamma\langle a_j b_k\rangle + \mathcal{E}_j^{(a)}\langle b_k\sigma_-\rangle + \mathcal{E}_k^{(b)}\langle a_j\sigma_-\rangle \end{pmatrix}, \tag{C.8a}$$

$$\frac{\mathrm{d}}{\mathrm{d}t}\langle a_j^\dagger b_k^\dagger \boldsymbol{\sigma}\rangle = \boldsymbol{M}_{jk}^{(a^\dagger b^\dagger)} a_j^\dagger b_k^\dagger \boldsymbol{\sigma}\rangle + \begin{pmatrix} -\frac{1}{2}\mathcal{E}_j^{(a)^*}\left(\langle b_k^\dagger\sigma_z\rangle + \langle b_k^\dagger\rangle\right) - \frac{1}{2}\mathcal{E}_k^{(b)^*}\left(\langle a_j^\dagger\sigma_z\rangle + \langle a_j^\dagger\rangle\right) \\ 0 \\ -\gamma\langle a_j^\dagger b_k^\dagger\rangle + \mathcal{E}_j^{(a)^*}\langle b_k^\dagger\sigma_+\rangle + \mathcal{E}_k^{(b)^*}\langle a_j^\dagger\sigma_+\rangle \end{pmatrix}, \tag{C.8b}$$

$$\frac{\mathrm{d}}{\mathrm{d}t}\langle a_j^\dagger a_k \boldsymbol{\sigma}\rangle = \boldsymbol{M}_{jk}^{(a^\dagger a)}\langle a_j^\dagger a_k \boldsymbol{\sigma}\rangle + \begin{pmatrix} -\frac{1}{2}\mathcal{E}_j^{(a)^*}\left(\langle a_k\sigma_z\rangle + \langle a_k\rangle\right) \\ -\frac{1}{2}\mathcal{E}_k^{(a)}\left(\langle a_j^\dagger\sigma_z\rangle + \langle a_j^\dagger\rangle\right) \\ -\gamma\langle a_j^\dagger a_k\rangle + \mathcal{E}_j^{(a)^*}\langle a_k\sigma_+\rangle + \mathcal{E}_k^{(a)}\langle a_j^\dagger\sigma_-\rangle \end{pmatrix}, \tag{C.8c}$$

$$\frac{\mathrm{d}}{\mathrm{d}t}\langle b_j^\dagger b_k \boldsymbol{\sigma}\rangle = \boldsymbol{M}_{jk}^{(b^\dagger b)}\langle b_j^\dagger b_k \boldsymbol{\sigma}\rangle + \begin{pmatrix} -\frac{1}{2}\mathcal{E}_j^{(b)^*}\left(\langle b_k\sigma_z\rangle + \langle b_k\rangle\right) \\ -\frac{1}{2}\mathcal{E}_k^{(b)}\left(\langle b_j^\dagger\sigma_z\rangle + \langle b_j^\dagger\rangle\right) \\ -\gamma\langle b_j^\dagger b_k\rangle + \mathcal{E}_j^{(b)^*}\langle b_k\sigma_+\rangle + \mathcal{E}_k^{(b)}\langle b_j^\dagger\sigma_-\rangle \end{pmatrix}, \tag{C.8d}$$

$$\frac{\mathrm{d}}{\mathrm{d}t}\langle a_j^\dagger b_k \boldsymbol{\sigma}\rangle = \boldsymbol{M}_{jk}^{(a^\dagger b)}\langle a_j^\dagger b_k \boldsymbol{\sigma}\rangle + \begin{pmatrix} -\frac{1}{2}\mathcal{E}_j^{(a)^*}\left(\langle b_k\sigma_z\rangle + \langle b_k\rangle\right) \\ -\frac{1}{2}\mathcal{E}_k^{(b)}\left(\langle a_j^\dagger\sigma_z\rangle + \langle a_j^\dagger\rangle\right) \\ -\gamma\langle a_j^\dagger b_k\rangle + \mathcal{E}_j^{(a)^*}\langle b_k\sigma_+\rangle + \mathcal{E}_k^{(b)}\langle a_j^\dagger\sigma_-\rangle \end{pmatrix}, \tag{C.8e}$$

$$\frac{\mathrm{d}}{\mathrm{d}t}\langle b_j^\dagger a_k \boldsymbol{\sigma}\rangle = \boldsymbol{M}_{jk}^{(b^\dagger a)}\langle b_j^\dagger a_k \boldsymbol{\sigma}\rangle + \begin{pmatrix} -\frac{1}{2}\mathcal{E}_j^{(b)^*}\left(\langle a_k\sigma_z\rangle + \langle a_k\rangle\right) \\ -\frac{1}{2}\mathcal{E}_k^{(a)}\left(\langle b_j^\dagger\sigma_z\rangle + \langle b_j^\dagger\rangle\right) \\ -\gamma\langle b_j^\dagger a_k\rangle + \mathcal{E}_j^{(b)^*}\langle a_k\sigma_+\rangle + \mathcal{E}_k^{(a)}\langle b_j^\dagger\sigma_-\rangle \end{pmatrix}, \tag{C.8f}$$

with

$$\boldsymbol{M}_{jk}^{(ab)} = \boldsymbol{M}^{(\sigma)} - \left[\kappa_a + \kappa_b + i\left(\Delta\omega_j^{(a)} + \Delta\omega_k^{(b)}\right)\right]\mathbb{1}, \tag{C.9a}$$

$$\boldsymbol{M}_{jk}^{(a^\dagger b^\dagger)} = \boldsymbol{M}^{(\sigma)} - \left[\kappa_a + \kappa_b - i\left(\Delta\omega_j^{(a)} + \Delta\omega_k^{(b)}\right)\right]\mathbb{1}, \tag{C.9b}$$

$$\boldsymbol{M}_{jk}^{(a^\dagger a)} = \boldsymbol{M}^{(\sigma)} - \left[2\kappa_a - i\left(\Delta\omega_j^{(a)} - \Delta\omega_k^{(a)}\right)\right]\mathbb{1}, \tag{C.9c}$$

$$\boldsymbol{M}_{jk}^{(b^\dagger b)} = \boldsymbol{M}^{(\sigma)} - \left[2\kappa_b - i\left(\Delta\omega_j^{(b)} - \Delta\omega_k^{(b)}\right)\right]\mathbb{1}, \tag{C.9d}$$

$$\boldsymbol{M}_{jk}^{(a^\dagger b)} = \boldsymbol{M}^{(\sigma)} - \left[\kappa_a + \kappa_b - i\left(\Delta\omega_j^{(a)} - \Delta\omega_k^{(b)}\right)\right]\mathbb{1}, \tag{C.9e}$$

$$\boldsymbol{M}_{jk}^{(b^\dagger a)} = \boldsymbol{M}^{(\sigma)} - \left[\kappa_a + \kappa_b - i\left(\Delta\omega_j^{(b)} - \Delta\omega_k^{(a)}\right)\right]\mathbb{1}. \tag{C.9f}$$

C.1.6 Third-order: Filter

$$\frac{\mathrm{d}}{\mathrm{d}t}\langle a_j^\dagger a_k b_l\rangle = -\left[2\kappa_a+\kappa_b - i\left(\Delta\omega_j^{(a)} - \Delta\omega_k^{(a)} - \Delta\omega_l^{(b)}\right)\right]\langle a_j^\dagger a_k b_l\rangle - \mathcal{E}_j^{(a)^*}\langle a_k b_l\sigma_+\rangle - \mathcal{E}_k^{(a)}\langle a_j^\dagger b_l\sigma_-\rangle - \mathcal{E}_l^{(b)}\langle a_j^\dagger a_k\sigma_-\rangle, \tag{C.10a}$$

$$\frac{\mathrm{d}}{\mathrm{d}t}\langle b_j^\dagger b_k a_l\rangle = -\left[\kappa_a+2\kappa_b - i\left(\Delta\omega_j^{(b)} - \Delta\omega_k^{(b)} - \Delta\omega_l^{(a)}\right)\right]\langle b_j^\dagger b_k a_l\rangle - \mathcal{E}_j^{(b)^*}\langle a_l b_k\sigma_+\rangle - \mathcal{E}_k^{(b)}\langle b_j^\dagger a_l\sigma_-\rangle - \mathcal{E}_l^{(a)}\langle b_j^\dagger b_k\sigma_-\rangle, \tag{C.10b}$$

$$\frac{\mathrm{d}}{\mathrm{d}t}\langle b_j^\dagger a_k^\dagger a_l\rangle = -\left[2\kappa_a+\kappa_b - i\left(\Delta\omega_j^{(b)} + \Delta\omega_k^{(a)} - \Delta\omega_l^{(a)}\right)\right]\langle b_j^\dagger a_k^\dagger a_l\rangle - \mathcal{E}_j^{(b)^*}\langle a_k^\dagger a_l\sigma_+\rangle - \mathcal{E}_k^{(a)^*}\langle b_j^\dagger a_l\sigma_+\rangle - \mathcal{E}_l^{(a)}\langle a_k^\dagger b_j^\dagger\sigma_-\rangle, \tag{C.10c}$$

$$\frac{\mathrm{d}}{\mathrm{d}t}\langle a_j^\dagger b_k^\dagger b_l\rangle = -\left[\kappa_a+\kappa_b - i\left(\Delta\omega_j^{(a)} + \Delta\omega_k^{(b)} - \Delta\omega_l^{(b)}\right)\right]\langle a_j^\dagger b_k^\dagger b_l\rangle - \mathcal{E}_j^{(a)^*}\langle b_k^\dagger b_l\sigma_+\rangle - \mathcal{E}_k^{(b)^*}\langle a_j^\dagger b_l\sigma_+\rangle - \mathcal{E}_l^{(b)}\langle a_j^\dagger b_k^\dagger\sigma_-\rangle. \tag{C.10d}$$

C.1.7 Third-order: Filter / Atom

$$\frac{\mathrm{d}}{\mathrm{d}t}\langle a_j^\dagger a_k b_l\boldsymbol{\sigma}\rangle = \boldsymbol{M}_{jkl}^{(a^\dagger ab)}\langle a_j^\dagger a_k b_l\boldsymbol{\sigma}\rangle + \begin{pmatrix} -\frac{1}{2}\mathcal{E}_j^{(a)^*}\left(\langle a_k b_l\sigma_z\rangle + \langle a_k b_l\rangle\right) \\ -\frac{1}{2}\mathcal{E}_k^{(a)}\left(\langle a_j^\dagger b_l\sigma_z\rangle + \langle a_j^\dagger b_l\rangle\right) - \frac{1}{2}\mathcal{E}_l^{(b)}\left(\langle a_j^\dagger a_k\sigma_z\rangle + \langle a_j^\dagger a_k\rangle\right) \\ -\gamma\langle a_j^\dagger a_k b_l\rangle + \mathcal{E}_j^{(a)^*}\langle a_k b_l\sigma_+\rangle + \mathcal{E}_k^{(a)}\langle a_j^\dagger b_l\sigma_-\rangle + \mathcal{E}_l^{(b)}\langle a_j^\dagger a_k\sigma_-\rangle \end{pmatrix}, \tag{C.11a}$$

$$\frac{\mathrm{d}}{\mathrm{d}t}\langle b_j^\dagger b_k a_l\boldsymbol{\sigma}\rangle = \boldsymbol{M}_{jkl}^{(b^\dagger ba)}\langle b_j^\dagger b_k a_l\boldsymbol{\sigma}\rangle + \begin{pmatrix} -\frac{1}{2}\mathcal{E}_j^{(b)^*}\left(\langle a_l b_k\sigma_z\rangle + \langle a_l b_k\rangle\right) \\ -\frac{1}{2}\mathcal{E}_k^{(b)}\left(\langle b_j^\dagger a_l\sigma_z\rangle + \langle b_j^\dagger a_l\rangle\right) - \frac{1}{2}\mathcal{E}_l^{(a)}\left(\langle b_j^\dagger b_k\sigma_z\rangle + \langle b_j^\dagger b_k\rangle\right) \\ -\gamma\langle b_j^\dagger b_k a_l\rangle + \mathcal{E}_j^{(b)^*}\langle a_l b_k\sigma_+\rangle + \mathcal{E}_k^{(b)}\langle b_j^\dagger a_l\sigma_-\rangle + \mathcal{E}_l^{(a)}\langle b_j^\dagger b_k\sigma_-\rangle \end{pmatrix}, \tag{C.11b}$$

$$\frac{\mathrm{d}}{\mathrm{d}t}\langle b_j^\dagger a_k^\dagger a_l\boldsymbol{\sigma}\rangle = \boldsymbol{M}_{jkl}^{(b^\dagger a^\dagger a)}\langle b_j^\dagger a_k^\dagger a_l\boldsymbol{\sigma}\rangle + \begin{pmatrix} -\frac{1}{2}\mathcal{E}_j^{(b)^*}\left(\langle a_k^\dagger a_l\sigma_z\rangle + \langle a_k^\dagger a_l\rangle\right) - \frac{1}{2}\mathcal{E}_k^{(a)^*}\left(\langle b_j^\dagger a_l\sigma_z\rangle + \langle b_j^\dagger a_l\rangle\right) \\ -\frac{1}{2}\mathcal{E}_l^{(a)}\left(\langle a_k^\dagger b_j^\dagger\sigma_z\rangle + \langle a_k^\dagger b_j^\dagger\rangle\right) \\ -\gamma\langle b_j^\dagger a_k^\dagger a_l\rangle + \mathcal{E}_j^{(b)^*}\langle a_k^\dagger a_l\sigma_+\rangle + \mathcal{E}_k^{(a)^*}\langle b_j^\dagger a_l\sigma_+\rangle + \mathcal{E}_l^{(a)}\langle a_k^\dagger b_j^\dagger\sigma_-\rangle \end{pmatrix}, \tag{C.11c}$$

$$\frac{\mathrm{d}}{\mathrm{d}t}\langle a_j^\dagger b_k^\dagger b_l\boldsymbol{\sigma}\rangle = \boldsymbol{M}_{jkl}^{(a^\dagger b^\dagger b)}\langle a_j^\dagger b_k^\dagger b_l\boldsymbol{\sigma}\rangle + \begin{pmatrix} -\frac{1}{2}\mathcal{E}_j^{(a)^*}\left(\langle b_k^\dagger b_l\sigma_z\rangle + \langle b_k^\dagger b_l\rangle\right) - \frac{1}{2}\mathcal{E}_k^{(b)^*}\left(\langle a_j^\dagger b_l\sigma_z\rangle + \langle a_j^\dagger b_l\rangle\right) \\ -\frac{1}{2}\mathcal{E}_l^{(b)}\left(\langle a_j^\dagger b_k^\dagger\sigma_z\rangle + \langle a_j^\dagger b_k^\dagger\rangle\right) \\ -\gamma\langle a_j^\dagger b_k^\dagger b_l\rangle + \mathcal{E}_j^{(a)^*}\langle b_k^\dagger b_l\sigma_+\rangle + \mathcal{E}_k^{(b)^*}\langle a_j^\dagger b_l\sigma_+\rangle + \mathcal{E}_l^{(b)}\langle a_j^\dagger b_k^\dagger\sigma_-\rangle \end{pmatrix}, \tag{C.11d}$$

with

$$\boldsymbol{M}_{jkl}^{(a^\dagger ab)} = \boldsymbol{M}^{(\sigma)} - \left[2\kappa_a + \kappa_b - i\left(\Delta\omega_j^{(a)} - \Delta\omega_k^{(a)} - \Delta\omega_l^{(b)}\right)\right]\mathbb{1}, \tag{C.12a}$$

$$\boldsymbol{M}_{jkl}^{(b^\dagger ba)} = \boldsymbol{M}^{(\sigma)} - \left[\kappa_a + 2\kappa_b - i\left(\Delta\omega_j^{(b)} - \Delta\omega_k^{(b)} - \Delta\omega_l^{(a)}\right)\right]\mathbb{1}, \tag{C.12b}$$

$$\boldsymbol{M}_{jkl}^{(b^\dagger a^\dagger a)} = \boldsymbol{M}^{(\sigma)} - \left[2\kappa_a + \kappa_b - i\left(\Delta\omega_j^{(b)} + \Delta\omega_k^{(a)} - \Delta\omega_l^{(a)}\right)\right]\mathbb{1}, \tag{C.12c}$$

$$\boldsymbol{M}_{jkl}^{(a^\dagger b^\dagger b)} = \boldsymbol{M}^{(\sigma)} - \left[\kappa_a + \kappa_b - i\left(\Delta\omega_j^{(a)} + \Delta\omega_k^{(b)} - \Delta\omega_l^{(b)}\right)\right]\mathbb{1}. \tag{C.12d}$$

C.1.8 Fourth-order: Filter

$$\begin{aligned}\frac{\mathrm{d}}{\mathrm{d}t}\langle a_j^\dagger b_k^\dagger b_l a_m\rangle = &-\left[2\kappa_a + 2\kappa_b - i\left(\Delta\omega_j^{(a)} + \Delta\omega_k^{(b)}\right) + i\left(\Delta\omega_l^{(b)} + \Delta\omega_m^{(a)}\right)\right]\langle a_j^\dagger b_k^\dagger b_l a_m\rangle \\ &- \mathcal{E}_j^{(a)*}\langle b_k^\dagger b_l a_m \sigma_+\rangle - \mathcal{E}_k^{(b)*}\langle a_j^\dagger a_m b_l \sigma_+\rangle \\ &- \mathcal{E}_l^{(b)}\langle b_k^\dagger a_j^\dagger a_m \sigma_-\rangle - \mathcal{E}_m^{(a)}\langle a_j^\dagger b_k^\dagger b_l \sigma_-\rangle.\end{aligned} \tag{C.13}$$

C.2 Filtered Cross-Correlation Function

The second-order cross-correlation function for the filtered output field is given by

$$G^{(2)}(\alpha, t; \beta, t+\tau) = \langle A^\dagger(t) B^\dagger B(t+\tau) A(t)\rangle = \sum_{j,k=-N}^{N} \langle A^\dagger(t) b_k^\dagger b_l(t+\tau) A(t)\rangle. \tag{C.14}$$

We use the quantum regression equations to solve for this with the following moment equations:

$$\frac{\mathrm{d}}{\mathrm{d}\tau}\langle A^\dagger(t)\boldsymbol{\sigma}(t+\tau)A(t)\rangle = \boldsymbol{M}^{(\sigma)}\langle A^\dagger(t)\boldsymbol{\sigma}(t+\tau)A(t)\rangle + \begin{pmatrix} 0 \\ 0 \\ -\gamma\langle A^\dagger A(t)\rangle \end{pmatrix}, \tag{C.15a}$$

and

$$\begin{aligned}\frac{\mathrm{d}}{\mathrm{d}\tau}\langle A^\dagger(t) b_j(t+\tau)A(t)\rangle = &-\left(\kappa_b + i\Delta\omega_j^{(b)}\right)\langle A^\dagger(t) b_j A(t)\rangle \\ &- \mathcal{E}_j^{(b)}\langle A^\dagger(t)\sigma_-(t+\tau)A(t)\rangle,\end{aligned} \tag{C.15b}$$

$$\begin{aligned}\frac{\mathrm{d}}{\mathrm{d}\tau}\langle A^\dagger(t) b_j^\dagger(t+\tau)A(t)\rangle = &-\left(\kappa_b - i\Delta\omega_j^{(b)}\right)\langle A^\dagger(t) a_j^\dagger A(t)\rangle \\ &- \mathcal{E}_j^{(b)*}\langle A^\dagger(t)\sigma_+(t+\tau)A(t)\rangle,\end{aligned} \tag{C.15c}$$

and

$$\frac{\mathrm{d}}{\mathrm{d}\tau}\langle A^\dagger(t)b_j\boldsymbol{\sigma}(t+\tau)A(t)\rangle = \boldsymbol{M}_j^{(b)}\langle A^\dagger(t)b_j\boldsymbol{\sigma}(t+\tau)A(t)\rangle + \begin{pmatrix} 0 \\ -\frac{1}{2}\mathcal{E}_j^{(b)}\left(\langle A^\dagger(t)\sigma_z(t+\tau)A(t)\rangle + \langle A^\dagger A(t)\rangle\right) \\ -\gamma\langle A^\dagger(t)b_j(t+\tau)A(t)\rangle + \mathcal{E}_j\langle A^\dagger(t)\sigma_-(t+\tau)A(t)\rangle \end{pmatrix}, \tag{C.15d}$$

$$\frac{\mathrm{d}}{\mathrm{d}\tau}\langle A^\dagger(t)b_j^\dagger\boldsymbol{\sigma}(t+\tau)A(t)\rangle = \boldsymbol{M}_j^{(b^\dagger)}\langle A^\dagger(t)b_j\boldsymbol{\sigma}(t+\tau)A(t)\rangle + \begin{pmatrix} -\frac{1}{2}\mathcal{E}_j^{(b)^*}\left(\langle A^\dagger(t)\sigma_z(t+\tau)A(t)\rangle + \langle A^\dagger A(t)\rangle\right) \\ 0 \\ -\gamma\langle A^\dagger(t)b_j^\dagger(t+\tau)A(t)\rangle + \mathcal{E}_j^{(b)^*}\langle A^\dagger(t)\sigma_+(t+\tau)A(t)\rangle \end{pmatrix}, \tag{C.15e}$$

and

$$\begin{aligned}\frac{\mathrm{d}}{\mathrm{d}\tau}\langle A^\dagger(t)b_j^\dagger b_k(t+\tau)A(t)\rangle = &-\left[2\kappa_b - i\left(\Delta\omega_j^{(b)} - \Delta\omega_k^{(b)}\right)\right]\langle A^\dagger(t)b_j^\dagger b_k(t+\tau)A(t)\rangle \\ &- \mathcal{E}_j^{(b)^*}\langle A^\dagger(t)b_k\sigma_+(t+\tau)A(t)\rangle \\ &- \mathcal{E}_k^{(b)}\langle A^\dagger(t)b_j^\dagger\sigma_-(t+\tau)A(t)\rangle.\end{aligned} \tag{C.15f}$$

We solve these differential equations with the initial conditions at $\tau = 0$,

$$\langle A^\dagger\boldsymbol{\sigma}A(t)\rangle = \sum_{j,m=-N}^{N}\langle a_j^\dagger a_m\boldsymbol{\sigma}(t)\rangle, \tag{C.16a}$$

$$\langle A^\dagger b_k^\dagger A(t)\rangle = \sum_{j,m=-N}^{N}\langle b_k^\dagger a_j^\dagger a_m(t)\rangle, \tag{C.16b}$$

$$\langle A^\dagger b_l A(t)\rangle = \sum_{j,m=-N}^{N}\langle a_j^\dagger a_m(t)b_l\rangle, \tag{C.16c}$$

$$\langle A^\dagger b_k^\dagger\boldsymbol{\sigma}A(t)\rangle = \sum_{j,m=-N}^{N}\langle b_k^\dagger a_j^\dagger a_m\boldsymbol{\sigma}(t)\rangle, \tag{C.16d}$$

$$\langle A^\dagger b_l\boldsymbol{\sigma}A(t)\rangle = \sum_{j,m=-N}^{N}\langle a_j^\dagger a_m b_l\boldsymbol{\sigma}(t)\rangle, \tag{C.16e}$$

$$\langle A^\dagger b_k^\dagger b_l A(t)\rangle = \sum_{j,m=-N}^{N}\langle a_j^\dagger b_k^\dagger b_l a_m(t)\rangle. \tag{C.16f}$$

D Derivation of the Dressed State Correlation Functions of the Three-Level Atom

Here we present a detailed derivation of the dressed state correlation functions of the three-level ladder type atom in Section 7.2.1. First we introduce some basic linear algebra theory, and then derive the dressed state operators in the general case. Finally we present the dressed state operators for the case of two-photon resonance, $\delta/\Gamma = 0$.

D.1 Linear Algebra: Changing Basis

For two bases $\mathcal{B} = \{\boldsymbol{b}_1, \boldsymbol{b}_2, \ldots, \boldsymbol{b}_n\}$ and $\mathcal{C} = \{\boldsymbol{c}_1, \boldsymbol{c}_2, \ldots, \boldsymbol{c}_n\}$ in some vector space $\mathcal{V}$, there exists some unique $n \times n$ matrix $\boldsymbol{P}_{\mathcal{B}\to\mathcal{C}}$ such that

$$[\boldsymbol{x}]_{\mathcal{C}} = \boldsymbol{P}_{\mathcal{B}\to\mathcal{C}}[\boldsymbol{x}]_{\mathcal{B}}, \tag{D.1}$$

where

$$\boldsymbol{P}_{\mathcal{B}\to\mathcal{C}} = \left[[\boldsymbol{b}_1]_{\mathcal{C}}, [\boldsymbol{b}_2]_{\mathcal{C}}, \ldots, [\boldsymbol{b}_n]_{\mathcal{C}}\right]. \tag{D.2}$$

For a diagonalisable matrix $\boldsymbol{M}$ in basis $\mathcal{A} = \{|g\rangle, |e\rangle, |f\rangle\}$ ($\mathcal{A}$ for atom), we have

$$\boldsymbol{D} = \boldsymbol{S}^{-1}\boldsymbol{M}\boldsymbol{S}, \tag{D.3}$$

with diagonal matrix

$$\boldsymbol{D} = \operatorname{diag}\left[\lambda_1, \lambda_2, \lambda_3\right], \tag{D.4}$$

and

$$\boldsymbol{S} = [\boldsymbol{v}_1, \boldsymbol{v}_2, \boldsymbol{v}_3] \tag{D.5}$$

for eigenvalues λ_i and eigenvectors $\boldsymbol{v}_i$. We can define a basis of eigenvectors $\mathcal{V} = \{\boldsymbol{v}_1, \boldsymbol{v}_2, \boldsymbol{v}_3\}$ such that we can rewrite the $\boldsymbol{S}$ matrix as

$$\boldsymbol{S} = \left[[\boldsymbol{v}_1]_{\mathcal{A}}, [\boldsymbol{v}_2]_{\mathcal{A}}, [\boldsymbol{v}_3]_{\mathcal{A}}\right] = \boldsymbol{P}_{\mathcal{V}\to\mathcal{A}}. \tag{D.6}$$

We can then find, for a vector $\boldsymbol{x}$,

$$[\boldsymbol{x}]_{\mathcal{A}} = \boldsymbol{S}\,[\boldsymbol{x}]_{\mathcal{V}}, \tag{D.7}$$

or, in the other direction,

$$[\boldsymbol{x}]_{\mathcal{V}} = \boldsymbol{S}^{-1}\,[\boldsymbol{x}]_{\mathcal{A}}. \tag{D.8}$$

D.2 Eigenvalues and Eigenstates

Expanding the atomic lowering operator, Eq. (7.6), as,

$$\Sigma_- = |g\rangle\langle e| + \xi\,|e\rangle\langle f| = \sigma_-^{eg} + \xi\sigma_-^{fe}, \tag{D.9}$$

we can then expand the master equation, Eq. (7.7), in terms of each dipole operator,

$$\begin{aligned}\frac{\mathrm{d}\rho}{\mathrm{d}t} = \frac{1}{i\hbar}[H_A,\rho] &+ \frac{\Gamma}{2}\left(2\sigma_-^{eg}\rho\sigma_+^{eg} - \sigma_+^{eg}\sigma_-^{eg}\rho - \rho\sigma_+^{eg}\sigma_-^{ge}\right)\\ &+ \frac{\xi^2\Gamma}{2}\left(2\sigma_-^{fe}\rho\sigma_+^{fe} - \sigma_+^{fe}\sigma_-^{fe}\rho - \rho\sigma_+^{fe}\sigma_-^{fe}\right)\\ &+ \Gamma\xi\left(\sigma_-^{eg}\rho\sigma_+^{fe} + \sigma_-^{fe}\rho\sigma_{eg}\right).\end{aligned} \tag{D.10}$$

If we write the atomic states as basis vectors:

$$|g\rangle \longrightarrow \begin{pmatrix}1\\0\\0\end{pmatrix}, \quad |e\rangle \longrightarrow \begin{pmatrix}0\\1\\0\end{pmatrix}, \quad |f\rangle \longrightarrow \begin{pmatrix}0\\0\\1\end{pmatrix}, \tag{D.11}$$

we can then write the Hamiltonian in matrix form:

$$H_A \longrightarrow \begin{pmatrix}0 & \frac{\Omega}{2} & 0\\ \frac{\Omega}{2} & -\left(\frac{\alpha}{2}+\delta\right) & \xi\frac{\Omega}{2}\\ 0 & \xi\frac{\Omega}{2} & -2\delta\end{pmatrix}. \tag{D.12}$$

D.2.1 Characteristic polynomial

To find the eigenvectors and eigenvalues (dressed states and frequencies), we must first solve the characteristic polynomial of the Hamiltonian in matrix form, Eq. (8):

$$\lambda^3 + \left(\frac{\alpha}{2}+3\delta\right)\lambda^2 + \left[\delta\left(2\delta+\alpha\right) - \left(1+\xi^2\right)\left(\frac{\Omega}{2}\right)^2\right]\lambda - 2\delta\left(\frac{\Omega}{2}\right)^2 = 0. \tag{D.13}$$

Solving this cubic equation, we can get the dressed states and dressed frequencies, which we generalise as

$$H_A\,|m\rangle = \hbar\omega_m\,|m\rangle, \quad H_A\,|u\rangle = \hbar\omega_u\,|u\rangle, \quad H_A\,|l\rangle = \hbar\omega_l\,|l\rangle, \tag{D.14}$$

where $|m\rangle, |u\rangle$, and $|l\rangle$ represent the dressed "middle", "upper", and "lower" states, respectively. As H_A is a diagonalisable matrix, we can write

$$\boldsymbol{D} = \boldsymbol{S}^{-1}H_A\boldsymbol{S}, \tag{D.15}$$

where

$$\boldsymbol{S} = \left(|m\rangle, |u\rangle, |l\rangle\right)^T \tag{D.16}$$

gives the dressed states in the bare state basis, and

$$\boldsymbol{S}^{-1} = \left(|g\rangle, |e\rangle, |f\rangle\right)^T \tag{D.17}$$

gives the bare states in the dressed state basis. This allows us to write

$$|g\rangle \longrightarrow \begin{pmatrix} g_m \\ g_u \\ g_l \end{pmatrix}, \quad |e\rangle \longrightarrow \begin{pmatrix} e_m \\ e_u \\ e_l \end{pmatrix}, \quad |f\rangle \longrightarrow \begin{pmatrix} f_m \\ f_u \\ f_l \end{pmatrix}. \tag{D.18}$$

D.2.2 Atomic operators

From these we can write the atomic operators in the dressed state basis:

$$|g\rangle\langle e| \longrightarrow \begin{pmatrix} g_m e_m & g_m e_u & g_m e_l \\ g_u e_m & g_u e_u & g_u e_l \\ g_l e_m & g_l e_u & g_l e_l \end{pmatrix}, \quad |e\rangle\langle f| \longrightarrow \begin{pmatrix} e_m f_m & e_m f_u & e_m f_l \\ e_u f_m & e_u f_u & e_u f_l \\ e_l f_m & e_l f_u & e_l f_l \end{pmatrix}, \tag{D.19}$$

and then

$$\begin{aligned} \Sigma_- = |g\rangle\langle e| + \xi\,|e\rangle\langle f| &\longrightarrow \begin{pmatrix} e_m\left(g_m + \xi f_m\right) & g_m e_u + \xi e_m f_u & g_m e_l + \xi e_m f_m \\ g_u e_m + \xi e_u f_m & e_u\left(g_u + \xi f_u\right) & g_u e_l + \xi e_u f_l \\ g_l e_m + \xi e_l f_m & g_l e_u + \xi e_l f_u & e_l\left(g_l + \xi f_l\right) \end{pmatrix} \\ &\longrightarrow \begin{pmatrix} |m\rangle \\ |u\rangle \\ |l\rangle \end{pmatrix} \begin{pmatrix} a_1 & a_2 & a_3 \\ a_4 & a_5 & a_6 \\ a_7 & a_8 & a_9 \end{pmatrix} \left(\langle m|, \langle u|, \langle l|\right) \end{aligned} \tag{D.20}$$

We can then transform into an interaction picture with unitary evolution operator

$$\mathcal{U}(t) = e^{\frac{1}{i\hbar}H_A t}, \tag{D.21}$$

and the following commutation relations:

$$[H_A, |m\rangle\langle m|] = 0, \quad [H_A, |m\rangle\langle u|] = \hbar\left(\omega_m - \omega_u\right)|m\rangle\langle u|, \quad [H_A, |m\rangle\langle l|] = \hbar\left(\omega_m - \omega_l\right)|m\rangle\langle l|, \tag{D.22a}$$

$$[H_A, |u\rangle\langle m|] = -\hbar\left(\omega_m - \omega_u\right)|u\rangle\langle m|, \quad [H_A, |u\rangle\langle u|] = 0, \quad [H_A, |u\rangle\langle l|] = \hbar\left(\omega_u - \omega_l\right)|u\rangle\langle l|, \tag{D.22b}$$

$$[H_A, |l\rangle\langle m|] = -\hbar\left(\omega_m - \omega_l\right)|l\rangle\langle m|, \quad [H_A, |l\rangle\langle u|] = -\hbar\left(\omega_u - \omega_l\right)|l\rangle\langle u|, \quad [H_A, |l\rangle\langle l|] = 0. \tag{D.22c}$$

The bare atomic operators then transform as

$$\tilde{\Sigma}_-(t) \longrightarrow \begin{pmatrix} a_1 & a_2 e^{i(\omega_m - \omega_u)t} & a_3 e^{i(\omega_m - \omega_l)t} \\ a_4 e^{-i(\omega_m - \omega_u)t} & a_5 & a_6 e^{i(\omega_u - \omega_l)t} \\ a_7 e^{-i(\omega_m - \omega_l)t} & a_8 e^{-i(\omega_u - \omega_l)t} & a_9 \end{pmatrix}, \tag{D.23a}$$

$$\tilde{\Sigma}_+(t) \longrightarrow \begin{pmatrix} a_1 & a_4 e^{i(\omega_m-\omega_u)t} & a_7 e^{i(\omega_m-\omega_l)t} \\ a_2 e^{-i(\omega_m-\omega_u)t} & a_5 & a_8 e^{i(\omega_u-\omega_l)t} \\ a_3 e^{-i(\omega_m-\omega_l)t} & a_6 e^{-i(\omega_u-\omega_l)t} & a_9 \end{pmatrix}. \tag{D.23b}$$

Transforming the master equation into the interaction picture,

$$\frac{\mathrm{d}\tilde{\rho}}{\mathrm{d}t} = \frac{\Gamma}{2}\left(2\tilde{\Sigma}_-\tilde{\rho}\tilde{\Sigma}_+ - \tilde{\Sigma}_+\tilde{\Sigma}_-\tilde{\rho} - \tilde{\rho}\tilde{\Sigma}_+\tilde{\Sigma}_-\right), \tag{D.24}$$

with

$$\rho = \mathcal{U}(t)\tilde{\rho}\,\mathcal{U}^\dagger(t), \tag{D.25}$$

we may drop any fast oscillating terms to find that the three components of this transformed master equation are:

$$\tilde{\Sigma}_+\tilde{\Sigma}_-(t) \longrightarrow \begin{pmatrix} a_1^2+a_4^2+a_7^2 & 0 & 0 \\ 0 & a_2^2+a_5^2+a_8^2 & 0 \\ 0 & 0 & a_3^2+a_6^2+a_9^2 \end{pmatrix}, \tag{D.26}$$

and

$$\begin{aligned}\tilde{\Sigma}_-\tilde{\rho}\tilde{\Sigma}_+ = {} & a_1^2\sigma_{mm}\tilde{\rho}\sigma_{mm} + a_5^2\sigma_{uu}\tilde{\rho}\sigma_{uu} + a_9^2\sigma_{ll}\tilde{\rho}\sigma_{ll} + a_2^2\sigma_{mu}\tilde{\rho}\sigma_{um} \\ & + a_3^2\sigma_{ml}\tilde{\rho}\sigma_{lm} + a_4^2\sigma_{um}\tilde{\rho}\sigma_{mu} + a_7^2\sigma_{lm}\tilde{\rho}\sigma_{ml} \\ & + a_6^2\sigma_{ul}\tilde{\rho}\sigma_{lu} + a_8^2\sigma_{lu}\tilde{\rho}\sigma_{ul} + a_1a_5\Big(\sigma_{mm}\tilde{\rho}\sigma_{uu} + \sigma_{uu}\tilde{\rho}\sigma_{mm}\Big) \\ & + a_1a_9\Big(\sigma_{mm}\tilde{\rho}\sigma_{ll} + \sigma_{ll}\tilde{\rho}\sigma_{mm}\Big) + a_5a_9\Big(\sigma_{uu}\tilde{\rho}\sigma_{ll} + \sigma_{ll}\tilde{\rho}\sigma_{uu}\Big).\end{aligned} \tag{D.27}$$

Putting all of the pieces together, and transforming back out of the interaction picture, we have

$$\begin{aligned}\frac{\mathrm{d}\rho}{\mathrm{d}t} = {} & -i[\omega_m\sigma_{mm} + \omega_u\sigma_{uu} + \omega_l\sigma_{ll}, \rho] \\ & + \frac{\Gamma a_1^2}{2}\Big(2\sigma_{mm}\rho\sigma_{mm} - \sigma_{mm}\rho - \rho\sigma_{mm}\Big) + \frac{\Gamma a_5^2}{2}\Big(2\sigma_{uu}\rho\sigma_{uu} - \sigma_{uu}\rho - \rho\sigma_{uu}\Big) \\ & + \frac{\Gamma a_9^2}{2}\Big(2\sigma_{dd}\rho\sigma_{dd} - \sigma_{dd}\rho - \rho\sigma_{dd}\Big) + \Gamma a_1a_5\Big(\sigma_{mm}\rho\sigma_{uu} + \sigma_{uu}\rho\sigma_{dd}\Big) \\ & + \Gamma a_1a_9\Big(\sigma_{mm}\rho\sigma_{ll} + \sigma_{ll}\rho\sigma_{mm}\Big) + \Gamma a_5a_9\Big(\sigma_{uu}\rho\sigma_{ll} + \sigma_{ll}\rho\sigma_{uu}\Big) \\ & + \frac{\Gamma a_2^2}{2}\Big(2\sigma_{mu}\rho\sigma_{um} - \sigma_{uu}\rho - \rho\sigma_{uu}\Big) + \frac{\Gamma a_4^2}{2}\Big(2\sigma_{um}\rho\sigma_{mu} - \sigma_{mm}\rho - \rho\sigma_{mm}\Big) \\ & + \frac{\Gamma a_3^2}{2}\Big(2\sigma_{ml}\rho\sigma_{lm} - \sigma_{ll}\rho - \rho\sigma_{ll}\Big) + \frac{\Gamma a_7^2}{2}\Big(2\sigma_{lm}\rho\sigma_{ml} - \sigma_{mm}\rho - \rho\sigma_{mm}\Big) \\ & + \frac{\Gamma a_6^2}{2}\Big(2\sigma_{ul}\rho\sigma_{lu} - \sigma_{ll}\rho - \rho\sigma_{ll}\Big) + \frac{\Gamma a_8^2}{2}\Big(\sigma_{lu}\rho\sigma_{ul} - \sigma_{uu}\rho - \rho\sigma_{uu}\Big).\end{aligned} \tag{D.28}$$

D.2.3 Dressed state operator moment equations

Expanding the reduced density operator into the dressed states, we find the matrix elements of the density operator evolve as:

$$\dot{\rho}_{mm} = -\Gamma\left(a_4^2 + a_7^2\right)\rho_{mm} + \Gamma a_2^2\rho_{uu} + \Gamma a_3^2\rho_{ll}, \tag{D.29a}$$

$$\dot{\rho}_{mu} = -\left[\frac{\Gamma}{2}\left(a_1^2 + a_2^2 + a_4^2 + a_5^2 + a_7^2 + a_8^2 - 2a_1a_5\right) + i\left(\omega_m - \omega_u\right)\right]\rho_{mu}, \tag{D.29b}$$

$$\dot{\rho}_{ml} = -\left[\frac{\Gamma}{2}\left(a_1^2 + a_3^2 + a_4^2 + a_6^2 + a_7^2 + a_9^2 - 2a_1a_9\right) + i\left(\omega_m - \omega_l\right)\right]\rho_{ml}, \tag{D.29c}$$

$$\dot{\rho}_{um} = -\left[\frac{\Gamma}{2}\left(a_1^2 + a_2^2 + a_4^2 + a_5^2 + a_7^2 + a_8^2 - 2a_1a_5\right) - i\left(\omega_m - \omega_u\right)\right]\rho_{um}, \tag{D.29d}$$

$$\dot{\rho}_{uu} = -\Gamma\left(a_2^2 + a_8^2\right)\rho_{uu} + \Gamma a_4^2\rho_{mm} + \Gamma a_6^2\rho_{ll}, \tag{D.29e}$$

$$\dot{\rho}_{ul} = -\left[\frac{\Gamma}{2}\left(a_2^2 + a_3^2 + a_5^2 + a_6^2 + a_8^2 + a_9^2 - 2a_5a_9\right) + i\left(\omega_u - \omega_l\right)\right]\rho_{ul}, \tag{D.29f}$$

$$\dot{\rho}_{lm} = -\left[\frac{\Gamma}{2}\left(a_1^2 + a_3^2 + a_4^2 + a_6^2 + a_7^2 + a_9^2 - 2a_1a_9\right) - i\left(\omega_m - \omega_l\right)\right]\rho_{lm}, \tag{D.29g}$$

$$\dot{\rho}_{lu} = -\left[\frac{\Gamma}{2}\left(a_2^2 + a_3^2 + a_5^2 + a_6^2 + a_8^2 + a_9^2 - 2a_5a_9\right) - i\left(\omega_u - \omega_l\right)\right]\rho_{lu}, \tag{D.29h}$$

$$\dot{\rho}_{ll} = -\Gamma\left(a_3^2 + a_6^2\right)\rho_{ll} + \Gamma a_7^2\rho_{mm} + \Gamma a_8^2\rho_{uu}. \tag{D.29i}$$

All of the off-diagonal terms are completely uncoupled. For easy implementation with the quantum regression equations, we write the density operator components as operator averages and rewrite the above equations as:

$$\frac{\mathrm{d}}{\mathrm{d}t}\begin{pmatrix}\langle\sigma_{mm}\rangle\\ \langle\sigma_{uu}\rangle\\ \langle\sigma_{ll}\rangle\end{pmatrix} = \begin{pmatrix}-\Gamma\left(a_4^2 + a_7^2\right) & \Gamma a_2^2 & \Gamma a_3^2\\ \Gamma a_4^2 & -\Gamma\left(a_2^2 + a_8^2\right) & \Gamma a_6^2\\ \Gamma a_7^2 & \Gamma a_8^2 & -\Gamma\left(a_3^2 + a_6^2\right)\end{pmatrix}\begin{pmatrix}\langle\sigma_{mm}\rangle\\ \langle\sigma_{uu}\rangle\\ \langle\sigma_{ll}\rangle\end{pmatrix}, \tag{D.30}$$

and, with $\sigma_-^{um} = |m\rangle\langle u|, \sigma_-^{ml} = |l\rangle\langle m|, \sigma_-^{ul} = |l\rangle\langle u|$,

$$\frac{\mathrm{d}}{\mathrm{d}t}\langle\sigma_-^{um}\rangle = -\left[\frac{\Gamma_{um}}{2} + i\left(\omega_u - \omega_0\right)\right]\langle\sigma_-^{um}\rangle, \tag{D.31a}$$

$$\frac{\mathrm{d}}{\mathrm{d}t}\langle\sigma_+^{um}\rangle = -\left[\frac{\Gamma_{um}}{2} - i\left(\omega_u - \omega_0\right)\right]\langle\sigma_+^{um}\rangle, \tag{D.31b}$$

$$\frac{\mathrm{d}}{\mathrm{d}t}\langle\sigma_-^{ml}\rangle = -\left[\frac{\Gamma_{ml}}{2} + i\left(\omega_0 - \omega_l\right)\right]\langle\sigma_-^{ml}\rangle, \tag{D.31c}$$

$$\frac{\mathrm{d}}{\mathrm{d}t}\langle\sigma_+^{ml}\rangle = -\left[\frac{\Gamma_{ml}}{2} - i\left(\omega_0 - \omega_l\right)\right]\langle\sigma_+^{ml}\rangle, \tag{D.31d}$$

$$\frac{\mathrm{d}}{\mathrm{d}t}\langle\sigma_-^{ul}\rangle = -\left[\frac{\Gamma_{ul}}{2} + i\left(\omega_u - \omega_l\right)\right]\langle\sigma_-^{ul}\rangle, \tag{D.31e}$$

$$\frac{\mathrm{d}}{\mathrm{d}t}\langle\sigma_+^{ul}\rangle = -\left[\frac{\Gamma_{ul}}{2} - i\left(\omega_u - \omega_l\right)\right]\langle\sigma_-^{ul}\rangle, \tag{D.31f}$$

where

$$\Gamma_{um} = \Gamma\left(a_1^2 + a_2^2 + a_4^2 + a_5^2 + a_7^2 + a_8^2 - a_1 a_5\right), \tag{D.32a}$$
$$\Gamma_{ml} = \Gamma\left(a_1^2 + a_3^2 + a_4^2 + a_6^2 + a_7^2 + a_9^2 - a_1 a_9\right), \tag{D.32b}$$
$$\Gamma_{ul} = \Gamma\left(a_2^2 + a_3^2 + a_5^2 + a_6^2 + a_8^2 + a_9^2 - a_5 a_9\right). \tag{D.32c}$$

For the coupled set of equations, we can use reduce the number of equations with

$$\rho_{mm} + \rho_{uu} + \rho_{ll} = 1 \Longrightarrow \rho_{ll} = 1 - \rho_{mm} - \rho_{uu}, \tag{D.33}$$

and hence

$$\frac{\mathrm{d}}{\mathrm{d}t}\begin{pmatrix}\langle\sigma_{mm}\rangle\\ \langle\sigma_{uu}\rangle\end{pmatrix} = \begin{pmatrix}-\Gamma z_1 & \Gamma z_2\\ \Gamma z_3 & -\Gamma z_4\end{pmatrix}\begin{pmatrix}\langle\sigma_{mm}\rangle\\ \langle\sigma_{uu}\rangle\end{pmatrix} + \begin{pmatrix}\Gamma a_3^2\\ \Gamma a_6^2\end{pmatrix}, \tag{D.34}$$

with

$$z_1 = a_4^2 + a_3^2 + a_7^2, \tag{D.35a}$$
$$z_2 = a_2^2 - a_3^2, \tag{D.35b}$$
$$z_3 = a_4^2 - a_6^2, \tag{D.35c}$$
$$z_4 = a_2^2 + a_6^2 + a_8^2. \tag{D.35d}$$

D.2.4 Solving the moment equations

The dressed state raising and lowering operator equations have simple solutions due to their uncoupled nature:

$$\langle\sigma_-^{um}(t)\rangle = \langle\sigma_-^{um}(0)\rangle e^{-\left[\frac{\Gamma_{um}}{2} + i\omega_{um}\right]t}, \tag{D.36a}$$
$$\langle\sigma_+^{um}(t)\rangle = \langle\sigma_+^{um}(0)\rangle e^{-\left[\frac{\Gamma_{um}}{2} - i\omega_{um}\right]t}, \tag{D.36b}$$
$$\langle\sigma_-^{ml}(t)\rangle = \langle\sigma_-^{ml}(0)\rangle e^{-\left[\frac{\Gamma_{ml}}{2} + i\omega_{ml}\right]t}, \tag{D.36c}$$
$$\langle\sigma_+^{ml}(t)\rangle = \langle\sigma_+^{ml}(0)\rangle e^{-\left[\frac{\Gamma_{ml}}{2} - i\omega_{ml}\right]t}, \tag{D.36d}$$
$$\langle\sigma_-^{ul}(t)\rangle = \langle\sigma_-^{ul}(0)\rangle e^{-\left[\frac{\Gamma_{ul}}{2} + i\omega_{ul}\right]t}, \tag{D.36e}$$
$$\langle\sigma_+^{ul}(t)\rangle = \langle\sigma_+^{ul}(0)\rangle e^{-\left[\frac{\Gamma_{ul}}{2} - i\omega_{ul}\right]t}. \tag{D.36f}$$

The diagonal moments have solutions

$$\begin{pmatrix}\langle\sigma_{mm}(t)\rangle\\ \langle\sigma_{uu}(t)\rangle\end{pmatrix} = \frac{C_1 e^{\lambda_+ t}}{z_1 - \lambda_+}\begin{pmatrix}-z_2\\ z_1 - \lambda_+\end{pmatrix} + \frac{C_2 e^{\lambda_- t}}{z_1 - \lambda_-}\begin{pmatrix}-z_2\\ z_1 - \lambda_-\end{pmatrix}, \tag{D.37}$$

where

$$\lambda_\pm = -\frac{\Gamma}{2}(z_1 + z_4) \pm \frac{\Gamma}{2}\sqrt{z_1^2 + z_4^2 - 2(z_1 z_4 + z_2 z_3)}. \tag{D.38}$$

E Moment Equations of the Three-Level Atom and Single Filter Cascaded System

Here we present all of the operator moment equations needed to calculate first- and second-order correlation functions for the multi-mode array filtered three-level atom. We first show the moment equations, as derived from Eq. (7.31). These are then followed by the coupled equations for both the filtered first- and second-order correlation functions.

The `Fortan90` code used to numerically calculate these equations can be found at the following Github repository: github.com/jnga773/multi-mode-filter.

E.1 Moment Equations

We write these coupled moment equations in matrix form, where we use the notation

$$\langle \boldsymbol{\Sigma} \rangle = \begin{pmatrix} \langle \sigma^{gg} \rangle \\ \langle \sigma^{eg}_{-} \rangle \\ \langle \sigma^{eg}_{+} \rangle \\ \langle \sigma^{ee} \rangle \\ \langle \sigma^{fe}_{-} \rangle \\ \langle \sigma^{fe}_{+} \rangle \\ \langle \sigma^{fg}_{-} \rangle \\ \langle \sigma^{fg}_{+} \rangle \end{pmatrix}, \quad \langle X\boldsymbol{\Sigma} \rangle = \begin{pmatrix} \langle X\sigma^{gg} \rangle \\ \langle X\sigma^{eg}_{-} \rangle \\ \langle X\sigma^{eg}_{+} \rangle \\ \langle X\sigma^{ee} \rangle \\ \langle X\sigma^{fe}_{-} \rangle \\ \langle X\sigma^{fe}_{+} \rangle \\ \langle X\sigma^{fg}_{-} \rangle \\ \langle X\sigma^{fg}_{+} \rangle \end{pmatrix}. \tag{E.1}$$

E.1.1 Atomic Operator Moments

$$\frac{\mathrm{d}}{\mathrm{d}t}\langle \boldsymbol{\Sigma} \rangle = \boldsymbol{M}\langle \boldsymbol{\Sigma} \rangle + \begin{pmatrix} 0 \\ 0 \\ 0 \\ \Gamma\xi^{2} \\ i\xi\frac{\Omega}{2} \\ -i\xi\frac{\Omega}{2} \\ 0 \\ 0 \end{pmatrix}, \tag{E.2}$$

where

$$\boldsymbol{M}^{(\Sigma)} = \begin{pmatrix} 0 & -i\frac{\Omega}{2} & i\frac{\Omega}{2} & \Gamma & 0 & 0 & 0 & 0 \\ -i\frac{\Omega}{2} & -\left[\frac{\Gamma}{2}-i\left(\frac{\alpha}{2}+\delta\right)\right] & 0 & i\frac{\Omega}{2} & \Gamma\xi & 0 & -i\xi\frac{\Omega}{2} & 0 \\ i\frac{\Omega}{2} & 0 & -\left[\frac{\Gamma}{2}+i\left(\frac{\alpha}{2}+\delta\right)\right] & -i\frac{\Omega}{2} & 0 & \Gamma\xi & 0 & i\xi\frac{\Omega}{2} \\ -\Gamma\xi^{2} & i\frac{\Omega}{2} & -i\frac{\Omega}{2} & -\Gamma\left(1+\xi^{2}\right) & -i\xi\frac{\Omega}{2} & i\xi\frac{\Omega}{2} & 0 & 0 \\ -i\xi\frac{\Omega}{2} & 0 & 0 & -i\xi\Omega & -\left[\frac{\Gamma}{2}\left(1+\xi^{2}\right)+i\left(\frac{\alpha}{2}-\delta\right)\right] & 0 & i\frac{\Omega}{2} & 0 \\ i\xi\frac{\Omega}{2} & 0 & 0 & i\xi\Omega & 0 & -\left[\frac{\Gamma}{2}\left(1+\xi^{2}\right)-i\left(\frac{\alpha}{2}-\delta\right)\right] & 0 & -i\frac{\Omega}{2} \\ 0 & -i\xi\frac{\Omega}{2} & 0 & 0 & i\frac{\Omega}{2} & 0 & -\left[\frac{\Gamma}{2}\xi^{2}-2i\delta\right] & 0 \\ 0 & 0 & i\xi\frac{\Omega}{2} & 0 & 0 & -i\frac{\Omega}{2} & 0 & -\left[\frac{\Gamma}{2}\xi^{2}+2i\delta\right] \end{pmatrix}. \tag{E.3}$$

E.1.2 First-order: Filter

$$\frac{\mathrm{d}}{\mathrm{d}t}\langle a_j\rangle = -\left(\kappa + i\Delta\omega_j\right)\langle a_j\rangle - \mathcal{E}_j\left(\langle\sigma_-^{eg}\rangle + \xi\langle\sigma_-^{fe}\rangle\right), \tag{E.4a}$$

$$\frac{\mathrm{d}}{\mathrm{d}t}\langle a_j^\dagger\rangle = -\left(\kappa - i\Delta\omega_j\right)\langle a_j^\dagger\rangle - \mathcal{E}_j{}^*\left(\langle\sigma_+^{eg}\rangle + \xi\langle\sigma_+^{fe}\rangle\right). \tag{E.4b}$$

E.1.3 First-order: Filter / Atom

$$\frac{\mathrm{d}}{\mathrm{d}t}\langle a_j\boldsymbol{\Sigma}\rangle = \boldsymbol{M}_j^{(a)}\langle a_j\boldsymbol{\Sigma}\rangle + \begin{pmatrix} -\mathcal{E}_j\langle\sigma_-^{eg}\rangle \\ -\mathcal{E}_j\xi\langle\sigma_-^{fg}\rangle \\ -\mathcal{E}_j\langle\sigma^{ee}\rangle \\ \Gamma\xi^2\langle a_j\rangle - \mathcal{E}_j\xi\langle\sigma_-^{fe}\rangle \\ i\xi\frac{\Omega}{2}\langle a_j\rangle \\ -i\xi\frac{\Omega}{2}\langle a_j\rangle - \mathcal{E}_j\xi(1-\langle\sigma^{gg}\rangle-\langle\sigma^{ee}\rangle) \\ 0 \\ -\mathcal{E}_j\langle\sigma_+^{fe}\rangle \end{pmatrix}, \tag{E.5a}$$

$$\frac{\mathrm{d}}{\mathrm{d}t}\langle a_j^\dagger\boldsymbol{\Sigma}\rangle = \boldsymbol{M}_j^{(a^\dagger)}\langle a_j\boldsymbol{\Sigma}\rangle + \begin{pmatrix} -\mathcal{E}_j{}^*\langle\sigma_+^{eg}\rangle \\ -\mathcal{E}_j{}^*\langle\sigma^{ee}\rangle \\ -\mathcal{E}_j{}^*\xi\langle\sigma_+^{fg}\rangle \\ \Gamma\xi^2\langle a_j^\dagger\rangle - \mathcal{E}_j{}^*\xi\langle\sigma_+^{fe}\rangle \\ i\xi\frac{\Omega}{2}\langle a_j^\dagger\rangle - \mathcal{E}_j{}^*\xi(1-\langle\sigma^{gg}\rangle-\langle\sigma^{ee}\rangle) \\ -i\xi\frac{\Omega}{2}\langle a_j^\dagger\rangle \\ -\mathcal{E}_j{}^*\langle\sigma_-^{fe}\rangle \\ 0 \end{pmatrix}, \tag{E.5b}$$

with

$$\boldsymbol{M}_j^{(a)} = \boldsymbol{M}^{(\Sigma)} - \left(\kappa + i\Delta\omega_j\right)\mathbb{1}, \tag{E.6a}$$

$$\boldsymbol{M}_j^{(a^\dagger)} = \boldsymbol{M}^{(\Sigma)} - \left(\kappa - i\Delta\omega_j\right)\mathbb{1}. \tag{E.6b}$$

E.1.4 Second-order: Filter

$$\begin{aligned}\frac{\mathrm{d}}{\mathrm{d}t}\langle a_j a_k\rangle = &-\left[2\kappa + i\left(\Delta\omega_j + \Delta\omega_k\right)\right]\langle a_j a_k\rangle \\ &- \mathcal{E}_j\left(\langle a_k\sigma_-^{eg}\rangle + \xi\langle a_k\sigma_-^{fe}\rangle\right) - \mathcal{E}_k\left(\langle a_j\sigma_-^{eg}\rangle + \xi\langle a_j\sigma_-^{fe}\rangle\right),\end{aligned} \tag{E.7a}$$

$$\begin{aligned}\frac{\mathrm{d}}{\mathrm{d}t}\langle a_j^\dagger a_k\rangle = &-\left[2\kappa - i\left(\Delta\omega_j - \Delta\omega_k\right)\right]\langle a_j^\dagger a_k\rangle - \mathcal{E}_j{}^*\langle a_k\sigma_+\rangle \\ &- \mathcal{E}_j{}^*\left(\langle a_k\sigma_+^{eg}\rangle + \xi\langle a_k\sigma_+^{fe}\rangle\right) - \mathcal{E}_k\left(\langle a_j^\dagger\sigma_-^{eg}\rangle + \xi\langle a_j^\dagger\sigma_-^{fe}\rangle\right),\end{aligned} \tag{E.7b}$$

$$\begin{aligned}\frac{\mathrm{d}}{\mathrm{d}t}\langle a_j^\dagger a_k^\dagger\rangle = &-\left[2\kappa - i\left(\Delta\omega_j + \Delta\omega_k\right)\right]\langle a_j^\dagger a_k^\dagger\rangle - \mathcal{E}_j{}^*\langle a_k^\dagger\sigma_+\rangle \\ &- \mathcal{E}_j{}^*\left(\langle a_k^\dagger\sigma_+^{eg}\rangle + \langle a_k^\dagger\sigma_+^{fe}\rangle\right) - \mathcal{E}_k{}^*\left(\langle a_j^\dagger\sigma_+^{eg}\rangle + \langle a_j^\dagger\sigma_+^{fe}\rangle\right).\end{aligned} \tag{E.7c}$$

E.1.5 Second-order: Filter / Atom

$$\frac{\mathrm{d}}{\mathrm{d}t}\langle a_j a_k \boldsymbol{\Sigma}\rangle = \boldsymbol{M}_{jk}^{(a^2)}\langle a_j a_k \boldsymbol{\Sigma}\rangle + \begin{pmatrix} -\mathcal{E}_j\langle a_k\sigma_-^{eg}\rangle - \mathcal{E}_k\langle a_j\sigma_-^{eg}\rangle \\ -\mathcal{E}_j\xi\langle a_k\sigma_-^{fg}\rangle - \mathcal{E}_k\xi\langle a_j\sigma_-^{fg}\rangle \\ -\mathcal{E}_j\langle a_k\sigma^{ee}\rangle - \mathcal{E}_k\langle a_j\sigma^{ee}\rangle \\ \Gamma\xi\langle a_j a_k\rangle - \mathcal{E}_j\xi\langle a_k\sigma_-^{fe}\rangle - \mathcal{E}_k\xi\langle a_j\sigma_-^{fe}\rangle \\ i\xi\frac{\Omega}{2}\langle a_j a_k\rangle \\ -i\xi\frac{\Omega}{2}\langle a_j a_k\rangle - \mathcal{E}_j\xi(\langle a_k\rangle - \langle a_k\sigma^{gg}\rangle - \langle a_k\sigma^{ee}\rangle) - \mathcal{E}_k\xi(\langle a_j\rangle - \langle a_j\sigma^{gg}\rangle - \langle a_j\sigma^{ee}\rangle) \\ 0 \\ -\mathcal{E}_j\langle a_k\sigma_+^{fe}\rangle - \mathcal{E}_k\langle a_j\sigma_+^{fe}\rangle \end{pmatrix}, \tag{E.8a}$$

$$\frac{\mathrm{d}}{\mathrm{d}t}\langle a_j^\dagger a_k \boldsymbol{\Sigma}\rangle = \boldsymbol{M}_{jk}^{(a^\dagger a)}\langle a_j^\dagger a_k \boldsymbol{\Sigma}\rangle + \begin{pmatrix} -\mathcal{E}_j{}^*\langle a_k\sigma_+^{eg}\rangle - \mathcal{E}_k\langle a_j^\dagger\sigma_-^{eg}\rangle \\ -\mathcal{E}_j{}^*\langle a_k\sigma^{ee}\rangle - \mathcal{E}_k\xi\langle a_j^\dagger\sigma_-^{fg}\rangle \\ -\mathcal{E}_j{}^*\xi\langle a_k\sigma_+^{fg}\rangle - \mathcal{E}_k\langle a_j^\dagger\sigma^{ee}\rangle \\ \Gamma\xi^2\langle a_j^\dagger a_k\rangle - \mathcal{E}_j{}^*\xi\langle a_k\sigma_+^{fe}\rangle - \mathcal{E}_k\xi\langle a_k^\dagger\sigma_-^{fe}\rangle \\ i\xi\frac{\Omega}{2}\langle a_j^\dagger a_k\rangle - \mathcal{E}_j{}^*\xi(\langle a_k\rangle - \langle a_k\sigma^{gg}\rangle - \langle a_k\sigma^{ee}\rangle) \\ -i\xi\frac{\Omega}{2}\langle a_j^\dagger a_k\rangle - \mathcal{E}_k\xi\Big(\langle a_j^\dagger\rangle - \langle a_j^\dagger\sigma^{gg}\rangle - \langle a_j^\dagger\sigma^{ee}\rangle\Big) \\ -\mathcal{E}_j{}^*\langle a_k\sigma_-^{fe}\rangle \\ -\mathcal{E}_k\langle a_j^\dagger\sigma_+^{fe}\rangle \end{pmatrix}, \tag{E.8b}$$

$$\frac{\mathrm{d}}{\mathrm{d}t}\langle a_j^\dagger a_k^\dagger \boldsymbol{\Sigma}\rangle = \boldsymbol{M}_{jk}^{(a^{\dagger 2})}\langle a_j^\dagger a_k^\dagger \boldsymbol{\Sigma}\rangle + \begin{pmatrix} -\mathcal{E}_j{}^*\langle a_k^\dagger\sigma_+^{eg}\rangle - \mathcal{E}_k{}^*\langle a_j^\dagger\sigma_+^{eg}\rangle \\ -\mathcal{E}_j{}^*\langle a_k^\dagger\sigma^{ee}\rangle - \mathcal{E}_k{}^*\langle a_j^\dagger\sigma^{ee}\rangle \\ -\mathcal{E}_j{}^*\xi\langle a_k^\dagger\sigma_+^{fg}\rangle - \mathcal{E}_k{}^*\xi\langle a_j^\dagger\sigma_+^{fg}\rangle \\ \Gamma\xi^2\langle a_j^\dagger a_k^\dagger\rangle - \mathcal{E}_j{}^*\xi\langle a_k^\dagger\sigma_+^{fe}\rangle - \mathcal{E}_k{}^*\xi\langle a_j^\dagger\sigma_+^{fe}\rangle \\ i\xi\frac{\Omega}{2}\langle a_j^\dagger a_k^\dagger\rangle - \mathcal{E}_j{}^*\xi\Big(\langle a_k^\dagger\rangle - \langle a_k^\dagger\sigma^{gg}\rangle - \langle a_k^\dagger\sigma^{ee}\rangle\Big) - \mathcal{E}_k{}^*\xi\Big(\langle a_j^\dagger\rangle - \langle a_j^\dagger\sigma^{gg}\rangle - \langle a_j^\dagger\sigma^{ee}\rangle\Big) \\ -i\xi\frac{\Omega}{2}\langle a_j^\dagger a_k^\dagger\rangle \\ -\mathcal{E}_j{}^*\langle a_k^\dagger\sigma_-^{fe}\rangle - \mathcal{E}_k{}^*\langle a_j^\dagger\sigma_-^{fe}\rangle \\ 0 \end{pmatrix}, \tag{E.8c}$$

with

$$\boldsymbol{M}_{jk}^{(a^2)} = \boldsymbol{M}^{(\Sigma)} - [2\kappa + i\,(\Delta\omega_j + \Delta\omega_k)]\,\mathbb{1}, \tag{E.9a}$$

$$\boldsymbol{M}_{jk}^{(a^\dagger a)} = \boldsymbol{M}^{(\Sigma)} - [2\kappa - i\,(\Delta\omega_j - \Delta\omega_k)]\,\mathbb{1}, \tag{E.9b}$$

$$\boldsymbol{M}_{jk}^{(a^{\dagger 2})} = \boldsymbol{M}^{(\Sigma)} - [2\kappa - i\,(\Delta\omega_j + \Delta\omega_k)]\,\mathbb{1}. \tag{E.9c}$$

E.1.6 Third-order: Filter

$$\begin{aligned}\frac{\mathrm{d}}{\mathrm{d}t}\langle a_j^\dagger a_k a_l\rangle = &-\left[3\kappa - i\left(\Delta\omega_j - \Delta\omega_k - \Delta\omega_l\right)\right]\langle a_j^\dagger a_k a_l\rangle \\ &- {\mathcal{E}_j}^*\left(\langle a_k a_l \sigma_+^{eg}\rangle + \xi\langle a_k a_l \sigma_+^{fe}\rangle\right) \\ &- \mathcal{E}_k\left(\langle a_j^\dagger a_l \sigma_-^{eg}\rangle + \xi\langle a_j^\dagger a_l \sigma_-^{fe}\rangle\right) \\ &- \mathcal{E}_l\left(\langle a_j^\dagger a_k \sigma_-^{eg}\rangle + \xi\langle a_j^\dagger a_k \sigma_-^{fe}\rangle\right), \end{aligned} \tag{E.10a}$$

$$\begin{aligned}\frac{\mathrm{d}}{\mathrm{d}t}\langle a_j^\dagger a_k^\dagger a_l\rangle = &-\left[3\kappa - i\left(\Delta\omega_j + \Delta\omega_k - \Delta\omega_l\right)\right]\langle a_j^\dagger a_k^\dagger a_l\rangle \\ &- {\mathcal{E}_j}^*\left(\langle a_k^\dagger a_l \sigma_+^{eg}\rangle + \xi\langle a_k^\dagger a_l \sigma_+^{fe}\rangle\right) \\ &- {\mathcal{E}_k}^*\left(\langle a_j^\dagger a_l \sigma_+^{eg}\rangle + \xi\langle a_j^\dagger a_l \sigma_+^{fe}\rangle\right) \\ &- \mathcal{E}_l\left(\langle a_j^\dagger a_k^\dagger \sigma_-^{eg}\rangle + \xi\langle a_j^\dagger a_k^\dagger \sigma_-^{fe}\rangle\right). \end{aligned} \tag{E.10b}$$

E.1.7 Third-order: Filter / Atom

$$\begin{aligned}\frac{\mathrm{d}}{\mathrm{d}t}\langle a_j^\dagger a_k a_l \boldsymbol{\Sigma}\rangle &= \boldsymbol{M}_{jkl}^{(a^\dagger a^2)}\langle a_j^\dagger a_k a_l \boldsymbol{\Sigma}\rangle \\ &+ \begin{pmatrix} -{\mathcal{E}_j}^*\langle a_k a_l \sigma_+^{eg}\rangle - \mathcal{E}_k\langle a_j^\dagger a_l \sigma_-^{eg}\rangle - \mathcal{E}_l\langle a_j^\dagger a_k \sigma_-^{eg}\rangle \\ -{\mathcal{E}_j}^*\langle a_k a_l \sigma^{ee}\rangle - \mathcal{E}_k\xi\langle a_j^\dagger a_l \sigma_-^{fg}\rangle - \mathcal{E}_l\xi\langle a_j^\dagger a_k \sigma_-^{fg}\rangle \\ -{\mathcal{E}_j}^*\xi\langle a_k a_l \sigma_+^{fg}\rangle - \mathcal{E}_k\langle a_j^\dagger a_l \sigma^{ee}\rangle - \mathcal{E}_l\langle a_j^\dagger a_k \sigma^{ee}\rangle \\ \Gamma\xi^2\langle a_j^\dagger a_k a_l\rangle - {\mathcal{E}_j}^*\xi\langle a_k a_l \sigma_+^{fe}\rangle - \mathcal{E}_k\xi\langle a_j^\dagger a_l \sigma_-^{fe}\rangle - \mathcal{E}_l\xi\langle a_j^\dagger a_k \sigma_-^{fe}\rangle \\ i\xi\frac{\Omega}{2}\langle a_j^\dagger a_k a_l\rangle - {\mathcal{E}_j}^*\xi(\langle a_k a_l\rangle - \langle a_k a_l \sigma^{gg}\rangle - \langle a_k a_l \sigma^{ee}\rangle) \\ -i\xi\frac{\Omega}{2}\langle a_j^\dagger a_k a_l\rangle - \mathcal{E}_k\xi\Big(\langle a_j^\dagger a_k\rangle - \langle a_j^\dagger a_l \sigma^{gg}\rangle - \langle a_j^\dagger a_l \sigma^{ee}\rangle\Big) - \mathcal{E}_l\xi\Big(\langle a_j^\dagger a_l\rangle - \langle a_j^\dagger a_k \sigma^{gg}\rangle - \langle a_j^\dagger a_k \sigma^{ee}\rangle\Big) \\ -{\mathcal{E}_j}^*\langle a_k a_l \sigma_-^{fe}\rangle \\ -\mathcal{E}_k\langle a_j^\dagger a_l \sigma_+^{fe}\rangle - \mathcal{E}_l\langle a_j^\dagger a_k \sigma_-^{fe}\rangle \end{pmatrix}, \end{aligned} \tag{E.11a}$$

$$\begin{aligned}\frac{\mathrm{d}}{\mathrm{d}t}\langle a_j^\dagger a_k^\dagger a_l \boldsymbol{\Sigma}\rangle &= \boldsymbol{M}_{jkl}^{({a^\dagger}^2 a)}\langle a_j^\dagger a_k^\dagger a_l \boldsymbol{\Sigma}\rangle \\ &+ \begin{pmatrix} -{\mathcal{E}_j}^*\langle a_k^\dagger a_l \sigma_+^{eg}\rangle - {\mathcal{E}_k}^*\langle a_j^\dagger a_l \sigma_+^{eg}\rangle - \mathcal{E}_l\langle a_j^\dagger a_k^\dagger \sigma_-^{eg}\rangle \\ -{\mathcal{E}_j}^*\langle a_k^\dagger a_l \sigma^{ee}\rangle - {\mathcal{E}_k}^*\langle a_j^\dagger a_l \sigma^{ee}\rangle - \mathcal{E}_l\xi\langle a_j^\dagger a_k^\dagger \sigma_-^{fg}\rangle \\ -{\mathcal{E}_j}^*\xi\langle a_k^\dagger a_l \sigma_+^{fg}\rangle - {\mathcal{E}_k}^*\xi\langle a_j^\dagger a_l \sigma_+^{fg}\rangle - \mathcal{E}_l\langle a_j^\dagger a_k^\dagger \sigma^{ee}\rangle \\ \Gamma\xi^2\langle a_j^\dagger a_k^\dagger a_l\rangle - {\mathcal{E}_j}^*\xi\langle a_k^\dagger a_l \sigma_+^{fe}\rangle - {\mathcal{E}_k}^*\xi\langle a_j^\dagger a_l \sigma_+^{fe}\rangle - \mathcal{E}_l\xi\langle a_j^\dagger a_k^\dagger \sigma_-^{fe}\rangle \\ i\xi\frac{\Omega}{2}\langle a_j^\dagger a_k^\dagger a_l\rangle - {\mathcal{E}_j}^*\xi\Big(\langle a_k^\dagger a_l\rangle - \langle a_k^\dagger a_l \sigma^{gg}\rangle - \langle a_k^\dagger a_l \sigma^{ee}\rangle\Big) - {\mathcal{E}_j}^*\xi\Big(\langle a_j^\dagger a_l\rangle - \langle a_j^\dagger a_l \sigma^{gg}\rangle - \langle a_j^\dagger a_l \sigma^{ee}\rangle\Big) \\ -i\xi\frac{\Omega}{2}\langle a_j^\dagger a_k^\dagger a_l\rangle - \mathcal{E}_l\xi\Big(\langle a_j^\dagger a_k^\dagger\rangle - \langle a_j^\dagger a_k^\dagger \sigma^{gg}\rangle - \langle a_j^\dagger a_k^\dagger \sigma^{ee}\rangle\Big) \\ -{\mathcal{E}_j}^*\langle a_k^\dagger a_l \sigma_-^{fe}\rangle - {\mathcal{E}_k}^*\langle a_j^\dagger a_l \sigma_-^{fe}\rangle \\ -\mathcal{E}_l\langle a_j^\dagger a_k^\dagger \sigma_+^{fe}\rangle \end{pmatrix}, \end{aligned} \tag{E.11b}$$

with

$$\boldsymbol{M}_{jkl}^{(a^\dagger a^2)} = \boldsymbol{M}^{(\Sigma)} - \left[3\kappa - i\left(\Delta\omega_j - \Delta\omega_k - \Delta\omega_l\right)\right]\mathbb{1}, \tag{E.12a}$$

$$\boldsymbol{M}_{jkl}^{({a^\dagger}^2 a)} = \boldsymbol{M}^{(\Sigma)} - \left[3\kappa - i\left(\Delta\omega_j + \Delta\omega_k - \Delta\omega_l\right)\right]\mathbb{1}. \tag{E.12b}$$

E.1.8 Fourth-order: Filter

$$\begin{aligned}\frac{\mathrm{d}}{\mathrm{d}t}\langle a_j^\dagger a_k^\dagger a_l a_m\rangle = &-\left[4\kappa - i\left(\Delta\omega_j + \Delta\omega_k\right) + i\left(\Delta\omega_l + \Delta\omega_m\right)\right]\langle a_j^\dagger a_k^\dagger a_l a_m\rangle \\ &- {\mathcal{E}_j}^*\left(\langle a_k^\dagger a_l a_m \sigma_+^{eg}\rangle + \xi\langle a_k^\dagger a_l a_m \sigma_+^{fe}\rangle\right) \\ &- {\mathcal{E}_k}^*\left(\langle a_j^\dagger a_l a_m \sigma_+^{eg}\rangle + \xi\langle a_j^\dagger a_l a_m \sigma_+^{fe}\rangle\right) \\ &- \mathcal{E}_l\left(\langle a_j^\dagger a_k^\dagger a_m \sigma_-^{eg}\rangle + \xi\langle a_j^\dagger a_k^\dagger a_m \sigma_-^{fe}\rangle\right) \\ &- \mathcal{E}_m\left(\langle a_j^\dagger a_k^\dagger a_l \sigma_-^{eg}\rangle + \xi\langle a_j^\dagger a_k^\dagger a_l \sigma_-^{fe}\rangle\right).\end{aligned} \tag{E.13}$$

E.2 Filtered First-Order Correlation Function

The first-order correlation function for the filtered output field is given by

$$G^{(1)}(t,\tau) = \langle A^\dagger(t+\tau)A(t)\rangle = \sum_{j=-N}^{N}\langle a_j^\dagger(t+\tau)A(t)\rangle. \tag{E.14}$$

We use the quantum regression equations to solve for this with the following moment equations:

$$\frac{\mathrm{d}}{\mathrm{d}\tau}\langle\boldsymbol{\Sigma}(t+\tau)A(t)\rangle = \boldsymbol{M}^{(\Sigma)}\langle\boldsymbol{\Sigma}(t+\tau)A(t)\rangle + \begin{pmatrix}0\\0\\-\gamma\langle A(t)\rangle\end{pmatrix}, \tag{E.15a}$$

and

$$\begin{aligned}\frac{\mathrm{d}}{\mathrm{d}\tau}\langle a_j^\dagger(t+\tau)A(t)\rangle = &-\left(\kappa - i\Delta\omega_j\right)\langle a_j^\dagger A(t)\rangle \\ &- {\mathcal{E}_j}^*\left(\langle\sigma_+^{eg}(t+\tau)A(t)\rangle + \xi\langle\sigma_+^{fe}(t+\tau)A(t)\rangle\right).\end{aligned} \tag{E.15b}$$

We solve these differential equations with the initial conditions at $\tau = 0$,

$$\langle\boldsymbol{\Sigma}A(t)\rangle = \sum_{k=-N}^{N}\langle a_k\boldsymbol{\Sigma}(t)\rangle, \tag{E.16a}$$

$$\langle a_j^\dagger A(t)\rangle = \sum_{k=-N}^{N}\langle a_j^\dagger a_k(t)\rangle. \tag{E.16b}$$

E.3 Filtered Second-Order Correlation Function

The second-order correlation function for the filtered output field is given by

$$G^{(2)}(t,\tau) = \langle A^\dagger(t)A^\dagger A(t+\tau)A(t)\rangle = \sum_{j,k=-N}^{N} \langle A^\dagger(t)a_k^\dagger a_l(t+\tau)A(t)\rangle. \tag{E.17}$$

We use the quantum regression equations to solve for this with the following moment equations:

$$\frac{\mathrm{d}}{\mathrm{d}\tau}\langle A^\dagger(t)\boldsymbol{\Sigma}(t+\tau)A(t)\rangle = \boldsymbol{M}^{(\Sigma)}\langle A^\dagger(t)\boldsymbol{\Sigma}(t+\tau)A(t)\rangle + \begin{pmatrix} 0 \\ 0 \\ 0 \\ \Gamma\xi^2\langle A^\dagger A(t)\rangle \\ i\xi\frac{\Omega}{2}\langle A^\dagger A(t)\rangle \\ -i\xi\frac{\Omega}{2}\langle A^\dagger A(t)\rangle \\ 0 \\ 0 \end{pmatrix}, \tag{E.18a}$$

and

$$\begin{aligned}\frac{\mathrm{d}}{\mathrm{d}\tau}\langle A^\dagger(t)a_j(t+\tau)A(t)\rangle =& -(\kappa + i\Delta\omega_j)\langle A^\dagger(t)a_jA(t)\rangle \\ & - \mathcal{E}_j{}^*\left(\langle A^\dagger(t)\sigma_-^{eg}(t+\tau)A(t)\rangle + \xi\langle A^\dagger(t)\sigma_-^{fe}(t+\tau)A(t)\rangle\right),\end{aligned} \tag{E.18b}$$

$$\begin{aligned}\frac{\mathrm{d}}{\mathrm{d}\tau}\langle A^\dagger(t)a_j^\dagger(t+\tau)A(t)\rangle =& -(\kappa - i\Delta\omega_j)\langle A^\dagger(t)a_j^\dagger A(t)\rangle \\ & - \mathcal{E}_j{}^*\left(\langle A^\dagger(t)\sigma_+^{eg}(t+\tau)A(t)\rangle + \xi\langle A^\dagger(t)\sigma_+^{fe}(t+\tau)A(t)\rangle\right),\end{aligned} \tag{E.18c}$$

and

$$\begin{aligned}\frac{\mathrm{d}}{\mathrm{d}\tau}\langle A^\dagger(t)a_j\boldsymbol{\Sigma}(t+\tau)A(t)\rangle =& \boldsymbol{M}_j^{(a)}\langle A^\dagger(t)a_j\boldsymbol{\Sigma}(t+\tau)A(t)\rangle \\ & + \begin{pmatrix} -\mathcal{E}_j\langle A^\dagger(t)\sigma_-^{eg}(t+\tau)A(t)\rangle \\ -\mathcal{E}_j\xi\langle A^\dagger(t)\sigma_-^{fg}(t+\tau)A(t)\rangle \\ -\mathcal{E}_j\langle A^\dagger(t)\sigma^{ee}(t+\tau)A(t)\rangle \\ \Gamma\xi^2\langle A^\dagger(t)a_j(t+\tau)A(t)\rangle - \mathcal{E}_j\xi\langle A^\dagger(t)\sigma_-^{fe}(t+\tau)A(t)\rangle \\ i\xi\frac{\Omega}{2}\langle A^\dagger(t)a_j(t+\tau)A(t)\rangle \\ -i\xi\frac{\Omega}{2}\langle A^\dagger(t)a_j(t+\tau)A(t)\rangle - \mathcal{E}_j\xi\big(1-\langle A^\dagger(t)\sigma^{gg}(t+\tau)A(t)\rangle - \langle A^\dagger(t)\sigma^{ee}(t+\tau)A(t)\rangle\big) \\ 0 \\ -\mathcal{E}_j\langle A^\dagger(t)\sigma_+^{fe}(t+\tau)A(t)\rangle \end{pmatrix},\end{aligned} \tag{E.18d}$$

$$\begin{aligned}\frac{\mathrm{d}}{\mathrm{d}\tau}\langle A^\dagger(t)a_j^\dagger\boldsymbol{\Sigma}(t+\tau)A(t)\rangle =& \boldsymbol{M}_j^{(a^\dagger)}\langle A^\dagger(t)a_j^\dagger\boldsymbol{\Sigma}(t+\tau)A(t)\rangle \\ & + \begin{pmatrix} -\mathcal{E}_j{}^*\langle A^\dagger(t)\sigma_+^{eg}(t+\tau)A(t)\rangle \\ -\mathcal{E}_j{}^*\langle A^\dagger(t)\sigma^{ee}(t+\tau)A(t)\rangle \\ -\mathcal{E}_j{}^*\xi\langle A^\dagger(t)\sigma_+^{fg}(t+\tau)A(t)\rangle \\ \Gamma\xi^2\langle A^\dagger(t)a_j^\dagger(t+\tau)A(t)\rangle - \mathcal{E}_j{}^*\xi\langle A^\dagger(t)\sigma_+^{fe}(t+\tau)A(t)\rangle \\ i\xi\frac{\Omega}{2}\langle A^\dagger(t)a_j^\dagger(t+\tau)A(t)\rangle - \mathcal{E}_j{}^*\xi\big(1-\langle A^\dagger(t)\sigma^{gg}(t+\tau)A(t)\rangle - \langle A^\dagger(t)\sigma^{ee}(t+\tau)A(t)\rangle\big) \\ -i\xi\frac{\Omega}{2}\langle A^\dagger(t)a_j^\dagger(t+\tau)A(t)\rangle \\ -\mathcal{E}_j{}^*\langle A^\dagger(t)\sigma_-^{fe}(t+\tau)A(t)\rangle \\ 0 \end{pmatrix},\end{aligned} \tag{E.18e}$$

and

$$\begin{aligned}\frac{\mathrm{d}}{\mathrm{d}\tau}\langle A^\dagger(t)a_j^\dagger a_k(t+\tau)A(t)\rangle = &-\left[2\kappa - i\left(\Delta\omega_j - \Delta\omega_k\right)\right]\langle A^\dagger(t)a_j^\dagger a_k(t+\tau)A(t)\rangle \\ &- {\mathcal{E}_j}^*\langle A^\dagger(t)a_k\sigma_+(t+\tau)A(t)\rangle \\ &- \mathcal{E}_k\langle A^\dagger(t)a_j^\dagger\sigma_-(t+\tau)A(t)\rangle. \end{aligned} \tag{E.18f}$$

We solve these differential equations with the initial conditions at $\tau = 0$,

$$\langle A^\dagger \mathbf{\Sigma} A(t)\rangle = \sum_{j,m=-N}^{N}\langle a_j^\dagger a_m \mathbf{\Sigma}(t)\rangle, \tag{E.19a}$$

$$\langle A^\dagger a_k^\dagger A(t)\rangle = \sum_{j,m=-N}^{N}\langle a_j^\dagger a_k^\dagger a_k(t)\rangle, \tag{E.19b}$$

$$\langle A^\dagger a_l A(t)\rangle = \sum_{j,m=-N}^{N}\langle a_j^\dagger a_l a_k(t)\rangle, \tag{E.19c}$$

$$\langle A^\dagger a_k^\dagger \mathbf{\Sigma} A(t)\rangle = \sum_{j,m=-N}^{N}\langle a_j^\dagger a_k^\dagger a_k \mathbf{\Sigma}(t)\rangle, \tag{E.19d}$$

$$\langle A^\dagger a_l \mathbf{\Sigma} A(t)\rangle = \sum_{j,m=-N}^{N}\langle a_j^\dagger a_l a_k \mathbf{\Sigma}(t)\rangle, \tag{E.19e}$$

$$\langle A^\dagger a_k^\dagger a_l A(t)\rangle = \sum_{j,m=-N}^{N}\langle a_j^\dagger a_k^\dagger a_l a_m(t)\rangle. \tag{E.19f}$$

F Moment Equations of the Three-Level Atom and Two-Filter Cascaded System

Here we present all of the operator moment equations needed to calculate second-order cross-correlation functions for the two-filter multi-mode array filtered three-level atom. We first show the moment equations, as derived from Eq. (7.39). These are then followed by the coupled equations for the second-order cross-correlation function.

The `Fortan90` code used to numerically calculate these equations can be found at the following Github repository: github.com/jnga773/multi-mode-filter.

F.1 Moment Equations

We write these coupled moment equations in matrix form, where we use the notation

$$\langle \boldsymbol{\sigma} \rangle = \begin{pmatrix} \langle \sigma^{gg} \rangle \\ \langle \sigma^{eg}_{-} \rangle \\ \langle \sigma^{eg}_{+} \rangle \\ \langle \sigma^{ee} \rangle \\ \langle \sigma^{fe}_{-} \rangle \\ \langle \sigma^{fe}_{+} \rangle \\ \langle \sigma^{fg}_{-} \rangle \\ \langle \sigma^{fg}_{+} \rangle \end{pmatrix}, \quad \langle X\boldsymbol{\sigma} \rangle = \begin{pmatrix} \langle X\sigma^{gg} \rangle \\ \langle X\sigma^{eg}_{-} \rangle \\ \langle X\sigma^{eg}_{+} \rangle \\ \langle X\sigma^{ee} \rangle \\ \langle X\sigma^{fe}_{-} \rangle \\ \langle X\sigma^{fe}_{+} \rangle \\ \langle X\sigma^{fg}_{-} \rangle \\ \langle X\sigma^{fg}_{+} \rangle \end{pmatrix}. \tag{F.1}$$

F.1.1 Atomic Operator Moments

$$\frac{\mathrm{d}}{\mathrm{d}t}\langle \boldsymbol{\sigma} \rangle = \boldsymbol{M}\langle \boldsymbol{\sigma} \rangle + \begin{pmatrix} 0 \\ 0 \\ 0 \\ \Gamma\xi^{2} \\ i\xi\frac{\Omega}{2} \\ -i\xi\frac{\Omega}{2} \\ 0 \\ 0 \end{pmatrix}, \tag{F.2}$$

where

$$\boldsymbol{M}^{(\Sigma)} = \begin{pmatrix} 0 & -i\frac{\Omega}{2} & i\frac{\Omega}{2} & \Gamma & 0 & 0 & 0 & 0 \\ -i\frac{\Omega}{2} & -\left[\frac{\Gamma}{2} - i\left(\frac{\alpha}{2}+\delta\right)\right] & 0 & i\frac{\Omega}{2} & \Gamma\xi & 0 & -i\xi\frac{\Omega}{2} & 0 \\ i\frac{\Omega}{2} & 0 & -\left[\frac{\Gamma}{2} + i\left(\frac{\alpha}{2}+\delta\right)\right] & -i\frac{\Omega}{2} & 0 & \Gamma\xi & 0 & i\xi\frac{\Omega}{2} \\ -\Gamma\xi^{2} & i\frac{\Omega}{2} & -i\frac{\Omega}{2} & -\Gamma\left(1+\xi^{2}\right) & -i\xi\frac{\Omega}{2} & i\xi\frac{\Omega}{2} & 0 & 0 \\ -i\xi\frac{\Omega}{2} & 0 & 0 & -i\xi\Omega & -\left[\frac{\Gamma}{2}\left(1+\xi^{2}\right) + i\left(\frac{\alpha}{2}-\delta\right)\right] & 0 & i\frac{\Omega}{2} & 0 \\ i\xi\frac{\Omega}{2} & 0 & 0 & i\xi\Omega & 0 & -\left[\frac{\Gamma}{2}\left(1+\xi^{2}\right) - i\left(\frac{\alpha}{2}-\delta\right)\right] & 0 & -i\frac{\Omega}{2} \\ 0 & -i\xi\frac{\Omega}{2} & 0 & 0 & i\frac{\Omega}{2} & 0 & -\left[\frac{\Gamma}{2}\xi^{2} - 2i\delta\right] & 0 \\ 0 & 0 & i\xi\frac{\Omega}{2} & 0 & 0 & -i\frac{\Omega}{2} & 0 & -\left[\frac{\Gamma}{2}\xi^{2} + 2i\delta\right] \end{pmatrix}. \tag{F.3}$$

F.1.2 First-order: Filter

$$\begin{aligned}
\frac{\mathrm{d}}{\mathrm{d}t}\langle a_j\rangle &= -\left(\kappa_a + i\Delta\omega_j^{(a)}\right)\langle a_j\rangle \\
&\quad - \mathcal{E}_j^{(a)}\left(\langle\sigma_-^{eg}\rangle + \xi\langle\sigma_-^{fe}\rangle\right), \qquad \text{(F.4a)}\\
\frac{\mathrm{d}}{\mathrm{d}t}\langle a_j^\dagger\rangle &= -\left(\kappa_a - i\Delta\omega_j^{(a)}\right)\langle a_j^\dagger\rangle \\
&\quad - \mathcal{E}_j^{(a)*}\left(\langle\sigma_+^{eg}\rangle + \xi\langle\sigma_+^{fe}\rangle\right). \qquad \text{(F.4b)}\\
\frac{\mathrm{d}}{\mathrm{d}t}\langle b_j\rangle &= -\left(\kappa_b + i\Delta\omega_j^{(b)}\right)\langle b_j\rangle \\
&\quad - \mathcal{E}_j^{(b)}\left(\langle\sigma_-^{eg}\rangle + \xi\langle\sigma_-^{eg}\rangle\right), \qquad \text{(F.4c)}\\
\frac{\mathrm{d}}{\mathrm{d}t}\langle b_j^\dagger\rangle &= -\left(\kappa_b - i\Delta\omega_j^{(b)}\right)\langle b_j^\dagger\rangle \\
&\quad - \mathcal{E}_j^{(b)*}\left(\langle\sigma_+^{eg}\rangle + \xi\langle\sigma_+^{eg}\rangle\right). \qquad \text{(F.4d)}
\end{aligned}$$

F.1.3 First-order: Filter / Atom

$$\frac{\mathrm{d}}{\mathrm{d}t}\langle a_j\boldsymbol{\sigma}\rangle = \boldsymbol{M}_j^{(a)}\langle a_j\boldsymbol{\sigma}\rangle + \begin{pmatrix}
-\mathcal{E}_j^{(a)}\langle\sigma_-^{eg}\rangle \\
-\mathcal{E}_j^{(a)}\xi\langle\sigma_-^{fg}\rangle \\
-\mathcal{E}_j^{(a)}\langle\sigma^{ee}\rangle \\
\Gamma\xi^2\langle a_j\rangle - \mathcal{E}_j^{(a)}\xi\langle\sigma_-^{fe}\rangle \\
i\xi\frac{\Omega}{2}\langle a_j\rangle \\
-i\xi\frac{\Omega}{2}\langle a_j\rangle - \mathcal{E}_j^{(a)}\xi(1-\langle\sigma^{gg}\rangle-\langle\sigma^{ee}\rangle) \\
0 \\
-\mathcal{E}_j^{(a)}\langle\sigma_+^{fe}\rangle
\end{pmatrix}, \qquad \text{(F.5a)}$$

$$\frac{\mathrm{d}}{\mathrm{d}t}\langle a_j^\dagger\boldsymbol{\sigma}\rangle = \boldsymbol{M}_j^{(a^\dagger)}\langle a_j^\dagger\boldsymbol{\sigma}\rangle + \begin{pmatrix}
-\mathcal{E}_j^{(a)*}\langle\sigma_+^{eg}\rangle \\
-\mathcal{E}_j^{(a)*}\langle\sigma^{ee}\rangle \\
-\mathcal{E}_j^{(a)*}\xi\langle\sigma_+^{fg}\rangle \\
\Gamma\xi^2\langle a_j^\dagger\rangle - \mathcal{E}_j^{(a)*}\xi\langle\sigma_+^{fe}\rangle \\
i\xi\frac{\Omega}{2}\langle a_j^\dagger\rangle - \mathcal{E}_j^{(a)*}\xi(1-\langle\sigma^{gg}\rangle-\langle\sigma^{ee}\rangle) \\
-i\xi\frac{\Omega}{2}\langle a_j^\dagger\rangle \\
-\mathcal{E}_j^{(a)*}\langle\sigma_-^{fe}\rangle \\
0
\end{pmatrix}, \qquad \text{(F.5b)}$$

$$\frac{\mathrm{d}}{\mathrm{d}t}\langle b_j\boldsymbol{\sigma}\rangle = \boldsymbol{M}_j^{(b)}\langle b_j\boldsymbol{\sigma}\rangle + \begin{pmatrix}
-\mathcal{E}_j^{(b)}\langle\sigma_-^{eg}\rangle \\
-\mathcal{E}_j^{(b)}\xi\langle\sigma_-^{fg}\rangle \\
-\mathcal{E}_j^{(b)}\langle\sigma^{ee}\rangle \\
\Gamma\xi^2\langle b_j\rangle - \mathcal{E}_j^{(b)}\xi\langle\sigma_-^{fe}\rangle \\
i\xi\frac{\Omega}{2}\langle b_j\rangle \\
-i\xi\frac{\Omega}{2}\langle b_j\rangle - \mathcal{E}_j^{(b)}\xi(1-\langle\sigma^{gg}\rangle-\langle\sigma^{ee}\rangle) \\
0 \\
-\mathcal{E}_j^{(b)}\langle\sigma_+^{fe}\rangle
\end{pmatrix}, \qquad \text{(F.5c)}$$

$$\frac{\mathrm{d}}{\mathrm{d}t}\langle b_j^\dagger \boldsymbol{\sigma}\rangle = \boldsymbol{M}_j^{(b^\dagger)}\langle b_j^\dagger \boldsymbol{\sigma}\rangle + \begin{pmatrix} -\mathcal{E}_j^{(b)^*}\langle \sigma_+^{eg}\rangle \\ -\mathcal{E}_j^{(b)^*}\langle \sigma^{ee}\rangle \\ -\mathcal{E}_j^{(b)^*}\xi\langle \sigma_+^{fg}\rangle \\ \Gamma\xi^2\langle b_j^\dagger\rangle - \mathcal{E}_j^{(b)^*}\xi\langle \sigma_+^{fe}\rangle \\ i\xi\frac{\Omega}{2}\langle b_j^\dagger\rangle - \mathcal{E}_j^{(b)^*}\xi(1-\langle\sigma^{gg}\rangle - \langle\sigma^{ee}\rangle) \\ -i\xi\frac{\Omega}{2}\langle b_j^\dagger\rangle \\ -\mathcal{E}_j^{(b)^*}\langle \sigma_-^{fe}\rangle \\ 0 \end{pmatrix}, \tag{F.5d}$$

with

$$\boldsymbol{M}_j^{(a)} = \boldsymbol{M}^{(\boldsymbol{\sigma})} - \left(\kappa_a + i\Delta\omega_j^{(a)}\right)\mathbb{1}, \tag{F.6a}$$

$$\boldsymbol{M}_j^{(a^\dagger)} = \boldsymbol{M}^{(\boldsymbol{\sigma})} - \left(\kappa_a - i\Delta\omega_j^{(a)}\right)\mathbb{1}, \tag{F.6b}$$

$$\boldsymbol{M}_j^{(b)} = \boldsymbol{M}^{(\boldsymbol{\sigma})} - \left(\kappa_b + i\Delta\omega_j^{(b)}\right)\mathbb{1}, \tag{F.6c}$$

$$\boldsymbol{M}_j^{(b^\dagger)} = \boldsymbol{M}^{(\boldsymbol{\sigma})} - \left(\kappa_b - i\Delta\omega_j^{(b)}\right)\mathbb{1}. \tag{F.6d}$$

F.1.4 Second-order: Filter

$$\begin{aligned}\frac{\mathrm{d}}{\mathrm{d}t}\langle a_j b_k\rangle =& -\left[\kappa_a + \kappa_b + i\left(\Delta\omega_j^{(a)} + \Delta\omega_k^{(b)}\right)\right]\langle a_j b_k\rangle \\ & - \mathcal{E}_j^{(a)}\left(\langle b_k\sigma_-^{eg}\rangle + \xi\langle b_k\sigma_-^{fe}\rangle\right) - \mathcal{E}_k^{(b)}\left(\langle a_j\sigma_-^{eg}\rangle + \xi\langle a_j\sigma_-^{fe}\rangle\right),\end{aligned} \tag{F.7a}$$

$$\begin{aligned}\frac{\mathrm{d}}{\mathrm{d}t}\langle a_j^\dagger b_k^\dagger\rangle =& -\left[\kappa_a + \kappa_b - i\left(\Delta\omega_j^{(a)} + \Delta\omega_k^{(b)}\right)\right]\langle a_j^\dagger b_k^\dagger\rangle \\ & - \mathcal{E}_j^{(a)^*}\left(\langle b_k^\dagger\sigma_+^{eg}\rangle + \xi\langle b_k^\dagger\sigma_+^{fe}\rangle\right) - \mathcal{E}_k^{(b)^*}\left(\langle a_j^\dagger\sigma_+^{eg}\rangle + \xi\langle a_j^\dagger\sigma_+^{eg}\rangle\right),\end{aligned} \tag{F.7b}$$

$$\begin{aligned}\frac{\mathrm{d}}{\mathrm{d}t}\langle a_j^\dagger a_k\rangle =& -\left[2\kappa_a - i\left(\Delta\omega_j^{(a)} - \Delta\omega_k^{(a)}\right)\right]\langle a_j^\dagger a_k\rangle \\ & - \mathcal{E}_j^{(a)^*}\left(\langle a_k\sigma_+^{eg}\rangle + \xi\langle a_k\sigma_+^{fe}\rangle\right) - \mathcal{E}_k^{(a)}\left(\langle a_j^\dagger\sigma_-^{eg}\rangle + \xi\langle a_j^\dagger\sigma_-^{fe}\rangle\right),\end{aligned} \tag{F.7c}$$

$$\begin{aligned}\frac{\mathrm{d}}{\mathrm{d}t}\langle b_j^\dagger b_k\rangle =& -\left[2\kappa_b - i\left(\Delta\omega_j^{(b)} - \Delta\omega_k^{(b)}\right)\right]\langle b_j^\dagger b_k\rangle \\ & - \mathcal{E}_j^{(b)^*}\left(\langle b_k\sigma_+^{eg}\rangle + \xi\langle b_k\sigma_+^{fe}\rangle\right) - \mathcal{E}_k^{(b)}\left(\langle b_j^\dagger\sigma_-^{eg}\rangle + \xi\langle b_j^\dagger\sigma_-^{fe}\rangle\right),\end{aligned} \tag{F.7d}$$

$$\begin{aligned}\frac{\mathrm{d}}{\mathrm{d}t}\langle a_j^\dagger b_k\rangle =& -\left[\kappa_a + \kappa_b - i\left(\Delta\omega_j^{(a)} - \Delta\omega_k^{(b)}\right)\right]\langle a_j^\dagger b_k\rangle \\ & - \mathcal{E}_j^{(a)^*}\left(\langle b_k\sigma_+^{eg}\rangle + \xi\langle b_k\sigma_+^{fe}\rangle\right) - \mathcal{E}_k^{(b)}\left(\langle a_j^\dagger\sigma_-^{eg}\rangle + \xi\langle a_j^\dagger\sigma_-^{fe}\rangle\right),\end{aligned} \tag{F.7e}$$

$$\begin{aligned}\frac{\mathrm{d}}{\mathrm{d}t}\langle b_j^\dagger a_k\rangle =& -\left[\kappa_a + \kappa_b - i\left(\Delta\omega_j^{(b)} - \Delta\omega_k^{(a)}\right)\right]\langle b_j^\dagger a_k\rangle \\ & - \mathcal{E}_j^{(b)^*}\left(\langle a_k\sigma_+^{eg}\rangle + \xi\langle a_k\sigma_+^{fe}\rangle\right) - \mathcal{E}_k^{(a)}\left(\langle b_j^\dagger\sigma_-^{eg}\rangle + \xi\langle b_j^\dagger\sigma_-^{fe}\rangle\right).\end{aligned} \tag{F.7f}$$

F.1.5 Second-order: Filter / Atom

$$\frac{\mathrm{d}}{\mathrm{d}t}\langle a_j b_k \boldsymbol{\sigma}\rangle = \boldsymbol{M}_{jk}^{(ab)}\langle a_j b_k \boldsymbol{\sigma}\rangle + \begin{pmatrix} -\mathcal{E}_j^{(a)}\langle b_k\sigma_-^{eg}\rangle - \mathcal{E}_k^{(b)}\langle a_j\sigma_-^{eg}\rangle \\ -\mathcal{E}_j^{(a)}\xi\langle b_k\sigma_-^{fg}\rangle - \mathcal{E}_k^{(b)}\xi\langle a_j\sigma_-^{fg}\rangle \\ -\mathcal{E}_j^{(a)}\langle b_k\sigma^{ee}\rangle - \mathcal{E}_k^{(b)}\langle a_j\sigma^{ee}\rangle \\ \Gamma\xi\langle a_j b_k\rangle - \mathcal{E}_j^{(a)}\xi\langle b_k\sigma_-^{fe}\rangle - \mathcal{E}_k^{(b)}\xi\langle a_j\sigma_-^{fe}\rangle \\ i\xi\frac{\Omega}{2}\langle a_j b_k\rangle \\ -i\xi\frac{\Omega}{2}\langle a_j b_k\rangle - \mathcal{E}_j^{(a)}\xi(\langle b_k\rangle - \langle b_k\sigma^{gg}\rangle - \langle b_k\sigma^{ee}\rangle) - \mathcal{E}_k^{(b)}\xi(\langle a_j\rangle - \langle a_j\sigma^{gg}\rangle - \langle a_j\sigma^{ee}\rangle) \\ 0 \\ -\mathcal{E}_j^{(a)}\langle b_k\sigma_+^{fe}\rangle - \mathcal{E}_k^{(b)}\langle a_j\sigma_+^{fe}\rangle \end{pmatrix}, \tag{F.8a}$$

$$\frac{\mathrm{d}}{\mathrm{d}t}\langle a_j^\dagger b_k^\dagger \boldsymbol{\sigma}\rangle = \boldsymbol{M}_{jk}^{(a^\dagger b^\dagger)} a_j^\dagger b_k^\dagger \boldsymbol{\sigma}\rangle + \begin{pmatrix} -\mathcal{E}_j^{(a)^*}\langle b_k^\dagger\sigma_+^{eg}\rangle - \mathcal{E}_k^{(b)^*}\langle a_j^\dagger\sigma_+^{eg}\rangle \\ -\mathcal{E}_j^{(a)^*}\langle b_k^\dagger\sigma^{ee}\rangle - \mathcal{E}_k^{(b)^*}\langle a_j^\dagger\sigma^{ee}\rangle \\ -\mathcal{E}_j^{(a)^*}\xi\langle b_k^\dagger\sigma_+^{fg}\rangle - \mathcal{E}_k^{(b)^*}\xi\langle a_j^\dagger\sigma_+^{fg}\rangle \\ \Gamma\xi^2\langle a_j^\dagger b_k^\dagger\rangle - \mathcal{E}_j^{(a)^*}\xi\langle b_k^\dagger\sigma_+^{fe}\rangle - \mathcal{E}_k^{(b)^*}\xi\langle a_j^\dagger\sigma_+^{fe}\rangle \\ i\xi\frac{\Omega}{2}\langle a_j^\dagger b_k^\dagger\rangle - \mathcal{E}_j^{(a)^*}\xi\Big(\langle b_k^\dagger\rangle - \langle b_k^\dagger\sigma^{gg}\rangle - \langle b_k^\dagger\sigma^{ee}\rangle\Big) - \mathcal{E}_k^{(b)^*}\xi\Big(\langle a_j^\dagger\rangle - \langle a_j^\dagger\sigma^{gg}\rangle - \langle a_j^\dagger\sigma^{ee}\rangle\Big) \\ -i\xi\frac{\Omega}{2}\langle a_j^\dagger b_k^\dagger\rangle \\ -\mathcal{E}_j^{(a)^*}\langle b_k^\dagger\sigma_-^{fe}\rangle - \mathcal{E}_k^{(b)^*}\langle a_j^\dagger\sigma_-^{fe}\rangle \\ 0 \end{pmatrix}, \tag{F.8b}$$

$$\frac{\mathrm{d}}{\mathrm{d}t}\langle a_j^\dagger a_k \boldsymbol{\sigma}\rangle = \boldsymbol{M}_{jk}^{(a^\dagger a)}\langle a_j^\dagger a_k \boldsymbol{\sigma}\rangle + \begin{pmatrix} -\mathcal{E}_j^{(a)^*}\langle a_k\sigma_+^{eg}\rangle - \mathcal{E}_k^{(a)}\langle a_j^\dagger\sigma_-^{eg}\rangle \\ -\mathcal{E}_j^{(a)^*}\langle a_k\sigma^{ee}\rangle - \mathcal{E}_k^{(a)}\xi\langle a_j^\dagger\sigma_-^{fg}\rangle \\ -\mathcal{E}_j^{(a)^*}\xi\langle a_k\sigma_+^{fg}\rangle - \mathcal{E}_k^{(a)}\langle a_j^\dagger\sigma^{ee}\rangle \\ \Gamma\xi^2\langle a_j^\dagger a_k\rangle - \mathcal{E}_j^{(a)^*}\xi\langle a_k\sigma_+^{fe}\rangle - \mathcal{E}_k^{(a)}\xi\langle a_k^\dagger\sigma_-^{fe}\rangle \\ i\xi\frac{\Omega}{2}\langle a_j^\dagger a_k\rangle - \mathcal{E}_j^{(a)^*}\xi(\langle a_k\rangle - \langle a_k\sigma^{gg}\rangle - \langle a_k\sigma^{ee}\rangle) \\ -i\xi\frac{\Omega}{2}\langle a_j^\dagger a_k\rangle - \mathcal{E}_k^{(a)}\xi\Big(\langle a_j^\dagger\rangle - \langle a_j^\dagger\sigma^{gg}\rangle - \langle a_j^\dagger\sigma^{ee}\rangle\Big) \\ -\mathcal{E}_j^{(a)^*}\langle a_k\sigma_-^{fe}\rangle \\ -\mathcal{E}_k^{(a)}\langle a_j^\dagger\sigma_+^{fe}\rangle \end{pmatrix}, \tag{F.8c}$$

$$\frac{\mathrm{d}}{\mathrm{d}t}\langle b_j^\dagger b_k \boldsymbol{\sigma}\rangle = \boldsymbol{M}_{jk}^{(b^\dagger b)}\langle b_j^\dagger b_k \boldsymbol{\sigma}\rangle + \begin{pmatrix} -\mathcal{E}_j^{(b)^*}\langle b_k\sigma_+^{eg}\rangle - \mathcal{E}_k^{(b)}\langle b_j^\dagger\sigma_-^{eg}\rangle \\ -\mathcal{E}_j^{(b)^*}\langle b_k\sigma^{ee}\rangle - \mathcal{E}_k^{(b)}\xi\langle b_j^\dagger\sigma_-^{fg}\rangle \\ -\mathcal{E}_j^{(b)^*}\xi\langle b_k\sigma_+^{fg}\rangle - \mathcal{E}_k^{(b)}\langle b_j^\dagger\sigma^{ee}\rangle \\ \Gamma\xi^2\langle b_j^\dagger b_k\rangle - \mathcal{E}_j^{(b)^*}\xi\langle b_k\sigma_+^{fe}\rangle - \mathcal{E}_k^{(b)}\xi\langle b_k^\dagger\sigma_-^{fe}\rangle \\ i\xi\frac{\Omega}{2}\langle b_j^\dagger b_k\rangle - \mathcal{E}_j^{(b)^*}\xi(\langle b_k\rangle - \langle b_k\sigma^{gg}\rangle - \langle b_k\sigma^{ee}\rangle) \\ -i\xi\frac{\Omega}{2}\langle b_j^\dagger b_k\rangle - \mathcal{E}_k^{(b)}\xi\Big(\langle b_j^\dagger\rangle - \langle b_j^\dagger\sigma^{gg}\rangle - \langle b_j^\dagger\sigma^{ee}\rangle\Big) \\ -\mathcal{E}_j^{(b)^*}\langle b_k\sigma_-^{fe}\rangle \\ -\mathcal{E}_k^{(b)}\langle b_j^\dagger\sigma_+^{fe}\rangle \end{pmatrix}, \tag{F.8d}$$

$$\frac{\mathrm{d}}{\mathrm{d}t}\langle a_j^\dagger b_k \boldsymbol{\sigma}\rangle = \boldsymbol{M}_{jk}^{(a^\dagger b)}\langle a_j^\dagger b_k \boldsymbol{\sigma}\rangle + \begin{pmatrix} -\mathcal{E}_j^{(a)^*}\langle b_k\sigma_+^{eg}\rangle - \mathcal{E}_k^{(b)}\langle a_j^\dagger\sigma_-^{eg}\rangle \\ -\mathcal{E}_j^{(a)^*}\langle b_k\sigma^{ee}\rangle - \mathcal{E}_k^{(b)}\xi\langle a_j^\dagger\sigma_-^{fg}\rangle \\ -\mathcal{E}_j^{(a)^*}\xi\langle b_k\sigma_+^{fg}\rangle - \mathcal{E}_k^{(b)}\langle a_j^\dagger\sigma^{ee}\rangle \\ \Gamma\xi^2\langle a_j^\dagger b_k\rangle - \mathcal{E}_j^{(a)^*}\xi\langle b_k\sigma_+^{fe}\rangle - \mathcal{E}_k^{(b)}\xi\langle a_k^\dagger\sigma_-^{fe}\rangle \\ i\xi\frac{\Omega}{2}\langle a_j^\dagger b_k\rangle - \mathcal{E}_j^{(a)^*}\xi(\langle b_k\rangle - \langle b_k\sigma^{gg}\rangle - \langle b_k\sigma^{ee}\rangle) \\ -i\xi\frac{\Omega}{2}\langle a_j^\dagger b_k\rangle - \mathcal{E}_k^{(b)}\xi\Big(\langle a_j^\dagger\rangle - \langle a_j^\dagger\sigma^{gg}\rangle - \langle a_j^\dagger\sigma^{ee}\rangle\Big) \\ -\mathcal{E}_j^{(a)^*}\langle b_k\sigma_-^{fe}\rangle \\ -\mathcal{E}_k^{(b)}\langle a_j^\dagger\sigma_+^{fe}\rangle \end{pmatrix}, \tag{F.8e}$$

$$\frac{\mathrm{d}}{\mathrm{d}t}\langle b_j^\dagger a_k \boldsymbol{\sigma}\rangle = \boldsymbol{M}_{jk}^{(b^\dagger a)}\langle b_j^\dagger a_k \boldsymbol{\sigma}\rangle + \begin{pmatrix} -\mathcal{E}_j^{(b)^*}\langle a_k\sigma_+^{eg}\rangle - \mathcal{E}_k^{(a)}\langle b_j^\dagger\sigma_-^{eg}\rangle \\ -\mathcal{E}_j^{(b)^*}\langle a_k\sigma^{ee}\rangle - \mathcal{E}_k^{(a)}\xi\langle b_j^\dagger\sigma_-^{fg}\rangle \\ -\mathcal{E}_j^{(b)^*}\xi\langle a_k\sigma_+^{fg}\rangle - \mathcal{E}_k^{(a)}\langle b_j^\dagger\sigma^{ee}\rangle \\ \Gamma\xi^2\langle b_j^\dagger a_k\rangle - \mathcal{E}_j^{(b)^*}\xi\langle a_k\sigma_+^{fe}\rangle - \mathcal{E}_k^{(a)}\xi\langle b_k^\dagger\sigma_-^{fe}\rangle \\ i\xi\frac{\Omega}{2}\langle b_j^\dagger a_k\rangle - \mathcal{E}_j^{(b)^*}\xi(\langle a_k\rangle - \langle a_k\sigma^{gg}\rangle - \langle a_k\sigma^{ee}\rangle) \\ -i\xi\frac{\Omega}{2}\langle b_j^\dagger a_k\rangle - \mathcal{E}_k^{(a)}\xi\Big(\langle b_j^\dagger\rangle - \langle b_j^\dagger\sigma^{gg}\rangle - \langle b_j^\dagger\sigma^{ee}\rangle\Big) \\ -\mathcal{E}_j^{(b)^*}\langle a_k\sigma_-^{fe}\rangle \\ -\mathcal{E}_k^{(a)}\langle b_j^\dagger\sigma_+^{fe}\rangle \end{pmatrix}, \tag{F.8f}$$

with

$$\boldsymbol{M}_{jk}^{(ab)} = \boldsymbol{M}^{(\boldsymbol{\sigma})} - \Big[\kappa_a + \kappa_b + i\left(\Delta\omega_j^{(a)} + \Delta\omega_k^{(b)}\right)\Big]\mathbb{1}, \tag{F.9a}$$

$$\boldsymbol{M}_{jk}^{(a^\dagger b^\dagger)} = \boldsymbol{M}^{(\boldsymbol{\sigma})} - \Big[\kappa_a + \kappa_b - i\left(\Delta\omega_j^{(a)} + \Delta\omega_k^{(b)}\right)\Big]\mathbb{1}, \tag{F.9b}$$

$$\boldsymbol{M}_{jk}^{(a^\dagger a)} = \boldsymbol{M}^{(\boldsymbol{\sigma})} - \Big[2\kappa_a - i\left(\Delta\omega_j^{(a)} - \Delta\omega_k^{(a)}\right)\Big]\mathbb{1}, \tag{F.9c}$$

$$\boldsymbol{M}_{jk}^{(b^\dagger b)} = \boldsymbol{M}^{(\boldsymbol{\sigma})} - \Big[2\kappa_b - i\left(\Delta\omega_j^{(b)} - \Delta\omega_k^{(b)}\right)\Big]\mathbb{1}, \tag{F.9d}$$

$$\boldsymbol{M}_{jk}^{(a^\dagger b)} = \boldsymbol{M}^{(\boldsymbol{\sigma})} - \Big[\kappa_a + \kappa_b - i\left(\Delta\omega_j^{(a)} - \Delta\omega_k^{(b)}\right)\Big]\mathbb{1}, \tag{F.9e}$$

$$\boldsymbol{M}_{jk}^{(b^\dagger a)} = \boldsymbol{M}^{(\boldsymbol{\sigma})} - \Big[\kappa_a + \kappa_b - i\left(\Delta\omega_j^{(b)} - \Delta\omega_k^{(a)}\right)\Big]\mathbb{1}. \tag{F.9f}$$

F.1.6 Third-order: Filter

$$\frac{\mathrm{d}}{\mathrm{d}t}\langle a_j^\dagger a_k b_l\rangle = -\Big[2\kappa_a + \kappa_b - i\left(\Delta\omega_j^{(a)} - \Delta\omega_k^{(a)} - \Delta\omega_l^{(b)}\right)\Big]\langle a_j^\dagger a_k b_l\rangle, \tag{F.10a}$$

$$\frac{\mathrm{d}}{\mathrm{d}t}\langle b_j^\dagger b_k a_l\rangle = -\Big[\kappa_a + 2\kappa_b - i\left(\Delta\omega_j^{(b)} - \Delta\omega_k^{(b)} - \Delta\omega_l^{(a)}\right)\Big]\langle b_j^\dagger b_k a_l\rangle, \tag{F.10b}$$

$$\frac{\mathrm{d}}{\mathrm{d}t}\langle b_j^\dagger a_k^\dagger a_l\rangle = -\Big[2\kappa_a + \kappa_b - i\left(\Delta\omega_j^{(b)} + \Delta\omega_k^{(a)} - \Delta\omega_l^{(a)}\right)\Big]\langle b_j^\dagger a_k^\dagger a_l\rangle, \tag{F.10c}$$

$$\frac{\mathrm{d}}{\mathrm{d}t}\langle a_j^\dagger b_k^\dagger b_l\rangle = -\Big[\kappa_a + 2\kappa_b - i\left(\Delta\omega_j^{(a)} + \Delta\omega_k^{(b)} - \Delta\omega_l^{(b)}\right)\Big]\langle a_j^\dagger b_k^\dagger b_l\rangle. \tag{F.10d}$$

F.1.7 Third-order: Filter / Atom

$$\frac{\mathrm{d}}{\mathrm{d}t}\langle a_j^\dagger a_k b_l \boldsymbol{\sigma}\rangle = \boldsymbol{M}_{jkl}^{(a^\dagger a b)}\langle a_j^\dagger a_k b_l \boldsymbol{\sigma}\rangle$$
$$+\begin{pmatrix}
-\mathcal{E}_j^{(a)^*}\langle a_k b_l \sigma_+^{eg}\rangle - \mathcal{E}_k^{(a)}\langle a_j^\dagger b_l \sigma_-^{eg}\rangle - \mathcal{E}_l^{(b)}\langle a_j^\dagger a_k \sigma_-^{eg}\rangle \\
-\mathcal{E}_j^{(a)^*}\langle a_k b_l \sigma^{ee}\rangle - \mathcal{E}_k^{(a)}\xi\langle a_j^\dagger b_l \sigma_-^{fg}\rangle - \mathcal{E}_l^{(b)}\xi\langle a_j^\dagger a_k \sigma_-^{fg}\rangle \\
-\mathcal{E}_j^{(a)^*}\xi\langle a_k b_l \sigma_+^{fg}\rangle - \mathcal{E}_k^{(a)}\langle a_j^\dagger b_l \sigma^{ee}\rangle - \mathcal{E}_l^{(b)}\langle a_j^\dagger a_k \sigma^{ee}\rangle \\
\Gamma\xi^2\langle a_j^\dagger a_k b_l\rangle - \mathcal{E}_j^{(a)^*}\xi\langle a_k b_l \sigma_+^{fe}\rangle - \mathcal{E}_k^{(a)}\xi\langle a_j^\dagger b_l \sigma_-^{fe}\rangle - \mathcal{E}_l^{(b)}\xi\langle a_j^\dagger a_k \sigma_-^{fe}\rangle \\
i\xi\tfrac{\Omega}{2}\langle a_j^\dagger a_k b_l\rangle - \mathcal{E}_j^{(a)^*}\xi(\langle a_k b_l\rangle - \langle a_k b_l \sigma^{gg}\rangle - \langle a_k b_l \sigma^{ee}\rangle) \\
-i\xi\tfrac{\Omega}{2}\langle a_j^\dagger a_k b_l\rangle - \mathcal{E}_k^{(a)}\xi\Big(\langle a_j^\dagger a_k\rangle - \langle a_j^\dagger b_l \sigma^{gg}\rangle - \langle a_j^\dagger b_l \sigma^{ee}\rangle\Big) - \mathcal{E}_l^{(b)}\xi\Big(\langle a_j^\dagger b_l\rangle - \langle a_j^\dagger a_k \sigma^{gg}\rangle - \langle a_j^\dagger a_k \sigma^{ee}\rangle\Big) \\
-\mathcal{E}_j^{(a)^*}\langle a_k b_l \sigma_-^{fe}\rangle \\
-\mathcal{E}_k^{(a)}\langle a_j^\dagger b_l \sigma_+^{fe}\rangle - \mathcal{E}_l^{(b)}\langle a_j^\dagger a_k \sigma_-^{fe}\rangle
\end{pmatrix}, \tag{F.11a}$$

$$\frac{\mathrm{d}}{\mathrm{d}t}\langle b_j^\dagger b_k a_l \boldsymbol{\sigma}\rangle = \boldsymbol{M}_{jkl}^{(b^\dagger b a)}\langle b_j^\dagger b_k a_l \boldsymbol{\sigma}\rangle$$
$$+\begin{pmatrix}
-\mathcal{E}_j^{(b)^*}\langle b_k a_l \sigma_+^{eg}\rangle - \mathcal{E}_k^{(b)}\langle b_j^\dagger a_l \sigma_-^{eg}\rangle - \mathcal{E}_l^{(a)}\langle b_j^\dagger b_k \sigma_-^{eg}\rangle \\
-\mathcal{E}_j^{(b)^*}\langle b_k a_l \sigma^{ee}\rangle - \mathcal{E}_k^{(b)}\xi\langle b_j^\dagger a_l \sigma_-^{fg}\rangle - \mathcal{E}_l^{(a)}\xi\langle b_j^\dagger b_k \sigma_-^{fg}\rangle \\
-\mathcal{E}_j^{(b)^*}\xi\langle b_k a_l \sigma_+^{fg}\rangle - \mathcal{E}_k^{(b)}\langle b_j^\dagger a_l \sigma^{ee}\rangle - \mathcal{E}_l^{(a)}\langle b_j^\dagger b_k \sigma^{ee}\rangle \\
\Gamma\xi^2\langle b_j^\dagger b_k a_l\rangle - \mathcal{E}_j^{(b)^*}\xi\langle b_k a_l \sigma_+^{fe}\rangle - \mathcal{E}_k^{(b)}\xi\langle b_j^\dagger a_l \sigma_-^{fe}\rangle - \mathcal{E}_l^{(a)}\xi\langle b_j^\dagger b_k \sigma_-^{fe}\rangle \\
i\xi\tfrac{\Omega}{2}\langle b_j^\dagger b_k a_l\rangle - \mathcal{E}_j^{(b)^*}\xi(\langle b_k a_l\rangle - \langle b_k a_l \sigma^{gg}\rangle - \langle b_k a_l \sigma^{ee}\rangle) \\
-i\xi\tfrac{\Omega}{2}\langle b_j^\dagger b_k a_l\rangle - \mathcal{E}_k^{(b)}\xi\Big(\langle b_j^\dagger b_k\rangle - \langle b_j^\dagger a_l \sigma^{gg}\rangle - \langle b_j^\dagger a_l \sigma^{ee}\rangle\Big) - \mathcal{E}_l^{(a)}\xi\Big(\langle b_j^\dagger a_l\rangle - \langle b_j^\dagger b_k \sigma^{gg}\rangle - \langle b_j^\dagger b_k \sigma^{ee}\rangle\Big) \\
-\mathcal{E}_j^{(b)^*}\langle b_k a_l \sigma_-^{fe}\rangle \\
-\mathcal{E}_k^{(b)}\langle b_j^\dagger a_l \sigma_+^{fe}\rangle - \mathcal{E}_l^{(a)}\langle b_j^\dagger b_k \sigma_-^{fe}\rangle
\end{pmatrix}, \tag{F.11b}$$

$$\frac{\mathrm{d}}{\mathrm{d}t}\langle b_j^\dagger a_k^\dagger a_l \boldsymbol{\sigma}\rangle = \boldsymbol{M}_{jkl}^{(b^\dagger a^\dagger a)}\langle b_j^\dagger a_k^\dagger a_l \boldsymbol{\sigma}\rangle$$
$$+\begin{pmatrix}
-\mathcal{E}_j^{(b)^*}\langle a_k^\dagger a_l \sigma_+^{eg}\rangle - \mathcal{E}_k^{(a)^*}\langle b_j^\dagger a_l \sigma_+^{eg}\rangle - \mathcal{E}_l^{(a)}\langle b_j^\dagger a_k^\dagger \sigma_-^{eg}\rangle \\
-\mathcal{E}_j^{(b)^*}\langle a_k^\dagger a_l \sigma^{ee}\rangle - \mathcal{E}_k^{(a)^*}\langle b_j^\dagger a_l \sigma^{ee}\rangle - \mathcal{E}_l^{(a)}\xi\langle b_j^\dagger a_k^\dagger \sigma_-^{fg}\rangle \\
-\mathcal{E}_j^{(b)^*}\xi\langle a_k^\dagger a_l \sigma_+^{fg}\rangle - \mathcal{E}_k^{(a)^*}\xi\langle b_j^\dagger a_l \sigma_+^{fg}\rangle - \mathcal{E}_l^{(a)}\langle b_j^\dagger a_k^\dagger \sigma^{ee}\rangle \\
\Gamma\xi^2\langle b_j^\dagger a_k^\dagger a_l\rangle - \mathcal{E}_j^{(b)^*}\xi\langle a_k^\dagger a_l \sigma_+^{fe}\rangle - \mathcal{E}_k^{(a)^*}\xi\langle b_j^\dagger a_l \sigma_+^{fe}\rangle - \mathcal{E}_l^{(a)}\xi\langle b_j^\dagger a_k^\dagger \sigma_-^{fe}\rangle \\
i\xi\tfrac{\Omega}{2}\langle b_j^\dagger a_k^\dagger a_l\rangle - \mathcal{E}_j^{(b)^*}\xi\Big(\langle a_k^\dagger a_l\rangle - \langle a_k^\dagger a_l \sigma^{gg}\rangle - \langle a_k^\dagger a_l \sigma^{ee}\rangle\Big) - \mathcal{E}_k^{(a)^*}\xi\Big(\langle b_j^\dagger a_l\rangle - \langle b_j^\dagger a_l \sigma^{gg}\rangle - \langle b_j^\dagger a_l \sigma^{ee}\rangle\Big) \\
-i\xi\tfrac{\Omega}{2}\langle b_j^\dagger a_k^\dagger a_l\rangle - \mathcal{E}_l^{(a)}\xi\Big(\langle b_j^\dagger a_k^\dagger\rangle - \langle b_j^\dagger a_k^\dagger \sigma^{gg}\rangle - \langle b_j^\dagger a_k^\dagger \sigma^{ee}\rangle\Big) \\
-\mathcal{E}_j^{(b)^*}\langle a_k^\dagger a_l \sigma_-^{fe}\rangle - \mathcal{E}_k^{(a)^*}\langle b_j^\dagger a_l \sigma_-^{fe}\rangle \\
-\mathcal{E}_l^{(a)}\langle b_j^\dagger a_k^\dagger \sigma_+^{fe}\rangle
\end{pmatrix}, \tag{F.11c}$$

$$\frac{\mathrm{d}}{\mathrm{d}t}\langle a_j^\dagger b_k^\dagger b_l \boldsymbol{\sigma}\rangle = \boldsymbol{M}_{jkl}^{(a^\dagger b^\dagger b)}\langle a_j^\dagger b_k^\dagger b_l \boldsymbol{\sigma}\rangle$$
$$+\begin{pmatrix}
-\mathcal{E}_j^{(a)^*}\langle b_k^\dagger b_l \sigma_+^{eg}\rangle - \mathcal{E}_k^{(b)^*}\langle a_j^\dagger b_l \sigma_+^{eg}\rangle - \mathcal{E}_l^{(b)}\langle a_j^\dagger b_k^\dagger \sigma_-^{eg}\rangle \\
-\mathcal{E}_j^{(a)^*}\langle b_k^\dagger b_l \sigma^{ee}\rangle - \mathcal{E}_k^{(b)^*}\langle a_j^\dagger b_l \sigma^{ee}\rangle - \mathcal{E}_l^{(b)}\xi\langle a_j^\dagger b_k^\dagger \sigma_-^{fg}\rangle \\
-\mathcal{E}_j^{(a)^*}\xi\langle b_k^\dagger b_l \sigma_+^{fg}\rangle - \mathcal{E}_k^{(b)^*}\xi\langle a_j^\dagger b_l \sigma_+^{fg}\rangle - \mathcal{E}_l^{(b)}\langle a_j^\dagger b_k^\dagger \sigma^{ee}\rangle \\
\Gamma\xi^2\langle a_j^\dagger b_k^\dagger b_l\rangle - \mathcal{E}_j^{(a)^*}\xi\langle b_k^\dagger b_l \sigma_+^{fe}\rangle - \mathcal{E}_k^{(b)^*}\xi\langle a_j^\dagger b_l \sigma_+^{fe}\rangle - \mathcal{E}_l^{(b)}\xi\langle a_j^\dagger b_k^\dagger \sigma_-^{fe}\rangle \\
i\xi\tfrac{\Omega}{2}\langle a_j^\dagger b_k^\dagger b_l\rangle - \mathcal{E}_j^{(a)^*}\xi\Big(\langle b_k^\dagger b_l\rangle - \langle b_k^\dagger b_l \sigma^{gg}\rangle - \langle b_k^\dagger b_l \sigma^{ee}\rangle\Big) - \mathcal{E}_k^{(b)^*}\xi\Big(\langle a_j^\dagger b_l\rangle - \langle a_j^\dagger b_l \sigma^{gg}\rangle - \langle a_j^\dagger b_l \sigma^{ee}\rangle\Big) \\
-i\xi\tfrac{\Omega}{2}\langle a_j^\dagger b_k^\dagger b_l\rangle - \mathcal{E}_l^{(b)}\xi\Big(\langle a_j^\dagger b_k^\dagger\rangle - \langle a_j^\dagger b_k^\dagger \sigma^{gg}\rangle - \langle a_j^\dagger b_k^\dagger \sigma^{ee}\rangle\Big) \\
-\mathcal{E}_j^{(a)^*}\langle b_k^\dagger b_l \sigma_-^{fe}\rangle - \mathcal{E}_k^{(b)^*}\langle a_j^\dagger b_l \sigma_-^{fe}\rangle \\
-\mathcal{E}_l^{(b)}\langle a_j^\dagger b_k^\dagger \sigma_+^{fe}\rangle
\end{pmatrix}. \tag{F.11d}$$

with

$$\boldsymbol{M}^{(a^\dagger ab)}_{jkl} = \boldsymbol{M}^{(\boldsymbol{\sigma})} - \left[2\kappa_a + \kappa_b - i\left(\Delta\omega_j^{(a)} - \Delta\omega_k^{(a)} - \Delta\omega_l^{(b)}\right)\right]\mathbb{1}, \tag{F.12a}$$

$$\boldsymbol{M}^{(b^\dagger ba)}_{jkl} = \boldsymbol{M}^{(\boldsymbol{\sigma})} - \left[\kappa_a + 2\kappa_b - i\left(\Delta\omega_j^{(b)} - \Delta\omega_k^{(b)} - \Delta\omega_l^{(a)}\right)\right]\mathbb{1}, \tag{F.12b}$$

$$\boldsymbol{M}^{(b^\dagger a^\dagger a)}_{jkl} = \boldsymbol{M}^{(\boldsymbol{\sigma})} - \left[2\kappa_a + \kappa_b - i\left(\Delta\omega_j^{(b)} + \Delta\omega_k^{(a)} - \Delta\omega_l^{(a)}\right)\right]\mathbb{1}, \tag{F.12c}$$

$$\boldsymbol{M}^{(a^\dagger b^\dagger b)}_{jkl} = \boldsymbol{M}^{(\boldsymbol{\sigma})} - \left[\kappa_a + 2\kappa_b - i\left(\Delta\omega_j^{(a)} + \Delta\omega_k^{(b)} - \Delta\omega_l^{(b)}\right)\right]\mathbb{1}. \tag{F.12d}$$

F.1.8 Fourth-order: Filter

$$\begin{aligned}\frac{\mathrm{d}}{\mathrm{d}t}\langle a_j^\dagger b_k^\dagger b_l a_m\rangle = &-\left[2\kappa_a + 2\kappa_b - i\left(\Delta\omega_j^{(a)} + \Delta\omega_k^{(b)}\right) + i\left(\Delta\omega_l^{(b)} + \Delta\omega_m^{(a)}\right)\right]\langle a_j^\dagger b_k^\dagger b_l a_m\rangle \\ &- \mathcal{E}_j^{(a)*}\langle b_k^\dagger b_l a_m \sigma_+^{eg}\rangle - \mathcal{E}_k^{(b)*}\langle a_j^\dagger a_m b_l \sigma_+^{eg}\rangle \\ &- \mathcal{E}_l^{(b)}\langle b_k^\dagger a_j^\dagger a_m \sigma_-^{eg}\rangle - \mathcal{E}_m^{(a)}\langle a_j^\dagger b_k^\dagger b_l \sigma_-^{eg}\rangle.\end{aligned} \tag{F.13}$$

F.2 Filtered Cross-Correlation Function

The second-order cross-correlation function for the filtered output field is given by

$$G^{(2)}(\alpha, t; \beta, t+\tau) = \langle A^\dagger(t) B^\dagger B(t+\tau) A(t)\rangle = \sum_{j,k=-N}^{N} \langle A^\dagger(t) b_k^\dagger b_l(t+\tau) A(t)\rangle. \tag{F.14}$$

We use the quantum regression equations to solve for this with the following moment equations:

$$\frac{\mathrm{d}}{\mathrm{d}\tau}\langle A^\dagger(t)\boldsymbol{\Sigma}(t+\tau)A(t)\rangle = \boldsymbol{M}^{(\Sigma)}\langle A^\dagger(t)\boldsymbol{\sigma}(t+\tau)A(t)\rangle + \begin{pmatrix} 0 \\ 0 \\ 0 \\ \Gamma\xi^2\langle A^\dagger A(t)\rangle \\ i\xi\frac{\Omega}{2}\langle A^\dagger A(t)\rangle \\ -i\xi\frac{\Omega}{2}\langle A^\dagger A(t)\rangle \\ 0 \\ 0 \end{pmatrix}, \tag{F.15a}$$

and

$$\begin{aligned}\frac{\mathrm{d}}{\mathrm{d}\tau}\langle A^\dagger(t) b_j(t+\tau)A(t)\rangle = &-\left(\kappa_b + i\Delta\omega_j^{(b)}\right)\langle A^\dagger(t) b_j(t+\tau)A(t)\rangle \\ &- \mathcal{E}_j^{(b)}\left(\langle A^\dagger(t)\sigma_-^{eg}(t+\tau)A(t)\rangle + \xi\langle A^\dagger(t)\sigma_-^{eg}(t+\tau)A(t)\rangle\right),\end{aligned} \tag{F.15b}$$

$$\begin{aligned}\frac{\mathrm{d}}{\mathrm{d}\tau}\langle A^\dagger(t) b_j^\dagger(t+\tau)A(t)\rangle = &-\left(\kappa_b - i\Delta\omega_j^{(b)}\right)\langle A^\dagger(t) b_j^\dagger(t+\tau)A(t)\rangle \\ &- \mathcal{E}_j^{(b)*}\left(\langle A^\dagger(t)\sigma_+^{eg}(t+\tau)A(t)\rangle + \xi\langle A^\dagger(t)\sigma_+^{eg}(t+\tau)A(t)\rangle\right),\end{aligned} \tag{F.15c}$$

and

$$\frac{\mathrm{d}}{\mathrm{d}\tau}\langle A^\dagger(t) b_j \mathbf{\Sigma}(t+\tau) A(t)\rangle = \boldsymbol{M}_j^{(b)} \langle A^\dagger(t) b_j \mathbf{\Sigma}(t+\tau) A(t)\rangle + \begin{pmatrix} -\mathcal{E}_j^{(b)} \langle A^\dagger(t)\sigma_-^{eg}(t+\tau)A(t)\rangle \\ -\mathcal{E}_j^{(b)} \xi \langle A^\dagger(t)\sigma_-^{fg}(t+\tau)A(t)\rangle \\ -\mathcal{E}_j^{(b)} \langle A^\dagger(t)\sigma^{ee}(t+\tau)A(t)\rangle \\ \Gamma\xi^2 \langle A^\dagger(t) b_j(t+\tau)A(t)\rangle - \mathcal{E}_j^{(b)} \xi \langle A^\dagger(t)\sigma_-^{fe}(t+\tau)A(t)\rangle \\ i\xi\frac{\Omega}{2}\langle A^\dagger(t) b_j(t+\tau)A(t)\rangle \\ -i\xi\frac{\Omega}{2}\langle A^\dagger(t) b_j(t+\tau)A(t)\rangle - \mathcal{E}_j^{(b)}\xi\big(1-\langle A^\dagger(t)\sigma^{gg}(t+\tau)A(t)\rangle - \langle A^\dagger(t)\sigma^{ee}(t+\tau)A(t)\rangle\big) \\ 0 \\ -\mathcal{E}_j^{(b)} \langle A^\dagger(t)\sigma_+^{fe}(t+\tau)A(t)\rangle \end{pmatrix}, \tag{F.15d}$$

$$\frac{\mathrm{d}}{\mathrm{d}\tau}\langle A^\dagger(t) b_j^\dagger \mathbf{\Sigma}(t+\tau) A(t)\rangle = \boldsymbol{M}_j^{(b^\dagger)} \langle A^\dagger(t) b_j^\dagger \mathbf{\Sigma}(t+\tau) A(t)\rangle + \begin{pmatrix} -\mathcal{E}_j^{(b)^*} \langle A^\dagger(t)\sigma_+^{eg}(t+\tau)A(t)\rangle \\ -\mathcal{E}_j^{(b)^*} \langle A^\dagger(t)\sigma^{ee}(t+\tau)A(t)\rangle \\ -\mathcal{E}_j^{(b)^*} \xi \langle A^\dagger(t)\sigma_+^{fg}(t+\tau)A(t)\rangle \\ \Gamma\xi^2 \langle A^\dagger(t) b_j^\dagger(t+\tau)A(t)\rangle - \mathcal{E}_j^{(b)^*} \xi \langle A^\dagger(t)\sigma_+^{fe}(t+\tau)A(t)\rangle \\ i\xi\frac{\Omega}{2}\langle A^\dagger(t) b_j^\dagger(t+\tau)A(t)\rangle - \mathcal{E}_j^{(b)^*}\xi\big(1-\langle A^\dagger(t)\sigma^{gg}(t+\tau)A(t)\rangle - \langle A^\dagger(t)\sigma^{ee}(t+\tau)A(t)\rangle\big) \\ -i\xi\frac{\Omega}{2}\langle A^\dagger(t) b_j^\dagger(t+\tau)A(t)\rangle \\ -\mathcal{E}_j^{(b)^*} \langle A^\dagger(t)\sigma_-^{fe}(t+\tau)A(t)\rangle \\ 0 \end{pmatrix}, \tag{F.15e}$$

and

$$\begin{aligned}\frac{\mathrm{d}}{\mathrm{d}\tau}\langle A^\dagger(t) b_j^\dagger b_k(t+\tau) A(t)\rangle = &-\left[2\kappa_b - i\left(\Delta\omega_j^{(b)} - \Delta\omega_k^{(b)}\right)\right]\langle A^\dagger(t) b_j^\dagger b_k(t+\tau)A(t)\rangle \\ &- \mathcal{E}_j^{(b)^*}\left(\langle A^\dagger(t) b_k \sigma_+^{eg}(t+\tau)A(t)\rangle + \xi\langle A^\dagger(t) b_k \sigma_+^{fe}(t+\tau)A(t)\rangle\right) \\ &- \mathcal{E}_k^{(b)}\left(\langle A^\dagger(t) b_j^\dagger \sigma_-^{eg}(t+\tau)A(t)\rangle + \xi\langle A^\dagger(t) b_j^\dagger \sigma_-^{fe}(t+\tau)A(t)\rangle\right)\end{aligned} \tag{F.15f}$$

We solve these differential equations with the initial conditions at $\tau = 0$,

$$\langle A^\dagger \mathbf{\Sigma} A(t)\rangle = \sum_{j,m=-N}^{N} \langle a_j^\dagger a_m \mathbf{\Sigma}(t)\rangle, \tag{F.16a}$$

$$\langle A^\dagger b_k^\dagger A(t)\rangle = \sum_{j,m=-N}^{N} \langle b_k^\dagger a_j^\dagger a_m(t)\rangle, \tag{F.16b}$$

$$\langle A^\dagger b_l A(t)\rangle = \sum_{j,m=-N}^{N} \langle a_j^\dagger a_m(t) b_l\rangle, \tag{F.16c}$$

$$\langle A^\dagger b_k^\dagger \mathbf{\Sigma} A(t)\rangle = \sum_{j,m=-N}^{N} \langle b_k^\dagger a_j^\dagger a_m \mathbf{\Sigma}(t)\rangle, \tag{F.16d}$$

$$\langle A^\dagger b_l \mathbf{\Sigma} A(t)\rangle = \sum_{j,m=-N}^{N} \langle a_j^\dagger a_m b_l \mathbf{\Sigma}(t)\rangle, \tag{F.16e}$$

$$\langle A^\dagger b_k^\dagger b_l A(t)\rangle = \sum_{j,m=-N}^{N} \langle a_j^\dagger b_k^\dagger b_l a_m(t)\rangle. \tag{F.16f}$$

References

1. Mollow, B. R. "Pure-state analysis of resonant light scattering: Radiative damping, saturation, and multiphoton effects". *Phys. Rev. A* **12,** 1919 (1975) (cit. on pp. 1, 47, 56).
2. Mollow, B. R. "Power spectrum of light scattered by two-level systems". *Phys. Rev.* **188,** 1969 (1969) (cit. on pp. 1, 47, 56).
3. Wu, F. Y., Grove, R. E. & Ezekiel, S. "Investigation of the spectrum of resonance fluorescence induced by a monochromatic field". *Phys. Rev. Lett.* **35,** 1426 (1975) (cit. on pp. 1, 47).
4. Cohen-Tannoudji, C. & Reynaud, S. "Dressed-atom description of resonance fluorescence and absorption spectra of a multi-level atom in an intense laser beam". *J. Phys. B: At. Mol. Phys.* **10,** 345 (1977) (cit. on pp. 1, 47, 56).
5. Cohen-Tannoudji, C., Reynaud, S., Bullough, R. K. & Vaughan, J. M. "Atoms in strong light-fields: Photon antibunching in single atom fluorescence". *Philos. Trans. Royal Soc. A* **293,** 223 (1979) (cit. on p. 1).
6. Kimble, H. J. & Mandel, L. "Theory of resonance fluorescence". *Phys. Rev. A* **13,** 2123 (1976) (cit. on pp. 1, 47).
7. Glauber, R. J. "The quantum theory of optical coherence". *Phys. Rev.* **130,** 2529 (1963) (cit. on pp. 1, 16, 23).
8. Glauber, R. J. "Photon correlations". *Phys. Rev. Lett.* **10,** 84 (1963) (cit. on pp. 1, 23, 58).
9. Walls, D. F. "Evidence for the quantum nature of light". *Nature* **280,** 451 (1979) (cit. on pp. 1, 47, 58).
10. Carmichael, H. J. & Walls, D. F. "A quantum-mechanical master equation treatment of the dynamical Stark effect". *J. Phys. B: At. Mol. Phys.* **9,** 1199 (1976) (cit. on pp. 1, 47).
11. Carmichael, H. J. & Walls, D. F. "Proposal for the measurement of the resonant Stark effect by photon correlation techniques". *J. Phys. B: At. Mol. Phys.* **9,** L43 (1976) (cit. on pp. 1, 47).
12. Kimble, H. J., Dagenais, M. & Mandel, L. "Photon antibunching in resonance fluorescence". *Phys. Rev. Lett.* **39,** 691 (1977) (cit. on pp. 1, 58).
13. Eberly, J. H. & Wódkiewicz, K. "The time-dependent physical spectrum of light". *J. Opt. Soc. Am.* **67,** 1252 (1977) (cit. on p. 1).
14. Arnoldus, H. F. & Nienhuis, G. "Photon correlations between the lines in the spectrum of resonance fluorescence". *J. Phys. B: At. Mol. Phys.* **17,** 963 (1984) (cit. on pp. 1, 65, 91).

15. Knöll, L., Weber, G. & Schafer, T. "Theory of time-resolved correlation spectroscopy and its application to resonance fluorescence radiation". *J. Phys. B: At. Mol. Phys.* **17,** 4861 (1984) (cit. on pp. 1, 65, 91).

16. Van Enk, S. J. "Time-dependent spectrum of a single photon and its positive-operator-valued measure". *Phys. Rev. A* **96,** 033834 (2017) (cit. on p. 1).

17. Shatokhin, V. N. & Kilin, S. J. "Second-order coherence and state reduction in resonance fluorescence with spectral resolution". *Opt. Commun.* **174,** 157 (2000) (cit. on pp. 1, 87).

18. Knöll, L., Vogel, W. & Welsch, D.-G. "Quantum noise in spectral filtering of light". *J. Opt. Soc. Am. B* **3,** 1315 (1986) (cit. on p. 1).

19. Cresser, J. D. "Intensity correlations of frequency-filtered light fields". *J. Phys. B: At. Mol. Phys.* **20,** 4915 (1987) (cit. on pp. 1, 65).

20. Knöll, L., Vogel, W. & Welsch, D.-G. "Spectral properties of light in quantum optics". *Phys. Rev. A* **42,** 503 (1990) (cit. on p. 1).

21. Apanasevich, P. A. & Kilin, S. J. "Light-induced correlations in spontaneous emission". *Phys. Lett. A* **62,** 83 (1977) (cit. on p. 1).

22. Apanasevich, P. A. & Kilin, S. J. "Multitime correlation in scattering and fluorescence". *J. Appl. Spectrosc.* **29,** 931 (1978) (cit. on p. 1).

23. Apanasevich, P. A. & Kilin, S. J. "Photon bunching and antibunching in resonance fluorescence". *J. Phys. B: At. Mol. Phys.* **12,** L83 (1979) (cit. on pp. 1, 59, 91).

24. Aspect, A., Roger, G., Reynaud, S., Dalibard, J. & Cohen-Tannoudji, C. "Time correlations between the two sidebands of the resonance fluorescence triplet". *Phys. Rev. Lett.* **45,** 617 (1980) (cit. on pp. 1, 65).

25. Apanasevich, P. A., Kilin, S. J. & Fedorov, A. F. "Photon correlation in resonance scattering – a new approach to the investigation of the excited states of atoms and molecules". *J. Phys. B: At. Mol. Phys.* **18,** L55 (1985) (cit. on p. 1).

26. Schrama, C. A., Nienhuis, G., Dijkerman, H. A., Steijsiger, C. & Heideman, H. G. M. "Destructive interference between opposite time orders of photon emission". *Phys. Rev. Lett.* **67,** 2443 (1991) (cit. on pp. 1, 90–91, 119).

27. Schrama, C. A., Nienhuis, G., Dijkerman, H. A., Steijsiger, C. & Heideman, H. G. M. "Intensity correlations between the components of the resonance fluorescence triplet". *Phys. Rev. A* **45,** 8045 (1992) (cit. on pp. 1, 65, 90–91, 119, 126–127).

28. Aichele, T., Reinaudi, G. & Benson, O. "Separating cascaded photons from a single quantum dot: Demonstration of multiplexed quantum cryptography". *Phys. Rev. B* **70,** 235329 (2004) (cit. on p. 1).

29. Ulhaq, A. *et al.* "Cascaded single-photon emission from the Mollow triplet sidebands of a quantum dot". *Nat. Photonics* **6,** 238 (2012) (cit. on pp. 1, 91).

30. Peiris, M. *et al.* "Two-color photon correlations of the light scattered by a quantum dot". *Phys. Rev. B* **91,** 195125 (2015) (cit. on pp. 1, 94–95).

31. Silva, B. *et al.* "The colored Hanbury Brown–Twiss effect". *Sci. Rep.* **6,** 37980 (2016) (cit. on p. 1).
32. Peiris, M., Konthasinghe, K. & Muller, A. "Franson interference generated by a two-level system". *Phys. Rev. Lett.* **118,** 030501 (2017) (cit. on pp. 1, 128).
33. Schleibner, J. *et al.* "Suppressed antibunching via spectral filtering: An analytical study in the two-photon Mollow regime". *Phys. Rev. A* **99,** 023813 (2019) (cit. on p. 1).
34. Phillips, C. L. *et al.* "Photon statistics of filtered resonance fluorescence". *Phys. Rev. Lett.* **125,** 043603 (2020) (cit. on pp. 1, 58, 65, 84).
35. Hanschke, L. *et al.* "Origin of antibunching in resonance fluorescence". *Phys. Rev. Lett.* **125,** 170402 (2020) (cit. on pp. 1, 58, 65, 84).
36. Nieves, Y. & Muller, A. "Third-order photon cross-correlations in resonance fluorescence". *Phys. Rev. B* **102,** 155418 (2020) (cit. on p. 1).
37. Shatokhin, V. N. & Kilin, S. J. "Correlation measurements in resonance fluorescence with spectral resolution and atomic inversion via detection of a spectrally filtered photon". *Phys. Rev. A* **63,** 023803 (2001) (cit. on p. 1).
38. Ng, B. L., Chow, C. H. & Kurtsiefer, C. "Observation of the Mollow triplet from an optically confined single atom". *Phys. Rev. A* **106,** 063719 (2022) (cit. on pp. 1, 65).
39. Nienhuis, G. "Spectral correlations in resonance fluorescence". *Phys. Rev. A* **47,** 510 (1993) (cit. on pp. 1, 35, 43, 86).
40. Nienhuis, G. "Spectral correlations within the fluorescence triplet". *Europhys. Lett.* **21,** 285 (1993) (cit. on pp. 1, 89).
41. Joosten, K. & Nienhuis, G. "Influence of spectral filtering on the quantum nature of light". *J. Opt. B: Quantum Semiclassical Opt.* **2,** 158 (2000) (cit. on pp. 1, 86, 89).
42. Cresser, J. D. "Theory of the spectrum of the quantised light field". *Phys. Rep.* **94,** 47 (1983) (cit. on p. 1).
43. del Valle, E., Gonzalez-Tudela, A., Laussy, F. P., Tejedor, C. & Hartmann, M. J. "Theory of frequency-filtered and time-resolved N-photon correlations". *Phys. Rev. Lett.* **109,** 183601 (2012) (cit. on pp. 1–2, 65).
44. del Valle, E., Gonzalez-Tudela, A., Laussy, F. P., Tejedor, C. & Hartmann, M. J. "Erratum: Theory of frequency-filtered and time-resolved N-photon correlations". *Phys. Rev. Lett.* **116,** 249902 (2016) (cit. on p. 1).
45. del Valle, E. "Distilling one, two and entangled pairs of photons from a quantum dot with cavity QED effects and spectral filtering". *New J. Phys.* **15,** 025019 (2013) (cit. on pp. 2, 94).
46. Gonzalez-Tudela, A., Laussy, F. P., Tejedor, C., Hartmann, M. J. & del Valle, E. "Two-photon spectra of quantum emitters". *New J. Phys.* **15,** 033036 (2013) (cit. on pp. 2, 84, 86, 93–94).
47. Muñoz, C. S., del Valle, E., Tejedor, C. & Laussy, F. P. "Violation of classical inequalities by photon frequency filtering". *Phys. Rev. A* **90,** 052111 (2014) (cit. on pp. 2, 93).

48. González-Tudela, A., del Valle, E. & Laussy, F. P. "Optimization of photon correlations by frequency filtering". *Phys. Rev. A* **91,** 043807 (2015) (cit. on pp. 2, 84, 93).

49. Muñoz, C. S., Laussy, F. P., Tejedor, C. & del Valle, E. "Enhanced two-photon emission from a dressed biexciton". *New J. Phys.* **17,** 123021 (2015) (cit. on p. 2).

50. Darsheshdar, E., Hugbart, M., Bachelard, R. & Villas-Boas, C. J. "Photon-photon correlations from a pair of strongly coupled two-level emitters". *Phys. Rev. A* **103,** 053702 (2021) (cit. on p. 2).

51. Laussy, F. P. "A new way to correlate photons". *Nat. Mater.* **16,** 398 (2017) (cit. on pp. 2, 93).

52. Holland, M. "Unraveling quantum dissipation in the frequency domain". *Phys. Rev. Lett.* **81,** 5117 (1998) (cit. on p. 2).

53. Carreño, J. C. L., del Valle, E. & Laussy, F. P. "Frequency-resolved Monte Carlo". *Sci. Rep.* **8,** 6975 (2018) (cit. on p. 2).

54. Bel, G. & Brown, F. L. H. "Theory for wavelength-resolved photon emission statistics in single-molecule fluorescence spectroscopy". *Phys. Rev. Lett.* **102,** 018303 (2009) (cit. on p. 2).

55. Holdaway, D. I. H., Notararigo, V. & Olaya-Castro, A. "Perturbation approach for computing frequency- and time-resolved photon correlation functions". *Phys. Rev. A* **98,** 063828 (2018) (cit. on p. 2).

56. Shatokhin, V. N. & Kilin, S. J. "Correlation functions in resonance fluorescence with spectral resolution: Signal-processing approach". *Phys. Rev. A* **94,** 033835 (2016) (cit. on pp. 2, 91).

57. Kamide, K., Iwamoto, S. & Arakawa, Y. "Eigenvalue decomposition method for photon statistics of frequency-filtered fields and its application to quantum dot emitters". *Phys. Rev. A* **92,** 033833 (2015) (cit. on pp. 2, 86).

58. Clauser, M. J. "Relaxation effects in spectra: Eigenvalue treatment of superoperators". *Phys. Rev. B* **3,** 3748 (1971) (cit. on p. 2).

59. Carmichael, H. J. "Quantum trajectory theory for cascaded open systems". *Phys. Rev. Lett.* **70,** 2273 (1993) (cit. on pp. 2, 25).

60. Gardiner, C. W. "Driving a quantum system with the output field from another driven quantum system". *Phys. Rev. Lett.* **70,** 2269 (1993) (cit. on pp. 2, 25).

61. Peng, Z.-a., Yang, G.-q., Wu, Q.-l. & Li, G.-x. "Monitoring for time ordering and time asymmetry of spectral correlations in filtered resonance fluorescence generated from a Λ-type atomic system". *Phys. Rev. A* **98,** 043828 (2018) (cit. on p. 2).

62. Peng, Z.-a., Yang, G.-q., Wu, Q.-l. & Li, G.-x. "Filtered strong quantum correlation of resonance fluorescence from a two-atom radiating system with interatomic coherence". *Phys. Rev. A* **99,** 033819 (2019) (cit. on p. 2).

63. Lax, M. "Formal theory of quantum fluctuations from a driven state". *Phys. Rev.* **129,** 2342 (1963) (cit. on pp. 2, 24–25).

64. Lax, M. "Quantum noise X. Density-matrix treatment of field and population-difference fluctuations". *Phys. Rev.* **157,** 213 (1967) (cit. on pp. 2, 24).

65. Gasparinetti, S. *et al.* "Correlations and entanglement of microwave photons emitted in a cascade decay". *Phys. Rev. Lett.* **119,** 140504 (2017) (cit. on pp. 4, 97–98, 119).

66. Gasparinetti, S. *et al.* "Two-photon resonance fluorescence of a ladder-type atomic system". *Phys. Rev. A* **100,** 033802 (2019) (cit. on pp. 4, 97–98).

67. Heisenberg, W. "Über quantentheoretische umdeutung kinematischer und mechanischer beziehungen". *Z. Phys.* **33,** 879 (1925) (cit. on p. 7).

68. Schrödinger, E. "Quantisierung als eigenwertproblem". *Ann. Phys.* **384,** 361 (1926) (cit. on p. 7).

69. Dirac, P. A. M. "On the theory of quantum mechanics". *Proc. R. Soc. Lond. A.* **112,** 661 (1926) (cit. on p. 7).

70. Dirac, P. A. M. "The quantum theory of the emission and absorption of radiation". *Proc. R. Soc. Lond. A.* **114,** 243 (1927) (cit. on pp. 7, 20).

71. Sakurai, J. J. & Napolitano, J. *Modern Quantum Mechanics* 2nd ed. (Pearson Education Inc., 2017) (cit. on pp. 7, 9).

72. Louisell, W. H. *Quantum Statistical Properties of Radiation* (Wiley, 1990) (cit. on p. 7).

73. Walls, D. F. & Milburn, G. J. *Quantum Optics* 2nd ed. (Springer Berlin Heidelberg, 2008) (cit. on pp. 11, 16, 23, 54, 58).

74. Glauber, R. J. "Coherent and incoherent states of the radiation field". *Phys. Rev.* **131,** 2766 (1963) (cit. on p. 16).

75. Carmichael, H. J. *Statistical Methods in Quantum Optics 1: Master Equations and Fokker-Planck Equations* 2nd ed. (Springer Berlin Heidelberg, 2002) (cit. on pp. 17, 24–25, 51, 53–54, 58).

76. Kolobov, M. I. & Sokolov, I. V. "Quantum theory of light interaction with an optical amplifier". *Opt. Spectrosc.* **62,** 69 (1987) (cit. on p. 25).

77. Carmichael, H. J. *Statistical Methods in Quantum Optics 2: Non-Classical Fields* (Springer Berlin Heidelberg, 2008) (cit. on p. 25).

78. Brooker, G. *Modern Classical Optics* (OUP Oxford, 2003) (cit. on pp. 31, 53, 56).

79. Born, M. & Wolf, E. *Principles of Optics: Electromagnetic Theory of Propagation, Interference and Diffraction of Light* (Elsevier, 2013) (cit. on p. 31).

80. Német, N., White, D., Kato, S., Parkins, S. & Aoki, T. "Transfer-matrix approach to determining the linear response of all-fiber networks of Cavity-QED systems". *Phys. Rev. Appl.* **13,** 064010 (2020) (cit. on p. 31).

81. Campos, R. A., Saleh, B. E. A. & Teich, M. C. "Quantum-mechanical lossless beam splitter: SU(2) symmetry and photon statistics". *Phys. Rev. A* **40,** 1371 (1989) (cit. on p. 31).

82. Smith, S. W. *Digital Signal Processing: A Practical Guide for Engineers and Scientists. a practical guide for engineers and scientists* (Newnes, 2003) (cit. on p. 37).

83. Carreño, J. C. L., Casalengua, E. Z., Silva, B., del Valle, E. & Laussy, F. P. "Loss of antibunching". *Phys. Rev. A* **105,** 023724 (2022) (cit. on pp. 43, 84, 87).

84. Schuda, F., Stroud, C. R. & Hercher, M. "Observation of the resonant Stark effect at optical frequencies". *J. Phys. B: At. Mol. Phys.* **7,** L198 (1974) (cit. on p. 47).

85. Guérin, S., Monti, F., Dupont, J.-M. & Jauslin, H. R. "On the relation between cavity-dressed states, Floquet states, RWA and semiclassical models". *J. Phys. A: Math. Gen.* **30,** 7193 (1997) (cit. on p. 47).

86. Sambe, H. "Steady states and quasienergies of a quantum-mechanical system in an oscillating field". *Phys. Rev. A* **7,** 2203 (1973) (cit. on p. 47).

87. Okuniewicz, J. M. "Quasiperiodic pointwise solutions of the periodic, time-dependent Schrödinger equation". *J. Math. Phys.* **15,** 1587 (1974) (cit. on p. 47).

88. Jaynes, E. T. & Cummings, F. W. "Comparison of quantum and semiclassical radiation theories with application to the beam maser". *Proc. IEEE* **51,** 89 (1963) (cit. on p. 47).

89. Loudon, R. *The Quantum Theory of Light* 1st ed. (OUP Oxford, 1973) (cit. on p. 47).

90. Puri, R. *Mathematical Methods of Quantum Optics* (Springer, Berlin, Heidelberg, 2001) (cit. on pp. 48, 50).

91. Bloch, F. "Nuclear induction". *Phys. Rev.* **70,** 460 (1946) (cit. on p. 51).

92. Hertel, I. V. & Schulz, C. P. *Atoms, Molecules and Optical Physics 2: Molecules and Photons - Spectroscopy and Collisions* (Springer Berlin Heidelberg, 2014) (cit. on p. 53).

93. Wiener, N. "Generalized harmonic analysis". *Acta Math.* **55,** 117 (1930) (cit. on p. 54).

94. Khinchin, A. "Korrelationstheorie der stationären stochastischen prozesse". *Math. Ann.* **109,** 604 (1934) (cit. on p. 54).

95. Hanbury Brown, R. & Twiss, R. Q. "Correlation between photons in two coherent beams of light". *Nature* **177,** 27 (1956) (cit. on p. 56).

96. Hanbury Brown, R. & Twiss, R. Q. "A test of a new type of stellar interferometer on Sirius". *Nature* **178,** 1046 (1956) (cit. on p. 56).

97. Hanbury Brown, R. & Twiss, R. Q. "Interferometry of the intensity fluctuations in light - I. Basic theory: the correlation between photons in coherent beams of radiation". *Proc. R. Soc. Lond. A* **242,** 300 (1957) (cit. on p. 56).

98. Paul, H. "Photon antibunching". *Rev. Mod. Phys.* **54,** 1061 (1982) (cit. on p. 58).

99. Mandel, L. "Squeezed states and sub-Poissonian photon statistics". *Phys. Rev. Lett.* **49,** 136 (1982) (cit. on p. 58).

100. Carmichael, H. J. "Photon antibunching and squeezing for a single atom in a resonant cavity". *Phys. Rev. Lett.* **55,** 2790 (1985) (cit. on p. 58).

101. Phillips, C. L. *et al. Photon statistics of filtered quantum dot resonance fluorescence.* in *Conference on Lasers and Electro-Optics* (Optica Publishing Group, 2021) (cit. on p. 65).

102. Carreño, J. C. L., del Valle, E. & Laussy, F. P. "Photon correlations from the Mollow triplet". *Laser Photonics Rev.* **11,** 1700090 (2017) (cit. on pp. 65, 91, 93–94).

103. Loredo, J. C. *et al.* "Generation of non-classical light in a photon-number superposition". *Nat. Photonics* **13,** 803 (2019) (cit. on p. 65).

104. Fischer, K. A. *et al.* "Signatures of two-photon pulses from a quantum two-level system". *Nat. Phys.* **13,** 649 (2017) (cit. on p. 65).

105. Müller, M., Bounouar, S., Jöns, K. D., Glässl, M. & Michler, P. "On-demand generation of indistinguishable polarization-entangled photon pairs". *Nat. Photonics* **8,** 224 (2014) (cit. on p. 65).

106. Wang, H. *et al.* "Near-transform-limited single photons from an efficient solid-state quantum emitter". *Phys. Rev. Lett.* **116,** 213601 (2016) (cit. on p. 65).

107. Greve, K. D. *et al.* "Quantum-dot spin–photon entanglement via frequency downconversion to telecom wavelength". *Nature* **491,** 421 (2012) (cit. on p. 65).

108. Anderson, E. *et al. LAPACK Users' Guide* Third (Society for Industrial and Applied Mathematics, Philadelphia, PA, 1999) (cit. on p. 70).

109. Runge, C. "Ueber die numerische auflōsung von differentialgleichungen". *Math. Ann.* **46,** 167 (1895) (cit. on p. 71).

110. Kutta, W. "Beitrag zur näherungsweisen integration totaler differentialgleichungen". *Z. Angew. Math. Phys.* **46,** 435 (1901) (cit. on p. 71).

111. Armstrong, J. A. "Theory of interferometric analysis of laser phase noise". *J. Opt. Soc. Am.* **56,** 1024 (1966) (cit. on p. 89).

112. Dalibard, J. & Reynaud, S. "Correlation signals in resonance fluorescence: Interpretation via photon scattering amplitudes". *J. Phys. (Paris)* **44,** 1337 (1983) (cit. on p. 91).

113. Kurpiers, P. *et al.* "Deterministic quantum state transfer and remote entanglement using microwave photons". *Nature* **558,** 264 (2018) (cit. on p. 97).

114. Potočnik, A. *et al.* "Studying light-harvesting models with superconducting circuits". *Nat. Commun.* **9,** 904 (2018) (cit. on p. 97).

115. Vivas-Viaña, A. & Muñoz, C. S. "Two-photon resonance fluorescence of two interacting nonidentical quantum emitters". *Phys. Rev. Research* **3,** 033136 (2021) (cit. on p. 97).

116. Lawande, S. V., D'Souza, R. & Puri, R. R. "Effects of detuning and fluctuations on fluorescence radiation from a strongly driven three-level atom: Some analytical results". *Phys. Rev. A* **36,** 3228 (1987) (cit. on p. 97).

117. Lawande, S. V., Puri, R. R. & D'Souza, R. "Optical-double-resonance spectra and intensity-intensity correlations under intense fields with finite bandwidths: Some analytical results". *Phys. Rev. A* **33,** 2504 (1986) (cit. on p. 97).

118. Ngaha, J. *Two-Photon Resonance Fluorescence in a Ladder System*. MSc. Thesis (The University of Auckland, 2019) (cit. on pp. 97, 100, 107).

119. Narducci, L. M., Scully, M. O., Oppo, G.-L., Ru, P. & Tredicce, J. R. "Spontaneous emission and absorption properties of a driven three-level system". *Phys. Rev. A* **42,** 1630 (1990) (cit. on p. 99).

120. Manka, A., Doss, H., Narducci, L., Rup, P. & Oppo, G.-L. "Spontaneous emission and absorption properties of a driven three-level system. II. The Λ and cascade models". *Phys. Rev. A* **43,** 3748 (1991) (cit. on p. 99).

121. Bounouar, S. *et al.* "Path-controlled time reordering of paired photons in a dressed three-level cascade". *Phys. Rev. Lett.* **118,** 233601 (2017) (cit. on p. 104).

122. Hargart, F. *et al.* "Cavity-enhanced simultaneous dressing of quantum dot exciton and biexciton states". *Phys. Rev. B* **93,** 115308 (2016) (cit. on p. 104).

123. Holm, D. A. & Sargent, M. "Theory of two-photon resonance fluorescence". *Opt. Lett.* **10,** 405 (1985) (cit. on p. 104).

124. Carmichael, H. J. & Walls, D. F. "Detailed balance in open quantum Markoffian systems". *Z. Phys. B* **23,** 299 (1976) (cit. on p. 123).

125. Denisov, A., Castro-Beltran, H. M. & Carmichael, H. J. "Time-asymmetric fluctuations of light and the breakdown of detailed balance". *Phys. Rev. Lett.* **88,** 243601 (2002) (cit. on p. 123).

126. Marquina-Cruz, E. R. & Castro-Beltran, H. M. "Nonclassicality of resonance fluorescence via amplitude-intensity correlations". *Laser Phys.* **18,** 157 (2008) (cit. on p. 123).